Tracking endogenous and grafted neural progenitor cells in normal and ischaemic brains using MRI contrast agents and genetic labelling.

Rachael Dobson

Thesis submitted for the degree of Doctor in Philosophy

September 2009

UCL Institute of Child Health

University College London

I, Rachael Dobson, confirm that the work presented in this thesis is my own work except where acknowledged in the text. This work is based on research that was undertaken by me at University College London during the period 1st October 2005 to 30th July 2009.

Abstract

Cerebral ischaemia is a major cause of mortality and morbidity globally. Neural stem and progenitor cells (NPC) have the potential to contribute to brain repair and regeneration after an ischaemic event. Both endogenous and grafted NPC have been shown to migrate towards the ischaemic lesion, and differentiate into neurons. This thesis investigates methods of labeling and tracking the migration neural progenitor cells to a site of cerebral ischaemic injury, using magnetic resonance imaging (MRI) contrast agents and transgenic lineage tracing techniques.

First, labeling of exogenous NPC populations was investigated, for use in cell tracking in grafting studies. Cell labeling was optimized *in vitro* with fetal NPC using the iron oxide-based MRI contrast agent. A labeling method was developed using the FePro contrast agent, which maximized iron oxide uptake, was non-toxic to NPC, and did not interfere with NPC proliferation and differentiation. Labelled cells were then grafted into the brain after cerebral ischaemia, and imaged over four weeks using MRI. NPC migration was not observed *in vivo*, but an endogenous contrast evolved over time within the lesioned tissue, which presented a source of confounding signal for cell tracking. Endogenous ferric iron was observed in the lesion on histological sections. Several limitations of using MRI-based iron oxide contrast agents were highlighted in this study. To circumvent these limitations, we considered the development of gadolinium-based MRI contrast agents for cellular labeling and tracking, in collaboration with Imperial College chemistry department. Polymeric Gd-DOTA chelates were synthesized and designed for maximal r_1 relaxivity, and their relaxivity and effects on cell viability were assessed. Through this approach, we identified a number of candidate polymeric Gd-DOTA chelates with high relaxivity and low cytotoxicity for use in cellular imaging and tracking studies.

Next, cell tracking of endogenous NPC was investigated, using MRI contrast agent and transgenic lineage tracing approaches. A method of *in situ* labeling of endogenous NPC with the MRI contrast agent FePro was developed. NPC were labeled with FePro *in situ*, and their normal migration to the olfactory bulb, where they contribute to neurogenesis, could be imaged *in vivo* and *ex vivo*. In a second study, the migration of NPC constitutively expressing green fluorescent protein (GPF) under the promoters of genes of two developmentally distinct cortical and striatal NPC populations, was investigated following cerebral ischaemia. Both cortical and striatal populations of NPC were observed to contribute to the migrating streams of NPC that were observed in the striatum after five weeks post-ischaemia.

These studies demonstrate that MRI contrast agents offer the potential for *in vivo*, longitudinal tracking of NPC migration, in both grafted and endogenous NPC populations. Coupled with transgenic lineage tracing, and used in animal models of CNS injury such as cerebral ischaemia, labeling and tracking the migration of NSC with MRI contrast agents can contribute to our understanding of NPC biology in pathological environments.

Table of Contents

Abbreviations

2D, two-dimensional

3D, three-dimensional

AMPA, α-amino-3-hydroxyl-5-methyl-4-isoxazole-propionate

ANOVA, analysis of variance

AP, anterior-posterior

ATP, adenosine triphosphate

BBB, blood brain barrier

BDNF, brain-derived neurotrophic factor

BrdU, bromodeoxyuridine

Ca^{2+}, calcium ion

Cb, calbindin

CBF, cerebral blood flow

CNP, 2′,3′-cyclic nucleotide 3′-phosphodiesterase myelin protein

CNS, central nervous system

CO_2, carbon dioxide

Crt, calretinin

CSF, cerebrospinal fluid

DCX, doublecortin

DMEM:F12, Dulbecco's modified

DOTA, gadoterate meglumine

DTPA, gadopentate dimeglumine

DV, dorsal-ventral

EBSS, Earl's balanced salt solution

ECM, extracellular matrix

EGF, epidermal growth factor

ELISA, Enzyme-linked immunosorbent assay

ES, embryonic stem cells

FePro, Endorem-protamine sulphate complex

FGF, fibroblast growth factor

FOV, field of view

Gd^{3+}, gadolinium ion

GDNF, glial cell-line derived neurotrophic factor

GFAP, glial fibrillary acid protein

GFP, green fluorescent protein

HCl, hydrogen chloride

HIF-1, hypoxia inducible factor 1

ICP, inductively coupled plasma mass spectrometry

IL, Interleukin

IR, inversion recovery

K, Kelvin

L-15, Leibovitz-15 medium

MCA, middle cerebral artery

MCAO, middle cerebral artery occlusion

MCP-1, monocyte chemotactic protein 1

ML, medial-lateral

MMP, matrix metalloproteinase

MRI, magnetic resonance imaging

MTB, methylthymol blue

MTT, 3-[4,5-dimethylthiazol-2-yl]-2,5-diphenyl tetrazolium bromide

MW, molecular weight

NeuN, neuronal nucleus

NG2, NG2 chondroitin sulphate proteoglycan

NHS, National Health Service

NMDA, N-methyl-D-aspartic acid

NO, nitrix oxide

NPC, neural stem and progenitor cells
NSC, neural stem cells

NPY, neuropeptide Y

OB, olfactory bulb

OLP, oligodendrocyte precursor cells

PBS, phosphate-buffered saline

PDGF, platelet-derived growth factor

PFA, paraformaldehyde

PSANCAM, polysialic acid neural cell adhesion molecule

RMS, rostral migratory stream
SVZ, subventricular zone

ROI, region of interest

ROS, reactive oxygen species

SOD, superoxide dismutase

SQUID, superconducting quantum interference device

T, Tesla

TE, echo time

tPA, tissue plasminogen activator

TNFα, tumor necrosis factor alpha

TR, repetition time

VCAM, vascular cell adhesion molecule

VEGF, vascular endothelial growth factor

YFP, yellow fluorescent protein

Zn^{2+}, zinc ion

Acknowledgements

I would like to thank the following people for their support and contributions:

Kaylene Young and the Richardson lab at the UCL Wolfson Institute for Biomedical Research
Jonathan Martinelli, Claire Grignolo and the Imperial College Chemistry Department
Ana Garcia -Prieto at the London Centre for Nanotechnology
My colleagues in the Developmental Biology Unit at ICH: Kingyin Lee, Weerapong Pasongchean, Yuri Dalfiume, Pati Pungchanchaikul, Jane Sowden
My colleagues at the RCS Unit of Biophysics and Centre for Advanced Biomedical Imaging: Jack Wells, Mankin Choy, Ken Cheung, Tanja Holand, Panos Kyrtatos, Jon Cleary, Anthony Price, Pauliina Lehtolainen, David Gadian, Martin King, David Thomas, Sally Dowsett, Ted Proctor
My supervisors, Patrizia Ferretti and Mark Lythgoe
My family, and Paolo.

This research was funded by the Child Health Research Appeal Trust (CHRAT).

Introduction

Cerebral ischaemia is a major cause of mortality and morbidity globally. Neural stem and progenitor cells (NPC) are a promising therapeutic candidate for the repair and regeneration of the ischaemic brain. Both endogenous and grafted NPC have been shown to migrate towards the ischaemic lesion, and differentiate into neurons. Understanding of the mechanism of action of NPC in the ischaemic brain is hindered by the limited methods of in vivo tracking of their distribution and migration. MRI contrast agents for cellular imaging might be suitable for NPC labeling and monitoring *in vivo* following engraftment. Some studies have achieved labeling and *in vivo* monitoring. New contrast agents and labeling methods have been described that have the potential to improve labeling efficiency, cell viability and *in vivo* detection. The aim of the research in this thesis is to optimize NPC labeling with MRI contrast agents to increase *in vivo* detection without affecting cell viability and NPC biology, for both exogenously and endogenously labeled NPC populations. This thesis investigates methods of labeling and tracking the migration neural progenitor cells to a site of cerebral ischaemic injury, using magnetic resonance imaging (MRI) contrast agents and transgenic lineage tracing techniques.

In the following chapters we will introduce the main topics discussed this thesis: cerebral ischaemia, neural stem cells, and magnetic resonance imaging (MRI). It is designed provide an overview of the literature, highlight important themes and issues relevant to the research chapters, and set the context within which we have approached our research aims.

1. *Cerebral ischaemia*

1.1. Overview

Stroke is a cardiovascular disease that affects blood flow in the brain. The most common type of stroke is cerebral ischaemia, which occurs as a result of the reduction of blood flow in a cerebral artery, in most cases the middle cerebral artery, causing a decrease in oxygen and glucose availability to the brain, and ultimately leads to localised energy failure and cell death. Energy failure contributes to cytotoxic oedema and the breakdown of the blood brain barrier (BBB), leading to vascular oedema and an inflammatory response. Central nervous system (CNS) injury from cerebral ischaemia is characterised by a necrotic core surrounded by an ischaemic penumbra. Further delayed neuronal death can occur in the peripheral penumbra days to weeks following the initial ischaemic insult.

The CNS has high oxygen consumption, a low level of antioxidants, little capability for glucose storage, and a high level of substrates for reactive oxidative species (ROS), in particular high iron levels and fatty acid membranes (Hayashi et al., 2003). Together, these factors make the CNS particularly sensitive to oxidative stress during cerebral ischaemia, and activate necrotic, apoptotic and inflammatory response pathways.

1.2. *Public health perspective*

Stroke is a major cause of mortality and disability worldwide: the third commonest cause of death after heart disease and all cancers, and the most common cause of disability. Cerebral ischaemia is the most common type of stroke, comprising 70% of stroke cases. Other types of stroke include intracerebral haemorrhage (13%) and subarachnoid haemorrhage (6%), with approximately 10% of strokes of unknown cause (The Stroke Association, 2006b). In the UK more than 130 000 people suffer from a stroke each year, of which one quarter result in mortality, and one third in disability (National Audit Office, 2005). Furthermore, there is a high risk – between 30-43% – of recurrent stroke within 5 years after the first stroke event, as well as a high risk of myocardial infarction.

In the past 30 years, stroke prevalence and mortality has decreased, but at a slower rate than for coronary heart disease. However, the risk of death from stroke has remained constant at 25%. The decrease in prevalence can be attributed to the reduction in smoking rates and saturated fat intake since the 1970s, both risk factors for stroke.

The risk factors for stroke are similar to those of other cardiovascular diseases: older age, male sex, smoking, a diet high in saturated fat, high blood pressure and serum cholesterol levels, obesity, diabetes, alcohol and low physical activity levels. Blood pressure is a causal risk factor for stroke, and is associated with 50% of all ischaemic strokes. Smoking accounts for 10% of strokes: smokers are at two to four times greater risk of stroke than non-smokers, cessation of smoking for five years reverses this difference in risk (The Stroke Association, 2006a). Though these are preventable risks, in the UK the public awareness for these risk factors, and how to manage them, is low.

A Western lifestyle might be associated with increased cardiovascular disease risk. A reduction in smoking rates and saturated fat intake has contributed to the declining mortality rates from cardiovascular disease since the 1970s, however a reduction in physical activity and increase in obesity and diabetes over the same period may have slowed the decline, and may cause an increase in prevalence in the future (Mokdad et al., 2003). Japan has the lowest incidence of cardiovascular disease of high income countries. In a study of Japanese emigrants, Robertson *et al* found that Japanese emigrating to the US were at increased risk of cardiovascular disease than those remaining in Japan (Robertson et al., 1977). Conversely, developing nations adopting Western lifestyle and dietary risk factors associated with economic development – such as urbanisation, tobacco use, a high fat diet, are experiencing an increase in cardiovascular disease prevalence, as well as diabetes, obesity and high blood pressure. For example, smoking rates are extremely high in China, where 60% of men and 4% of women smoke – over 300 million smokers. Globally, two thirds of stroke mortality now occurs in developing countries (The Stroke Association, 2006), and rates are higher in urban areas.

Socioeconomic status is another strong indicator of cardiovascular disease risk. There is an inverse relationship between social status and stroke risk, where risk decreases with income in a 'dose-

dependent' effect (The Stroke Association, 2006), which suggests that the social environment is a determinant of risk. This is supported by the Whitehall study, which found that cardiovascular disease risk was inversely related to employment grade in civil servants (Brunner et al., 1993; Hemingway et al., 2000; Marmot et al., 1991). This health inequality has also been demonstrated in terms of the reduction in cardiovascular disease prevalence – while the prevalence of cardiovascular disease has decreased since the 1970s, the majority of the decrease has occurred in higher socioeconomic groups, with almost no difference in prevalence in low socioeconomic class. Even at the global level, socioeconomic factors influence stroke risk. National per capita income is a strong predictor of stroke mortality and morbidity (Johnston et al., 2009).

Of perhaps greatest concern is the increasing risk of stroke with advancing age. Over 80% of strokes occur in those aged 65 or above, and 56% occur over 75 years of age. The population of the UK is ageing, and life expectancy is also increasing. The Office of Health Economics estimates that by mid-century, the percentage of UK citizens over 65 years of age will increase to 25% of the population, compared to 15.7% in 2006 and 15% in 1981. As life expectancy is also increasing, the growing number of people above 65 will live longer, and are therefore at greater risk of a number of diseases including stroke and other cardiovascular diseases for a longer period of life. The result is that the overall health burden to the NHS is growing quickly as the population ages. Reducing risk of cardiovascular disease in the population, and maintaining health into old age, is therefore a major health priority, in order to reduce the health burden of stroke or even maintain it at current levels. But there are also great opportunities for the development of novel treatments for stroke patients, which is discussed in the following sections, and investigated further in this thesis.

1.3. Clinical perspective

The health burden of stroke in the UK is already large. Approximately 450 000 people are living disabled from stroke in England (National Audit Office, 2005), and only 5-9% of stroke patients are fully independent one year after stroke. This represents a huge cost to the NHS and wider economy: £2.8 billion in direct costs to the NHS, and £2.4 billion in additional care costs, such as nursing home and community care, annually, or £15 000 per person for 5 years of direct care, rising to £29 000 to include additional care costs. This is greater than the costs associated with coronary heart disease. One quarter of all long-term hospital beds, and one fifth of acute beds, are occupied by stroke patients – the largest of any patient group. The average length of stay in a hospital is 28 days after stroke, but there is high variability among hospitals across the UK (National Audit Office, 2005).

There is clear evidence that appropriate clinical management of stroke and effective care can improve stroke outcome, reducing death, disability and complications from stroke (Royal College of Physicians, 2007). Access to an acute stroke services in hospitals is linked to recovery from stroke (National Audit Office, 2005), and increasing the number of stroke units in hospitals is estimated to

have saved the NHS £82 million (The Stroke Association, 2006). In the UK, 91% of hospitals have a stroke unit, and 50% have an acute stroke unit. However, only 65% of stroke patients are treated in stroke unit, and only 10% of patients are admitted directly to a stroke unit (within four hours of admission) (Royal College of Physicians, 2007). These data present clear implications for stroke outcome, as the only effective intervention requires treatment within three hours of stroke onset. Furthermore, 75% of patients who experienced a mild stroke or transient ischaemic attack (TIA) were not treated in a stroke unit. Treating patients with minor stroke or TIA in specialist units has been shown to reduce hospital admissions for recurrent stroke, patient disability, and ultimately healthcare costs (Luengo-Fernandez et al., 2009). As this group is at high risk of having a recurrent stroke, lack of access to a stroke unit may also miss opportunity for prevention.

Clinical guidelines recommend that all patients with acute stroke should have a brain scan – magnetic resonance imaging (MRI) or computed tomography (CT) – within 24 hours of onset of symptoms, for stroke subtype diagnosis before treatment (Department of Health, 2007). Currently, most patients wait 48 hours on average (National Audit Office 2005), and only 9% have access to MRI or CT within three hours of admission (Royal College of Physicians, 2007). The most cost-effective management of stroke would include scanning all stroke patients immediately (National Audit Office, 2005).

Currently the only approved intervention that improves outcome for cerebral ischaemia is the thrombolysis drug tissue plasminogen activator (tPA), which requires diagnosis of cerebral ischaemia and rtPA treatment within 3 hours of the ischaemic event. This treatment option is not currently routine in the NHS, with fewer than 1% of patients receiving rtPA treatment. This is partly due to clinical management, access to imaging facilities and radiologists, as well as a lack of public awareness of stroke as a medical emergency. In Australia, 9% of stroke patients are treated with rtPA, of which 40% make a full recovery from stroke, which represents a saving of £16 million in rehabilitation and care costs.

The middle cerebral artery (MCA) supplies a large portion of the cortex, including the frontal, parietal and temporal lobes, as well as the basal ganglia, posterior and anterior internal capsules. As such, occlusion of the MCA and resulting cerebral ischaemia leads to diverse neurological sequelae. Disability from stroke includes paralysis, speech impediments, aphasia, dysphagia, reduced mobility and locomotion, reduced motor control including hemiplegia or hemiparesis, memory loss and dementia, urinary incontinence, and depression. Long term care for stroke is focussed around rehabilitation, and can include physiotherapy; speech therapy; and occupational therapy. Dieticians and psychologists may also be involved in long term care, to reduce lifestyle and diet risk factors associated with recurrent stroke, and to address mental health issues, respectively.

There is an urgent need for improved stroke care. A coordinated approach of stroke risk prevention, improved clinical management, and drug development will be required to reduce the health burden of stroke. Stroke prevention and reduced exposure to risk factors will lower stroke incidence in the

population, and integrated clinical and social care management can improve outcome, reducing death and disability. There is also huge scope for development of treatments that will improve neurological outcome after stroke, however to date there have been few successful drug developments. Regenerative medicine may provide an alternative approach to neuroregeneration, which is discussed in the following sections.

1.4. *Acute ischaemia*

In the brain, reduced cerebral blood flow (CBF) leads to energy failure and necrosis in neurons. The necrotic core of an ischaemic lesion develops via acute excitotoxic events, accumulation of toxic metabolites and mitrochondrial dysfunction (Durukan and Tatlisumak, 2007). In neurons, excitotoxicity occurs as energy-dependent functions fail in the absence of glucose and oxygen (Sugawara et al., 2004). Energy failure leads to the abnormal depolarisation of the neuronal membrane, activation of voltage-gated calcium channels, and release of neurotransmitters into the extrasynaptic space. Extrasynaptic glutamate accumulates and can activate AMPA and NMDA receptors on adjacent neurons and glia, causing further Ca^{2+} influx into cells. This influx causes a disruption in ion homeostasis in the cell, and activates intracellular signalling pathways, such as further neurotransmitter release; activation of proteolytic enzymes to degrade the cytoskeleton and extracellular matrix (ECM); and the production of free radicals such as superoxide, hydrogen peroxide, the hydroxyl radical and nitric oxide. The disruption in ion homeostasis also results in an influx of water into the cell, causing cytotoxic oedema and osmotic lysis of cells. Together, these pathways lead to necrosis in neurons (Lai and Todd, 2006).

Mitochondrial dysfunction in the absence of oxygen also leads to cellular necrosis. Oxidative stress results in the overproduction of the free radicals hydrogen peroxide and superoxide in mitochondria, which is normally scavenged by the superoxide dismutase (SOD) antioxidant. The free radicals can react with cellular components such as DNA, phospholipids, amino acids and carbohydrates, causing the rupture of mitochondria, release of proapoptotic molecules (Mergenthaler et al., 2004), and at high concentrations cell disintegration (Sugawara et al., 2004). Free radical production is an important contributor to CNS damage following ischaemia: in transgenic mice, overexpression of SOD has been shown to be neuroprotective in cerebral ischaemia, whereas SOD deletion increases ischaemic infarct size (Sugawara et al., 2004).

1.5. *Inflammatory mediators in ischaemia*

A number of pro-inflammatory cytokines, chemokines, growth factors and extracellular matrix (ECM) proteins are upregulated and activated following cerebral ischaemia. These can persist for hours to days, and contribute to the change in CNS environment following stroke. As such, they may mediate endogenous or engrafted neural stem and progenitor cell (NPC) behaviour following

ischaemia, which will be discussed further in Chapters 4 and 7.

Pro-inflammatory cytokines are upregulated during ischaemia, and are associated with neuronal death. Interleukin (IL)-1β, IL-6 and TNF-α are upregulated, stimulating upregulation of P- and E-selectin cell adhesion molecules in endothelial cells (Huang et al., 2006). P- and E-selectin are initiators of the peripheral inflammatory cascade, and promote leukocyte adherence to the endothelium and infiltration into the brain parenchyma (Huang et al., 2006). Membrane proteins of the integrin family modify the basal lamina and ECM, disrupting the BBB and further promoting the inflammatory cascade (Huang et al., 2006; Nawashiro et al., 1997). Endothelial cells express vascular cell adhesion molecule VCAM-1 and ICAM-1, with which β-integrin-expressing leukocytes also interact (Mergenthaler et al., 2004). Pharmacoogical inhibition of ICAM-1 blocks leukocyte infiltration, and reduces ischaemic infarct volume (Soriano et al., 1996). Overexpression of TNF-α can exacerbate ischaemic damage, whereas pharmacological inhibition decreases infarct volume (Wang et al., 2007a).

Anti-inflammatory cytokines involved in the acute inflammatory response include TGF-β, IL-10 and MCP-1, which downregulate inflammation and are neuroprotective (Mergenthaler et al., 2004).

Infiltration of leukocytes, such as neutrophils and monocytes, across the vascular endothelium into the brain parenchyma occurs as early as 30 minutes following ischaemia (Huang et al., 2006). Leukocytes contribute to microvessel obstruction, edema, tissue infarction and necrosis, independent of neuronal excitotoxicity and mitochondrial dysfunction. Neutrophils also express selectins and glycoproteins that mediate endothelial-leukocyte interactions. They release free radicals and matrix metalloproteases which contribute to tissue infarction (Huang et al., 2006).

Chemokines are cytokines that promote chemotaxis and recruitment of immune cells. Following ischaemia, these are released by neurons and glia into the interstitial space and cerebrospinal fluid (CSF) and influence the recruitment of microglia and macrophages to the injury site (Lai and Todd, 2006; Wang et al., 2007a). The neurotrophin brain-derived neurotrophic factor (BDNF) is transiently expressed in neurons and microglia following ischaemia, and exogenously administered BDNF can decrease infarct volume (Lai and Todd, 2006; Benraiss et al., 2001; Pencea et al., 2001b). Microglia upregulate epidermal growth factor receptor (EGFR), vascular endothelial growth factor (VEGF), and platelet-derived growth factor (PDGF) following ischaemia, and exogenous administration of VEGF can rescue neurons from ischaemic damage (Kuhn et al., 1997).

Matrix metalloproteases (MMP) are Zn^{2+} endopeptidases that primarily modulate ECM homeostasis (Gasche et al., 2006). Following ischaemia, MMPs are involved in the inflammatory response, BBB disruption, and ECM remodelling through enzymatic degradation of basal lamina and ECM proteins (del Zoppo et al., 2007; Asahi et al., 2001; Kamada et al., 2007; Tejima et al., 2007). MMP activity may also contribute to hemorrhagic transformation (Gasche et al., 2006) and regulation of neuronal death (Cunningham et al., 2005). Neurons and astrocytes produce pro-MMP that can be activated following ischaemia. MMP-2 is activated immediately during ischaemia, and its expression overlaps

the area of necrotic core, whereas MMP-9 is activated from 3-24 h post-ischaemia.

Inhibition of MMP-9 following ischaemia exacerbates infarct volume, reduces neurovascular remodelling, and reduced functional recovery from ischaemia (Zhao 2006). Administration of exogenous VEGF partially attenuates the increase in lesion volume from MMP inhibition (Zhao et al., 2006). ECM remodelling through MMP activity may contribute to tissue regeneration and neurogenesis, and facilitate cell migration.

1.6. Cellular responses to cerebral ischaemia

Early ischaemic events such as blood brain barrier (BBB) breakdown create a hypoosmotic environment around the vasculature as water moves into the brain parenchyma, which is known as vasogenic oedema (Panickar and Norenberg, 2005). *In vitro,* hypoosmotic conditions are sufficient to induce reactive astrocytosis, which is characterised by astrocyte hypertrophy; fibrous morphology, proliferation (Faulkner et al., 2004), migration, and upregulation of the intermediate filament GFAP in astrocytes (Panickar and Norenberg, 2005). Proliferation and hypertrophy begins within minutes of ischaemia and peaks at two weeks post-ischaemia (Panickar and Norenberg, 2005).

1.6.1. Reactive astrocytes

Reactive astrocytes contain the area of inflammation and prevent the spread of injury, by demarcating and surrounding ischaemic tissue, separating the inflammatory response from viable neural tissue. Reactive astrocytes form scar tissue with fibroblasts (Pekny and Nilsson, 2005). They release taurine, which reduces local tissue oedema, produce the antioxidant glutathione (Pekny and Nilsson, 2005), and secrete VEGF, which is neuroprotective following ischaemia. In transgenic models, GFAP deletion prevents reactive astrocytosis, and increases infarct volume, decreases local cerebral blood flow (CBF) and increases cytotoxic oedema following ischaemia. There is no glial scar formation, no restoration of the BBB, and no containment of inflammation These data suggests that reactive astrocytes have a protective role following cerebral ischaemia.

However, reactive astrocytes may also exacerbate tissue damage and inhibit axon regeneration via the formation of the glial scar (Sofroniew, 2005). Hyper-reactive astrocytes contribute to inflammation by producing nitric oxide (NO) and reactive oxygen species (ROS). Gap junctions in astrocytes may also have the negative effect of propagating inflammatory damage though distal communication with astrocytes in non-ischaemic regions (Panickar and Norenberg, 2005).

1.6.2. Activated microglia

Microglial activity may be both protective and damaging following cerebral ischaemia, and microglia

interact with neural stem and progenitor cells (NPC) in the normal and injured brain. Understanding microglial activity in the ischaemic brain is therefore central to understanding the NSC response and lesion progression over time. The microglial contribution to the evolution of the ischaemic lesion is investigated in Chapter 4.

Microglia form part of the CNS immune system. Their developmental origin is the bone marrow mesenchyme, and they populate the CNS during development (Aloisi, 2001; Napoli and Neumann, 2009). There is both an endogenous microglial and peripheral macrophage response to ischaemia (Ladeby et al., 2005b; Ladeby et al., 2005a). Activated microglia and macrophages are morphologically and immunologically equivalent, and behave as a single cell type following ischaemia (Ekdahl et al., 2009). Macrophages have been distinguished from microglia experimentally by bone marrow irradiation and GFP bone marrow transplantation, where repopulated peripheral blood cells express GFP and resident microglia do not (Tanaka et al., 2003). Priller *et al* estimate that peripheral macrophages account for 1/3 of the activated microglial population (Priller et al., 2001). Microglia represent the first immune response against injury, preceding the infiltration of peripheral macrophages and leukocytes (Tanaka et al., 2003; Schilling et al., 2003). Microglia are activated within minutes of cerebral ischaemia onset, whereas macrophages infiltration peaks at 24-28 hours post-ischaemia (Jander et al., 2007; Kleinschnitz et al., 2003; Schilling et al., 2003). Macrophage/microglia remain at the ischaemic boundary for weeks to months (Ekdahl et al., 2009).

Activated microglia take on an amoeboid morphology, migrate to sites of injury and upregulate inflammatory markers in response to cerebral ischaemia. Their major role following ischaemia is the mediation of the local inflammatory response and programmed cell death (Lai and Todd, 2006). Activated microglia act as sensors of excitotoxicity and necrosis through the upregulation of glutamate transporter 1 and ATP receptor, and synthesise and release a combination of cytokines, chemokines and growth factors such as BDNF and GDNF (Shaked et al., 2005). Microlia proliferate after ischaemia (Flugel et al., 2001; Djukic et al., 2006; Ajami et al., 2007). They respond to soluble factors and the loss of neuronal input following ischaemia by migration toward the lesion (Ekdahl et al., 2009; Hanisch and Kettenmann, 2007).

Microglia can also become overactivated in response to injury, and have been implicated in secondary delayed neuronal death in the penumbra (Block and Hong, 2007). Overactivated microglia increase nitric oxide (NO) and TNF-α secretion, thereby increasing inflammation at the injury site (Butovsky et al., 2006). Inhibition of the immune response exacerbates ischaemic damage (Lalancette-Hebert et al., 2007), but inhibition of microglia by minocyline has been shown to be neuroprotective (Yrjanheikki et al., 1999). Upregulation of IL-10 or prostaglandin E2 suppresses the pro-inflammatory funtion of microglia and is also neuroprotective (Cacci et al., 2008).

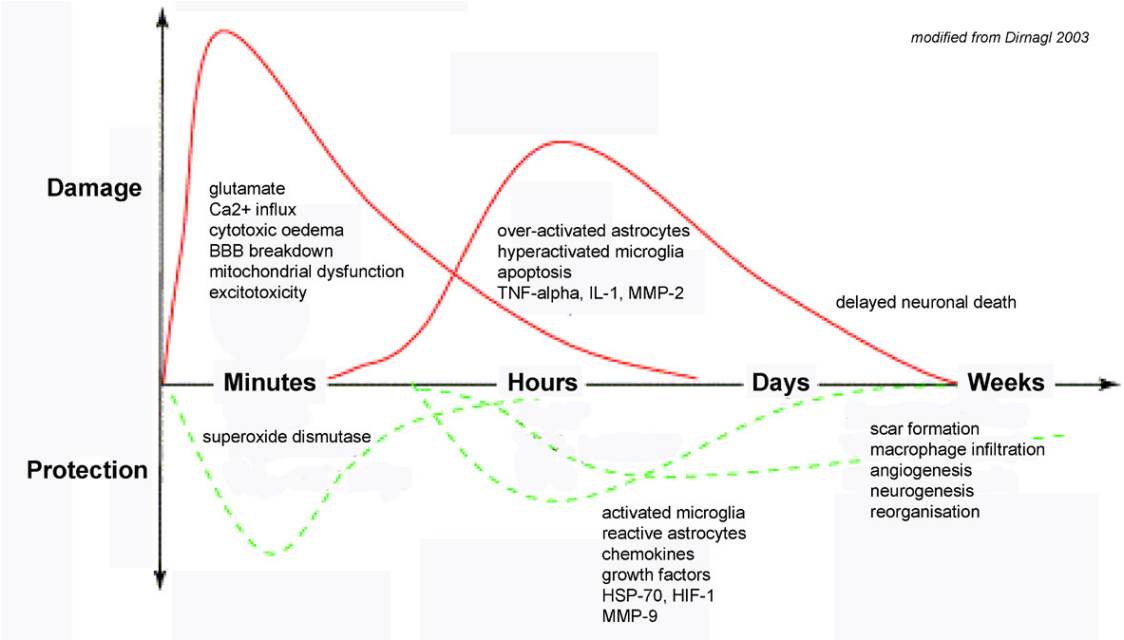

Figure 1.6.2.1 Schematic timeline of inflammatory and protective events after cerebral ischaemia (modified from Durukan *et al*).

Both microglia and astrocytes have been implicated in secondary delayed neuronal death in the penumbra, which is discussed further in section 1.7, and is investigated in this thesis (Block et al., 2007; Panickar and Norenberg, 2005). In the case of both astrocytes and microglia, a moderate, local inflammatory response from reactive astrocytes and activated microglia is protective in CNS injury, whereas overactivation of astrocytes and microglia propagates the injury. However, lack of any inflammatory response in the CNS also exacerbates the injury. Therefore, there is an intermediate level of inflammatory response that is optimal for neuroprotection. This may underlie the limited regenerative capacity of the mammalian CNS, where the severity of ischaemic insults leads to overactivation of microglia and astrocytes, and prevents regeneration. Targeting pro-inflammatory cytokines and their cellular mediators may therefore have therapeutic potential. Cellular therapy may also act via mitigating the inflammatory response and creating a supportive environment for regeneration.

1.7. The penumbra and delayed neuronal death

The penumbra can be defined as a region of ischaemic tissue peripheral to the necrotic core where viable neurons may be salvaged. It is therefore an important therapeutic target for CNS regeneration.

The physiological profile of the penumbra has been characterised using a variety of methods. First defined in 1977 by Astrup *et al*, the penumbra is an area of ischaemic injury that experiences low CBF and residual circulation during the ischaemic event, but not the total membrane potential failure of neurons, where "neurons remain structurally intact but functionally inactive" and have the potential to be rescued with the restoration of perfusion (Astrup et al., 1977; Weinstein et al., 2004; Lo, 2008;

Fisher, 2004). It has also been described as a region with reduced CBF, oxygen and glucose consumption (Ginsberg, 1990; Powers, 1984), , increased excitotoxicity, oxidative stress and apoptosis (Lo et al., 2005; Sharp et al., 2000). Neurons in the penumbra may become dysfunctional but do not undergo acute necrosis during ischaemia (Lo et al., 2005). The penumbra may later progress to infarction via delayed apoptosis hours to days after the ischaemic event, due to secondary cell damage from chronic inflammation and mild excitotoxicity (Mergenthaler et al., 2004). Therefore, a time window exists between the ischaemic event and latent neuronal death where cells in the penumbra are potentially salvageable.

Cell protective programmes are upregulated within the penumbra (Mergenthaler et al., 2004). Heat shock protein 70 (HSP70) and Hypoxia-inducible factor-1 (HIF-1) are immediately upregulated following ischaemia, and their expression overlap demarcates the penumbra(Weinstein et al., 2004b). The penumbra vasculature is characterised by vasoparalysis, decreased reactivity of vessels and decreased autoregulation. There is a decreased metabolic response to neuronal activity, as well as decreased neuronal activity. Furthermore, reactive astrocytosis, expression of superoxide dismutase (SOD), and delayed neuronal death from apoptosis peak at 14 days post injury (Girouard and Iadecola, 2006). This indicates a slow degenerative process following the initial ischaemic insult and the onset of a chronic injury.

Nestin expression is also upregulated in the penumbra, in GFAP+ reactive astrocytes (Li and Chopp, 1999; Duggal et al., 1997; Lin et al., 1995), in a distinct GFAP- population of astrocytes (Burns et al., 2007), and in infiltrating peripheral macrophages. Upregulation has been reported from 6 hours, peaking at 7 days, and persisting up to 4 weeks post-ischaemia (Duggal et al., 1997; Li and Chopp, 1999). A small proportion of nestin+ cells have originated from the SVZ and migrated toward the penumbra (Burns et al., 2007). It is possible that nestin expression is linked to cell proliferation in the penumbra, though there are no BrdU co-labelling studies to date. Astrocyte proliferation occurs in the penumbra, and nestin expression may represent a recapitulation of developmental processes in the astrocyte population, as a mechanism of repair and regeneration (Wiese et al., 2004).

1.8. Animal models of cerebral ischaemia

Human stroke is typically a small vessel occlusion, or an arterial embolism. Distinctive features of human stroke are the presence of the ischaemic penumbra that progresses to infarction subsequent to the initial damage; reperfusion of the occlusion; and functional reorganisation of neuronal circuits affected by ischaemic damage. Animal models of cerebral ischaemia aim to mimic some or most of these features in mammals with similar cerebral physiology to the human.

The Koizumi middle cerebral artery occlusion (MCAO) model is a model of focal ischaemia, which can be transient or permanent. It is presently the most common animal model of ischaemia(Koizumi J, 1986). It is this model that is used in chapters 4 and 7 to investigate cellular therapy and the

endogenous neural stem cell response following ischaemia. To perform the procedure, a tipped suture is inserted into the carotid artery and advanced through the skull into the circle of Willis, where it occludes the MCA (Figure 1.8.1) (Durukan and Tatlisumak, 2007; Lythgoe et al., 2003). For a transient ischaemic injury with reperfusion, the suture occludes the MCA for a fixed amount of time, between 20 – 120 minutes, and is then withdrawn slowly to reperfuse and restore bloodflow to the occluded region. The procedure creates a volume of ischaemic injury in the ipsilateral hemisphere that encompasses the dorsolateral striatum and the anterior cortex, but excludes the hippocampus. Focal ischaemia requires surgical occlusion of the MCA because the circle of Willis provides sufficient collateral blood supply to the MCA region via non-affected vessels.

To date, most cerebral ischaemia studies are performed in the rat. The surgery is easier in a larger animal, and a more reproducible lesion can be achieved. The most reproducible lesions can be achieved between 60-90 minutes of occlusion, however with increasing occlusion time the volume of necrotic to penumbral tissue decreases, and less tissue is salvageable (Durukan and Tatlisumak, 2007). The MCAO surgery has also been developed in the mouse (Hata et al., 1998; Fujimura et al., 1999; Chen et al., 2005). While the surgery is more difficult in a smaller animal and lesion reproducibility is more difficult to achieve (Carmichael, 2005), the major advantage of performing surgery in mouse is the opportunity to study ischaemia by combining the MCAO surgery in transgenic animal models (Tureyen et al., 2005).

The advantages of the Koizumi MCAO model are that it avoids the need for invasive craniotomy to access and occlude the MCA, it is a transient occlusion, and the animals can recover and survive weeks to months post-ischaemia. Many elements of the surgery can be modified: for example the suture width, length and coating material, and MCA occlusion time. The MCA occlusion model can also be modified to create permanent focal ischaemia, where the suture is not withdrawn after surgery, no reperfusion occurs, and the MCA region experiences a chronic decrease in blood flow (Lythgoe et al., 2003).

The disadvantages are that the infarct size can be variable and may incorporate the thalamus, hypothalamus and substantia nigra. These structures are rarely infarcted in human, and hypothalamic injury may lead to hyperthermia (Durukan and Tatlisumak, 2007). Furthermore, the area of infarct in this model is significantly larger than in human stroke (Carmichael, 2005). Different rat and mouse strains have different cerebrovascular anatomy, and this may produce different infarct volumes, poor occlusions or subarachnoid hemorrhages, for example in the Fischer rat (Dittmar et al., 2006).

The Koizumi MCAO procedure is performed under anaesthesia, and this may itself be neuroprotective (Kitano et al., 2007). Estrogen may also be neuroprotective, as female rats have smaller stroke volumes than male or ovariectomized rats (Alkayed et al., 1998), and estrogen administration can reduce lesion volume in ovariectomized females (Rusa et al., 1999).

A disadvantage common to all animal models of ischaemia is the lack of associated diseases which may complicate the pathology, which are common in the clinical setting: surgery is typically

performed in young healthy animals. Apoptosis at the lesion is known to be increased in older (18 months) rather than younger (3 months) ischaemic rats (Chen and Sun, 2007). Furthermore, this study also showed that post-ischaemic neurogenesis was also reduced in older rats. The typical human stroke patient is of old age and may have other diseases such as atherosclerosis, diabetes or dementia, or conditions such as obesity and high blood pressure and cholesterol, all of which could complicate ischaemic pathology and patient recovery.

Several other animal models of focal cerebral ischaemia exist. Photothrombotic ischaemia involves intravenous administration of a photosensitive dye – typically Rose Bengal – followed by selective irradiation over a specific area of cortex which activates the dye, causing endothelial damage, BBB disruption and ischaemia (Busza et al., 1992; Durukan and Tatlisumak, 2007). This procedure creates exclusively cortical lesions due to the limited penetration depth of the irradiation, and the infarct lacks a penumbra.

Microembolic and thromboembolic ischaemia models generate heterogeneous multifocal lesions within the brain (Mayzel-Oreg et al., 2004; Papadopoulos et al., 1987; Vise et al., 1977). These models involve the intracarotid injection of microspheres, fibrin, fat or air emboli, silicone or collagen clots to produce embolism in intracranial arteries. The lesion volume and localisation is not reproducible, but the mechanism of infarction is similar to human stroke conditions. Following microembolism, the blood brain barrier breaks down immediately due to severe irritation of the vascular wall (Vise et al., 1977),(Vise 1977), in contrast to the human stroke where the blood brain barrier breaks down after several hours as a consequence of the ischaemic event.

The MCAO occlusion can also be achieved by craniotomy to expose the MCA and electrocoagulation of the artery to achieve occlusion (Clark et al., 1993; Tamura et al., 1981). While the reproducibility of this method is high, the occlusion is permanent, and the surgery introduces factors that are not common in human stroke such as exposure to air, local temperature change, and disruption of CSF homeostasis and intracranial pressure.

The spontaneously hypertensive rat is naturally prone to stroke, and some studies have been undertaken using this strain of rat (Nabika et al., 2004). In this rat the circle of Willis is incomplete and the system of compensatory collateral vessels is compromised.

Characterisation of animal models of ischaemia and effectiveness of treatment can be assessed by several parameters. Lesion volume can be assessed by MRI (discussed further in section 3.5.6); TTC staining, or hematoxylin-eosin histology. Total lesion volume and lesion volume as a percentage of hemisphere volume can be expressed (Tatlisumak et al., 1998a; Tatlisumak et al., 1998b; Gerriets et al., 2004). The advantage of *in vivo* imaging modalities such as MRI is that no tissue processing or fixation is required prior to analysis, which can alter tissue volumes through dehydration, mounting, and removal from the skull.

Ischaemic injury can also be assessed through behavioural tests such as skilled limb movements (Gharbawie and Whishaw, 2006; Gharbawie et al., 2006), neurological score, beam walking, the

rotarod test or the sticky label test (Hunter et al., 2000) These tests assess the sensory and motor capabilities of animals and can be used as markers of functional recovery after ischaemia (Modo et al., 2002c).

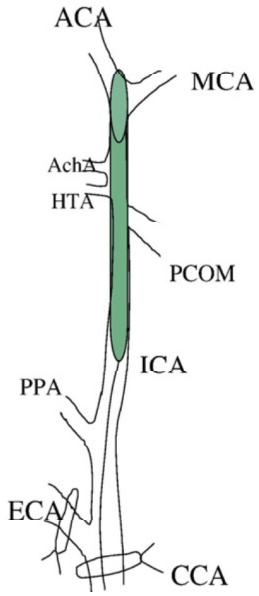

Figure 1.8.1 The middle cerebral artery occlusion surgery (modified from Durukan et al.). ACA, anterior cerebral artery. MCA, middle cerebral artery. ICA, internal carotid artery. ECA, external carotid artery. CCA, common carotid artery. Green filament illustrates the tipped suture advanced to the MCA bifurcation, causing MCA occlusion.

2. *Stem cells*

2.1. Definition

A stem cell is a cell that has the capacity for unlimited self-renewal and the ability to terminally differentiate into multiple cell types. Thus, at each cell division the stem cell replicates itself; two cells are generated that will either commit to differentiation, or remain as stem cells. This pairing of continuous cell division with developmental plasticity is what defines a stem cell, and is the mechanism by which the developing embryo can give rise to a mature adult organism with multiple organs and cell types.

Theories of stem cells and regeneration are historically linked. Regeneration has been observed in reptiles, amphibians and invertebrates for centuries, and was investigated with much interest in the eighteenth century at the height of the expansion of the biological sciences. Starfish limbs, newt tails and eyes were severed and observed to re-grow into functional units, and the concept of an embryonal centre that could regenerate a missing limb was proposed. The isolation and study of stem cells in vitro began with the study of teratocarcinomas in the mid-twentieth century. Teratocarcinomas are spontaneously arising gonadal tumours and are unique in that they contain differentiated cells as well as undifferentiated cells of all the embryonic germ layers. *In vitro* the teratocarcinomas can expand continuously. The study of these tumours gave rise to the concept that a single cell can proliferate and generate multiple mature cell types. The resemblance of teratomas to a disorganised embryo suggested a developmental origin of these cells and stimulated the search for the isolation of stem cells in the developing embryo (Friel et al., 2005a).

The extent to which a stem cell can produce differentiated cells of any lineage *in vivo* is temporally and spatially regulated, and is determined by the developmental stage and the position within the embryo or adult organism. Stem cells derived from blastomeres can give rise to all 3 germ layers and placenta (Friel et al., 2005b). These cells are termed totipotent, for their capacity to generate all cells required for a new embryo. Cells of the inner cell mass (ICM) can give rise to endoderm, mesoderm and ectoderm but not placenta *in vitro* (Keller, 2005). These cells are termed pluripotent. Multipotent stem cells are somatic or adult stem cells that are developmentally restricted and can only generate cells of a specific lineage. Progenitor cells have a limited number of cell divisions before they will terminally differentiated, and are not considered true stem cells for this reason.

Murine embryonic stem (ES) cells were first isolated and cultured from the ICM of the blastocyst (Friel et al., 2005c), and only relatively recently human ES cells were successfully isolated and cultured from the 8 stage pre-implantation embryo (Thomson et al., 1998). ES cells can give rise to endoderm, mesoderm and ectoderm *in vitro*, and develop into teratomas *in vivo* when implanted into immunodeficient adult mice, thus demonstrating their pluripotency (Trounson, 2005). ES cells can differentiate into specific lineages if prompted by specific genes, growth factors or if presented with

specific environmental cues. For example, ES cells transplanted into the subventricular zone of the normal adult brain migrate throughout the brain and differentiate into all neural lineages (Trounson, 2005). Developmental pathways regulating cell division, differentiation, and lineage have been elucidated through the study of ES cells. Transcription factors such as Nanog, Oct4, Sox2 and BMP4 have been identified as important regulators of self-renewal and maintaining an undifferentiated cell state (Friel et al., 2005d).

Mature adult cells can also be reprogrammed to an embryonic state, to generate induced pluripotent stem cells. Takahashi and Yamanaka demonstrated that by introducing four key transcription factor genes – c-myc, Oct3/4, Sox2 and Klf – to adult mouse fibroblasts, the cells returned to an embryonic-like state (Takahashi and Yamanaka, 2006). The authors could also create iPS cells from human fibroblasts (Takahashi et al., 2007). These cells are similar to ES cells, but do not require the destruction of an embryo for their generation. Other groups have improved this protocol to exclude the oncogenic c-myc gene (Yu et al., 2007), and without the use of retrovirus (Kaji et al., 2009), successfully generating pluripotent iPS cells.

Stem cells exist in many mature adult organs in the mammal, including the brain. Stem cells have been identified in other tissues such as muscle, kidney, heart, gut, blood and skin. Hematopoietic cells normally give rise to mature blood cells in the adult, and are positive for markers such as CD34, c-kit and CD133, but not mature myeloid, lymphoid or erythrocyte markers. They can be isolated from the bone marrow, peripheral blood or enriched in umbilical cord blood. Mesenchymal stem cells give rise to cell types of the mesenchyme, including bone, cartilege, muscle, and fat. They are also derived from the bone marrow, and are defined as the adherent fibroblast population of white blood cells from the bone marrow, capable of differentiating into mesenchymal cell lineages.

2.2. Neural stem cells and neurogenesis

This thesis investigates the activity of neural stem and progenitor cells (NPC) after cerebral ischaemia, and what follows is an overview of NPC biology in the adult brain. Neural stem cells (NSC) are multipotential stem cells with the capacity for unlimited cell division, but whose progeny are restricted to producing cells of neural lineage: astrocytes, oligodendrocytes and neurons. Neurogenesis is the process of generating new neurons, from the cell division of stem or progenitor cells, to commitment to a neural lineage, the migration and differentiation of the newborn cells, and functional integration into CNS pathways.

NSC exist in the developing embryo and give rise to the majority of cell types in the CNS. More recently, newborn neurons have been identified in the adult mammalian brain, raising the question of the persistence of NSC in the adult CNS. Neurogenic regions have been identified in the subventricular zone of the lateral ventricles and the subgranular zone of the hippocampus (Merkle and varez-Buylla, 2006; varez-Buylla and Garcia-Verdugo, 2002; varez-Buylla and Lim, 2004; Gage,

2000). Cells originating from these regions contribute to cell replacement in the olfactory bulb and hippocampus, respectively (Lois and varez-Buylla, 1993; Merkle and varez-Buylla, 2006); (Gage et al., 1998; Gage et al., 1995). Cell division has also been reported in brain regions that are not normally neurogenic: the retina, spinal cord, olfactory bulbs, cerebellum, striatum and neocortex. Cells from the cortex, striatum, retina, and spinal cord have been shown to proliferate *in vitro*, and could be multipotent (Palmer et al., 1995; Palmer et al., 2000; Lledo et al., 2006a).

Postnatal neurogenesis was originally suggested by Hamilton in 1902, and again by Altman in the 1960s. In 1977 Kaplan and Hinds demonstrated that newborn neurons in the dentate gyrus can integrate into the hippocampal neural network (Kaplan and Hinds, 1977). The occurrence of neurogenesis begged the question of the presence of stem cells in the adult CNS. In the early 1990s, retroviral cell labelling and the development of bromodeoxyuridine facilitated cell tracing, and Reynolds and Weiss successfully isolated adult NSC (aNSC) from the adult mouse SVZ, and expanded and characterised these cells *in vitro* (Reynolds and Weiss, 1992; Morshead et al., 1994b). Adult neurogenesis has also been confirmed in primates (Pencea et al., 2001a) and humans (Bernier et al., 2000; Sgubin et al., 2007; Bedard and Parent, 2004).

The function of adult neurogenesis may be an adaptive response by the brain to changes in the external environment or the internal state of the animal.

Neurogenesis also occurs at the hippocampus, in the subgranular zone (SGZ) (Kaplan and Hinds, 1977). Newborn cells migrate into the granule cell layer of the dentate gyrus, where they differentiate into mature granule cell neurons and extend projections into the hippocampal region CA3 and receive synaptic input from the entorhinal cortex (van et al., 2002). Cell death in the granule cell layer occurs at the same rate as neurogenesis, which suggests a controlled feedback exists between the DG and SGZ (Gage, 2000).

2.3. Development of adult neural stem cells

Through lineage tracing studies, it has been suggested that the developmental origin of the SVZ, the main proliferative region in the adult mammalian CNS, is the neuroepithelium (Malatesta et al., 2003; Merkle et al., 2004; Noctor et al., 2002b). In the embryo, this sheet of cells committed to neural lineage folds to develop into the neural tube, creating a ventricular space in the centre, and a surrounding germinative ventricular zone (Bonfanti and Peretto, 2007a). Cell division occurs by nuclear translocation, where mitosis takes place at the ventricle, the nuclei migrate to the pial surface during interphase, and return to the ventricular surface during subsequent rounds of mitosis. NSC at the ventricle extend processes that contact the pial surface. Symmetrical cell division results in the generation of two stem cells and leads to an exponential increase in cells and growth. Asymmetrical cell division generates a daughter cell that migrates away from the ventricle into the CNS and differentiates into a mature cell (Merkle and varez-Buylla, 2006).

Radial glia appear in the ventricular zone of the embryonic CNS during cortical neurogenesis, and have been identified as the neural stem cells that give rise to the majority of cells in the embryonic forebrain (Malatesta et al., 2003; Noctor et al., 2002a; Merkle et al., 2004). Like neuroepithelial cells, they also have projections to the pial surface and contact the ventricle. During cortical neurogenesis, radial glia support the migration of newborn neurons by providing a scaffold for radial migration (Ghashghaei et al., 2007b). Following neurogenesis, radial glia generate astrocytes that migrate throughout the cortex (Merkle and varez-Buylla, 2006), and themselves differentiate into astrocytes postnatally (Figure 2.1.1.i). In addition, some radial glia persist into adulthood and give rise to the population of neural stem cells in the adult SVZ.

It has recently been reported that SVZ stem cells have a mixed developmental origin, with a population derived from the embryonic cortex and a population derived from the embryonic striatum (Young et al., 2007b; Willaime-Morawek and van der, 2008). Stem cells derived from embryonic cortex, expressing the Emx1 transcription factor, migrate ventrally and intermix with striatal stem cell population, expressing the Gsh2 transcription factor. In the adult, Emx1-derived NSC populate the dorsolateral corner of the SVZ, and Gsh2-derived stem cells reside in both the lateral wall and dorsolateral corner. The two populations contribute differentially to neurogenesis at the olfactory bulb, where Gsh2-derived NSC give rise to all calbindin-positive and the majority of tyrosine-hydroxylase-positive interneurons, whereas Emx1-derived NSC give rise to the majority of calretinin-positive interneurons (Young et al., 2007c). The contribution of these NSC populations to neurogenesis post-ischaemia is investigated further in Chapter 7.

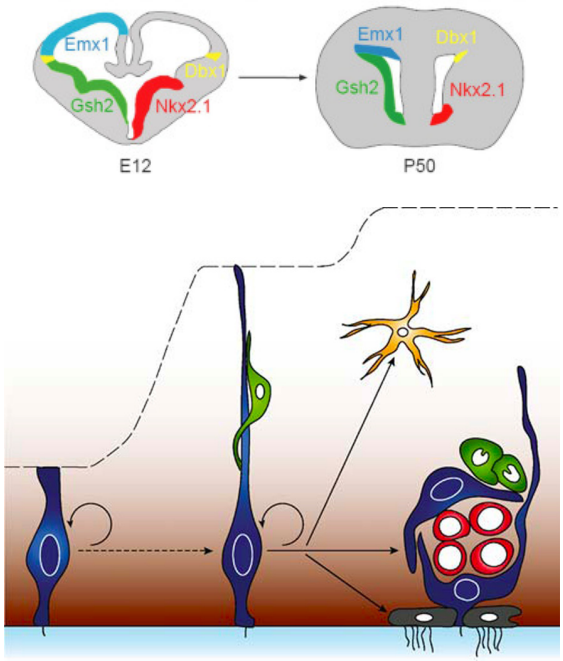

Figure 2.3.1 Development of adult neural stem cells (modified from Young *et al* (top) and Ihrie *et al* (bottom)). Top, transcription factor expression in the periventricular zone at embryonic stage 12, and anatomical localisation of adult SVZ stem cell populations derived from embryonic transcription factor regions. Bottom, neural crest neural stem cell (left); radial glial cell at embryonic stage 14

(middle), and adult subventricular zone (right). Blue, stem cell. Green, progenitor cell. Red, migrating neuroblast. Grey, ependymal cell. Yellow, astrocyte.

2.4. *SVZ anatomy*

The cytoarchitecture of the SVZ bears resemblance to the ventricular zone of the developing CNS, and is likely to originate from this structure. Cell types in the SVZ have been well characterised. GFAP-expressing astrocytes (type B cells) are neural stem cells that generate transit-amplifying progenitor cells (type C cells), which then generate postmitotic migrating neuroblasts (type A cells)(Fig 1.1.iii)(Merkle and varez-Buylla, 2006; Lim et al., 2007).

Doetsch *et al* identified the population of GFAP-positive(+) astrocytes (type B) as the stem cell pool in the SVZ (Doetsch et al., 1999a). These cells have several characteristics in common with radial glia of the developing cortex. Type B cells extend processes that contact the ventricle, and both they and radial glia express GFAP and the intermediate filament protein nestin (Doetsch, 2003f; Doetsch, 2003c). Type B astrocytes undergo asymmetrical cell division and generate daughter cells that are type C transit-amplifying cells (Doetsch, 2003b; Doetsch et al., 1999a). In the normal brain, this population is quiescent with a cell cycle of 15 days (Chiasson et al., 1999). Following ablation of rapidly-dividing cells in the SVZ by arabinofuranoside-C (Ara-C), type B cells are the only remaining proliferative cell type, and over the course of weeks the SVZ is repopulated with type C and type A cells (Doetsch et al., 1999a). Furthermore, genetic tagging of type B cells demonstrates that type C and type A cells are derived from type B stem cells (Doetsch et al., 1999a). While 12% of SVZ cells are GFAP+, only 1% of SVZ cells are capable of proliferating and generating neurospheres *in vitro* (Bonfanti and Peretto, 2007b). This suggests either that not all GFAP+ cells are stem cells, or that *in vitro* culture conditions are suboptimal for stem cell proliferation. Other markers expressed by SVZ NSC include nestin, vimentin, Sox2, Pax6 and CD133.

Type C progenitor cells are a fast-dividing population (Noctor et al., 2004) with a 12hr cell cycle (Chiasson et al., 1999). They express the markers Dlx2 and nestin, but not GFAP (Doetsch, 2003e). They also express the EGF receptor (EGFR) and may therefore be important in regulating the rate of proliferation in the SVZ (Doetsch, 2003a). Type C cells generate type A migrating neuroblasts. Type A cells express Dlx2, doublecortin (DCX), and polysialated neural cell adhesion molecule (PSA-NCAM)(Ming and Song, 2005). Neuroblasts migrate away from the SVZ, through the rostral migratory stream (RMS) to the olfactory bulb (OB), where they differentiate into granule cells and periglomerular inhibitory interneurons, over 90% of which are GABAergic (Ghashghaei et al., 2007c; Lledo et al., 2008). In the normal brain, 30 000 neuroblasts are generated per day in mice (Lledo et al., 2006b). Neuroblasts can migrate to the OB in 6 days and fully differentiate within 14 days from their birth (Lledo et al., 2006c).

Ependymal cells are derived from radial glia (Spassky et al., 2005), form a single layer of ciliated cells around the ventricle and express nestin, an early neural marker (Chiasson et al., 1999). Limited cell

division of this population *in vivo*, as well as limited expansion *in vitro* has been reported. However, ependymal cells are not multipotential and thus are not the source of stem cells in the SVZ (Chiasson et al., 1999). Ependymal cells may support neurogenesis in the SVZ through the expression of Noggin (Lim et al., 2000). Inhibition of the Noggin antagonist BMP4 increases the GFAP+ stem cell pool at the SVZ, and overexpression of BMP4 increases glial differentiation (Bonaguidi et al., 2005).

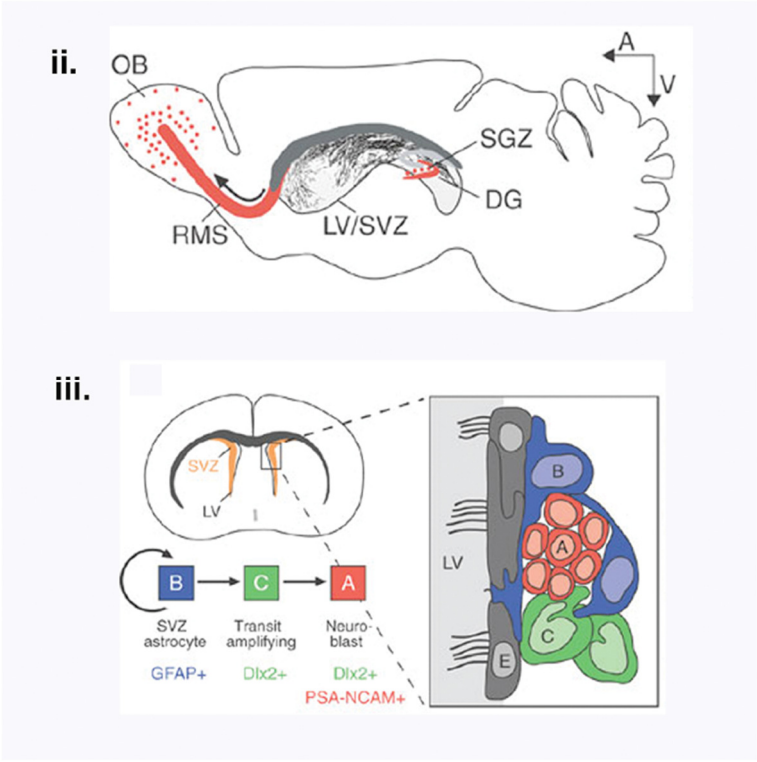

Figure 2.4.1 SVZ Anatomy. Top, sagittal section of rodent brain. Red areas denote regions of neurogenesis in the adult brain. LV, lateral ventricle. SVZ, subventricular zone. SGZ, subgranular zone. DG, dentate gyrus. RMS, rostral migratory stream. OB, olfactory bulb. Bottom, coronal section of the lateral ventricles (yellow), and SVZ cytoarchitecture (inset). B, GFAP+ SVZ stem cell astrocytes. C, transit-amplifying progenitor cells. A, migrating neuroblasts. E, ependymal cells.

2.5. *The subventricular zone niche*

The SVZ has a unique capacity for neurogenesis in the adult CNS and has been identified as a neurogenic niche (Merkle and varez-Buylla, 2006; Lim et al., 2007; Gage, 2000). This begs the question whether there is a unique population of cells in the SVZ capable of neurogenesis, or whether the environment is uniquely permissive for neurogenesis? It is likely that the answer is both, however there is strong evidence that the cytoarchitecture and extracellular environment of the SVZ play a critical role in enabling neurogenesis (Palmer et al., 2000; Palmer et al., 1995; Palmer et al., 1999b; Song et al., 2002), as SVZ-derived aNSC transplanted into non-neurogenic regions in the adult CNS are gliogenic and incapable of neurogenesis (Gage et al., 1995).

The cytoarchitecture of the SVZ bears resemblance to the neurogenic ventricular zone of the

developing CNS, and originates from this structure developmentally. The mammalian SVZ may represent a developmental artefact persisting into adulthood, with a quiescent population of neural stem cells of embryonic origin. In avians and reptiles, the ventricular zone persists into adulthood, and ventricular radial glia are capable of neurogenesis throughout adult life (Lindsey and Tropepe, 2006).

These neural stem cells (B cells) have been identified as being GFAP-expressing astrocytes (Doetsch et al., 1999a). Astrocytes in non-neurogenic regions can proliferate and generate new glia in the normal brain (Doetsch, 2003), and express SSEA-1, an early embryonic marker of cell proliferation (Doetsch, 2003). *In vitro*, astrocytes proliferate when exposed to growth factors. It is possible that the SVZ provides a permissive environment for astrocytes, which are capable of proliferation and gliogenesis in other brain regions, to undergo neurogenesis, rather than there being a subpopulation of astrocytes unique to the SVZ.

The non-NSC astrocytes in the SVZ may enable neurogenesis through the expression of developmental genes and maintenance of a germinal niche. Some astrocytes span the SVZ and are in contact with both the CSF and vasculature, suggesting that they modulate neurogenesis by monitoring these environments. Wnt signalling by astrocytes promotes neuronal fate specification of NSC *in vitro* and *in vivo* (Lledo, 2006). Sonic hedgehog (Shh) is secreted by SVZ astrocytes, and stimulates NSC proliferation (Jiao and Chen, 2008). Application of exogenous Shh induces neurogenesis in the normally non-neurogenic cortex (Jiao and Chen, 2008). Astrocytes derived from the SVZ increase neurogenesis in cultured aNSC *in vitro*, whereas astrocytes derived from spinal cord do not (Doetsch, 2003).

Some studies have found that ependymal cells are capable of cell proliferation, and suggest that this cell type may be a candidate neural stem cell in the SVZ. Johansson et al demonstrated that ependymal cells labeled with intraventricularly-injected DiI contributed to neurogenesis at the olfactory bulb (Johansson et al, 1999). The authors also demonstrated that the DiI+ ependymal cells could generate neurospheres in vitro. Some GFAP+ NSC are known to contact the ventricular surface, and may have incorporated the DiI label as well. Other studies have found that ependymal cells express the stem cell marker CD133, and demonstrate that CD133+ cells contribute to neurogenesis at the OB and can generate neurospheres (Coskun et al, 2008). However in this study the authors used CD133 and not an ependymal-specific marker, and other studies have found that CD133 is expressed in GFAP+ NSC (Mirzadeh et al, 2008). Other studies indicate that ependymal cells cannot generate neurospheres indefinitely, and that ependymal-derived neurospheres do not differentiate into neurons, oligodendrocytes and glia (Chiasson et al, 1999). Spassky et al did not find evidence of ependymal cell proliferation in the adult brain (Spassky et al, 2005). Not all ependymal or GFAP+ cells are SVZ NSC. Ependymal cells and GFAP+ NSC are both derived from radial glia developmentally, and SVZ NSC share many properties with radial glial cells. There is also evidence that ependymal cells respond to cerebral ischaemia injury by proliferation (Zhang et al, 2007).

A 'vascular plexus' exists at the SVZ, where blood vessels are in close association with astrocytes and neuroblasts (Shen et al., 2008). The blood brain barrier is partially open at the SVZ, where regions of vasculature do not have astrocytic endfeet and small molecules (<400 Da) can enter the brain (Tavazoie et al., 2008). This has led to the theory of a neurovascular niche that promotes neurogenesis in the SVZ (Palmer et al., 2000); (Lim et al., 2007). Endothelial cells promote neurogenesis in SVZ-derived aNSC *in vitro* (Lledo et al., 2006d). Endothelial cells secrete growth factors important for neurogenesis including fibroblast growth factor-2 (FGF-2), epidermal growth factor (EGF), vascular endothelial growth factor (VEGF), brain-derived neurotrophic factor (BDNF), and p-derived growth factor (PDGF)(Doetsch, 2003i).

A similar vasculature exists in the RMS, where blood vessels are oriented in parallel to the migratory neuroblasts (Shen et al., 2008), and the RMS may also be a neurogenic niche (Mendoza-Torreblanca 2008). Astrocytes in the RMS have been shown to proliferate, migrate and differentiate into olfactory bulb granule and periglomerular interneurons (Alonso et al., 2008).

The extracellular matrix (ECM) proteins in the SVZ and surrounding blood vessels can activate, cleave, and sequester signalling molecules and thus play a role in regulating neurogenesis. Progenitor cells and migrating neuroblasts express the laminin receptor ab1-integrin and interact with ECM proteins including tenascin C and laminin (Ghashghaei et al., 2007d). Blocking $\alpha\beta$1-integrin inhibits NSC adherence to endothelial cells, and reduces cell proliferation, demonstrating the effect of the ECM and vasculature on SVZ neurogenesis (Shen et al., 2008). Tenascin C is implicated in niche maintenance through control of growth factor signalling and EGFR expression, and the modulation of sensitivity to growth factors(Garcion et al., 2004). Heparin sulphate proteoglycans (HSPG) bind to growth factors and migratory guidance cues such as the slit proteins (Ghashghaei et al., 2007e), and thus play an integral role in regulating cell proliferation and migration.

The ECM environment outside of the SVZ may be anti-neurogenic. The oligodendrocyte transcription factor and marker Olig2 may be a repressor of neurogenesis, and blocking Olig2 expression has been shown to enhance neurogenesis following injury (Buffo et al., 2005). Ephrin-A2 and A3 is expressed in astrocytes outside of SVZ niche, and is inhibitory to neurogenesis. In Ephrin-A2 and -A3 knock out transgenic mice, neurogenesis occurs throughout the CNS (Jiao et al., 2008).

2.6. Neuroblast migration

Neuroblast migration to the olfactory bulb (OB) is investigated in Chapter 6. Migration along the RMS occurs within 2 weeks of neuroblast generation at the SVZ, and differentiation at the olfactory bulb between 15-45 days (Petreanu and varez-Buylla, 2002). Using ^{3}H-thymidine labelling of newborn neuroblasts, the authors also observed a decrease of 50% of newborn neurons in the olfactory bulb at 15-45 days, suggesting that apoptosis occurs at the differentiation phase.

Type A cells orient themselves away from the SVZ, forming a leading process. Chains of neuroblasts

migrate within a glial tube through the RMS (Figure 2.4.1)(Lois et al., 1996; Lois and varez-Buylla, 1994). While neuroblasts are primarily postmitotic, they are capable of proliferation when in contact with astrocytes in the glial tube (Gritti et al., 2002).

DCX is a microtubule-associated protein required for migration along the RMS. Mutation in the DCX gene results in slow migration, but does not affect the orientation of neuroblasts or their responsiveness to cues (Kappeler et al., 2006). Deletion of DCX does not result in abnormal migration to the OB, suggesting that there may be some functional redundancy of structural proteins involved in migration (Ocbina et al., 2006). DCX deletion does result in morphologic defects in neuroblasts and delayed migration through the RMS (Koizumi et al., 2006). PSA-NCAM regulates the organisation of chain migration and contact between neuroblasts (Ghashghaei et al., 2007). Deletion of the PSA-NCAM gene decreases the size of the OB through a decrease in cell replacement by neuroblasts (Gage, 2000b). In PSA-NCAM-mutant mice, odor discrimination but not odor detection was disrupted, indicating a functional role for neurogenesis at the OB (Gheusi et al., 2000).

Repulsive and attractive guidance cues are likely to influence neuroblast migration. Removal of the OB does not alter neuroblast migration (Kirschenbaum et al., 1999), therefore attractive cues from the OB are not the primary driving force for migration. Neurogenesis is not reduced or disrupted in anosmic mice (Petreanu and varez-Buylla, 2002). However, other studies have demonstrated that odor-enriched environments increase neurogenesis exclusively at the olfactory bulb, suggesting that cues from the olfactory bulb may be important in neurogenesis regulation (Rochefort et al., 2002).

The long-distance repulsive cue Slit is expressed in the septum, striatum, choroid plexus and in type C cells (Ghashghaei et al., 2007f; Abrous et al., 2005), and regulate the motility and directionality of neuroblast migration (Ming and Song, 2005); (Zhao et al., 2008). Long distance gradients of repulsive cues such as Slits are created by directional CSF flow generated by the movement of ciliary epithelium in the lateral ventricles (Sawamoto et al., 2006). Heparin sulphate proteoglycans in the ECM can modulate the Slit signal (Ghashghaei et al., 2007a). Neuroblasts express the Slit receptor ROBO and the netrin receptor DCC.

The astroglial tube surrounding the RMS is a source of local repulsive cues and creates short distance gradients (Ghashghaei et al., 2007h). Neuroblasts express integrins on their cell membranes that interact with ECM proteins and receptors for migration guidance cues in the SVZ and RMS (Lledo et al., 2006e). Other cues implicated in neuroblast migration are the ephrins/Ephs(Conover et al., 2000), GABA, and netrin (Ghashghaei et al., 2007i). At the OB, reelin causes neuroblasts to exit the RMS, re-orient their direction of migration, and migrate into OB granule cell layers where they differentiate(Ghashghaei et al., 2007; (Gong et al., 2007).

2.7. *Control of neurogenesis and the potential of NSC*

Various growth factors and neurotransmitters regulate neurogenesis. FGF-2 is secreted by astrocytes and endothelial cells in the SVZ (Hagg, 2005), and exogenous FGF-2 increases neurogenesis and the number of type B stem cells (Wagner et al., 1999; Kuhn et al., 1997). Infusion of EGF into the lateral ventricles increases cell proliferation in the SVZ (Kuhn et al., 1997; Doetsch et al., 2002), and infusion of EGF into the 4th ventricle stimulates neurogenesis in the normally non-proliferative subventricular zone (Martens et al., 2002). VEGF induces neurogenesis and angiogenesis in the CNS, and can stimulate the release of BNDF (Hagg, 2005). BDNF promotes neuroblast survival and increases neurogenesis (Hagg, 2005). TGFα is a ligand of EGFR and increases neurogenesis (Hagg, 2005). Type C transit-amplifying cells express growth factor receptors, NMDA receptors sensitive to glutamate and electrical activity, and Ca^{2+} channels. Extrasynaptic GABA levels affect both proliferation and the rate of migration in the RMS (Lledo et al., 2006f).

Developmental transcription factors are also implicated in neurogenesis. Noggin is expressed in ependymal cells (Ming and Song, 2005), and astrocytes in the SVZ express neurogenesin and wnt. Other developmental factors associated with neurogenesis are sonic hedgehog (Ahn and Joyner, 2005), bone morphogenic protein-4, notch1, pax6, and mash1 (Lledo et al., 2006a).

Several environmental factors have been shown to influence neurogesis. Positive modulators include an odor-enriched environment, exercise, learning, and caloric restriction of diet (van et al., 1999; Gould et al., 1999; Gould et al., 1997; Mirescu et al., 2004; Lichtenwalner and Parent, 2006; Komitova et al., 2005; Naylor et al., 2005a; Lee et al., 2002; Hauser et al., 2000; Raber et al., 2004; Ekdahl et al., 2003; Lindqvist et al., 2006). Negative modulators include stress, depression, drug or alcohol abuse, a high fat diet, diabetes, inflammation and irradiation (Herrera et al., 2003; Gould et al., 1997; Malberg et al., 2000; Dranovsky and Hen, 2006; Powrozek et al., 2004; Mirescu et al., 2004; Beauquis et al., 2006).

The potential of aNSC can be examined in vitro using cell culture systems. aNSC are isolated from the SVZ, mechanically and chemically dissociated, and cultured in a defined medium that supports the survival and proliferation of neural stem cells but not other cell types, or that induces the differentiation of neural stem cells (Reynolds et al., 1992; Vescovi et al., 1993).This population is enhanced and enriched over subsequent passages. The SVZ stem cell population is capable of proliferation, and can differentiate into all neural lineages. Clonal analysis through lineage tagging with a genetic marker establishes that a subset of differentiated cells are derived from a single, original stem cell (Morshead et al., 1994a). Together, these techniques establish the potential of aNSC to proliferate and differentiate. These in vitro techniques are applied to assess the effects of MRI contrast agents on NPC behaviour in Chapter 4.

Transplantation studies can demonstrate the potential of NSC *in vivo*. Embryonic NSC transplanted into embryonic CNS migrate extensively and follow endogenous migratory routes (Brustle et al., 1997; Brustle et al., 1998). Similarly, embryonic NSC transplanted into the adult CNS migrate and

differentiate into all neural cell types (Wichterle et al., 1999). Adult NSC transplanted into embryonic CNS have limited potential and do not migrate extensively (Lim et al., 1997). Adult NSC transplanted into non-neurogenic regions of the adult CNS are gliogenic and do not generate neurons (Gage et al., 1995; Seidenfaden et al., 2006), and adult NSC transplanted into the SVZ or SGZ follow normal migratory routes and differentiate appropriately (Herrera et al., 1999; Suhonen et al., 1996). -derived NSC can also differentiate into cerebellar interneurons after cerebellar transplantation, which indicates that their neurogenic capacity is not restricted to the SVZ (Milosevic et al., 2008). These studies suggest that adult NSC are more committed and lineage-restricted than embryonic NSC, but also emphasize the role of the neurogenic niche in determining neurogenic potential.

2.8. Oligodendrocyte precursor cells

Oligodendrocyte precursor cells (OLPs) represent an additional population of proliferating cells in the adult brain, and are known to proliferate throughout adult life. We investigate the fate of OLPs following ischaemia, alongside the fate of NPC, in Chapter 7, and an overview of OLP biology is summarised below. The majority of mature oligodendrocytes are generated from OLPs between postnatal day 7 and 14. The developmental origin of OLPs is in the ventricular zone of the developing brain, but they migrate and are distributed throughout all regions of the brain, including white matter, the cortex and striatum, by postnatal stages.

Following the postnatal burst of oligodendrocyte production, a population of OLPs persists into adulthood (Wolswijk and Noble, 1989). OLPs coexpress platelet-derived growth factor receptor alpha (PDGFRα) and NG2 proteoglycan (Nishiyama et al., 1997). PDGF is a chemoattractant for OLPs *in vitro* and *in vivo* (Noble et al., 1988; Zhang et al., 2004a), and PDGFRα expression in OLPs is required for proliferation and differentiation (Woodruff et al., 2004; Pringle et al., 1992; Richardson et al., 1988). PDGF has been shown to maintain OLP cell cycling (Bogler et al., 1990). Loss of PDGF results in loss of PDGFRα+ OLPs and hypomyelination (Fruttiger et al., 1999). PDGFRα expression can lead to neural tube defects, gliomas and hypomyelination (Fruttiger et al., 1999; Li et al., 1996; Payne et al., 1997).NG2 can also be expressed in vascular smooth muscle cells (Ozerdem et al., 2001), and blood-borne macrophage (Dawson et al., 2000; Bu et al., 2001). Other lineage markers – transcription factors SOX10 and Olig2 – are expressed all cells of oligodrendroglial lineage, including both OLPs and oligodendrocytes.

OLPs contribute to mature oligodendrocyte generation and myelination (Bu et al., 2004; Franklin et al., 1997; Zhu et al., 2008). Upon differentiation, OLPs downregulate PDGFRα and NG2 proteoglycan, upregulate myelin and myelinate axons (McTigue and Tripathi, 2008). The number of oligodendrocytes in the brain is determined by the number of axons. During development, more oligodendrocytes are generated than required. Those that are not in contact with axons undergo apoptosis within 2-3 days, due to lack of survival cues from axons (Barres et al., 1992; Raff et al., 1993).

In vitro, adult OLPs can differentiate into oligodendrocytes and astrocytes (Wren et al., 1992; Engel and Wolswijk, 1996; Yoo and Wrathall, 2007). *In vivo*, OLPs do not contribute to astrogliogenesis in the normal brain (Groves et al., 1993), but when transplanted into a glia-depleted environment are capable of differentiation into both oligodendrocytes and astrocytes (Franklin et al., 1997). OLPs have also been shown to differentiate into astrocytes *in vivo* after injury (Alonso, 2005).

NG2+ OLPs may also receive synaptic input, and can form synapse-like connections with neurons. OLPs express AMPA, NMDA and GABA receptors (Bergles et al., 2000), and AMPA-mediated currents have been described in OLPs (Kukley et al., 2007; Ziskin et al., 2007), as well as electrophysiological action potential-like 'spiking' (Karadottir et al., 2008). This OLP responsiveness to synaptic activity results in activity-dependent intracellular signaling pathway activation, which may be involved in the regulation of OLP proliferation, differentiation and migration (Nishiyama et al., 2009). OLPs may be vulnerable to excitotoxicity due to their expression of glutamate receptors.

It has recently been reported that OLPs can also generate forebrain neurons in the normal adult brain in the piriform cortex (Rivers et al., 2008), and postnatal OLPs can generate neurons *in vitro* (Kondo and Raff, 2000; Belachew et al., 2003; Aguirre and Gallo, 2004). can also differentiate into neurons when grafted into neurogenic brain regions (Windrem et al., 2004). the normal brain, OLP contribution to projection neurons in the piriform cortex was found to be approximately 1.4%, however the function of these cells is unknown (Rivers et al., 2008).

Following an injury involving demyelination, such as EAE, remyelination can occur and is mediated by OLPs (Nishiyama, 1998; Nishiyama, 2007). OLPs respond to injury through proliferation, differentiation and remyelination (Levine and Reynolds, 1999). NG2+ cells may be a diverse heterogeneous population, as only a subset respond to cerebral injury (McTigue and Tripathi, 2008).

2.9. Neurogenesis and cerebral ischaemia

2.9.1. Cell proliferation at the subventricular zone

Expansion of the SVZ and neural stem cell proliferation ipsilateral to the lesion has been reported following cerebral ischaemia in several rodent models (Parent et al., 2002; Arvidsson et al., 2002; Kokaia et al., 2006; Jin et al., 2001; Dempsey et al., 2003; Yan et al., 2006). Neurogenesis has also been reported following human stroke (Minger et al., 2007; Sgubin et al., 2007).

Cell proliferation, as well as proliferation rate, increases within 24 hours of the initial insult, peaks at 7 days(Zhang et al., 2004c; Zhang et al., 2004b), decreases by 2-4 weeks (Takasawa et al., 2002; Dempsey et al., 2003; Zhu et al., 2003), but remains elevated relative to contralateral and baseline non-ischaemic SVZ for several weeks and up to a year post-ischaemia (Thored et al., 2006). Even a short period of ischaemia (15 minutes) is sufficient to increase neurogenesis at the SVZ, without causing inflammation or infarction (Naylor et al., 2005b).

SVZ isolated from the ischaemic hemisphere generate more neurospheres than non-ischaemic SVZ (Zhang et al., 2004b). Furthermore, the same result is obtained following Ara-C ablation of type C

cells, suggesting that proliferation predominantly occurs from the stem cell pool following ischaemia. Asymmetric cell division increases from 40% in normal SVZ to 60% in ischaemic SVZ, reflecting an increase in proliferation in type B cells and expansion of the SVZ (Zhang et al., 2004c). Ependymal cell early proliferation, upregulation of CD133, and de-differentiation into radial glia-like cells has also been reported (Zhang et al., 2007a; Coskun et al., 2008; Carlen et al., 2009).

2.9.2. Factors influencing neurogenesis post-stroke

A mechanism of early neural stem cell response to ischaemia may be glutamate sensitivity. Blocking NMDA receptors in the SVZ blocks an increase in neurogenesis following ischaemia, indicating a role for glutamate excitotoxicity in early activation of SVZ neural stem cells (Arvidsson et al., 2001).

Growth factors also modulate neurogenesis post-ischaema. A number of experimental methods have been used to investigate the action of growth factors on neural stem cells. The effect of application of exogenous growth factors on neurogenesis can be assessed *in vitro* and *in vivo* after ischaemia. Growth factor expression can be upregulated locally by adenoviral transduction after ischaemia, or by overexpression in a transgenic mouse model.

FGF-2 is known to influence the neural stem cell popultation in the normal brain (Kuhn et al., 1997), and is implicated in the neurogenic response after ischaemia. FGF-2 is upregulated at the SVZ following ischaemia for up to 14 days (Endoh et al., 1994; Yoshimura et al., 2001), coinciding with peak SVZ expansion and enhancing neurogenesis (Leker et al., 2007; Yoshimura et al., 2001). Overexpression of FGF-2 enhances the neurogenic response after ischaemia by increasing SVZ cell proliferation and migration (Dayer et al., 2007). Gene profiling changes at 7 days post-ischaemia show upregulation of the FGF family genes and the FGF receptor 1 (as well as members of the Sox family genes; integrins; MMP-2; Hif-1α; Notch signalling genes; Bmp4 and TGF-β superfamily genes) (Liu et al., 2007a). Exogenous FGF-2 has been shown to enhance NPC proliferation (Ay et al., 2001). Intranasal administration of FGF-2 from 2 hours post-ischaemia has been shown to improve neurological function and reduce infarct volume (Ma et al., 2008).

Insulin-like growth factor-1 (IGF-1) promotes NPC proliferation in the presence of FGF-2, and neuronal differentiation in the absence of FGF-2 (Kalluri et al., 2007; Camarero et al., 2003; Otaegi et al., 2006). The IGF-1 receptor is expressed on SVZ NSC (Yan 2006). IGF-1 is also upregulated after ischaemic injury in the penumbra (Yan et al., 2006), and is associated with neuronal and oligodendroglial differentiation (Hsieh et al., 2004; McCurdy et al., 2005; Yan et al., 2006). Inhibition of IGF-1 by intraventricular infusion of IGF-1 antibody inhibits cell proliferation at the SVZ (Yan et al., 2006).

The growth factor EGF can inflence the rapid amplification of cells by neural progenitor cells. Heparin-binding EGF (HB-EGF) is upregulated after ischaemia (Tanaka et al., 1999; Yan et al., 2006), and the EGF receptor (EGFR) is upregulated in neural progenitor cells after ischaemia (Ninomiya et al., 2006). HB-EGF has been shown to increase neural stem cell proliferation *in vitro*

(Jin et al., 2005), and injection of a HB-EGF adenovirus increases progenitor cell proliferation post-ischaemia (Sugiura et al., 2005). FGF-2 and EGF intraventricular infusions demonstrated an increased cell replacement in the striatum following ischaemia (Tureyen et al., 2005).

BDNF and GDNF upregulation has been reported following ischaemia, and increase neurogenesis (Takami et al., 1992; Kokaia et al., 1995; Kitagawa et al., 1999). BDNF adenoviral injection into the lateral ventricle results in increased neurogenesis, differentiation and functional integration into damaged tissue (Benraiss et al., 2001). A similar result was achieved with BDNF infusion after ischaemia (Hazell, 2007). GDNF has been shown to protect against neurotoxicity (Wong et al., 2005) and provide trophic support to cells locally (Kobayashi et al., 2006).

Erythropoeitin (EPO) and VEGF expression are regulated by the transcription factor hypoxia-inducible factor-1 (HIF-1). HIF-1, EPO and VEGF are all upregulated after ischaemia (Jiang et al., 2001; Hayashi et al., 1997). Erythropoeitin treatment increases neurogenesis after stroke (Jin et al., 2002; Wang et al., 2004), and proliferation in the SVZ is reduced in EPO knock-out transgenic mice (Tsai et al., 2006) Exogenous EPO infusion has been shown to increase neuroblast migration towards ischaemia and proliferation at the SVZ (Shingo et al., 2001). EPO has been shown to be protective after ischaemia, and its therapeutic effects is being trialled in the clinic (Ehrenreich et al., 2002). VEGF increases neurogenesis *in vitro* and *in vivo* (Jin et al., 2002), and mice overexpressing VEGF show increased neurogenesis after ischaemia (Wang et al., 2007b). Roitbak *et al* demonstrated that the neuroprotective effect of VEGF was mediated via HIF-1α and VEGF (Roitbak et al., 2008). VEGF and the VEGF receptor 2/Flk-1 are expressed in adult NSC, and VEGF has been shown to promote neurogenesis *in vitro*, though not through increasing cell proliferation (Schanzer et al., 2004).

BrdU studies also demonstrate an increase in neurogenesis in the striatum and cortex, normally non-neurogenic brain regions, following ischaemia (Parent et al., 2002; Arvidsson et al., 2002). Cells from the SVZ may migrate into the striatum or cortex and differentiate into neurons, or cerebral ischaemia may activate a quiescent population of cells with proliferative capacity in the striatum and cortex to undergo neurogenesis. The origin of post-ischaemic neurogenesis is investigated further in Chapter 7.

2.9.3. Migration of neuroblasts in response to ischaemia

Neuroblast migration into the infarcted region has also been reported following cerebral ischaemia, from 24 hours to 16 weeks post-ischaemia (Kokaia et al., 2006). We investigate NPC subpopulations associated with post-ishaemic neurblast migration in Chapter 7. Neuroblasts exit the RMS and migrate into the striatum towards the ischaemic infarct (Arvidsson et al., 2002). Lateral migration into the striatum from the SVZ has also been observed, with chains of DCX+ cells migrating out of the SVZ, in close proximity to astrocytes and blood vessels (Parent et al., 2002c), toward the ischaemic infarct (Magavi et al., 2000; Hicks et al., 2008; Wang et al., 2007b; Thored et al., 2006; Thored et al., 2007). Most DCX+ cells colabel with BrdU (Kokaia et al., 2006), suggesting that they are generated post-ischaemia.

The origin of migrating DCX+ cells following ischaemia is thought to be the progeny of SVZ neural progenitor cells, and the identification of DiI+ DCX+ migrating neuroblasts in tracing studies after ventricular DiI infusion supports the SVZ origin (Jin et al., 2003) In the non-ischaemic SVZ, DCX+ cells co-express neural progenitor markers Sox2 and Nestin, but co-express the mature interneuron marker tyrosine hydroxlase following ischaemia, suggesting that they become committed to neuronal differentiation (Hou et al., 2008; Lai et al., 2008). However other studies have suggested that the DCX+ cells may originate from local progenitor cells. Hua et al observed DiI+ cells in the olfactory bulb and rostral migratory stream after intraventricular DiI injection in ischaemic mice, but did not observe DiI in DCX+ cells at the ischaemic lesion (Hua et al., 2008). The authors suggest that a local progenitor cell can give rise to neuroblasts and contribute to neurogenesis. In a similar study, DiI was injected intraventricularly in the nestin-EGFP transgenic mouse, and the authors report that only a subset of GFP+DCX+ neuroblasts was DiI+ (Burns et al., 2007) Cell labelling and longitudinal tracking of cell migration following ischaemia would help to elucidate the origin of DCX+ cells in the ischaemic brain, and a method of endogenously labelling and imaging SVZ NPC with MRI contrast agent for this purpose is developed in Chapter 6.

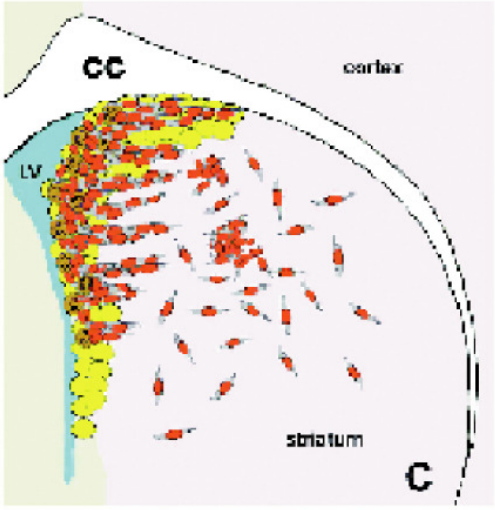

Figure 2.9.3.1 Neuroblast migration following cerebral ischaemia (from Chopp et al, 2005). LV, lateral ventricle. CC, corpus callosum. Yellow, neural stem can progenitor cells. Red, migrating neuroblasts.

It is likely that multiple attractive cues together with a permissive ECM environment contribute to neuroblast migration. The matrix metalloproteinase MMP-9 may be involved in the neurogenic response (Fowlkes et al., 2004; Karagiannis and Popel, 2006; Lee et al., 2006; Son et al., 2006). It is increased in the SVZ at 7-14 days post-ischaemia, where it co-localises with DCX (Zhao et al., 2006). Inhibition of MMPs reduces DCX migration from the SVZ following ischaemia (Lee et al., 2006; Wang et al., 2006; Zhao et al., 2006), and upregulation of MMP-9 has also been shown to promote migration MMPs are involved in ECM remodelling and may create an ECM environment that is permissive to neuroblast migration. MMPs may also promote neurogenesis by cleaving pro-growth

factor proteins and releasing proliferation or migration cues from the ECM. MMP-9 has been shown to cleave ECM matrix-bound signalling molecules such as VEGF (Zhao et al., 2007)and IGF-1 (Zhao et al., 2007), growth factors which promote neurogenesis.

The chemokine stromal cell-derived factor-1α (SDF-1α) may mediate neuroblast migration after ischaemia (Ohab et al., 2006). It is also regulated by the transcription factor HIF-1 (Chang et al., 2007), is expressed during development and is important in neuronal migration (Lazarini et al., 2003; McGrath et al., 1999). Its normal function in the adult is as a chemoattractant, to recruit bone marrow cells expressing the CXCR-4 receptor into the circulation (Dar et al., 2006). SDF1α is expressed in endothelial cells in the brain (Stumm et al., 2002), and reactive astrocytes in the ipsilateral striatum up to four weeks post-ischaemia (Imitola et al., 2004). receptor for SDF-1α – CXCR4 – is expressed in SVZ progenitor cells (Ni et al., 2004; Thored et al., 2006), and SDF1α-CXCR4 signalling is implicated in neural progenitor cell proliferation and migration (Imitola et al., 2004). SVZ-derived neurospheres migrate towards a gradient of SDF-1α *in vitro*. Pharmacological inhibition of SDF-1α prevents migration *in vitro* and *in vivo* in response to cerebral ischaemia (Kokaia et al., 2006; Robin et al., 2006). SDF1α administration promotes neuroprotection and angiogenesis after ischaemia (Shyu et al., 2008). Overexpression of CXCR4 receptor in neural progenitors in the SVZ causes a decrease in neurogenesis in the absence of SDF1α, and increased neurogenesis after application of exogenous SDF1α (Liu et al., 2008).

2.9.4. Differentiation of neuroblasts in response to cerebral ischaemia

Newborn, BrdU+ neurons in the striatum differentiate into regionally appropriate neurons, expressing markers for early – Meis2 and Pbx – and mature – DARPP-32 – striatal medium spiny neurons (Arvidsson et al., 2002), or calbindin-positive interneurons (Jin et al., 2003), and several studies have confirmed neuronal differentiation of newly generated cells in the striatum after an ischaemic even (Yamashita et al., 2006; Parent et al., 2002). 4 weeks after ischaemia, newborn cells develop polarity, form dendrites and receive excitatory and inhibitory synaptic input, and are themselves electrophyisiologically active and capable of generating action potentials (Hou et al., 2008). These cells express mature neuronal markers such as NeuN, MAP-2, synapsin 1, the GABAergic neuronal marker glutamic acid decarboxylase, and the cholinergic neuronal marker choline acetyltransferase (Hou et al., 2008).

While newborn neurons are capable of differentiation into the correct phenotype, the majority die within 2 to 5 weeks post-ischaemia. Aarvidsson *et al* estimate that neuronal replacement after ischaemia by neurogenesis is 0.2% of total cell loss (Arvidsson et al., 2002). This may be due to an increasingly inhibitory environment as the ischaemic lesion progresses, scar tissue forms, and the inflammatory profile changes. Neurogenesis and cell survival can be increased after ischaemia by treatment with FGF-2 (Ay et al., 2001; Dayer et al., 2007).

2.10. *Inflammation, microglia and neurogenesis*

Microglia and the peripheral immune system can also be mediators of neurogenesis. In the normal brain, microglia depletion decreases neurogenesis (Ziv et al., 2006), and SVZ extracts co-cultured with microglia increase neurogenesis (Aarum et al., 2003; Walton et al., 2006). In the hippocampus, environmental enrichment increases neurogenesis and recruits microglia to the dentate gyrus. Decreased neurogenesis is observed in immunodefficient SCID (severe combined immunodefficient) mice, and no increase in neurogenesis is observed following environmental enrichment. This effect can be rescued with bone marrow replenishment (Ziv et al., 2006). These results suggest that microglia may be required for neurogenesis. Furthermore, in Boyden chamber migration assays, there is an increase in directional migration of adult NSC towards microglia (Aarum et al., 2003), which suggests a soluble factor released from microglia may be involved in the regulation of neurogenesis (Nakanishi et al., 2007; Morgan et al., 2004).

However, overactivated microglia may have a negative effect on neurogenesis. Chronic inflammation can inhibit neurogenesis (Ekdahl et al., 2003; Monje et al., 2003). Inhibition of activated microglia by minocycline increases neurogenesis *in vivo* (Liu et al., 2007b). *In vitro*, exposure to the cytokine IL-4 causes microglial activation, whereas exposure to bacterial endotoxin causes microglial overactivation. Exposure of microglia to the former increases neurogenesis in co-culture, while exposure to the latter decreases neurogenesis (Butovsky et al., 2006). Together, this data suggests that a moderate inflammatory environment is optimal for neurogenesis and NPC migration after ischaemia. Conditioned media from bacterial endotoxin-treated microglia can also decrease neural stem cell survival *in vitro*, suggesting a soluble factor secreted by microglia mediates this response (Cacci et al., 2008).

IL-6 is one candidate factor – IL-6 decreases neurogenesis *in vitro*, and overexpression of IL-6 in astrocytes *in vivo* also decreases neurogenesis (Vallieres et al., 2002). The pro-inflammatory cytokine TNFα may also be a negative mediator of neurogenesis. It is normally upregulated after ischaemia (Ekdahl et al., 2009), and is expressed in microglia (Gregersen et al., 2000). Low levels of TNFα increase proliferation and neuronal differentiation of NPC *in vitro* via the TNFα receptor 1, whereas high levels of TNFα initiate apoptosis in NPC (Bernardino et al., 2008). Pharmacological inhibition of TNFα decreases neurogenesis after ischaemia (Heldmann et al., 2005). Iosif *et al* also demonstrated that the TNFα receptor 1 is expressed in SVZ nestin-expressing progenitor cells, and in transgenic mice with TNFα receptor 1 knock out, neurogenesis was increased after ischaemia compared to mice that did not lack the receptor (Iosif et al., 2008).

Microglial expression of chemokines or growth factors may also a mechanism of neurogenesis regulation. Microglia express BDNF and GDNF, which have been shown to be neuroprotective and promote neurogenesis. The chemokine monocyte chemotactic protein-1 (MCP-1) is expressed in

microglia following ischaemia, and has been shown to modulate neuroblast migration *in vitro* (Widera et al., 2004). Neuroblasts express chemokine receptors such as CCR2, and may therefore be responsive to chemokine levels *in vivo* (Tran et al., 2004). Increased levels of iNOS and eNOS, expressed in microglia, have also been shown to increase neurogenesis and angiogenesis (Chen et al., 2005; Zhu et al., 2003).

2.11. *Non-SVZ neurogenesis*

While the contribution of SVZ stem cells to neurogenesis following stroke has been extensively studied, it has been suggested that other cell types may also contribute to neurogenesis. A local progenitor cell may exist in the cortex, and proliferate to generate neuroblast that go onto differentiate into mature neurons, much like the SVZ neuroblast. There is some conflicting evidence for the existence of such a cell type.

Several studies have reported cortical neurogenesis following cerebral ischaemia (Gu et al., 2000; Jiang et al., 2001; Palmer et al., 1995; Palmer et al., 1999b; Magavi et al., 2000; Rakic, 2002), while others have reported that newborn neurons originate exclusively from the SVZ and migrate to their final destination for differentiation (Bhardwaj et al., 2006; Yamashita et al., 2006). NPC marker nestin is upregulated after ischaemia and is widely expressed in the ischaemic lesion (Duggal et al., 1997; Li and Chopp, 1999; Nakamura et al., 2003). In an inducible transgenic model where cells express GFP under the nestin promotor, the majority of GFP+ cells differentiate into neurons (Lagace et al., 2007), suggesting that nestin is a marker for NPC. However, it is uncertain whether nestin expression is exclusive to neural stem and progenitor cells (Ernst and Christie, 2005), or whether it can be expressed in other cell types after ischaemia. Astrocytes have been shown to reexpress developmental markers such as nestin and vimentin after injury (Hartfuss et al., 2001; Malatesta et al., 2003). Nestin expression may not be an indicator of neurogenesis after ischaemia.

As discussed above, in cell tracing studies involving intraventricular DiI infusions, Hua *et al* did not observe DiI in DCX+ cells at the lesion site, and Burns *et al* also observed DiI-negative DCX+ cells after ischaemia (Hua et al., 2008; Burns et al., 2007). The capacity of SVZ-derived neuroblasts to migrate into the cortex is also in dispute, and different animal models of ischaemia frequently give different contradicting results. In models that result in striatal and cortical injury, such as the MCAO model, few DCX+ cells are typically observe in the cortex (Arvidsson et al., 2002; Kokaia et al., 2006; Thored et al., 2006; Thored et al., 2007). In exclusively cortical models of ischaemia, such as photothrombolysis, DCX+ cells have been observed in the cortex (Jin et al., 2003). However, it is unclear whether these neuroblasts originate in the SVZ or from a local progenitor source. Longitudinal cell tracking would help to resolve these issues, and a method of labelling SVZ NPC is described in Chapter 6.

2.12. *Other sources of cell proliferation and DNA synthesis*

Development of cell tracking techniques is essential to resolve these issues of cell migration and neurogenesis. Labelling methods that can track a population of cells and its progeny, such as retroviral labelling and the CRE-lox system, will be able to address the question of the origin of neurogenic cells following ischaemia. Additionally, while BrdU incorporates into newly synthesised DNA in S-phase during cell division, aberrant DNA synthesis during apoptosis and in damaged neurons has been reported in ischaemia (Burns et al., 2007; Gage, 2000), however DNA repair at this level may not be detectable by BrdU immunohistochemistry (Taupin, 2007). It is important to be able to distinguish between these forms of DNA synthesis in CNS damage, and understand the limitations of using BrdU and mitotoic markers as indicators of cell proliferation.

OLPs have been shown to proliferate and accumulate in the corpus callosum and border of the ischaemic lesion within 7 days, co-localising with reactive astrocytes and microglia at the infarct border (Gottlieb et al., 2000; Mabuchi et al., 2000; Mandai et al., 1997; Ohta et al., 2003). Young *et al* have also demonstrated that OLPs are capable of neurogenesis in the normal adult brain (Young et al., 2007a). In Chaper 7, we investigate the contribution of OLPs to post-ischaemic neurogenesis further. Furthermore, reactive astrocyte and microglia proliferation have been reported following ischaemia and represents a major contribution to total cell proliferation, particularly outside of the SVZ. In inducible nestin-Cre transgenic mice – where GFP is expressed under the nestin promoter and induced by tamoxifen administration, and permanently expressed in the cell and its progeny thereafter – the majority of BrdU+ cells were not GFP+, indicating that they were not derived from the nestin+ SVZ progenitor or stem cell populations (Burns et al., 2007).

2.13. *Stem cell therapy in cerebral ischaemia*

Cellular therapy is a promising treatment for cerebral ischaemia and other neurodegenerative diseases such as multiple sclerosis, Parkinson's and Huntington's disease, which are characterised by extensive neuronal cell death. The main goal of cellular therapy is to replace cells lost during the injury event with stem cells that will respond to the injury environment and differentiate appropriately. For example, following cerebral ischaemia it is estimated that endogenous neurogenesis replaces only 0.2% of lost cells, and the aim of cellular therapy is to increase this cell replacement via the introduction of exogenous cells.

The process of cellular therapy involves the culture and expansion stem cells *in vitro*, and grafting of stem cells into a tissue, where they contribute to repair. Several study parameters can influence the treatment outcome, such as the stem cell type used (for example, embryonic, fetal, adult, haematopoietic, umbilical cord blood, iPS, or cell lines); the number of grafted cells; the delivery route (intravenous; intracarotid; grafting into the ipsilateral or contralateral cortex, striatum, corpus callosum; or intraventricular injections); the time point of delivery (acute or delayed). The

mechanism of action of stem cells has yet to be fully elucidated, but may involve not only cell replacement of injured tissue, but also neuroprotection.

Cellular therapy has been successful in several neurodegenerative disease models. In a rodent model of Parkinson's disease, a range of cell types have been used to replace degenerating neurons in the substantia nigra, including dopaminergic neurons (Lindvall and Kokaia, 2004), fetal mesencephalic cells (Wenning et al., 1997), neural-differentiated ES cells (Barberi et al., 2003; Bjorklund et al., 2002), and neural stem cells (Ourednik et al., 2002). These studies have been only partially successful, with results showing some functional improvement and only some neuronal differentiation of grafted cells.

In rodent models of Huntington's disease, grafting of fetal NPC into the striatum has resulted in behavioural recovery, graft survival and some GABAergic cell replacement (Clelland et al., 2008; McBride et al., 2004). These studies have led to clinical trials using fetal NPC, whose results indicate that the cellular therapy slows disease progression and improves motor and cognitive functions in patients (Bachoud-Levi et al., 2000; Hauser et al., 2002; Reuter et al., 2008). Patient autopsies confirm graft survival and neuronal differentiation (Keene et al., 2007).

Neurodegeneration in multiple sclerosis is chronic and dispersed, which present challenges for cell delivery to sites of degeneration. Several cell types have been studies in the EAE rodent model of MS, including oligodendrocyte precursors, embryonic stem cells and adult neural stem cells (Einstein et al., 2006; Groves et al., 1993; Pluchino and Martino, 2005; Windrem et al., 2004; Wolswijk, 2002). Pluchino *et al* demonstrated that adult neural stem cells injected intravenously home to sites of injury, accumulate in perivascular areas, and improve functional outcome (Pluchino and Martino, 2005; Pluchino et al., 2003). Many cells remain undifferentiated, with only some going onto oligodendrocyte differentiation and remyelination. A small clinical trial using haematopoietic stem cells has reported a delay in disease progression as well as functional improvement in 80% of patients treated (Burt et al., 2009). Other clinical trials have also observed at least a delay in disease progression (Saccardi et al., 2006).

Several cell replacement studies in cerebral ischaemia in rodents have demonstrated an improved functional outcome with a range of cell types, summarized in Table 2.13.1.4.1. Cellular therapy can contribute to neurogenesis and angiogenesis in the post-ischaemic brain (Kelly et al., 2004), as well as neuroprotection. Clinical trials involving cellular therapy have also been partially successful in improving motor and cognitive function after cerebral ischaemia (Kondziolka et al., 2002; Kondziolka et al., 2000; Kondziolka et al., 2005; Bang et al., 2005; Savitz et al., 2005). *et al* observed mild improvement in neurological score after intravenous infusion of mesenchymal stem cells in stroke patients. Similarly, Kondziolka and Savitz both observed some functional improvement after neural stem cell grafts in stroke patients and demonstrated the clinical safety of cellular therapy. However in all studies improvements were minor.

2.13.1. Cell type

One important consideration for cellular therapy in all disease models including cerebral ischaemia is the cell type used, which can range from ES cells, foetal NPC, and immortalised neural stem cell lines to haematopoietic, mesenchymal and umbilical cord stem cells. Linked to the cell type choice is the hypothesis as to the mechanism of recovery. The primary hypothesis of neural stem cell grafts is the contribution to cell replacement and functional integration of graft cells into host tissue; while haematopoietic cells are thought to promote endogenous neurogenesis, angiogenesis and cell survival in the lesion, through the release of growth factors and cytokines locally, and interaction with the host immune system. Furthermore, for appropriate cell integration and differentiation, the developmental stage of the cell appears to be important. While adult stem cells can be restricted in their differentiation capacity, embryonic stem cells can be tumorigenic when grafted into disease models. Fetal cells, taken from the stage of development that commitment to the desired cell type occurs, are lineage-restricted but retain some developmental plasticity, and can differentiate appropriately when grafted.

2.13.1.1. Embryonic stem cells

Embryonic stem (ES) cells derived from the inner cell mass of the embryo are pluripotent and can generate cells of the endoderm, mesoderm and ectoderm. *In vitro*, ES cells can be prompted to differentiate into the neural lineage at low density culture or when exposed to signalling factors (Barberi et al., 2003; Liour and Yu, 2003; Schmandt et al., 2005; Smukler et al., 2006; Tropepe et al., 2001; Wichterle et al., 2002; Ying et al., 2003).

ES cells can be expanded *in vitro*, but can form teratomas *in vivo* when transplanted into adult tissue in rodents (Bjorklund et al., 2002). Transplantation of ES cells into the ischaemic rodent brain has been shown to improve motor function, and some ES cells differentiate into neurons at the infarct border (Buhnemann et al., 2006; Hayashi et al., 2006), some studies have also observed no change in lesion size following cell therapy with ES cells (Hicks et al., 2008).

2.13.1.2. Bone marrow stem cells

Stem cells of haematopoietic and mesenchymal lineage have also been used in cell therapy studies in rodents, and have been summarised in the table below (Table 2.13.1.4.1) (Athiraman et al., 2009; Chen et al., 2001; Chopp and Li, 2002; Li and Chopp, 2009; Li et al., 2005; Li et al., 2002; Li et al., 2001b; Li et al., 2001a; Li et al., 2000; Shen et al., 2007; Shen et al., 2006); (Rempe and Kent, 2002; Kurozumi et al., 2004; Kurozumi et al., 2005). For cellular therapy following ischaemia, haematopoeitic and mesenchymal cells are typically injeceted systemically – intravenously or via the carotid artery – and home to the ischaemic lesion. Because of their pathotropism, they can be

exploited as a vehicle for drug delivery, modified to overexpress growth factors or other neuroprotective factors.

Haematopoietic and mesenchymal stem cells may also be able to differentiate into neurons (Dezawa et al., 2005). However, it is also likely that these cells have a predominantly neuroprotective effect after cerebral ischaemia. Chopp and colleagues have shown in several studies that bone marrow-derived mesenchymal stem cells improve functional outcome, reduce infarct size and apoptosis, increase VEGF, FGF-2, BDNF and IGF-1 expression in the lesion (Hardy et al., 2008; Chen et al., 2003), and increase neurogenesis and angiogenesis following cerebral ischaemia. Neovascularisation of the ischaemic infarct is associated with improved functional outcome, and haematopoietic cells have been shown to directly integrate into new vessel formation, and increase endogenous angiogenesis through expression of angiogenic factors such as VEGF and BDNF (Chen et al., 2003; Li et al., 2002; Zhang et al., 2005a).

2.13.1.3. Umbilical cord blood cells

Umbilical cord blood (UCB) cells are another stem cell source that has demonstrated neuroprotection, cell replacement and differentiation into neural, glial and endothelial cell types after grafting in cerebral ischaemia rodent models (Borlongan et al., 2004; Lu et al., 2002; Vendrame et al., 2004). UCB are easily available and enriched for haematopoietic stem cells (Sanberg et al., 2005). A number of studies have suggested that UCB can differentiate into neurons and glia (Bicknese et al., 2002; Sanchez-Ramos et al., 2001; Zigova et al., 2002). Improved behavioural outcome has been observed following cellular therapy with UCB, sometimes with little or no cell engraftment, which suggests a neuroprotection mechanism (Taguchi et al., 2004).

2.13.1.4. Neural stem cells

Immortalised neural stem cell lines such as C17.2 cerebellar external granule cell layer progenitors (Snyder et al., 1997), MHP36 hippocampal progenitors (Modo et al., 2002a) have been used for cell transplantation after cerebral ischaemia in rodents. These studies demonstrate moderate functional improvement and some neuronal differentiation of transplanted cells. Veizovic *et al* found that grafting of MHP36 cell line decreased lesion volume and improved functional outcome (Veizovic et al., 2001), and Modo *et al* demonstrated that this cell type is capable of neuronal differentiation at the lesion (Modo et al., 2002a; Modo et al., 2004). Chu *et al* have observed similar results with an immortalised human neural stem cell line, and also observed neuronal differentiation in the ischaemic brain (Chu et al., 2004; Chu et al., 2008). In some studies, the cell lines are also modified to express growth factors such as VEGF (Maurer et al., 2008). advantages of the immortalised cell lines are that they can be rapidly expanded *in vitro*, and are a clonally derived homogeneous population. However, the cells are immortalised with an

oncogene and may therefore be tumorigenic under certain conditions. Temperature-sensitive immortalised stem cells, which are capable of proliferation at 33°C, but inhibited at 37-39°C, could prevent tumorigenicity of grafted cells. The ST14A neural stem cell line, derived from embryonic striatal tissue and immortalised by retroviral transduction of the temperature-sensitive SV40 Large T Antigen oncogene (Cattaneo and Conti, 1998), is one candidate cell type, and is described further in Chapters 4 and 5.

For cell replacement, the lineage commitment of stem cells plays an important role in their differentiation potential after engraftment into injured tissue. Radial glia-like cells give rise to the cortical neuron layers in the normal developing embryo, and may have the appropriate migratory capacity and neurogenic potential to give rise to neurons after engraftment into host injury tissue, compared to adult neural stem cells or embryonic stem cells. It is this cell type that is of particular interest to our research, and the focus of cell engraftment and cell MRI contrast agent labelling studies in Chapter 4. Several of the immortalised stem cell lines are originally derived from fetal neural stem cells. Recent research has demonstrated that fetal telencephalic neural progenitor cells are able to migrate towards the ischaemic infarct, differentiate into neurons in the peri-infarct area, and can improve behavioural recovery (Darsalia et al., 2007; Kelly et al., 2004; Lee et al., 2008; Ishibashi et al., 2004; Zhang et al., 2009; Takahashi et al., 2008). In addition, Jiang *et al* found that neural progenitor cells derived from adult tissue did not differentiate into neurons after grafting into the ischaemic brain, though the authors observed that cell treatment decreased lesion volume and improved functional outcome (Jiang et al., 2005).

Kelly *et al* found that grafting of human fetal neural progenitor cells into the ischaemic brain resulted in NPC migration toward the lesion site and differentiation into neurons (Kelly et al., 2004), and Darsalia *et al* oberseved a similar result (Darsalia et al., 2007). Zhu *et al* also found that fetal NPC could migrate and differentiate at the lesion, and also observed behavioural improvement (Zhu et al., 2005). The disadvantage of using this cell type is that primary NSC, derived from foetal and adult CNS, are more difficult to source and expand *in vitro* than immortalised cell lines, and are a heterogeneous population of cells.

Bible *et al* have also used a bio-scaffold to support neural stem cell integration into host tissue. MHP36 cells were co-injected with a synthetic scaffold material directly into the lesion necrotic core (Bible et al., 2009), which was shown to aid cell distribution throughout the lesion cavity. Grafted cells were in close association with the bio-scaffold. Cell proliferation of grafted cells was not assessed, but by seven days post-ischaemia some grafted cells expressed neuronal and glial markers. In future studies, co-injection of stem cells with bio-scaffolds coated with growth factors may further enhance cell survival and neurogenesis.

Reference	Cell Type	Origin	Delivery	Timepoint	Cell Survival	Cell Migration	Neuronal Differentiation	Decrease Lesion Size	Functional Improvement
Buhnemann 2006	ES	Mouse	IC						
Erdo 2003	ES	Mouse	IC	14 D					
Hoehn 2002	ES	Mouse	IC	14 D					
Takagi 2005	ES	Mouse	IC	2 D					
Hayashi 2006	ES	Primate	IC	1 D					
Lappalainen 2008	ES-NSC	Rat	IV	Immediate					
Theus 2008	ES-NSC		IC	2 D					
Daadi 2008	ES-NSC	Human	IC						
Hicks 2008	ES-NSC	Human							
Jiang 2005	NPC (A)	Rat	Cisternal	2 D					
Kameda 2007	NPC (A)	Rat	IC	Prior					
Zhang 2004	NPC (A)	Rat	Cisternal	2 D					
Zhang 2009	NPC (F)	Human	IC	1 D					
Darsalia 2007	NPC (F)	Human	IC						
Fukunaga 1999	NPC (F)	Rat	IC	Immediate					
Ishibashi 2004	NPC (F)	Human	IC	4 D					
Jeong 2003	NPC (F)	Human	IV	1 D					
Kelly 2004	NPC (F)	Human	IC	1 D					
Lee 2008	NPC (F)	Human	IV						
Jin 2005	NPC (F)	Mouse	IC	1 D					
Takahashi 2008	NPC (F)	Rat	IC	Immediate					
Zhang 2008	NPC (F)	Rat	IC	7 D					
Zhu 2005	NPC (F)	Rat	IC	3 D					
Pastori 2008	NPC (P)	Mouse	ICa	Immediate					
Bliss 2006	NSC CL	Human	IC	7 D					
Borlongan 1998	NSC CL	Human	IC	28 D					
Chu 2005	NSC CL	Human	IC	1 D					
Chu 2004	NSC CL	Human	IC	1 D					
Chu 2008	NSC CL	Human	IC	Prior					
Lee 2007	NSC CL	Human	IC	7 D					
Pollock 2006	NSC CL	Human	IC						
Sapporta 1999	NSC CL	Human	IC	28 D					

Stroemer 2008	NSC CL	Human	IC						
Guzman 2008	NSC CL	Mouse	IC						
Guzman 2008	NSC CL	Mouse	IV	2 D					
Kim 2004	NSC CL	Mouse	IC	Immediate					
Mochizuki 2008	NSC CL	Mouse	IC	Immediate					
Modo 2002	NSC CL	Mouse	IC	14 D					
Modo 2008	NSC CL	Mouse	IC	14 D					
Modo 2002	NSC CL	Mouse	IC	14 D					
Modo 2002	NSC CL	Mouse	IC	14D					
Veizovic 2001	NSC CL	Mouse	IC	14 D					
Shyu 2008	OEC	Human							
Borlongan 2005	Haem	Human	IV	Immediate					
Shyu 2006	Haem	Human	IC	7D					
Willing Sanberg 2003	Haem	Human	IV	1 D					
Schwarting 2008	Haem	Rat	IV	1 D					
Chen 2008	Haem		IC						
Yoo 2008	MSC	Human	IC	3 D					
Chen 2003	MSC	Human	IV	1 D					
Kurozumi 2004	MSC	Human	IC	1 D					
Li 2002	MSC	Human	IV	1 D					
Zhao 2002	MSC	Human	IC	7D					
Chen 2001	UCB	Human	IV	1 D					
Ding 2007	UCB	Human	IC						
Kozlowska 2007	UCB	Human	IC	2 D					
Taguchi 2004	UCB	Human	IV	2 D					
Vendrame 2004	UCB	Human	IV	1 D					
Willing 2003	UCB	Human	IC	1 D					
Xiao 2005	UCB	Human	IV	2 D					

Table 2.13.1.4.1 Table of cellular therapy studies for cerebral ischaemia. Green, improved outcome relative to control. Yellow, no difference in outcome relative to control. Red, poor outcome relative to control. Grey, not assessed. ES, embryonic stem cell. ES NSC, embryonic stem cell-derived neural stem cell. NPC (F), fetal neural progenitor cell. NPC (P), postnatal neural progenitor cells. NPC (A), adult neural progenitor cells. NSC CL, neural stem cell immortalised cell line. OEC, olfactory ensheathing cells. Haem, haematopoietic stem cells. MSC, mesenchymal stem cells. UCB, umbilical cord blood cells. IV, intravenous. IC, intracerebral. ICa, intracarotid.

2.13.2. Mechanism of action in cellular therapy

While many cell types have demonstrated functional improvement in cell therapy studies, the mechanism of action is not well understood. Several actions have been observed: neuronal differentiation and cell replacement; trophic support of endogenous cells; neuroprotection; and immunomodulation. Understanding the mechanisms of action is important, and this knowledge will determine study parameters such as the optimal cell type, delivery route and timepoint. A primarily immunomodulatory role for stem cells suggests that systemic cell delivery would be appropriate, whereas a neuronal differentiation role would require cell grafting at or near the injury site for maximum cell replacement.

A number of studies have demonstrated some neuronal differentiation of graft stem cells after cerebral ischaemia (Table 2.13.1.4.1). The graft cells differentiate appropriately and can integrate into local circuitry. However, this cell replacement occurs at relatively low levels, and it is unlikely that the low level of neuronal differentiation accounts for the functional improvement reported following NSC cell therapy. Neuroprotection, immunomodulation and trophic support are likely important roles of graft cells that contribute to the improved outcome.

The concept of the ectopic neurovascular niche has been proposed for NSC and bone marrow stem cell therapy, where transplanted cells support endogenous neurogenesis by recreating the components of the SVZ neurovascular niche at the lesion site, by increasing neovascularisation; increasing the recruitment of endogenous NSC to the lesion; and inducing plasticity in the ischaemic hemisphere (Martino and Pluchino, 2006; Bliss et al., 2007). Transplanted NSC are able to home to lesion areas, termed 'pathotropism', migrating towards gradients of proinflammatory cytokines and chemokines (Aboody et al., 2000; Ben-Hur et al., 2003), are closely associated with endothelial cells and astrocytes at the lesion (Chang et al., 2007).

Grafted cells may also act by neuroprotection and prevention of cell death. NSC and BMSC grafts are associated with reduced apoptosis and latent cell loss at the lesion, reduced glial scar formation, and increased survival of neurons and endogenous neuroblasts at the penumbra (Camarero et al., 2003; Otaegi et al., 2006). Grafted cells may also modulate the immune response to injury locally and peripherally. In the EAE model, grafted NPC reduce brain inflammation via reduced immune cell infiltration and reduction of proinflammatory cytokines (Einstein et al., 2007). This effect has also been observed in cerebral ischaemia. Lee *et al* demonstrated that acute intravascular administration of neural stem cells reduced neuroinflammation after cerebral ischaemia, but this effect was reversed if rats received splenectomy prior to ischaemia, indicating a peripheral immunomodulatory effect of NSC rather than local CNS effect (Lee et al., 2008).

These neuroprotective and trophic effects of stem cell grafts promote the expression of growth factors at the ischaemic lesion, and stem cells themselves secrete growth factors. The protective

and neurogenic actions of growth factors were previously described, and stem cell grafts may act by promoting these pathways after stroke. SDF1α is normally expressed in bone marrow stromal cells (Stumm et al., 2002). The receptor CXCR4 is expressed in SVZ NPC (Ni et al., 2004; Thored et al., 2006), and this may be one pathway by which bone marrow grafts enhance neurogenesis after stroke. Capone et al demonstrated that following neural progenitor cell transplantation, several growth factors were upregulated at the ischaemic lesion - IGF-1, VEGF, TGFb1, BDNF, SDF1α (Capone et al., 2007).

3. *Magnetic resonance imaging in cerebral ischaemia*

Magnetic resonance imaging (MRI) is a powerful non-invasive imaging modality for cerebral ischaemia that can provide anatomical and physiological information for the normal and pathological CNS. Relative to other *in vivo* imaging modalities, it has high spatial resolution, but weak sensitivity and signal to noise.

MRI is a technique based on the detection of protons (^1H) of water molecules. Water protons in different tissues will have different relaxation times based on their unique physiochemical environment, and this difference can be exploited to maximise contrast between tissues and generate an anatomical image. Furthermore, through the development of MRI contrast agents that can label cells or bind to specific cellular markers, a new field cellular and molecular imaging is emerging.

Some atomic nuclei, such as ^1H, ^{13}C and ^{31}P, possess spin. The classical approach is to visualise the nucleus of a proton spining around its own axis, generating a magnetic moment. The sum of all spins in a sample is the net magnetisation vector (M_z). Under normal conditions its polarity is random and net magnetisation is 0. The magnetic moment is dependent on the gyromagnetic ratio, which varies depending on the structure of a given nucleus. ^1H has a unique gyromagnetic ratio compared to ^{13}C or ^{31}P. The spin quantum number I for ^1H protons is ½.

3.1. *Relaxation*

When an external magnetic field (B_0) is applied along the z-axis, net magnetisation (M_z) becomes aligned parallel to B_0 (figure 3.1.1). Spins precess around B_0 at the Larmor frequency (ω_0), which is proportional to the strength of the applied magnetic field and the gyromagnetic ratio of the nucleus. This is given by the equation:

$$\omega_0 = B_0 \times \lambda$$

where ω_0 is the Larmor frequency at which nuclei precess; B_0 is the external magnetic field strength, and λ is the gyromagnetic ratio.

The Larmor frequency is specific to protons at a given field strength. Nuclei will adopt an energy state, *m*, parallel or anti-parallel to the applied magnetic field B_0, where a greater proportion will adopt the lower energy parallel state (Fig 3.1.1). Transition between energy states can occur, and this change is used to detect an NMR signal. Because of the small energy difference between spin states, NMR sensitivity is inherently low. The energy difference between parallel and antiparallel nuclei is proportional to the applied field strength B_0. At greater field strength there is a greater energy difference and greater net signal, generating better signal to noise.

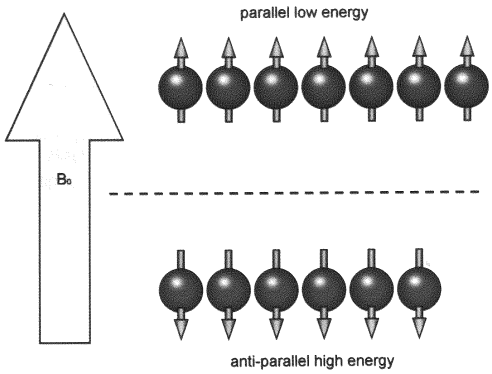

Figure 3.1.1 Net magnetization of nuclear magnetic moments parallel to applied magnetic field B_0 (from Westbrook et al.)

When a 90° radiofrequency (RF) pulse is applied in the xy plane at the Larmor frequency ω_0, this tilts magnetization into the transverse *xy* plane M_{xy}, which returns to equilibrium, parallel to the *z* plane, over time. This relaxation can be described according to two time constants, the longitudinal relaxation time T_1, and the transverse relaxation time T_2. The longitudinal relaxation time T_1 is the time constant for the recovery of M_z magnetization parallel to B_0. The transverse relaxation time T_2 is the time constant for the decay of transverse magnetisation. The T_1 and T_2 values for different samples and tissues will vary according to the molecular environment of the ^1H protons, and in this way image contrast between tissues can be generated.

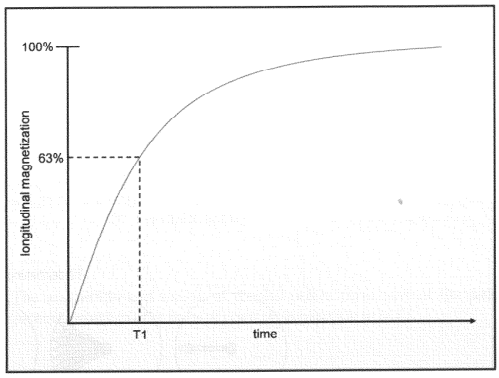

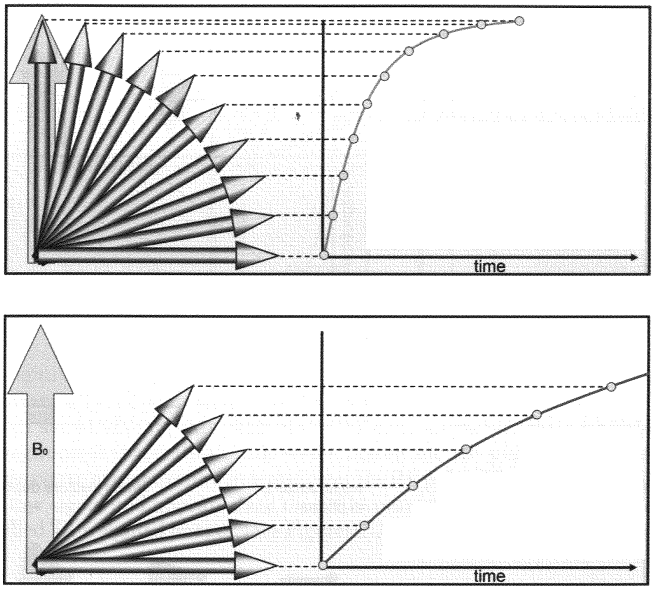

Figure 3.1.2 Longitudinal Relaxation, recovery of M_z magnetization (from Westbrook et al.). Top, T_1 time constant. Middle and bottom, example of recovery of M_z magnetization in water (bottom), and contrast agent solution (middle), which accelerates the longitudinal relaxation rate. Contrast agents are discussed further in Section 3.7.

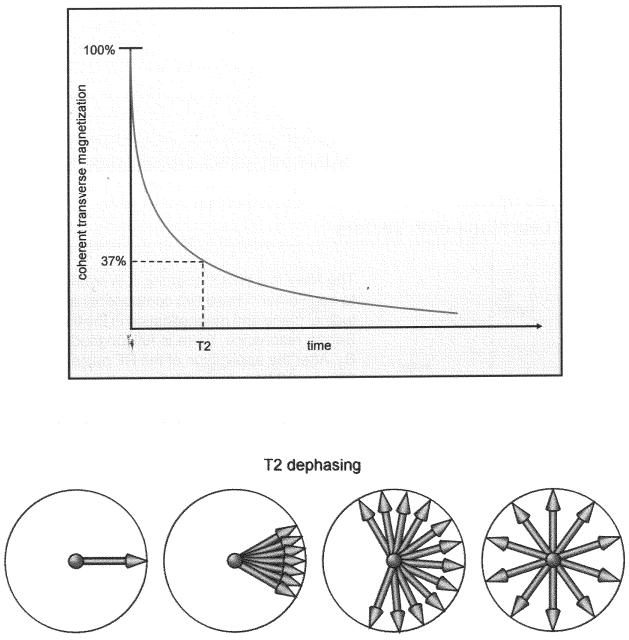

Figure 3.1.3 Transverse Relaxation, decay of transverse magnetization (from Westbrook et al.). Top, T_2 time constant. Bottom, schematic of loss of M_{xy} phase coherence.

3.2. Signal detection

Using a transmitter coil near the sample, an RF pulse of defined frequency and duration is sent through the transmitter coil by the transmitter, generating an oscillating magnetic field B_1 in the sample. Nuclei absorb energy at the Larmor frequency, and signal at the resonant frequency is detected by a receiver coil. This signal is termed the free induction decay (FID), and is a waveform expressed as a function of time, with many frequency components. By Fourier transformation, spatial and contrast information can be resolved from the FID signal, and an image can be constructed. Signal to noise is affected by the magnetic field strength B_0, the voxel size, the T_1 and T_2 of the sample, and pulse sequence parameters.

3.3. Spin echo sequence and measurement of T_2

When a 90° RF pulse is applied, the phase coherence of M_{xy} also decays over time (Figure 3.1.3). Protons in different molecular environments precess at slightly different frequencies, causing a spread in magnetization and loss of signal. Loss of M_{xy} phase coherence can be accelerated by local magnetic field inhomogeneities of tissues, which dephase spins in the *xy* plane. The time constant T_2* reflects the combined T_2 and local field inhomogeneity effects. A 180° refocusing pulse is used to reduce the effects of the T_2* component, reversing the decay to produce a spin echo. At time TE/2, the magnetisation phase is inverted and the direction of precession is reversed, eventually returning to phase coherence at the echo time TE. The 180° pulse counteracts the dephasing effects of local field inhomogeneities, and the dephasing from T_2 relaxation effects is predominantly detected. T_2-weighting is proportional to TE, where greater T_2 weighting occurs at longer echo times. The T_2 relaxation time of a sample can be measured by taking a series of T_2 measurements at varying echo times, which generates a relaxation curve from which the T_2 constant can be measured.

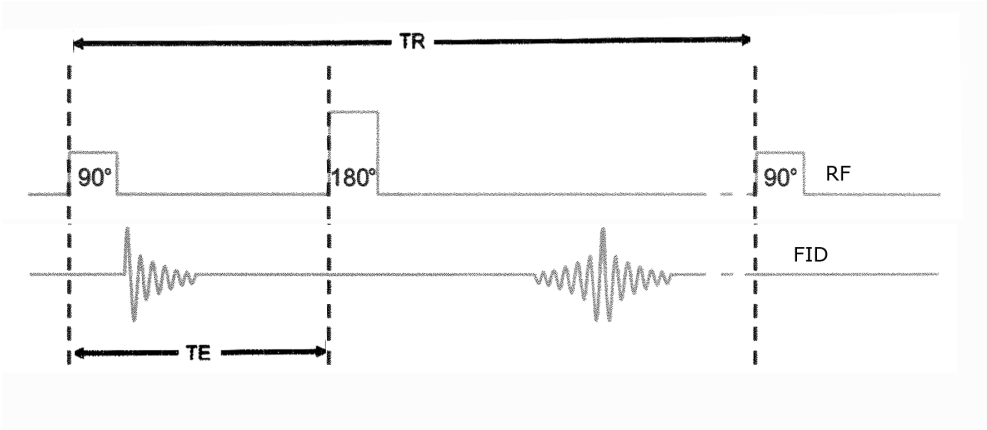

Figure 3.3.1 The spin echo sequence (modified from Westbrook et al.). RF, radiofrequency

pulse. FID, free induction decay. TR, repetition time. TE, echo time.

*3.4. Gradient echo sequence and measurement of T_2**

Rather than using a 180° RF refocusing pulse, for the gradient echo sequence, the frequency encoding gradient is used to rephase the FID. The first gradient dephases the magnetisation, and on reversal of the gradient, magnetisation rephases, where the maximum rephasing occurs at full reversal, producing a gradient echo signal. The gradient echo does not refocus the dephasing effects of the local field inhomogeneities, generating a T_2*-weighted image. The gradient echo sequence is sensitive to local field inhomogeneities generated from the presence of superparamagnetic conrast agents in a sample. The gradient echo sequence is used to detect iron oxide-based MRI contrast agents in vivo in Chapters X and X.

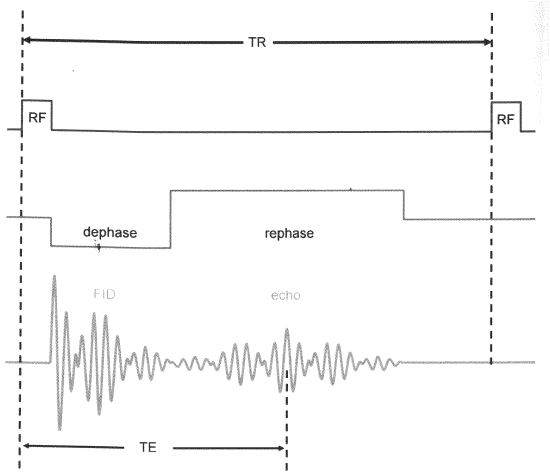

Figure 3.4.1 The gradient echo sequence (from Westbrook et al.)

3.5. Inversion recovery sequence and measurement of T_1

The T_1 constant of a sample can be measured using the inversion recovery pulse sequence. A 180° pulse is applied and magnetisation is inverted, antiparallel to the z axis. The spins relax towards M_0 equilibrium at a rate dependent on the T_1 time constant. After a give inversion time TI , another 90° pulse is then applied to rotate M_z into the xy plane. The FID signal amplitude is dependent on M_z at the time of the 90° pulse, which is determined by the T_1 relaxation constant. If a series of measurements are taken at varying inversion times TI, then an inversion recovery curve can be generated and the T_1 constant measured. The inversion recovery pulse sequence is used to measure the T1 or gadolinium-based MRI contrast agents in Chapter 5.

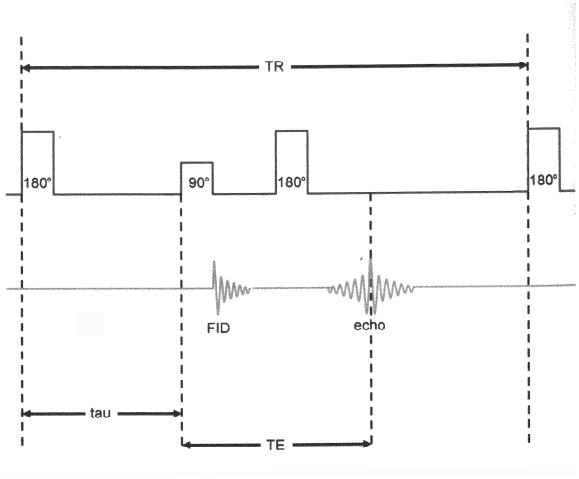

Figure 3.5.1 The inversion recovery sequence (from Westbrook et al.).

3.6. MRI and ischaemia

Magnetic resonance imaging is an important non-invasive imaging modality in cerebral ischaemia. In experimental animal models, it can provide longitudinal data for individual subjects, both anatomical and physiological. Relative to other non-invasive imaging modalities, MRI provides a high spatial resolution and sensitivity.

In the normal CNS, the cerebrospinal fluid (CSF) has a long T_1 and T_2, whereas grey and white matter have shorter T_1 and T_2. Under pathological conditions such as cerebral ischaemia, the water distribution in affected tissues changes, changing the T_1 and T_2 values of the tissue, and in this way pathological anatomy can be imaged. During and subsequent to cerebral ischaemia, changes in water compartment occur due to cytotoxic and vasogenic oedema, and BBB breakdown. Cerebral blood flow changes occur during ischaemia and reperfusion (Calamante et al., 1999b; Thomas et al., 2000; Lythgoe et al., 2003),(Calamante et al., 1999a; Lythgoe et al., 2003; Thomas et al., 2000), as well as inflammation and infiltration of peripheral leukocytes and macrophages. These water movements and pathological events can be imaged using MRI. T_2-weighted imaging can detect the acute ischaemic response (Calamante et al., 1999a), and demarcate the mature and evolving lesion (Wegener et al., 2006). This closely correlates to histological data. Diffusion-weighted imaging (DWI) is sensitive to cytotoxic oedema in the acute phase of ischaemia, as cell swelling causes a change in water diffusivity within ischaemic cells relative to normal cells. These diffusion changes correspond to regions of periinfarct acidosis and infarct core. Cerebral perfusion can be measured non-invasively using arterial spin labelling (ASL), and the infarct core and surrounding region of reduced perfusion can be detected (Weber et al., 2006; Dijkhuizen and Nicolay, 2003). The penumbra can be identified where DWI and ASL images do not overlap and only perfusion changes are observed, outside of the ischaemic core, but where tissue has experienced reduced perfusion but not cytotoxic oedema and cell death

(Neumann-Haefelin et al., 2000; Lythgoe et al., 2003; Thomas et al., 2000).

Breakdown of the BBB can be imaged using MRI contrast agents. Systemically injected gadolinium leaks into the brain parenchyma from the CNS vasculature at areas of BBB disruption and endothelial damage. This generates an area of hyperintensity in T_1-weighted images (Dijkhuizen and Nicolay, 2003). Furthermore, the peripheral immune response to ischaemia can be imaged. Ferumoxide agents taken up by peripheral macrophages can be visualised in the ischaemic brain upon macrophage infiltration (Jander et al., 2007; Rausch et al., 2001; Rausch et al., 2002; Weber et al., 2005). MRI contrast agents will be discussed in further detail in the following section.

Other imaging modalities can be used for imaging cerebral ischaemia. Ischaemic lesions can be detected by PET imaging by observing the uncoupling of regional cerebral blood flow (rCBF) and the cerebral metabolic rate of oxygen consumption ($CMRO_2$) (Marchal et al., 1996).

3.7. MRI contrast agents

A novel application of magnetic resonance imaging is the use of contrast agents for cellular imaging. Cellular imaging has been defined as the "non-invasive and repetitive imaging of targeted cells and cellular processes in living organisms" (Bulte and Kraitchman, 2004a). Traditionally, contrast on MR images is achieved by exploiting differences in relaxation rates of different tissues in the body, or between normal and pathological tissue, on T_1- or T_2-weighted images, but in many cases tissue contrast is insufficient. Contrast agents (CA) are designed to accelerate relaxation rates of surrounding water protons, decreasing local T_1 and T_2 and generate contrast against non-contrast agent enhanced tissue. They can be categorised based on their predominant effect on T_1 or T_2 relaxation: a dominant T_1 reduction effect will increase signal intensity and generate positive contrast on a T_1-weighted image; whereas a predominantly T_2-shortening effect will reduce signal intensity and generate negative contrast on T_2-weighted images (Modo et al., 2005). Relaxivity – the ability of a contrast agent to reduce the T_1 or T_2 relaxation rate – is the unit of measurement of contrast enhancement. Increased relaxivity will lead to increased contrast on an MR image, or the same contrast can be achieved with a smaller dose of contrast agent. Relaxivity (r_1 or r_2) is calculated using the equation:

$$\frac{1}{T_1^{obs}} = \frac{1}{T_1^{0}} + r_1[Gd]$$

or

$$\frac{1}{T_2^{obs}} = \frac{1}{T_2^{0}} + r_2[Gd]$$

respectively, and measured as mM^{-1} sec^{-1}.

3.7.1. Paramagnetic contrast agents

Paramagnetic agents are typically organic compounds that form a complex with lanthanide or transition metal ions. The majority of paramagnetic agents are complexes synthesised with the Gd^{3+} ion (Hermann et al., 2008). The first gadolinium-based contrast agents were developed in the 1980s (Kabalka et al., 1987). Gadolinium-DTPA [Gd(DTPA)(H2O)$_2$] (Magnevist ®) was the first to be licensed for clinical MRI by the Food and Drug Administration (FDA), and now over 30% of clinical MRI scans use gadolinium for contrast enhancement (Caravan et al., 1999). Typical applications of gadolinium-based contrast MRI imaging include renal, tumour, blood brain barrier imaging, and angiography, or to decrease the total acquisition time in anatomical imaging. Relaxivity and cytotoxicity of novel gadolinium-based contrast agents, designed and synthesized for cellular imaging, are assessed in Chapter 5.

The Gd^{3+} ion has 7 unpaired electrons and a high magnetic moment. The greater access and proximity of water to the Gd^{3+} ion, the better it can affect proton spin and increase the relaxation of water protons. There are two main mechanisms by which gadolinium affects water protons, via inner sphere and outer sphere effects. Inner sphere effects refer to water directly coordinated to the Gd^{3+} ion. Gadolinium-bound water protons relax, and water molecules undergo rapid chemical exchange with each other. The net effect is that gadolinium enhances the relaxation rate of surrounding water. The outer sphere effect refers to the remote relaxation effect gadolinium has on nearby diffusing water that is not bound to the Gd^{3+} ion.

3.7.1.1. Paramagnetic contrast agent design

Several factors affect relaxivity of gadolinium contrast agents: the number of free sites available for inner sphere water proton coordinated to the Gd^{3+} ion, *q*; the water exchange rate, τ_M; the rotational correlation time, or molecular tumbling time, of the contrast agent, τ_R; and outer sphere indirect water interaction with gadolinium (Hermann et al., 2008) All of these parameters can be altered through ligand design.

Gadolinium must be coordinated in a ligand that has high thermodynamic stability and is kinetically inert. Because of the toxicity of the free Gd^{3+} ion, it must remain encapsulated in the ligand. Gadolinium contrast agents are typically 9-coordinate structures: an 8-coordinate organic ligand and a single water molecule coordinated to a Gd^{3+} ion. Structures that allow two coordinated water molecules have less thermodynamic stability, and may lead to dissociation of the toxic Gd^{3+} ion into a biological environment. *In vivo*, endogenous Zn^{2+} and Ca^{2+} ions are the main competitors to Gd^{3+} (Hermann et al., 2008), so the contrast agent must also resist transchelation and loss of the Gd^{3+} ion. Other chelating agents found *in vivo* include phosphate, citrate and bicarbonate.

Gadolinium contrast agents achieve the optimum relaxivity when the rotational diffusion τ_R of the molecule approaches the Larmor frequency ω_0, which is typically slower than the rotational diffusion of the contrast agent. Slower τ_R allows for more water exchange to occur, and therefore increased relaxation of surrounding water by gadolinium via inner sphere effects. *In vivo*, slower rotational diffusion can be achieved by increasing the effective molecular weight of the complex, through non-covalent binding of the complex to larger proteins, or by covalent binding to become part of a larger polymer (Caravan et al., 1999). A number of clinical gadolinium-based contrast agents have been designed to non-covalently bind to human serum albumin (HSA) in the blood to increase relaxivity, for example MS-325, Vasovist and Multihance (Hermann et al., 2008). An additional advantage of this strategy is that contrast agent relaxivity is enhanced only in areas of high physiological concentration of HSA, eg in the blood pool.

3.7.1.2. Cellular imaging with paramagnetic contrast agents

Cellular imaging using gadolinium-based contrast agents is less common than with iron oxide-based agents. Gadolinium T_1 relaxivity is an order of magnitude weaker than iron oxide T_2 relaxivity and this is a disadvantage for cellular imaging that depends on high sensitivity and spatial resolution for cellular detection. However, T_1 relaxivity is desirable as it can produce increased and hyperintense signal on T_1-weighted images, and can be distinguished from magnetic susceptibility effects, unlike superparamagnetic contrast agents.

A number of gadolinium-based approaches to cellular labelling have been successful. Rudelius *et al* used the transfection agent lipofectin to label embryonic stem cells with gadolinium DTPA (Rudelius et al., 2003). Gd-DTPA was localised in the cytoplasm, as assessed by electron microscopy, and labelled cells generated positive contrast on MRI images. However the study also found that the labelling efficiency was low (less than 50%) and caused reduced cell viability. Other studies have similarly found that cells can be labelled with gadolinium contrast agents and generate positive contrast *in vitro*, for example mononuclear cell labelling with gadophorin-2 using lipofectin transfection agent; monocyte labelling with gadofluorine-M (Henning et al., 2007); and mesenchymal cell labelling with gadolinium fullerene (Anderson et al., 2006). However several of these studies report, where viability has been assessed, that the contrast agent labelling is associated with reduced cell viability.

Brekke *et al* found, using the rhodamine-conjugated gadolinium contrast agent GRID, that labelling neural stem cells resulted in localisation of the contrast agent in the cytoplasm (Brekke et al., 2007). The GRID contrast agent, however, acts primarily as a T_2 agent, generating hypointensity *in vitro* and *in vivo* (Brekke et al., 2007; Modo et al., 2002a; Modo et al., 2004). Labelling with GRID also induced cellular stress, decreased viability and proliferation, although

labelling did not affect cell differentiation or migration (Modo et al., 2008).

Another gadolinium cellular imaging approach has been used to image tumor cells *in vivo*. Exploiting the fact that proliferating tumor cells have upregulated glutamine transporter systems on the cell memebrane, Lattuada *et al* covalenetly bound glutamine to gadolinium DOTA and found that the gadolinium-glutamine agent preferentially localised to tumor cells, generating T_1 hyperintensity (Lattuada et al., 2006). This enhancement of T_1 contrast in tumor cells was also demonstrated in an *in vivo* tumor in mouse (Geninatti et al., 2006).

Macromolecular gadolinium contrast agents have also been developed for cellular imaging tumour targeting. Fu *et al* describe a polymer with a polyethylene glycol/polylysine backbone and Gd-DTPA compenents at the ends, developed for tumour angiogenesis detection (Fu et al., 2007). Wiener *et al* describe a folate-conjugated DTPA- polyamidoamine dendrimer structure (Wiener et al., 1997). The highly branched dendrimer contrast agents were observed to accumulate in tumour cells expressing the folate receptor, and decreased the T_1 relaxation time of cells relative to unlabelled tumour cells. In Chapter 5, we investigate the relaxivity and cytotoxicity of gadolinium polymer contrast agents designed and synthesised for cellular imaging.

3.7.2. Superparamagnetic contrast agents

Superparamagnetic contrast agents are typically iron oxide-based agents composed of a magnetite crystal core embedded in a biocompatible coating (Modo et al., 2005). Magnetite crystals possess a large magnetic moment in the presence of an external magnetic field, and create a local magnetic field inhomogeneity. This causes remote dephasing of water protons, which decreases the T_1 and T_2 locally (Bulte and Kraitchman, 2004b; Modo et al., 2005).

r_2* relaxivity, or the susceptibility effect, describes the increase in T_2* relaxation due to magnetisation differences between neighbouring regions or adjacent voxels. Non-homogeneous distribution of iron oxide particles in a tissue will give rise to local field inhomogeneities around the iron oxide particles. T_2*-weighted sequences are sensitised to the proton dephasing caused by local magnetic field inhomogeneities, and are typically used to detect susceptibility effects from superparamagnetic iron oxide contrast agents (Bulte and Kraitchman, 2004a). For cellular imaging, the magnetic field distortion can extend beyond the volume of a single cell containing iron oxide (Magnitsky et al., 2005), and this has been termed a 'blooming effect' (Bulte et al., 2001). No water has access to or is bound directly to the magnetite crystals, therefore there are no inner sphere effects associated with superparamagnetic contrast agents (Modo et al., 2005).

Superparamagnetic iron oxide (SPIO) particles, or ferumoxide particles, are composed of multiple magnetite crystals forming the core, with an average particle diameter of 200 nm. Ultrasmall SPIO (USPIO), or ferumoxtran particles, consist of a single crystal core and have an

average particle diameter of 50 nm (Modo et al., 2005). For SPIO and USPIO, the magnetite core size is in the range of 4-10 nm. Relaxivity increases with increasing crystal density, and so SPIO – with several magnetite crystals per core and a large magnetic moment – can generate more contrast per mol of iron than USPIO (Bulte and Kraitchman, 2004a). The extent of in vivo r_2* relaxivity of an SPIO contrast agent is dependent on several other factors including the compartmentalisation or aggregation of the agent in tissue, cells or the bloodstream, and the imaging sequence and parameters used.

The compounds are typically coated in a biocompatible material, most commonly dextran or other polysaccharides. These surface modifications are required for stabilisation – to prevent crystal aggregation – as well as for solubility and biocompatibility. The composition of the coating provides possible conjugates for ligand binding such as antibodies, proteins or peptides etc, for targeted labelling. Other surface modification strategies designed to increase specificity, biocompatibility, or cell labelling include magnetite encapsulation in an apoferritin protein shell (Bulte et al., 1994); magnetodendrimers (Bulte et al., 2001); biotin-streptavidin system – binding biotinylated antibodies to streptavidin-SPIO (Artemov et al., 2004), and covalent linking of dextran to antibodies by (Bulte and Kraitchman, 2004a). The latter method pre-dates molecular imaging and was originally designed for isolation of specific cell types by antibody recognition and separation through a magnetic column (Dutton et al., 1979).

The most commonly used category of superparamagnetic contrast agents is the SPIO. This category includes Endorem/Ferridex, an FDA-approved iron oxide-based contrast agent. This is a dextran-coated particle with an average diameter of 150-200 nm, and has been licensed for use in MRI of the liver. Other contrast agents that will be discussed in further sections include the USPIO Sinerem and Bangs particles. These are larger micron-sized iron oxide nanoparticles, with a divinyl benzene coating and conjugated to a fluorophore, which allows for fluorescent microscopy of the Bangs particles in histological sections.

SPIO cellular uptake commonly occurs by endocytosis, and SPIO localise intracellularly in endosomes. Cellular internalisation and particle clustering increases particle susceptibility effects (Kraitchman and Bulte, 2008). Cell iron content after SPIO uptake is in the range of 10-20 pg iron per cell, whereas non-labelled cells contain 0.01-0.1 pg iron per cell (Arbab et al., 2003). SPIO degrade in acidic environments such as the lysosome, and SPIO-containing endosomes have been observed to fuse with lysosomes after 5 days. Once in the lysosome, iron in SPIO particles may enter endogenous iron homeostasis pathways and be stored as ferritin or hemosiderin. Iron homeostasis pathways in the CNS are discussed in section 3.9.

3.7.2.1. Cell labelling strategies using SPIO

Cellular internalisation of SPIO can occur via several mechanisms of endocytosis. Phagocytosis is the internalisation of cellular debris, bacteria, virus, etc., by macrophages or microglia. It is known that peripheral macrophages preferentially uptake SPIO and USPIO via this mechanism, and phagocytosis has been exploited to label macrophages endogenously with superparamagnetic contrast agent for cellular imaging of inflammation processes. This is described in further detail in section 3.7.2.3 (Bulte and Kraitchman, 2004a). Pinocytosis describes the internalisation of molecules via non-specific binding to the cell membrane into an intracellular pinosome. This is an active process and can occur in all cell types and is the likely method of SPIO uptake for most cell types including stem cells (Modo et al., 2005). Clathrin- or caveolin-mediated endocytosis rely on specific receptor-ligand or protein transport interactions on the cell membrane, and can be exploited in SPIO design to increase cellular uptake. For example, transferrin-transferrin receptor interactions lead to clathrin-mediated invagination of the cell membrane and internalisation of transferrin into intracellular endosomes (Kresse et al., 1998; Moore et al., 1998).

Cell labelling with SPIO can occur through incubation of SPIO in the culture media alone, and has been achieved in a variety of non-phagocytic cells: human, rat and mouse stem and progenitor cells, glioma cells, dendritic cells, lymphocytes, fibroblasts, cancer cells and several cell lines. Cellular uptake is proportional to the SPIO concentration in the culture media (Modo et al., 2005). Labelling by incubation can be modified to improve cellular uptake efficiency or to reduce labelling time, for example by transfection, electroporation, magnetoliposomes, and the CLIO-Tat system.

Transfection agents (TA) used are typically polycations that form complexes with the SPIO through electrostatic interactions and facilitate SPIO binding to the cell membrane, initiating endocytosis of the TA-SPIO complex (Politi 2007). A number of commercially available TA have been successfully used to increase SPIO uptake (FuGene, lipofectamine, Polyfect, etc), as well as poly-L-lysine and protamine sulphate (Arbab 2004).

Protamine sulphate is an attractive TA for cell labelling and cellular imaging because it has a higher transfection efficiency than poly-L-lysine (Cornetta and Anderson, 1989; Sorgi et al., 1997), and has FDA approval for administration to humans. It is commonly used to reverse heparin anticoagulation, but has also been used as a contrast agent in clinical gene therapy trials (Porter et al., 1998; Cornetta and Anderson, 1989). In conjunction with the SPIO Endorem which is also licensed by the FDA, cellular labelling with the Endorem-protamine sulphate complex (termed FePro) has a high possibility of translating to the clinic for application in cellular therapy clinical trials. The FePro complex has been tested for cell viability in several cell types and demonstrated to be well-tolerated (Arbab et al., 2003; Arbab et al., 2004; Arbab et al.,

2005b). We investigate the cytotoxicity and effects on NPC behaviour of FePro in Chapter 4.

Cell labelling through electroporation is less favoured as this method is not well tolerated by many cell types, and can decrease cell viability (Suzuki et al., 2007). This method involves generating transient pores in the cell membrane by applying an electrical current to the cells. Material such as DNA or MRI contrast agents can then enter the cell via these pores. Walczak et al describe successful magnetoelectroporation in the C17.2 neural stem cell line, with minimal effects on cell viability (Walczak et al., 2006). Magnetoliposomes are SPIO within liposomes. The liposome exterior facilitates cell internalisation (Bulte and Kraitchman, 2004a; De and Joniau, 1988), and has been used in several cell types.

The CLIO-Tat system links iron oxide particles to peptides with membrane translocation properties, to improve particle internalisaion. The human immunodeficiency virus-1 transactivator transcription (HIV-1 Tat) protein has been conjugated with cross-linked iron oxide particles (CLIO) to form the CLIO-Tat complex (Josephson et al., 1999; Lewin et al., 2000). Cell labelling with the CLIO-Tat system has been shown to be increased 100-fold compared to using iron oxide particles alone. The FITC fluorophore has also been conjugated to the CLIO-Tat complex to form a bimodal contrast agent (Pittet et al., 2006).

3.7.2.2. Cellular imaging with superparamagnetic contrast agents

The large T_2* relaxivity of the superparamagnetic contrast agents increases the sensitivity greatly over paramagnetic agents, and cellular detection has been achieved at the single cell level in *in vitro* systems (Shapiro et al., 2006b). Sensitivity is dependent on the concentration of the label within the cell, as well as the field strength of the system and the imaging sequence used. It has been estimated that approximately 1.4-3.0 pg iron per cell is required for detection. By contrast, unlabelled cells contain 0.1pg of endogenous iron (Arbab and Frank, 2008).

Several studies have successfully labelled stem cells and monitored them after transplantation *in vivo* over a period of time (Bulte and Kraitchman, 2004a). Cellular imaging in the brain was first described by Norman and Hawrylak, who transplanted fetal neural progenitor cells labelled with ferrite particles into the normal adult brain, and detected transplanted cells with MRI (Hawrylak et al., 1993). Hoehn *et al* (Hoehn et al., 2002) demonstrated that cells could be labelled with USPIO, transplanted into the ischaemic brain, and their response to ischaemia imaged. Immortalised neural stem cells were transplanted in the contralateral hemisphere and observed to migrate into the ischaemic hemisphere via the corpus callosum over a period of weeks using MRI. Zhang and Guzman report monitoring C17.2 neural stem cell migration (Guzman et al., 2008) or primary neural progenitor cells (Zhang et al., 2003) after cerebal ischaemia by SPIO labelling.

In vivo cellular imaging with MRI has been achieved in other models of neurodegenerative disorders, for example EAE (Ben Hur et al., 2004; Ben Hur et al., 2007; Pluchino et al., 2003); Parkinson's disease (Savitt et al., 2006) and brain tumours (Hakumaki et al., 2002; Zhang et al., 2004d). Recently, MRI contrast agents have been used to label the endogenous population of stem cells in the SVZ of the adult rat, and to track their normal migration through the RMS to the olfactory bulb (Shapiro et al., 2006a; Sumner et al., 2009).

There are many limitations to stem cell imaging using MRI contrast agents. As with other cellular markers, issues surrounding contrast agent toxicity and labelling efficacy are important to ensure that cells, once labelled, do not alter their molecular identity and normal behaviour. The negative contrast can be difficult to discriminate from other image artefacts. *In vivo* quantitation is difficult, as signal is dependent on sequence parameters, and not directly proportional to iron oxide concentration. Cellular resolution and adequate signal must be achieved *in vivo* for cellular tracking studies. To date, single-cell resolution has only been achieved *in vitro* (Shapiro et al., 2006b). Cell tracking in injury models is also complicated by the presence of macrophages. If a labelled cell dies in this situation, leaked contrast agent from the cell may be phagocytosed by surrounding macrophages, and these events would be indistinguishable on MRI images. However, Guzman *et al* were able to distinguish between living and non-living contrast agent-labelled neural stem cells, where cell death resulted in increased T2* signal over time, indicating a reduction in contrast agent at the implantation site (Guzman et al., 2007).

3.7.2.3. Macrophage imaging

SPIO particles with particle size of 200 nm can be rapidly internalised *in vivo* by phagocytic cells, including circulating macrophages, which take up the nanoparticles and store them in cytoplasmic vesicles (Raynal et al., 2004). Smaller USPIO have a longer plasma half-life. Macrophages have been shown to upregulate the transferring receptor TfR-1 and ferritin following uptake (Pawelczyk et al., 2008).

SPIO and USPIO uptake by macrophages has been exploited to investigate the peripheral immune response in a number of models of neurodegenerative diseases including cerebral ischaemia and EAE. In cerebral ischaemia, macrophage infiltration into the lesion and boundary zone was observed from 24 hours, where negative T_2 contrast was observed against positive T_2 oedema (Kleinschnitz et al., 2003; Rausch et al., 2001; Rausch et al., 2002; Schroeter et al., 2004). Peak infiltration was estimated at 5-8 days post-ischaemia (Kleinschnitz et al., 2003). USPIO accumulation occurred outside of the stroke lesion, which may predict the area of delayed neuronal death (Rausch et al., 2002). Saleh *et al* also described USPIO-macrophage accumulation in human stroke patients (Saleh et al., 2004). Macrophage accumulation has been observed in EAE at sites of inflammation and blood brain barrier breakdown (Berger et al., 2006; Dousset et

al., 1999; Floris et al., 2004).

3.8. Other Imaging Modalities for Cellular Imaging

As discussed, MRI has high spatial resolution, but relatively low sensitivity and signal to noise. MRI can also simultaneously integrate cellular imaging with anatomical and physiological imaging. Other imaging modalities have been used for cellular imaging with superior sensitivity, at the expense of spatial resolution.

Optical or bioluminescence imaging has been used to image neural stem cell CNS transplants (Bradbury et al., 2007; Shah, 2009; Ogawa et al., 2009), including in a model of cerebral ischaemia (Kim et al., 2004) and endogenous neural stem cells (Reumers et al., 2008). These studies typically involve lentiviral transduction of cells to express the firefly luciferase gene under the promoter of a gene of interest. Firefly luciferase spontaneously generates light as a byproduct of an enzymatic reaction, and this can be detected by an ultra-sensitive CCD camera. Very little light is generated by the luciferase reaction, and the CCD camera, while highly sensitive to light, has low spatial resolution. An additional limitation is the maximum tissue depth through which signal can be detected. These can be an impediment to small animal imaging studies.

Single photon emission computed tomography (SPECT), x-ray computed tomography (CT) and positron emission tomography (PET) all require the use of high energy radiation (gamma or x-rays), which can be toxic at accumulated or high doses. SPECT uses the contrast agents Indium-III-oxine or Iodine I-123 or I-131, which can be taken up by cells but have short half-lives. SPECT/CT has been used to image the accumulation of Indium-III-oxine-labelled human embryonic and rat hippocampal stem cells in the brain following cerebral ischaemia (Lappalainen et al., 2008). The authors injected labelled cells intravenously or intra-arterially via the common carotid artery, and observed accumulation of cells in the ischaemic hemisphere after intra-arterial injection. Intravenously injected cells predominantly accumulated in the liver, spleen and kidneys, from immediately after injection. The SPECT/CT had relatively high sensitivity and could detect approximately 1000 labelled cells. Spatial resolution in the brain was low, however, and anatomical localisation was limited.

3.9. Iron homeostasis in the brain

Iron is present in high concentrations in the brain relative to other tissues, in particular in the subsantia nigra and globus pallidus (Gaasch et al., 2007) and has independent metabolic pathways from non-CNS tissues. Disruption of these pathways can lead to degenerative disease in the brain (Sipe 2002). Iron is an enzyme co-factor, and is involved in the synthesis of neurotransmitters

dopamine and serotonin, the formation of myelin by oligodendrocytes, the synthesis of cholesterol and other CNS lipids, as well as as in the mitochondria (Sipe et al., 2002). Physiologically, iron can exist in two states, as ferrous (Fe2+) or ferric (Fe3+) iron, and systemic and CNS iron paythways are tightly, but independently, regulated.

Iron uptake from the blood stream occurs in endothelial cells of the blood brain barrier (BBB). Transferrin-bound ferrous iron binds to transferrin receptor 1 (TfR1) on endothelial cells and endocytosis occurs (Moos, 2002). Plasma transferrin is recycled back into the plasma, and iron is transported out of the endothelial cells into the interstitial fluid by the transmembrane protein ferrotportin (Rouault and Cooperman, 2006). Brain transferrin – synthesised by oligodendrocytes and the choroid plexus – binds to the interstitial iron. This active transport of iron into the brain via endothelial cells means that brain iron levels are decoupled from plasma iron levels, and plasma iron levels do not alter brain iron levels (Moos, 2002). Free iron is in excess relative to transferrin in the brain by a ratio of 2 to 1, meaning that iron-bound transferrin is saturated in the brain (Gaasch et al., 2007). Ferrous iron can be oxidised into ferric iron by the membrane protein cerulosplasmin in astrocytic end feet processes in contact with endothelial cells (Sipe et al., 2002).

Transferrin and a parallel non-transferrin mechanism of iron regulation exist in the brain. TfR1 is expressed in neurons, with regional variability in expression levels across the brain (Gaasch et al., 2007). Transferrin has been observed in the cytoplasm and lysosomes of neurons, which suggests that neurons participate in the transferrin pathway (Moos, 2002). The transferrin-iron bond is weaker in acidic environments such as the endosome, and ferrous iron is released here.

Extracellular transferrin-bound iron is excreted back into the blood via the choroid plexus, and high levels of transferrin, sythesised by the choroid plexus, are present in the ventricular CSF (Moos, 2002). This is regulated by epithelial cell control of solute movement between the CSF and systemic circulation, as the choroids plexus vasculature is different from the rest of the CNS in that it has fenestrated blood vessels instead of a tightly regulated blood brain barrier (Carbonell and Rama, 2007).

Ferritin is an iron sequestration protein, which is the main source of iron within cells. The ferritin protein is a hollow spherical shell with 24 subunits. Heavy ferritin is the catalytically active ferroxidase subunit that oxidises ferrous Fe2+ into ferric Fe3+ iron for storage as a solid crystalline nanoparticle in the ferritin core. Ferritin can encapsulate 2000-4500 iron atoms (Carbonell and Rama, 2007). The light ferritin subunit is involved in mineralization of iron in the ferritin core. Ferritin protein synthesis has been observed in neuronal and glial cell bodies. However, no TfR1 or transferrin has been identified in glial cells. Ferric iron is reduced to ferrous iron on release from the ferritin core.

Excess free iron present in the interstitial space can bind to other proteins or low molecular weight molecules such as citrate or phosphate. Oligodendrocytes and neurons express divalent

metal transporter-1 (DMT1) on the cell membrane, which transports free iron into intracellular endosomes (Carbonell and Rama, 2007; Gaasch et al., 2007; Sipe et al., 2002). Within the neuron, free and ferritin-bound iron can be transported along axons, and the iron transport protein ferroportin is expressed at the synapse, suggesting iron transport out of neurons occurs at the synapse (Rouault and Cooperman, 2006). Brain iron pathways are discussed further in Chapter 4, in relation to ischaemic environments and interactions with iron oxide from an MRI contrast agent source.

Constitutive expression of ferritin, transferrin, or both of these genes in cells results in increased uptake of endogenous iron from the blood pool or extracellular space (Deans et al., 2006; Genove et al., 2005). This represents an interesting crossover between MRI and genetic studies and may become a valuable tool in transgenic imaging, and with high levels of extracellular free and transferrin-bound iron, the brain is an ideal organ for these studies. There are several advantages to this genetic strategy over conventional MRI contrast agents, particularly the possibility of integration into the cellular genome in cell transplant studies, or as an in vivo marker of gene expression in lineage tracing transgenic studies. Overexpression of ferritin or transferrin has been achieved by adenoviral and lentiviral transduction (Cohen et al., 2005; Deans et al., 2006; Genove et al., 2005).

4. *Investigation of cell labelling with ferumoxides and the evolution of MR contrast and in a model of cell transplantation in cerebral ischaemia*

4.1. Introduction

Stroke remains a common cause of mortality and disability worldwide, with few effective treatments available. Cerebral ischaemia, caused by the reduction of blood flow in a cerebral artery, is the most common type of stroke, accounting for 80% of strokes. Cellular therapy is an emerging and promising avenue for treatment of cerebral ischaemia. Several experimental studies have demonstrated that treatment with stem cells after an ischaemic event improves neurological score and behavioural recovery, and can reduce infarct volume (Arvidsson et al., 2002; Kokaia and Lindvall, 2003; Lindvall and Kokaia, 2006). These findings have led to a small number of clinical trials of cellular therapy in stroke patients, with only modest effects on neurological outcome and motor skill recovery observed (Aarum et al., 2003; Bang et al., 2005; Kondziolka et al., 2003; Kondziolka et al., 2000; Savitz et al., 2005). It is clear that further optimisation of cell type and delivery, and a greater understanding of the behaviour of engrafted cells is required for improved therapeutic outcome.

For cell replacement, the lineage commitment of stem cells plays an important role in their differentiation potential after engraftment into injured tissue. Recent research has demonstrated that fetal telencephalic neural progenitor cells (NPC) are able to migrate towards the ischaemic infarct, differentiate into neurons in the peri-infarct area, and can improve behavioural recovery (Abrous et al., 2005; Darsalia et al., 2007; Ishibashi et al., 2004; Kelly et al., 2004; Lee et al., 2007; Takahashi et al., 2008; Zhang et al., 2009; Zhu et al., 2005). Developmentally, these radial glia-like cells give rise to the cortical neuron layers in the normal developing embryo, and may have the appropriate migratory capacity and neurogenic potential to give rise to neurons after engraftment into host injury tissue.

Cellular imaging with MRI contrast agents can be used to monitor the distribution of transplanted cells in models of cerebral ischaemia. Cells are labelled *in vitro* with iron oxide- or gadolinium-based compounds prior to engraftment, and generate contrast on MRI images *in vivo*. Hoehn *et al*.. demonstrated that C17.2 immortalised cerebellar stem cells could be labelled with the iron oxide-based agent Sinerem (Hoehn et al., 2002), and subsequently migrate into the infarcted area from the contralateral hemisphere. Modo *et al*.. demonstrated similar results with MHP36 immortalised hippocampal stem cells and a gadolinium-based contrast agent (Modo et al., 2002a; Modo et al., 2004).

As yet, no MRI contrast agents have been approved for use in clinical trials of cellular therapy in stroke or other disease. Characterisation of the effect of MRI contrast agent labelling on stem

and progenitor cells is essential prior to use in a clinical setting. Previous studies have described a contrast agent complex comprising the ferumoxide Endorem and the transfection agent protamine sulphate, both of which have FDA approval for use in humans (Arbab et al., 2004; Arbab et al., 2005b; Panizzo et al., 2009). Endorem is a dextran-coated superparamagnetic iron oxide agent, and can form a complex with the polycationic protamine sulphate – the FePro complex. In previous studies it has been shown to have little effect on cell viability (Arbab et al., 2005b).

The aim of this study was to assess whether neural progenitor cell labeling and *in vivo* imaging could be optimized by using the FePro complex to label cells. We assessed the effect of FePro labelling on fetal neural progenitor cell (NPC) metabolism, proliferation and differentiation capacity. FePro-labelled NPC were engrafted into the ipsilateral parenchyma at 48 hours post-ischaemia and monitored over 4 weeks using MRI. Assessment of NPC viability demonstrated no difference in the behaviour of FePro-labelled NPC compared to unlabelled NPC. Furthermore, cells could proliferate and differentiate into neurons, oligodendrocytes and astrocytes. *In vivo*, we observed the evolution of hypointense T2 contrast in the ischaemic striatum over several weeks in both control and FePro-NPC engrafted animals. We noted that from day 14 following ischaemia the observed hypointensities could be attributed to areas of labelled cells or tissue damage. We did not observe migration of FePro-NPC into the ischaemic striatum. This study highlights the need to characterise the long-term profile of cerebral ischaemia, and points to confounding image contrast at later timepoints that must be overcome in order for iron oxide based cellular imaging to be a viable method of cell tracking.

4.2. Methods

4.2.1. Neurosphere dissection and cell culture

Forebrain tissue was dissected from E13.5 CD1 mouse embryos and digested in 1X trypsin with DNase for 7 minutes at 37°C. Cells were washed in trypsin inhibitor and EBSS, and plated in 6 well culture dishes. Proliferation medium contained DMEM:F12 with glutamax (Invitrogen), N2 supplement (GIBCO), 10 ng/ml EGF (Peprotech), 20 ng/ml FGF-2 (Peprotech), 0.05% heparin and 1% Penicillin-Streptomycin. Cells were incubated at 37°C with 5% CO_2, and medium was replaced 24 hours after dissection. Cells were passaged 7 days after dissection once neurosphere formation had occurred, and replated into 6 well culture dishes. NPC were passaged every 7 days. For each assay, NPC from the same litter and passage number (passage 2 or 3) were used.

4.2.2. ST14A cell culture

Cells were cultured as described. The ST14A cell line was established by immortalisation of fetal

striatal cells through retroviral transduction of the SV40 Large T Antigen oncogene (Cattaneo 1998). The cells proliferate at 33°C, and proliferation is inactivated at 39°C. Cells were cultured on adherent flasks in DMEM (Invitrogen) with 10% foetal calf serum and 1% Penicillin-Streptomycin. Cells were incubated at 33°C with 5% CO2 and 100% humidity. Cells were passaged every 48 hours, using 1X Trypsin-EDTA to detach cells from adherent flasks, collected and centrifuged in 10ml culture medium, replated 1:3 in fresh culture medium, and returned to the incubator.

4.2.3. Cell labelling with contrast agent

Endorem: Cells were incubated with 500 μg/ml Endorem for 24 hours in cell culture medium to allow contrast agent internalisation.

FePro complex: Endorem was incubated with protamine sulphate in a ratio of 9:5 for 10 minutes to form the FePro complex, to make a final concentration of 100 μg/ml Endorem and 10 μg/ml protamine sulphate in culture medium. The FePro complex was added to proliferation medium without heparin, and cells were incubated in FePro-proliferation medium for 24 hours. Cells were washed in EBSS with heparin to wash excess FePro and dissociate the extracellular complex.

For adherent ST14A cells, cells were washed after labelling by replacing culture medium with Earl's balanced salt solution without Ca2+ or Mg2+ (EBSS) to remove and dilute the contrast agent. This was repeated three times, then cells were trypsinised and passaged as described.

For NPC labelling, neurospheres at 6 days after passage were dissociated as described above, and replated into medium containing Endorem or FePro contrast agent for cell labelling. NPC were incubated with contrast agent for 24 hours, then culture medium was diluted in 1:5 in EBSS and centrifuged to retain the pellet of labelled cells and discard the excess contrast agent and medium. The dilution and centrifugation process was repeated three times to wash cells. NPC were dissociated as described above for replating or use in intracerebral microinjections.

4.2.4. Cellular viability assays

Cells were incubated with Endorem, FePro, or no contrast agent (control) for 24 hours. Cells were washed three times, trypsinised, and replated into 96 well plates at a density of 10^4 cells per well for cell metabolic activity assays as a measure of cell viability.

MTT assay: MTT (3-[4,5-dimethylthiazol-2-yl]-2,5-diphenyl tetrazolium bromide; Sigma) is an indicator dye that measures the metabolic activity and proliferation of cells. Soluble MTT is mild-yellow in colour in the absence of viable cells. Purple MTT formazan crystals are formed when the tetrazolium component of the MTT molecule is cleaved by mitochondrial dehydrogenase enzymes during normal metabolic activity. The crystals are insoluble and retained within viable

cells. They can be dissolved and quantified as a measure of cell metabolism using a spectrophotometer.

Cells were replated into 96 well culture plates at a density of 10^4 cells per well, and 8 wells per treatment, in 100 ul growth medium with 10% MTT. Cells were incubated for 4 hours, then culture medium was removed and replaced with 100 ul per well MTT solvent 0.04M HCl in isopropanol. Plates were left on a gyratory shaker for 30 minutes to allow the formazan crystals to dissolve. Absorbance was measured at 570nm using an ELISA microplate spectrophotometer. Three readings were taken for each assay, and the assay was repeated twice.

Alamar Blue assay: Alamar Blue is a non-toxic oxidation-reduction (redox) indicator dye used to quantify cell metabolism and growth. Reduction of NADH occurs during cell metabolism and growth, and the Alamar Blue dye changes colour in a reduced environment. This change is exploited to measure the metabolism of cells under various conditions.

Labelled cells were replated into 96-well plates at a density of 10^4 cells per well, and 8 wells per treatment, in 100 μl growth medium with 10% Alamar Blue solution. Cells were incubated for 4 hours, then absorbance was measured at 570nm using an ELISA microplate spectrophotometer. Three readings were taken for each assay, and the assay was repeated twice.

Trypan blue assay: The Trypan Blue exclusion dye is internalised by non-viable cells that have lost cell membrane integrity, and all non-viable cells in a sample appear blue. Viable cells exclude the dye and appear normal and colourless under a light microscope.

Cells were resuspended 10:1 in 0.5% Trypan Blue, and transferred to a haemocytometer for counting. Under a light microscope, non-viable blue-stained cells and total viable cells were counted. For each assay, two samples were counted for each treatment group, and the assay was repeated three times.

4.2.5. Cellular proliferation assays

To assess the neurosphere-forming capacity of NPC following treatment with MRI contrast agents, cells were plated at a density of 10^4 cells per ml in neurosphere proliferation medium. Cells were plated into 96 well plates, where each well contained 100 μl of proliferation medium and 1000 cells. After 5 days in culture, the number of neurospheres generated per 10^3 cells was counted, and neurosphere diameter was measured. For each assay, a minimum of 8 wells per treatment group was counted, and each assay was repeated twice.

4.2.6. Prussian blue stain for iron in neurospheres

In some assays, neurospheres were also stained with the Prussian Blue stain for iron. NPC cultured at a density of 10^4 cells per ml for 7 days were transferred to polyornithine-coated coverslips in 24 well plates for one hour to allow neurosphere adherence to coverslips. NPC were

then fixed in 4% PFA in PBS for 10 minutes, incubated in 6% hydrochloric acid and 4% potassium ferrocyanide for 20 minutes, then washed in PBS washed and mounted.

4.2.7. Cellular differentiation assays

Neurospheres at 6 days after passage were transferred onto polyornithine-coated coverslips in 24 well plates, and cultured in differentiation medium containing DMEM:F12 with B27 medium (Invitrogen) and 10% foetal calf serum for 6 days to allow differentiation to occur. Differentiated neurospheres were fixed in 4% PFA at 4^{o}C for immunohistochemical analysis of cellular differentiation.

For immunocytochemistry, coverslips were incubated in blocking solution (10% goat serum with 0.1% Triton-X) for 30 minutes, then incubated in primary antibody in blocking solution for one hour at 37oC: mouse anti-β3-tubulin (1:1000, Promega); rabbit anti-GFAP (1:1000, Chemicon); monoclonal O4 IgM (1:2, generous gift Prof Rhona Mirsky). Coverslips were washed three times in PBS, then incubated with secondary antibody for 30 min at 37oC cy3-conjugated goat anti-mouse (1:100); Alexa 488-conjugated goat anti-rabbit 1gG (1:1000, Invitrogen); and Alexa 680-conjugated goat anti-mouse IgM (1:1000, Invitrogen). Coverslips were washed in PBS and mounted onto slides with Citifluor mountant medium for fluorescence microscopy. Sections were photographed using a Zeiss Axiophot microscope, OpenLab imaging software and Jenoptik digital camera.

4.2.8. Measurement of iron using super quantum interference device (SQUID)

Contrast agent-labelled cells were fixed in 4% PFA, and washed in PBS with heparin to remove excess contrast agent. Cells were transferred to gelatin pill caps containing cotton wool, at a density of 1.25 X 10^{6} per gel cap. Iron content was measured using SQUID and amount of iron per cell was calculated.

Sample magnetization was measured over a range of magnetic field strengths at 300K (Kelvin; room temperature) and 10K, and hysteresis loops were plotted. To calculate the amount of iron in each sample, remanent magnetization and saturation magnetization of the samples were compared to the magnetization of a sample with Endorem alone, that has a known iron content against which cell magnetisation can be calibrated. Remanent magnetization is the magnetization at 0 field strength, and saturation magnetisation is the maximum magnetization of the sample. To calculate the iron content based on saturation magnetisation, the diamagnetic component of the sample hysteresis curves was subtracted. The diamagnetic signal is produced by organic material in the cells, and is not a component of the Endorem-only hysteresis curve. At remanence magnetization, diamagnetism is 0, therefore no subtraction is required.

4.2.9. *Middle cerebral artery (MCA) occlusion*

All procedures were in accordance with the UK Animals (Scientific) Procedures Act of 1986. Eleven 250g male Sprague-Dawley rats (Charles Rivers UK) were used. Animals were anaesthetised with 2% isofluorane and 100% O_2. Temperature was monitored with a rectal probe. The right common carotid artery was exposed. A sterile 4-0 suture with an epoxy resin tip (Araldite®, Huntsman Advanced Materials) was inserted into the carotid artery and advanced 17mm into the brain to occlude the MCA for 30 minutes. Following occlusion, the MCA was reperfused, the suture removed and animals recovered.

4.2.10. *Intracerebral microinjections of FePro-labelled cells*

Animals were anaesthetised with 2% isofluorane and 100% O_2, and their head secured and aligned in a stereotactic frame. Animals were injected with 1.25 X 10^5 in a maximum of 3µl FePro-labelled cells at 0.2l min^{-1} into the right corpus callosum, 48 hours after MCA occlusion surgery. The coordinates used were AP +1.0, ML -0.30; DV -0.2 to Bregma. The injection needle was left in place for 10 minutes following injection, slowly removed and the animals recovered.

4.2.11. *MRI*

For *in vitro* MRI, contrast agent-labelled cells were washed and fixed in 4% PFA. Cells were transferred to 250µl Eppendorf tubes and centrifuged to produce a cell pellet. Eppendorfs were placed in a custom-made rack inside a 50 ml falcon tube filled with 2.5 mg/ml copper sulphate solution. Cell pellets were imaged using a 2.35T system. A 2D spin echo sequence was used with the following parameters: TR = 1500 ms; TE = 80 ms; FOV 25 mm; slice thickness 1mm.

For *in vivo* MRI, animals were anaesthetised with 2% isofluorane and 100% O_2, and secured on a stereotactic probe. Animals were imaged using a 2.35T system. A 2D gradient echo (T2*-weighted) sequence was used with the following parameters: TR = 500ms; TE = 30ms; FOV 30mm; 128 X 128 voxels; 1mm slice thickness; and 16 averages. A 2D spin echo (T2-weighted) sequence was also used: TR = 1500ms; TE = 120ms; FOV 30mm; 128 X 128 voxels; slice thickness 1mm; 16 averages. Animals were imaged at 3, 7, 14, 21, and 28 days post MCA occlusion surgery.

4.2.12. *Perfusion Fixation*

Following MRI, animals were transcardially perfused with 0.9% saline at 4°C then perfused fixed with 4% PFA. Brains were removed from the skull and transferred to 30% sucrose in PBS for 48 hours until no longer buoyant, then frozen and stored at -80°C for tissue processing.

4.2.13. *Histology and immunohistochemistry*

Coronal brain sections of 30 μm thickness were taken on a cryostat. For Prussian blue staining, sections were incubated in 6% hydrochloric acid and 4% potassium ferrocyanide for 20 minutes, then washed in PBS. For fluorescence immunohistochemistry, sections were incubated in 10% foetal calf serum with 0.1% Triton-X (Sigma) for 30 minutes, followed by anti-doublecortin (1:50), anti-nestin (1:100), or anti-GFP (1:1000, Chemicon) in 10% foetal calf serum with 0.1% Triton-X, overnight at 4°C. Sections were washed in PBS, and incubated in cy3-conjugated secondary antibodies with 1:1000 Hoechst (anti-goat; anti-mouse; anti-rabbit respectively) for one hour at 37°C. Sections washed in PBS and mounted with Citifluor.

4.2.14. *Generation of cerebral ischaemia homogenate for ischaemia-conditioned medium*

The MCA occlusion surgery was performed as described. MRI was performed at 24 hours post-ischaemia using a 2D spin echo sequence to determine the lesion volume, as described. Animals were sacrificed by Schedule 1 method at 24 or 48 hours post-ischaemia. Brains were extracted and stored in L-15 medium on ice. Under sterile conditions, the area of infarct as determined by MRI was dissected from the brain. The contralateral hemisphere was used as non-ischaemic control tissue. Tissue was homogenized using a glass homogenizer, then resuspended in L-15 medium. The homogenate was filtered through a 0.4 m sterile filter to remove large debris and to sterilize. Protein content of the homogenate was calculated against an albumin standard using the Pierce BCA Protein Assay Kit.

4.2.15. *Neurosphere migration assay*

Neurospheres after two passages were used for the migration study. 96 well plates were incubated with 12.5% polyornithine for one hour at 37°C. Polyornithine is a substrate on which neurospheres adhere. Single neurospheres were transferred into individual wells of the 96 well plates, and 100 μl of control medium was added to each neurosphere-containing well. Individual neurospheres were photographed on a Zeiss AxioVert inverted microscope with a Hamamatsu digital camera and using OpenLab imaging software, then tissue homogenate or growth factors were added to the control medium. Treatment groups were as follows: 1400, 700, 300 g/ml MCAO homogenate from 24 hours time point; 1400, 700, 300 g/ml MCAO homogenate from 48 hours time point; 10 ng/ml EGF in N2 medium; 10 ng/ml FGF in N2 medium; 25 ng/ml VEGF in N2 medium. Control groups were as follows: DMEM:F12 with N2 medium; DMEM:F12 with control tissue homogenate. Neurospheres were photographed at 24 hours, 48 hours and 72 hours following treatment. Assays were repeated three times, 8 wells per assay.

4.2.16. *Data Analysis*

Data are expressed as mean +/- standard deviation. Data analysis was performed using ImageJ for MRI image analysis and neurosphere area measurements; Adobe Photoshop for microscopy image analysis, and SPSS software for statistical analysis and graphical dislplay.

For *in vitro* assays, neurosphere area was measured using ImageJ, and MCAO homogenate treatment conditions were compared to control homogenate using analysis of variance (ANOVA) contrast tests. Homogeneity of variance was assessed with the Levine test. The Tukey test was used for post-hoc analysis. Significance level $p=0.05$.

For *in vivo* lesion volume analysis, lesion volumes were expressed as total volume, volume at the central MCA territory slice, and as a percentage of the total ipsilateral hemisphere volume. The ratio of lesion volume at day 28 to day 7 was also calculated, and two-tailed independent samples t-tests were performed to test for a difference in lesion volume change between control and treatment group animals.

4.3. *Results*

4.3.1. *FePro cell labelling and viability*

The effects of iron oxide-based MRI contrast agents on cell viability were first assessed in a fetal neural stem cell line. ST14A cells were incubated with Endorem or FePro for 24 hours, and cell viability was assessed using metabolic activity assays. Figure 4.3.1.1 shows the results of the MTT and Alamar Blue assays, where data are expressed as a percentage of control unlabelled cells. No significant difference in viability was observed between Endorem, FePro and control non-treated cells for the MTT assay (ANOVA, $p>0.05$; Figure 4.3.1.1a). The Alamar Blue assay showed a significant difference between the treatment groups (ANOVA, $p=0.005$; Figure 3.1.1b), where decreased metabolic activity was observed in cells treated with Endorem, relative to control untreated cells, but no difference was observed in the FePro cells. Therefore, treatment with the FePro complex did not significantly affect cell viability of ST14A cells, whereas treatment with Endorem may have a small negative effect on cell viability. Figure 4.3.1.1c-e show Prussian Blue labeling in control, Endorem- and FePro-labelled cells, demonstrating that unlabelled cells do not contain iron oxide (Figure 4.3.1.1c), and that cells can be labeled with Endorem (Figure 4.3.1.1d) and FePro (Figure 4.3.1.1e).

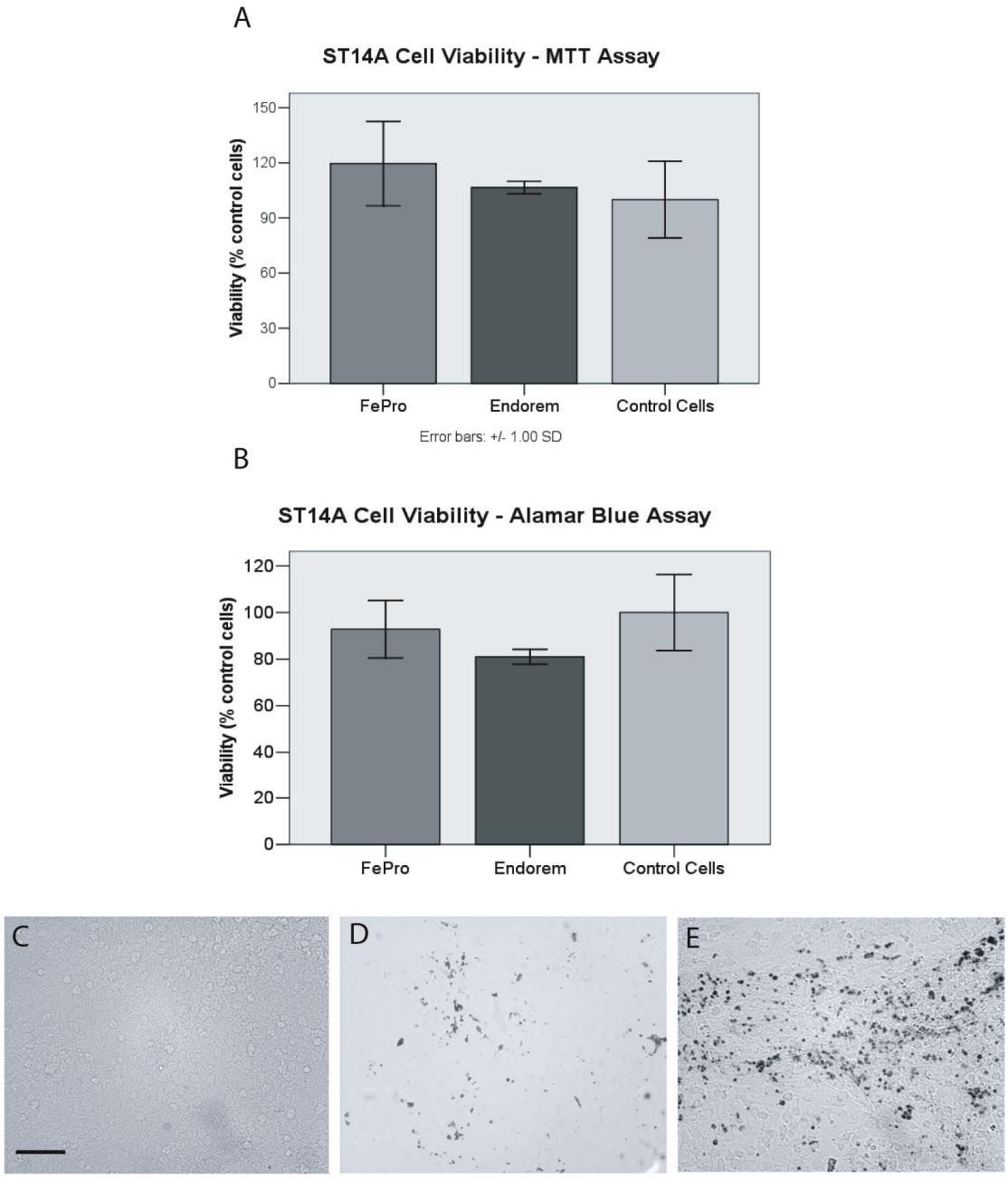

Figure 4.3.1.1 ST14A cell viability after FePro-labelling. A, MTT assay. No significant difference observed between control, Endorem-, and FePro-labelled cells after 24 h treatment with MRI contrast agent (ANOVA, $p>0.05$). **B**, Alamar Blue assay. No significant difference between FePro-labelled and control unlabelled cells. Decrease in metabolic activity of Endorem-labelled cells relative to control unlabelled cells (ANOVA, $p<0.01$). C-E, Prussian blue stain of ST14A cell monolayer. **C**, control. **D**, Endorem. **E**, FePro.

4.3.2. Superconducting quantum interference device SQUID analysis of iron uptake

Iron uptake was compared for cells incubated with Endorem or the FePro complex, using a superconducting quantum interferece device (SQUID) to quantify the amount of iron oxide present in each sample. With remanent magnetization as the reference point, cell uptake was 3.75 pg Fe/cell for Endorem-labelled cells, and 13 pg Fe/cell for FePro-labelled cells. With saturation magnetisation as a reference point, cell uptake was 4.1 pg Fe/cell for Endorem-labelled cells and 16 pg Fe/cell for FePro-labelled cells (Figure 4.3.2.1). Together, these results suggest that FePro labelling increases cell uptake of iron by 3.4-3.9 fold.

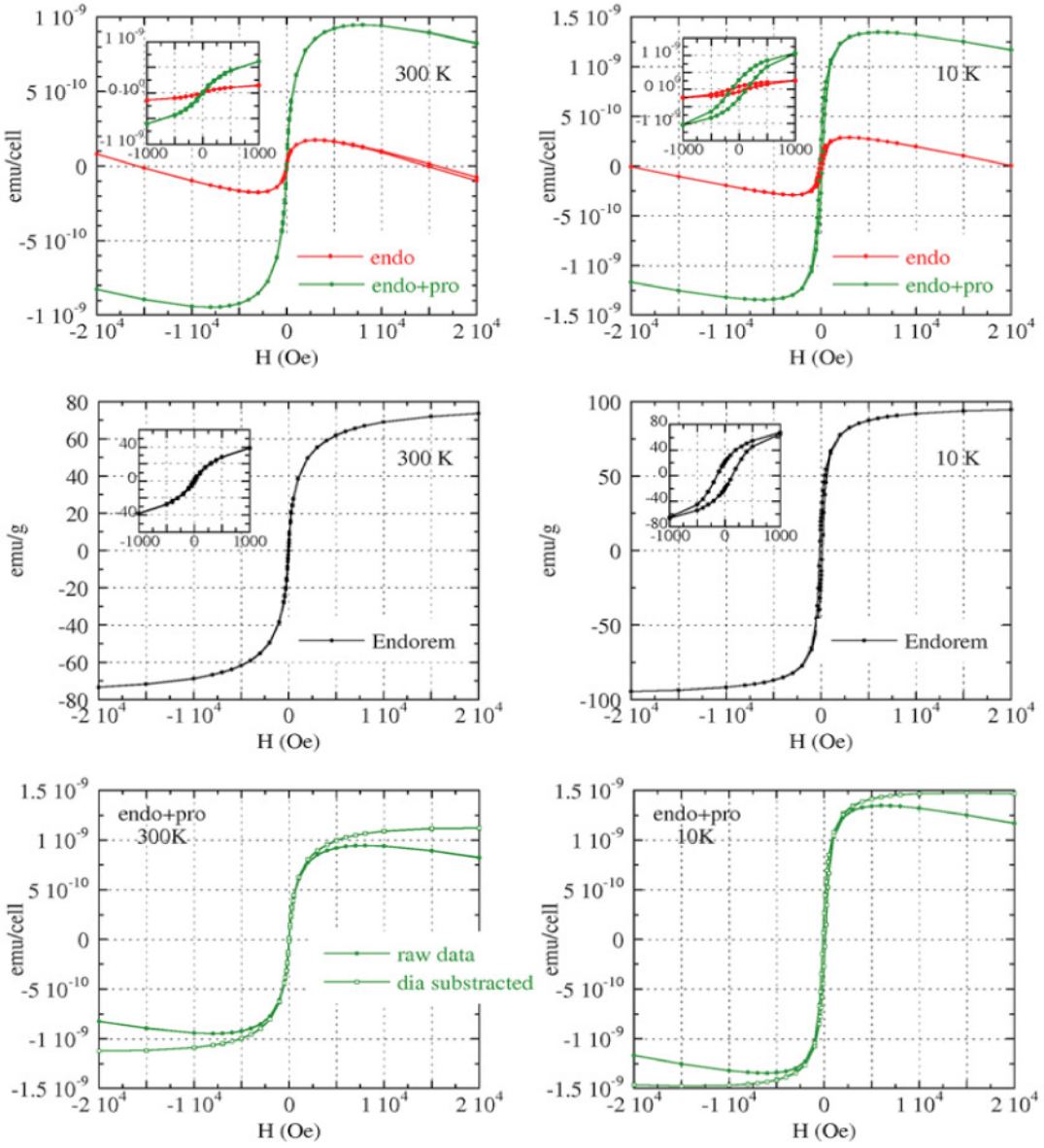

Figure 4.3.2.1Analysis of iron uptake by cells using superconducting quantum interference

device (SQUID). Hysteresis curves of Endorem- and FePro-labelled cells at 300K (Kelvin) (top left), and 10K (top right). Hysteresis curves of Endorem CA at 300K (middle left) and 10K (middle right). Hysteresis curve of FePro-labelled cells as raw data, and with diamagnetic component subtracted, at 300K (bottom left) and 10K (bottom right). FePro-labelling results in greater iron oxide uptake than Endorem labeling.

In summary, iron oxide content was greater in FePro-labelled cells than Endorem-labelled cells, suggesting the protamine sulphate increases efficiency of contrast agent uptake.

4.3.3. NPC viability, proliferation and differentiation capacity

Next, the effect of cell labelling with the FePro complex and Endorem on cell viability and proliferative capacity was assessed in primary fetal neural stem and progenitor cells (NPC). Figure 4.3.3.1a and 4.3.3.1b show the effects of Endorem and FePro on NPC viability in the Trypan Blue exclusion assay and Alamar blue assay. No significant difference between control, Endorem- or FePro-treated NPC was observed in the Trypan Blue exclusion assay (ANOVA, $p=0.91$) or the Alamar Blue assay (ANOVA, $p=0.49$), indicating that both Endorem and the FePro complex have little effect on cell viability or metabolism.

The neurosphere forming assays measured the number of neurospheres generated per 1000 cells and the average neurosphere diameter per sample, which are indicators of the number of stem and progenitor cells in the sample and their rate of proliferation, respectively. Figure 4.3.1.1c and 4.3.3.1d show the effect of Endorem and FePro on NPC proliferative capacity. No significant difference in neurospheres per 1000 cells plated was observed between control, Endorem- and FePro-labelled NPC (Figure 4.3.3.1d; ANOVA, $p=0.833$). For Endorem-labelled NPC, the mean neurosphere diameter was larger than control neurospheres (Figure 4.3.3.1c; ANOVA $p=0.001$).

Figure 4.3.3.1e and 4.3.3.1f show Prussian Blue-stained neurospheres from Endorem- and FePro-labelled NPC after 7 days in culture, respectively. The iron is distributed within the neurosphere, indicating that the contrast agent is retained within cells across cell divisions.

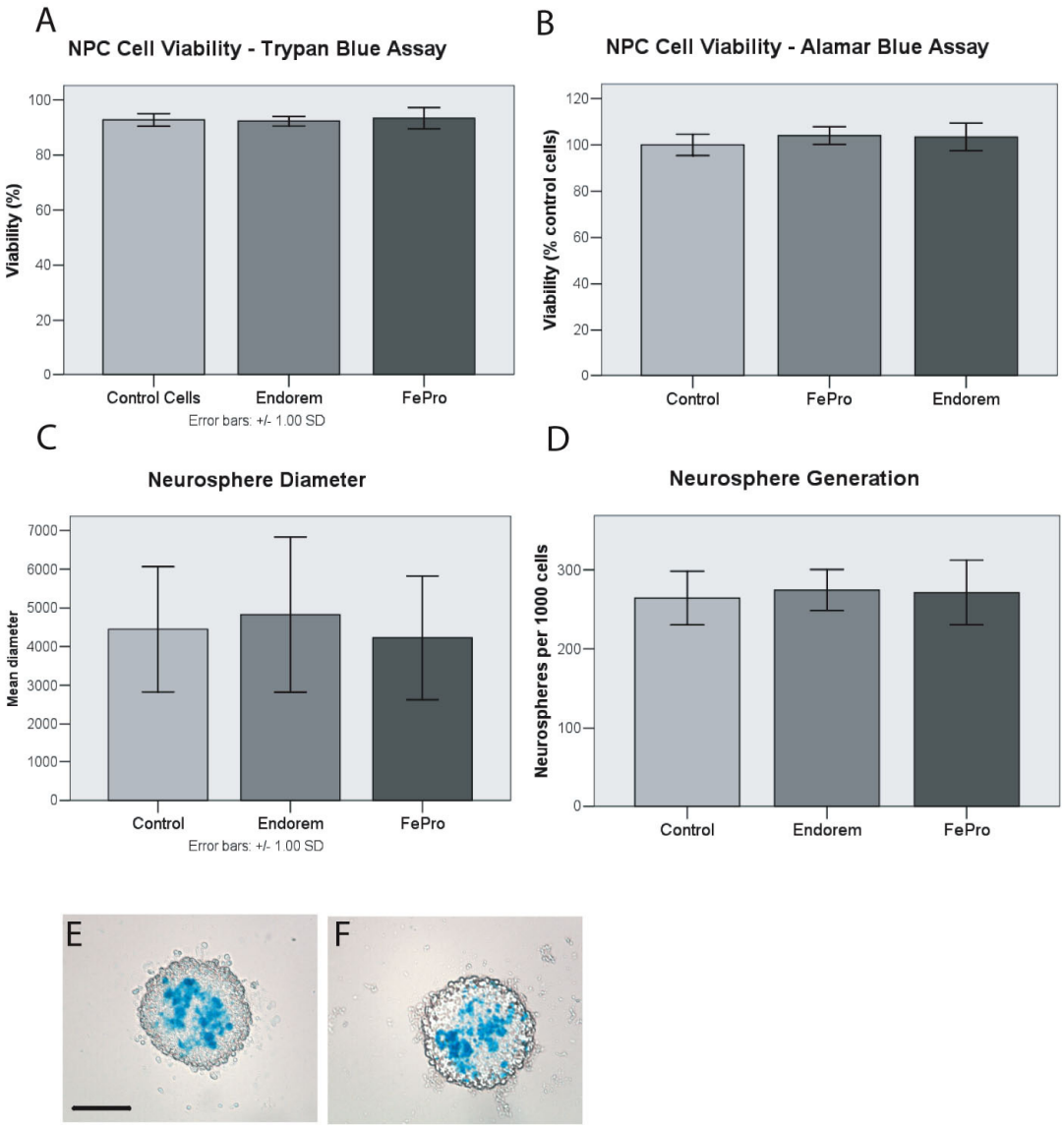

Figure 4.3.3.1 NPC viability, proliferation and differentiation capacity in control, FePro- and Endorem-labelled NPC. A, Trypan Blue assay. No significant difference in cell survival (ANOVA, p=0.91). **B**, Alamar Blue assay. No significant difference in cell metabolism (ANOVA, p=0.45). **C**, Neurosphere diameter. Neurosphere diameter of Endorem-labelled neurospheres significantly different from control unlabelled neurospheres (ANOVA, p<0.05). **D**, Neurosphere generation. No significant difference in neurosphere generation per 1000 cells (ANOVA, p=0.83). **E, F**. Prussian Blue stain for iron in Endorem (E) and FePro (F) labelled neurospheres.

4.3.4. NPC differentiation

To further characterise the effects of Endorem and FePro, the differentiation capacity of contrast agent-labelled NPC was assessed. The differentiation assay is a measure of the capacity of neurospheres to generate the cell types of neural lineage - neurons, oligodendrocytes and astrocytes. Figures 4.3.4.1a-f show that FePro and Endorem-labelled NPC can differentiate into

neurons, oligodendrocytes, and astrocytes. Figures 4.3.4.1g-h demonstrates that cells retain the contrast agent label following differentiation, as shown by the Prussian blue stain for iron. A pellet of FePro-labelled cells were imaged in a Eppendorf tube using a 2.35T MRI system, and produce hypointensity relative to control, unlabelled cells (Figure 4.3.4.1i).

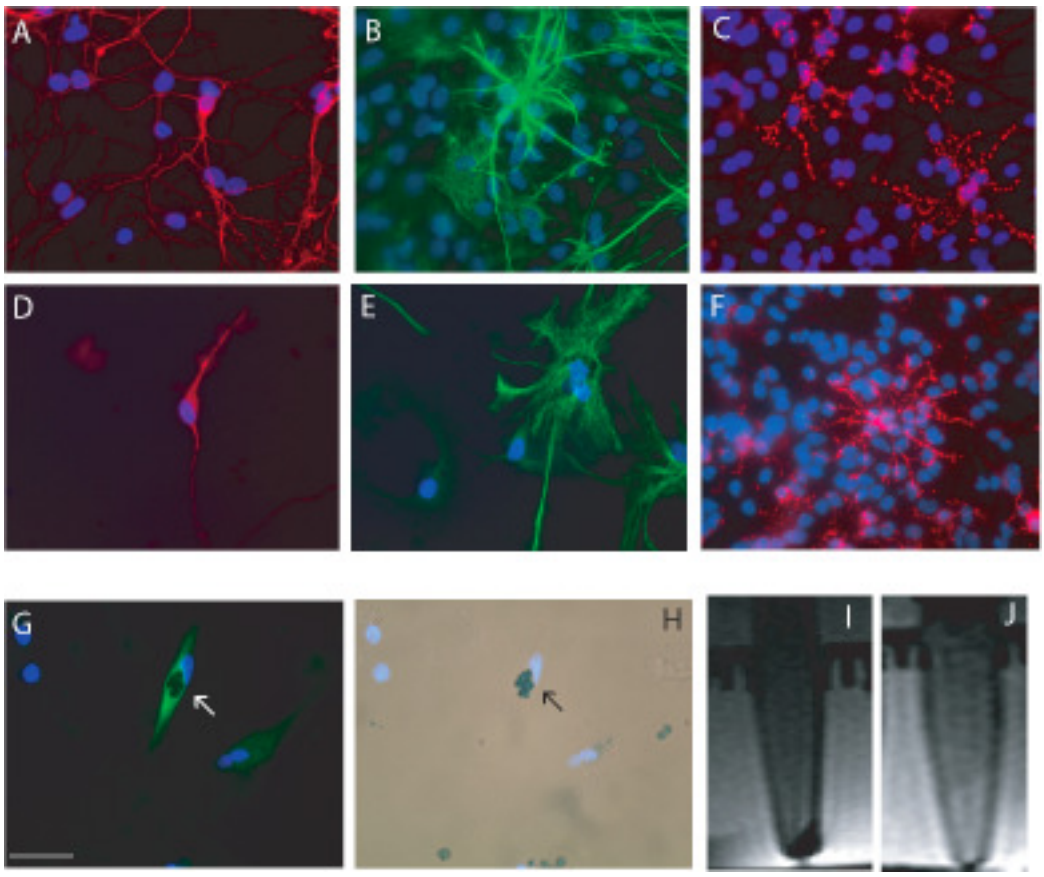

Figure 4.3.4.1 Differentiation capacity of FePro-labelled NPC. A-F. Immunocytochemistry of FePro (A-C) and Endorem (D-F) labelled neurospheres. A,D, anti-b3-tubulin (neuron, red). B,E, anti-GFAP (astrocyte, green). C,F, anti-O4 (oligodendrocyte, red). Blue, Hoescht nuclear stain. FePro-labelled neurospheres can differentiate into neurons (A,D), astrocytes (B,E), and oligodendrocytes (C,F). **G**, immunocytochemistry of FePro-labelled astrocyte (GFAP, green). **H**, corresponding light micrograph showing Prussian blue stain. **I**,**J** MRI T2-weighted image of FePro-labelled neurosphere pellet (I) and control unlabelled neurospheres (J). FePro-labelled cell pellets produce hypointensity on MRI images. Scale bars, 20um.

4.3.5. Serial MRI of cerebral ischaemia following FePro-NPC injection

Next, *in vivo* MRI imaging of FePro-labelled NPC was assessed in a model of cerebral ischaemia. FePro-labelled NPC (FePro-NPC) were injected into the ipsilateral corpus callosum 48 hours following cerebral ischaemia and animals were imaged at 3, 7, 14, 21, and 28 days post-ischaemia, to determine whether NPC could be identified and monitored over time with MRI, relative to a

control uninjected group. Figure 3.5.1a shows the temporal profile of a FePro-NPC-treated animal and control on spin echo images across the 28 day time period. The T2-weighted images revealed heterogeneous ischaemic lesions in both groups, with hypointense regions developing in the striatum and medium cortical layers, from day 7 and persisting until day 28. This lesion heterogeneity was present in all control animals as well as the FePro-NPC group. Signal intensity in hypointense ischaemic striatum regions was significantly different from corresponding contralateral region (Figure 4.3.5.2E; $p<0.001$). However, on T2*-weighted images, contrast between ischaemic and normal tissue was less apparent (Figure 4.3.5.2A-D).

To determine whether cell injections have an effect on the outcome of cerebral ischaemia, change in lesion volume over time was compared between control stroke and FePro-NPC groups. For both total lesion and MCAO territory, no significant difference in lesion volume change over time was observed (Figure 4.3.5.1b-d; ANOVA, $p=0.321$ and $p=0.136$, respectively). The ratio of ipsilateral to contralateral hemisphere volume at the SVZ level was assessed. We observed that the ipsilateral total hemisphere volume was decreased by 28 days post-ischaemia relative to the contralateral hemisphere in both groups (ANOVA $p<0.001$; Figure 4.3.5.1e), but did not observe a difference between FePro-NPC and control groups. This reduction in ipsilateral hemisphere volume over time may represent secondary, delayed neuronal death in the ischaemic hemisphere, lesion compaction, brain reorganisation or a combination of these factors.

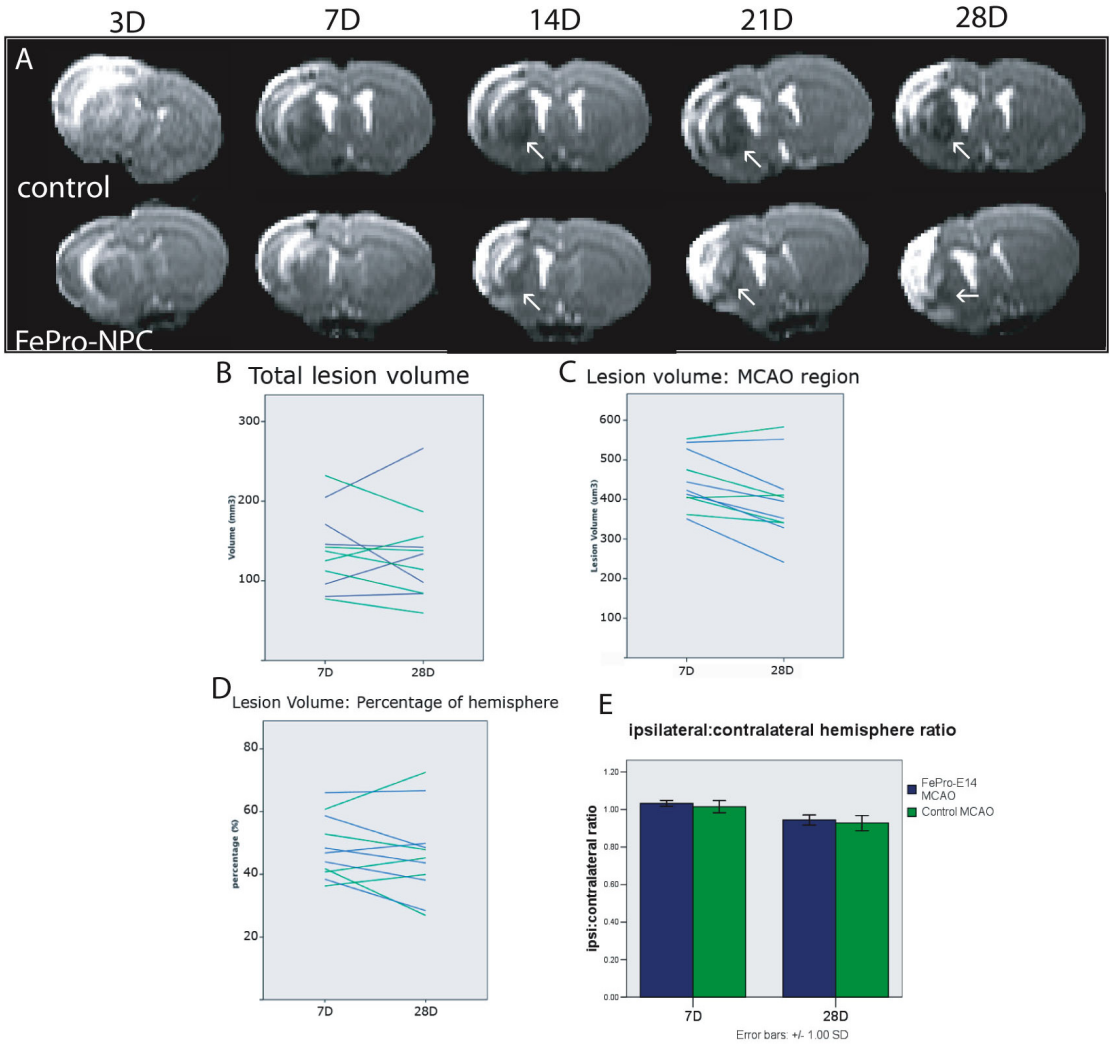

Figure 4.3.5.1 In vivo MRI. A, serial T2-weighted imaging up to 28 days post-ischaemia in FePro-NPC and control. Regions of T2 hypointensity develop in the lesion at later timepoints, and the injection site of FePro-labelled cells can be identified in the FePro-NPC group. B-E, analysis of lesion volume change at 7 days and 28 days in FePro-NPC and control. **B**, total lesion volume. No significant difference between control and FePro-NPC lesion volumes (ANOVA, p=0.921). **C**, lesion volume at MCA region. No significant difference between control and FePro-NPC lesion volumes at the MCA slice (ANOVA, p=0.577). **D**, lesion volume: ipsilateral hemisphere volume. No significant difference between control and FePro-NPC in lesion size as a proportion of ipsilateral hemisphere volume (ANOVA, p=0.922). For all graphs, variability within groups is high. **E**, ipsi:contralateral hemisphere volume. Change in ipsi:contralateral hemisphere volume ratio over time (ANOVA, p<0.0001), but no significant difference between control and FePro-NPC ipsi:contralateral hemisphere volume ratios.

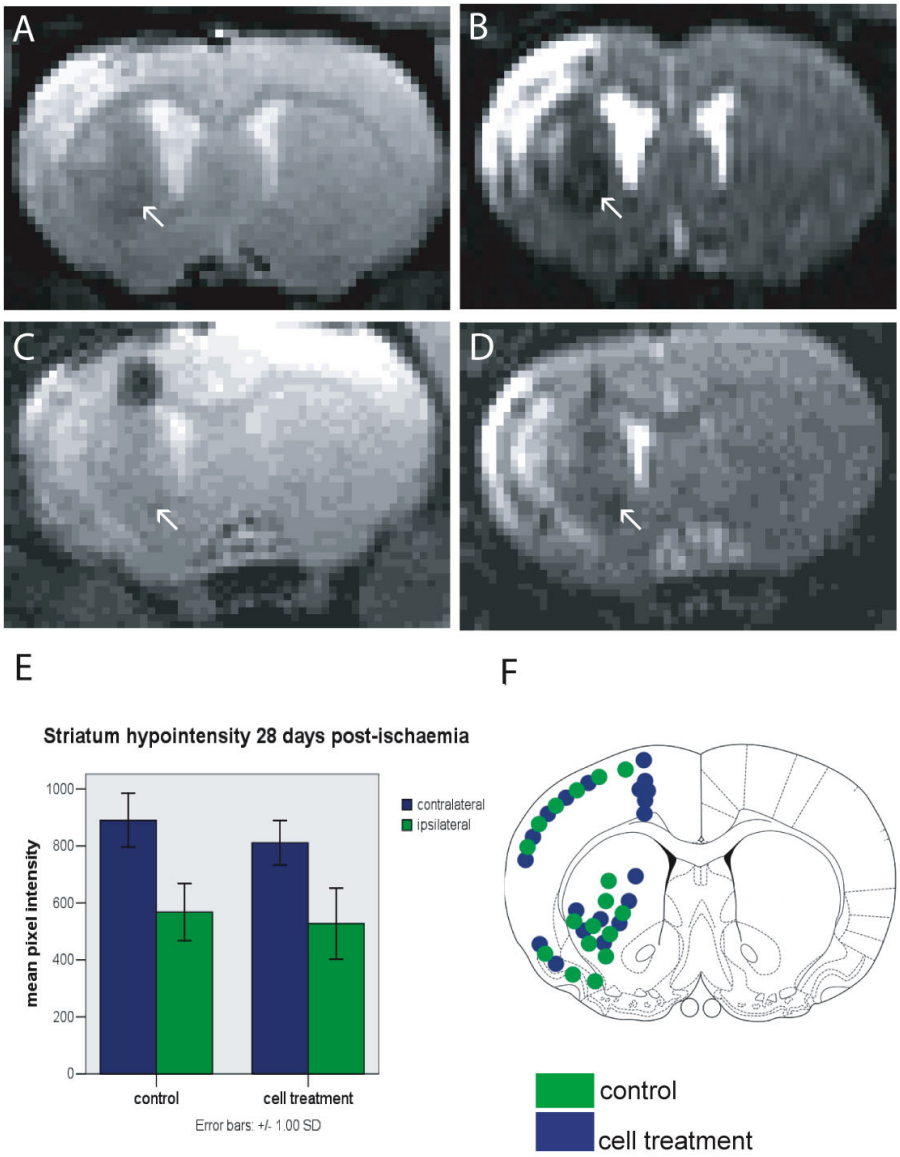

Figure 4.3.5.2Hypointensity at 28 days post-ischaemia. **A-D**, T2- (B,D) and T2*-weighted (A,C) images of MCA region in one control (A,B) and one FePro-NPC (C,D) animal. Hypointense regions within the ischaemic lesion (arrows) were observed in both T2- and T2*-weighted images, in particular on T2-weighted images. **E**, Signal intensity in regions of T2 hypointense ipsilateral striatum at 28 days post-ischaemia, and in corresponding contralateral regions in control (green) and FePro-NPC (blue) groups. Signal intensity in the ischaemic striatum was lower than in the ontralateral striatum. Signal intensity was significantly different between contralateral and ipsilateral hemispheres ($p<0.001$). **F**, Diagram of T2 hypointensity in control (green) and cell treatment (blue) groups. Composite of all imaged animals at 28 days.

4.3.6. Histological analysis

No GFP was detected outside of the injection tract in the FePro-NPC group, suggesting that no migration toward the ischaemic lesion occurred. We investigated the origin of the hypointense

signal on T2-weighted MRI images on histological sections. Iron oxide can be a source of T2 hypointensity, and we assessed its distribution in the brain in both groups with the Prussian blue stain for iron. No iron was detected in the contralateral cortex or striatum in either the control or FePro-NSC group (Figure 4.3.6.1K-L). However, in both groups, iron oxide was detected in the ipsilateral (ischaemic) striatum at the ischaemic border, and in the cortex in some animals (Fig 4.3.6.1A-D), which may indicate that factors other than Endorem are contributing to the hypointensity. Iron accumulation was detected in the mid-striatum at the lesion border, which approximates the area of hypointensity on MRI images. Additionally in the FePro-NSC group, iron oxide was detected at the injection site.

We investigated whether the MRI image hypointensity was linked to the distribution of macrophage/microglia in the brain. We observed macrophage/microglia in the infarcted cortex and striatum in both FePro-NSC and control groups (Figure 4.3.6.1g-j). The majority of macrophage/microglia were negative for Prussian blue. Prussian blue-positive cells were a mixture of OX-42-positive and OX-42-negative. No macrophage/microglia were observed in the contralateral hemisphere. In some animals, we observed red blood cells in the ischaemic striatum, which were not positive for Prussian blue (Fig 4.3.6.1M). This may represent the development of microhemorrhages within the lesion over time..

In summary, on histological sections we observed a number of possible sources of the hypointensity in the spin echo and gradient echo MRI images. We observed the accumulation of iron oxide at the lesion boundary, associated with blood vessels, and red blood cells in the ischaemic striatum. The contribution these sources may make to hypointensity on MRI images is addressed in detail in the Discussion section.

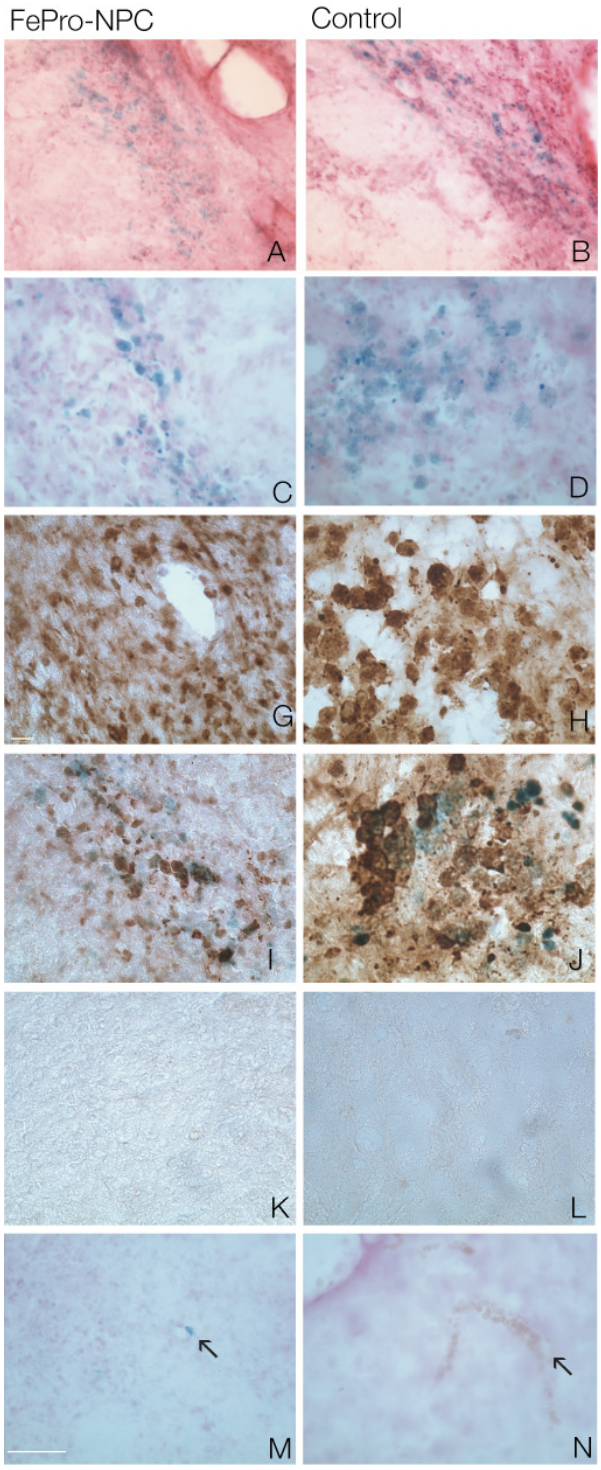

Figure 4.3.6.1Histological analysis at 28 days at the ipsilateral striatum. **A,b**, Prussian blue stain for iron and hematoxylin-eosin staining at the ipsilateral striatum. Iron oxide detected in the ischaemic lesion. **C,D**, Prussian blue stain with nuclear fast red counterstain in the ipsilateral striatum. **G-J**, OX-42 immunohistochemistry stain for macrophages, and Prussian blue stain for iron. Prussian blue-positive and –negative macrophages are present at the ischaemic lesion. K,L OX-42 immunohistochemistry and Prussian blue stain for macrophages in the contralateral hemisphere. No macrophages or iron oxide were observed in the striatum or cortex of the contralateral hemisphere. **M**, Prussian blue stain for iron at blood vessel (arrow). **N**, Prussian blue-negative red blood cells (arrow). Scale bars, 30um.

4.3.7. E14 neurosphere response to cerebral ischaemia

We did not observe NPC migration into the ischaemic lesion *in vivo* on MRI images or histological sections. Although fetal NPC migration has been previously reported, one possibility is that the NPC were not responsive to the ischaemic environment. We therefore assessed the migration capacity of NPC *in vitro*, and developed an assay to assess the response of NPC neurospheres to cerebral ischaemia. The migratory capacity of the NPC was assessed at two different timepoints – 24 and 48 hours – representing different inflammatory environments following ischaemia. Tissue homogenates were generated from the brain at 24 and 48 hours post-ischaemia.

Figure 4.3.7.1 demonstrates the migratory response of NPC to 24 hr and 48 hr ischaemic tissue. Migration in both 24 hr and 48 hr post-ischaemia groups was significantly different to control migration (ANOVA, $p<0.001$). Post hoc analysis showed that at 24 hr, the 1400 μg/ml concentration, and at 48 hr the 300 and 700 μg/ml concentrations, were significantly different from control non-ischaemic homogenate. Figure 4.3.7.1b shows the percentage of neurospheres per assay that respond to homogenate or growth factors by migration. The majority of MCAO homogenate treated neurospheres migrate after 72 hours of treatment, whereas few neurospheres treated with contralateral hemisphere homogenate or N2 medium respond by migration after 72 hours. That not 100 per cent of neurospheres respond by migration in different treatment groups also accounts for the large standar deviations in the treatment groups. In summary, NPC demonstrate a migratory response to both 24 and 48 hr ischaemic homogenate, and the migratory cue is likely a soluble extracellular factor. These results indicate that fetal NPC are responsive to cerebral ischaemia factors *in vitro*.

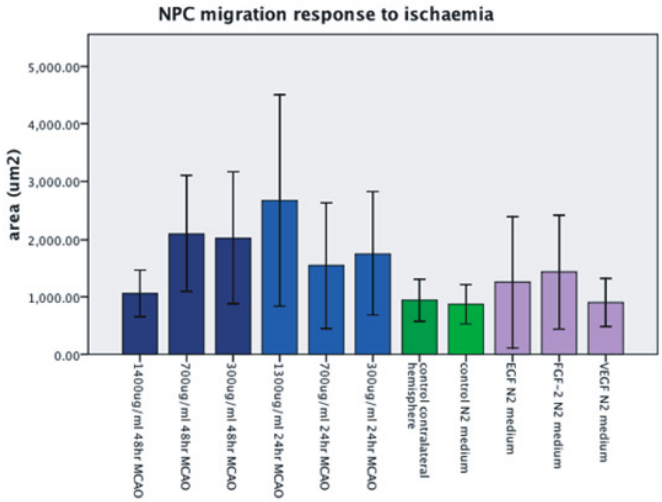

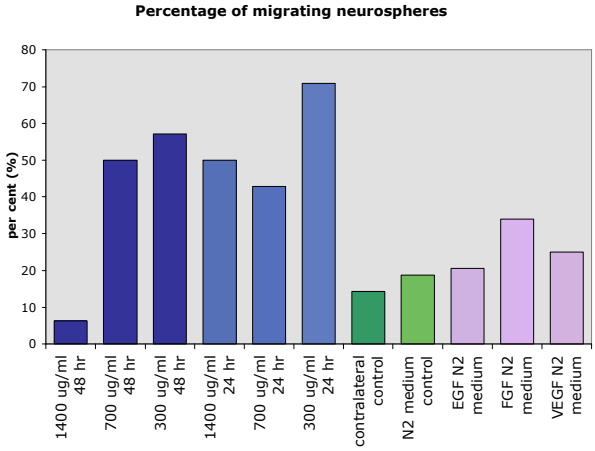

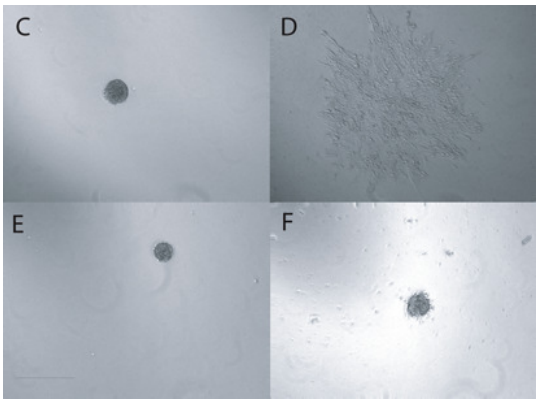

Figure 4.3.7.1 E14 Neurosphere response to cerebral ischaemia. A, migration of E14 neurospheres at 72 hours post-treatment. **B,** percentage of neurospheres that responded by migration to homogenate or growth factors., showing a high response rate to MCAO homogenate, but not contralateral control homogenate. **C,** D, migration of individual neurosphere in response to 1400 ug/ml 24 hr MCAO homogenate, at t=0 hr (C) and t=72 hr (D). **E, F,** migration of individual neurosphere in response to contralateral hemisphere MCAO homogenate at t=0 hr (E) and t=72 hr (F). Scale bar, 400 um.

4.4. *Discussion*

This study raises important issues surrounding the use of MRI and MRI contrast agents for longitudinal cell tracking studies in models of injury, where the evolution of endogenous contrast over time within lesioned tissue can be a source of uncertainty in image interpretation. We found that labeling with the FePro complex did not affect NPC viability, proliferation or differentiation capacity *in vitro*. However, in the *in vivo* studies we identified a source of T2 image contrast in the ischaemic lesion that develops over time, creating a challenge for longitudinal cellular imaging studies. These results are discussed in the following sections.

4.4.1. *In vitro characterisation of FePro labelling*

In summary, we observed NPC can be labelled with the FePro complex with no significant effect on cell viability or proliferation relative to control, unlabelled cells, and labelled NPC can differentiate into neurons, oligodendrocytes and astrocytes. The FePro label is retained throughout multiple cell divisions during the formation of new neurospheres, and FePro-labelled neurospheres produced hypointensity on MRI images. Endorem labelling may have a small effect on proliferation rate, but no effect on NPC number, viability or differentiation. In addition, data from the ST14A cell line also confirm that FePro does not affect cell viability, and has greater labelling efficiency than Endorem. By these observations, FePro is a superior MRI contrast agent for NPC cell labelling than Endorem.

The effects of the FePro complex on fetal NPC were characterized *in vitro*. The FePro complex did not alter the metabolic activity of the NPC, suggesting that there were no cytotoxic effects associated with FePro labelling. FePro-labelled NPC were able to proliferate to generate neurospheres, and retain the label through several cell divisions. FePro-NPC could differentiate appropriately into neurons, oligodendrocytes and astrocytes, and retain the FePro contrast agent through differentiation. Imaging NPC *in vitro* demonstrated that FePro uptake under the described labeling conditions was sufficient to generate MRI contrast. SQUID measurement of iron oxide uptake also confirmed and quantified cellular uptake of FePro. Other studies have similarly shown that cytotoxicity of FePro is low in other cell types, and that FePro uptake is sufficient to generate contrast on T2*-weighted images (Arbab et al., 2003; Arbab et al., 2004; Arbab et al., 2005b; Arbab et al., 2006).

Similarly, labeling with Endorem alone was assessed, and Endorem was generally found to be non-toxic and have little effect on NPC behaviour. However, the mean diameter of neurospheres generated from Endorem-labelled NPC was greater than non-labelled NPC, suggesting that Endorem may interfere with cell proliferation pathways. Furthermore, cell metabolism was

reduced in Endorem-labelled ST14A cells, an effect which was not observed in FePro-labelled cells. Other studies have similarly found that labeling with Endorem, or Endorem + transfection agent, to have little effect on cell metabolic processes (Arbab et al., 2005b).

SQUID measurements indicated that iron oxide uptake by NPC was less when cells were labelled with Endorem than with FePro. The concentration of iron oxide in culture medium was five times greater with Endorem labeling than FePro complex labeling, yet Endorem labeling resulted in less iron oxide uptake by cells. This result demonstrates the superior labeling efficiency of the FePro complex. Even if we conclude that both contrast agent labeling methods have little effect on NPC viability and behaviour, labeling with the FePro complex results in increased iron oxide uptake.

Protamine sulphate may facilitate SPIO internalization via increased complex contact with the cell membrane. Transfection agent-membrane interaction has been shown to initiate internalization of SPIO via endocytosis (Politi et al., 2007), whereas free Endorem is likely internalized via non-specific membrane binding and pinocytosis of Endorem particles (Modo et al., 2005). This possible difference in cellular uptake between Endorem and the FePro complex may explain both the difference in total particle uptake, as well as the observed differences in cell viability and metabolism between Endorem and FePro, where cellular uptake by pinocytosis may be less efficient and more toxic to cells.

4.4.2. Evolution of MRI T_2 contrast and heterogeneity following cerebral ischaemia

In this study, cellular imaging was in part hampered by the evolution of T_2 heterogeneity in the ischaemic lesion in all animals, obscuring cell detection on MRI. The evolution of T_2 hypointensity might be related to the accumulation of macrophages and granulocytes to the lesion over time, leading to localized hypercellularity. Sibson *et al* have previously shown in a model of multiple sclerosis that accumulation of MHC Class II-expressing cells (such as macrophages, dendritic and B cells) are spatially coincident with regions of T2 hypointensity and reduced ADC. In this study, hypercellularity increases from one week, peaks at 3 weeks and persists in later timepoints, and regions of T_2 hypointensity develop by 3 weeks, which is consistent with our results (Broom et al, 2005). Further studies found similar results (Newman et al, 2001; Sibson et al, 2002).

The T_2 heterogeneity may also arise as a consequence of the accumulation of iron in the lesion, the development of microhemorrhages, the degradation of blood products, macrophage activity, paramagnetic properties of inflammatory cells, or neuronal degeneration. In the FePro-NSC group, an additional factor is clearly the presence of iron oxide particles in the FePro contrast

agent.

Palweczyk *et al.* have shown that iron exchange can occur between labeled cells and macrophages *in vitro*, although the transfer of iron to macrophages is low (Pawelczyk et al., 2008). In our study, macrophages were observed at the injection site, and it is likely that FePro-NPC cell death occurred over weeks following injection, releasing iron to the surrounding parenchyma. In another study, Lepore *et al.* observed some macrophage uptake of Endorem from labeled NPC in a model of spinal cord injury (Lepore et al., 2006). However, Stuckey *et al.* did not observe macrophage uptake of iron following transplantaion of bone marrow stromal cells in a model of myocardial infarction (Stuckey et al., 2006).(Stuckey 2006). Endorem from labeled cells may enter endogenous iron degradation pathways: Arbab *et al.* have shown that cell labeling results in sequestration of Endorem in endosomes, which fuse with lysosomes and degrade into hemosiderin over time (Arbab et al., 2005a).

Weber *et al.* observed the evolution of hypointensity in ischaemic striatum on T_2*-weighted MRI images at 2 and 10 weeks post-ischaemia, but not changes in T_2, in a 60 minute MCA occlusion model (Weber et al., 2005). These T_2* hypointense regions colocalised with iron-containing macrophages, and were distinct from T_2* patterns observed in hemorrhagic transformation. The authors attributed the iron in macrophages to the phagocytosis of red blod cells from damaged blood vessels, distinct from hemorrhage.

Macrophages are involved in the normal recycling of senescent erythrocytes: heme oxygenase-1 (HO-1) is a component of this pathway, and is expressed in macrophages (Sipe et al., 2002). The development of microhemorrhages following delayed vascular degradation and erythrocyte degradation may be sources of iron in the ischaemic lesion (Hoehn et al., 2007). Koistinaho *et al.*. also observed HO-1-positive microglia in the ischaemic striatum (Koistinaho et al., 1996), and HO-1 has also been detected in neurons and oligodendrocytes following ischaemia in the ipsilateral cortex and thalamus (Bidmon et al., 2001). Danielisova *et al.*. have observed iron deposition in the striatum and pyramidal cells of cortical layers III and V following 20 minute MCA occlusion (Danielisova et al., 2002).

Delayed neuronal death after shorter occlusion times may be another mechanism that contributes to the evolution of T_2 hypointensity in the lesion. Garcia *et al.*. observed delayed neurodegeneration following short periods of ischaemia (Garcia et al., 1997). The authors report selective neuronal necrosis in the striatum and cortex, predominantly in layer III, after 10 or 20 minutes MCA occlusion. Sbarbati *et al* also describe the delayed development of T_2 hypointensity in the medium cortical layers, where they observe neuronal death and macrophage accumulation around blood vessels (Sbarbati et al., 2002). Van Lookeren Campagne *et al.*. also describe delayed neuronal death, increased cerebral blood volume and a reduction in lesion volume from 14 days post-ischaemia following shorter 30 minute MCA occlusion times (van Lookeren et al., 1999).

Justicia *et al.*. have linked iron accumulation and T_2 hypointensity to delayed neuronal death in the thalamus between 3 and 7 weeks following cerebral ischaemia (Justicia et al., 2008). The authors suggested that iron accumulation was mediated by heme oxygenase-1-positive (HO-1) microglial activity and neuronal degradation, although they did not describe iron accumulation in the infarcted striatum or cortex. Other studies observe retrograde neurodegeneration over weeks following ischaemia, where reactive astrocytes and microglia accumulate in the thalamus, neuronal degerneration occurs and thalamic volume decreases (Fujie et al., 1990; Iizuka et al., 1990). These studies suggest that iron accumulation may be linked to neurodegeneration, lesion contraction and microglial activity. Iron accumulation is associated with other neurodegenerative diseases such as Alzheimer's, Parkinson's and Huntington's disease (Berg and Youdim, 2006; Gaasch et al., 2007; Palmer et al., 1999a; Simmons et al., 2007; Thompson et al., 2001).

Following cerebral ischaemia, dysregulation of iron homeostasis also occurs, and leads to non-heme iron accumulation surrounding the necrotic core (Carbonell and Rama, 2007). The dysregulation may result from blood brain barrier breakdown and inflammatory events following ischaemia (Selim and Ratan, 2004), where plasma transferrin and iron in endothelial cells may enter the parenchyma, as well as hemoglobin-containing erythrocytes (Carbonell and Rama, 2007). Iron can become unbound from brain storage proteins under hypoxic-ischaemic conditions. Release of ferric iron by ferritin or tranferrin is facilitated by low pH, superoxide and nitric oxide, which are present during ischaemia. Ferritin upregulation has been reported in microglia and oligodendrocytes following ischaemia, and is correlated to neurodegeneration (Bishop and Robinson, 2001; Danielisova et al., 2002; Kondo et al., 1997). Iron deprivation in the diet decreases necrosis, and excess dietary iron increases necrosis after cerebral ischaemia. Treatment with iron chelating compounds after ischaemia decreases neuronal damage and recovery. In the clinical setting, increased plasma iron stores and CSF ferritin levels correlate with stroke progression and poor clinical outcome (Armengou and Davalos, 2002).

Together with our results, these studies support the hypothesis that microglial activity, heme-oxygenase-1 expression, microhemmorrhage iron accumulation and delayed neuronal death may account for change in T2 and T2* at later time points following ischaemia. In summary, BBB breakdown, microhemorrhage and iron dysregulation after ischaemia, leading to iron accumulation in the lesion, are possible causes of delayed neuronal death and the evolution of T_2 hypointensity. Brain iron accumulation after the ischaemic event may contribute to the development of a neurotoxic environment that leads to delayed neuronal death. The sources of iron are likely from both the blood and brain iron stores. Together, the studies described above confirm our observation that the evolution of the ischaemic lesion is a dynamic process occurring over several weeks following cerebral ischaemia, and delayed neuronal death may reshape the lesion at later time points.

4.4.3. Cell treatment and cerebral ischaemia

In this study, E14 forebrain-derived neural stem and progenitor cells were injected into the ipsilateral corpus callosum 48 hours following cerebral ischaemia. Our hypothesis was that the cells would migrate towards the ischaemic boundary, but we did not observe cell migration from the injection site. *In vitro*, these cells demonstrated a migratory response to cerebral ischaemia. The developmental stage of progenitor cells may determine their capacity to differentiate appropriately and contribute to repair. Foetal forebrain tissue is a source of neural stem cells, and the cells can be expanded *in vitro*. NPC are cultured from the embryonic stage E14, which is within the period of cortical neurogenesis: at this stage NPC proliferate at the ventricular zone and progeny migrate radially to establish the neuronal layers of the cortex. Fetal NPC might therefore be highly migratory and capable of neurogenesis. Furthermore, in transplantation studies in the normal brain, fetal NPC are capable of migrating through the adult brain and differentiating into neurons, whereas adult neural stem cells predominantly generate astrocytes when transplanted into non-neurogenic tissue (Brustle, 1999; Brustle et al., 1997; Doetsch et al., 1999b; Gage, 2000). Ourednik *et al.* have also suggested that NPC have an inherent cell rescue response, and spontaneous express neuroprotective agents such as GDNF following cell injection (Ourednik et al., 2002; Ourednik et al., 2000). The time point of 48 hours post-ischaemia was chosen as the acute inflammatory response has subsided and cytokines and growth factors are being upregulated at this time point (Durukan and Tatlisumak, 2007; Darsalia et al., 2005; Fisher, 2004; Huang et al., 2006). White matter tracts may provide a scaffold for migration of neurons (Ben-Hur et al., 2003), and so the ipsilateral corpus callosum was chosen as the injection site.

In the *in vitro* migration assay, the filtered ischaemic homogenate did not contain cells, only soluble extracellular cues that may be produced by a combination of inflammatory cells, astrocytes, endothelial cells and ischaemic neurons. Under these conditions, the ischaemic environment was non-toxic to NPC and promoted cell migration. It is possible that macrophages phagocytosed FePro-NPC *in vivo*, as macrophages were identified at the injection site. Other studies have shown significant cell death of injected cells (Bliss et al., 2007). The contralateral hemisphere was used as control, non-ischaemic tissue. While this tissue was not affected from the MCAO ischaemic event, the tissue may have experienced acute ischaemia during the tissue processing stage prior to filtration and freezing. Any factors produced by the tissue as a result of this acute ischaemic event did not lead to neuroblast migration.

In this study immunosuppression was not used following cell injection. Other cellular therapy studies have demonstrated an improved functional outcome and neurogenesis with (Kelly et al., 2004; Pollock et al., 2006) and without (Daadi et al., 2008; Darsalia et al., 2007) the use of

cyclosporine A. Modo *et al.* also concluded that cyclosporine A had no effect on cell survival in their model of cerebral ischaemia (Modo et al., 2002b). Cyclosporine A has been shown to be neuroprotective following brain injury, including cerebral ischaemia (Korde et al., 2007; Ravikumar et al., 2007; Shin et al., 2007; Yamaguchi et al., 2006).

4.4.4. Future work

Following the results of this study, there is scope for further work. There is significant scope for refining the cell delivery strategy by optimisation of the injection site, the timepoint of cell delivery following ischaemia and the option of immunosuppression.

For cellular imaging using MRI to be successful, a method of distinguishing between labelled cells and the evolving ischaemic lesion must be established. Several approaches may be considered. Firstly, optimisation of T2 and T2*-weighted imaging may improve discrimination between concentrated iron in FePro-labelled cells and iron accumulating in the ischaemic lesion. In this study we observed that the hypointensity within the lesion was less on T2*-weighted images than T2-weighted images, and this finding can be further optimised and explored. However, if the likely source of the observed T2 hypointensity is iron deposition in the ischaemic lesion, the problem of distinguishing endogenous iron from FePro-derived iron will always exist, and may not be possible to overcome.

A second option is to explore other MRI contrast agents. Gadolinium agents that generate positive contrast on T1 images are an attractive option, and could be distinguished from endogenous iron accumulation. However, the relaxivity of gadolinium agents can be an order of magnitude less than for superparamagnetic iron oxide agents, which may present a challenge for cell detection. Additionally, few gadolinium contrast agents for cellular imaging currently exist, and free gadolinium (Gd3+) is toxic to cells. A gadolinium agent of low toxicity and high relaxivity is therefore required.

5. *Assessment of relaxivity, cell labelling and cytotoxicity in novel monomeric and polymeric gadolinium contrast agents*

5.1. Introduction

Iron oxide-based contrast agents are more commonly used for cellular imaging because of their strong r_2 relaxivity, however gadolinium-based agents have different advantages. Although gadolinium r_1 relaxivity is an order of magnitude weaker than iron oxide r_2 relaxivity, r_1 relaxivity is a desirable property for cellular detection because it produces an increased and hyperintense signal on T_1-weighted images, and can be distinguished from susceptibility effects due to magnetic field inhomogeneities, unlike superparamagnetic contrast agents. The ideal gadolinium contrast agent would have high r_1 relaxivity, generate positive contrast on T_1-weighted images, and be non-toxic when internalised by cells. There are relatively few gadolinium-based contrast agents that exist to date that fulfil both the low toxicity criteria as well as having high relaxivity values. As discussed in section 3.7.1.2, many gadolinium contrast agents with high r_1 relaxivity have been shown to be toxic when internalised by cells.

Relaxivity of gadolinium complexes can be altered through ligand design. As discussed in section 3.7.1.1, several factors affect r_1 relaxivity of gadolinium contrast agents: the number of inner sphere water molecules coordinated to the Gd^{3+} ion, *q*; the water exchange rate, τ_M; the rotational correlation rate, or molecular tumbling rate, of the contrast agent, τ_R; and outer sphere water interactions (Hermann et al., 2008). All of these parameters can be altered through ligand design.

Gadolinium contrast agents achieve the optimum relaxivity when the rotational diffusion of the contrast agent τ_R is slow, allowing more water exchange to occur and affect the relaxation of surrounding water. This can be achieved by non-covalent binding of the complex to larger proteins, or by covalent binding to become part of a larger molecule, thereby increasing the effective molecular weight of the complex (Caravan et al., 1999); (Modo et al., 2005) If the conjugation of gadolinium chelates is restricted to the surface or periphery of a macromolecule, as in HSA-conjugated DOTA, the freedom of rotation around their linker and the molecular tumbling rate of a single chelate can still be high relative to the tumbling rate of the whole macromolecule, diminishing the effect of greater molecular weight on molecular tumbling time and relaxivity.

The aim of this study is to develop a gadolinium-based contrast agent suitable for cell labeling, to overcome some of the limitations experienced using an iron oxide-based contrast agent approach: the optimal gadolinium-based contrast agent would have low toxicity, high labeling efficiency and high T1 relaxivity. We investigate whether hyperbranched polymers synthesised from gadolinium chelates increase r_1 relaxivity of a contrast agent. Polymerisation of several gadolinium chelate monomers into a rigid hyperbranched polymer structure is one strategy to achieve slower

molecular tumbling and increased r_1 relaxivity per mol of gadolinium, which may overcome the limitations of peripheral conjugation discussed above. Incorporating gadolinium chelates internally in the macromolecular structure would further reduce the freedom of rotation of the chelates and increase their individual molecular tumbling time, with a predicted increase in relaxivity (Aime 2005). And in terms of the molar r_1 relaxivity for the polymer contrast agent, this should also be increased due to more Gd^{3+} ions per polymer unit.

An additional advantage to this approach is the possibility of controlling the polymer branching and gadolinium loading during synthesis. This can be achieved by altering the ratio of chelate to linker and other reaction parameters to influence the final polymer size and structure. For example, a very large polymer size may reduce access of the internal gadolinium to water molecules, which should have a negative effect on r_1 relaxivity. Polymer synthesis with 'empty' chelate and subsequent gadolinium loading allows control of the amount of gadolinium loading per macromolecule. Partial loading may confer non-toxicity to the polymer, because any Gd^{3+} ion that becomes free within the polymer could coordinate with an 'empty' neighbour, thus trapping Gd^{3+} and preventing its release into a biological compartment, in which it would be toxic. This strategy of Gd^{3+} partial loading may therefore protect against *in vivo* gadolinium toxicity if the compounds remain in living systems for long term cell tracking.

In this study, novel monomeric and polymeric gadolinium chelates were synthesised, and their relaxivity and effects on cell viability were assessed. Monomeric chelates were composed of DOTA-tetraamides with different branching arms– allyl, styryl or propargyl (Figure 5.2.3.1). Polymeric chelates were composed of DOTA-tetraamides and diazide linkers, either synthesised as empty polymer with subsequent partial gadolinium loading, or synthesised with gadolinium-coordinated Gd-DOTA-tetraamides, resulting in 100% loading. DOTA was used due to its high stability in biological environments (Aime et al., 2002; Tweedle, 1992), and the possibility for structural modification. Diazides were used as linkers because they have reactions sites at both ends of the linker and are water soluble. Up to four linkers can bind to each gadolinium chelate, and this is expected to reduce rotational freedom of the chelate.

We observed a lower r_1 relaxivity in all monomeric chelates than gadoterate meglumine (Gd-DOTA, Dotarem®) or gadopentate dimeglumine (Gd-DTPA, Magnevist®) at 2.35T and 9.4T. Monomeric chelates had minimal cytotoxicity effects on neural stem cells, which could be labelled and imaged. Several polymeric chelates had higher relaxivity per mol Gd^{3+} than their monomeric units, however cytotoxicity also varied considerably among polymers, with many polymers toxic at even low concentrations. This study characterises the relaxivity and toxicity of novel monomeric and polymeric gadolinium chelates, and demonstrates that relaxivity can be increased by a hyperbranched polymer structure.

5.2. Methods

5.2.1. MRI

MRI was performed using a 2.35T horizontal magnet with a 120 mm bore (Oxford Instruments Eynsham,UK), interfaced to a Surrey Medical Imaging Systems (SMIS, UK) console. A volume coil (60 mm length) was used to transmit radiofrequency excitation pulses. Signal was detected using a passively decoupled, single loop, surface coil of 2 cm diameter positioned over the samples. Concentrations of monomer (0.1-2.5mM) or polymer (0.5-2.0mM) were imaged in 250µl Eppendorf tubes placed in a rack within a water-filled 50ml Falcon tube. T_1 relaxation times were measured for each concentration by acquiring a series of spin echo sequences with a fixed TE (30 ms) and an array of TR (100; 120; 130; 150; 180; 200; 250; 300; 400; 500; 600; 700; 800; 900; 1000; 1200; 1500; 1800; 2500; 4000; 8000 ms). T_2 relaxation times were measured for each concentration by acquiring a series of spin echo sequences with a fixed TR (1000 ms) and an array of TE (30; 40; 60; 80; 100; 120; 140; 160; 200 ms). For all sequences, FOV = 30 x 30 mm, resolution 128 x 64 voxels, slice thickness 1mm and 1 average. A 0.2mM Magnevist sample was included in each scan as a standard. Data analysis was performed using an in-house Matlab programme (Jack Wells, unpublished), which calculates T_1 and T_2 values of self-selected ROI across the TR array or TE array for T_1 and T_2 measurement, respectively.

MRI was also performed using a 9.4T horizontal 20 cm bore Varian VNMRS system. T1 relaxation times were measured for each concentration by acquiring an inversion recovery sequence, where TR = 17500 ms, TE = 13.34 ms, IR array = 15; 30; 60; 100; 150; 200; 300; 450; 600; 900; 1500; 3000; 6000; 17000 ms. T2 relaxation times were measured by acquiring a spin echo sequence, where TR = 2000; TE array = 20; 30; 40; 50; 60; 90; 120; 180; 250 ms. For all sequences, FOV = 100 x 40 mm; slice thickness 2 mm, resolution 64 x 64 voxels. Data analysis was performed using an in-house C++ programme (Andrew Lowe, unpublished) to create T1 or T2 maps. ROI were drawn using ImageJ software, and mean T1 or T2 times at each concentration were calculated.

5.2.2. Cell culture

ST14A cells were cultured as described in Chapter 4. Cells were cultured on adherent flasks (TPP) in DMEM (Invitrogen) with 10% foetal calf serum (Gibco) and 1% Penicillin-Streptomycin. Cells were incubated at 33°C with 5% CO2 and 100% humidity. Cells were passaged every 48 hours, using 1X Trypsin-EDTA to detach cells from adherent flasks, collected and centrifuged in 10ml culture medium, replated 1:3 in fresh culture medium, and returned to the incubator.

For viability experiments, 10^4 cells in 100 µl culture medium were plated per well in 96-well plates. Monomeric (0.01 – 3mM) or polymeric (0.01 – 1.0mM) chelates were incubated with cells for 24

hours, with 8 wells per concentration. At 24 hours, prior to cell viability testing, contrast agents were removed, and cells washed in EBSS 3 times.

MTT assay: Cells were incubated in growth medium with 10% MTT for 4 hours, then culture medium was removed and replaced with 100 μl per well MTT solvent 0.04M HCl in isopropanol. Plates were left on a gyratory shaker for 30 minutes to allow the formazan crystals to dissolve. Absorbance was measured at 570nm using an ELISA microplate spectrophotometer. Three readings were taken for each assay, and the assay was repeated twice.

Alamar Blue assay: Cells were incubated in 100ul growth medium with 10% Alamar Blue solution for 4 hours, then absorbance was measured at 570nm using an ELISA microplate spectrophotometer. Three readings were taken for each assay, and the assay was repeated twice.

Data analysis: To assess whether absorbance readings for each monomeric and polymeric gadolinim chelate were different to control unlabelled cells, analysis of variance test was performed, with significance level $p<0.05$ and Tukey post-hoc test. Mean absorbance readings for each concentration and gadolinium chelate were expressed as a percentage of control cells for graphical display.

5.2.3. Gadolinium Complexes

All chelates were synthesised, purified and characterised at Imperial College Chemistry Department by Jonathan Martinelli or Claire Grignolo. For monomeric chelates, allyl-, styryl- and propargyl-derivatives of DOTA-tetraamide were sythesised. Gadolinium was complexed to the DOTA amides by reacting with $GdCl_3$ salt and purification by filtration or extraction (Figure 2.3.1; Table 2.3.1). Methylthymol blue (MTB) or xylenol orange were used as an indicator of free Gd^{3+} ion in solution. The gadolinium chelates were characterised by mass spectrometry and x-ray chrystallography to confirm the structure and the coordination sites of four nitrogen atoms, four carboxylate groups and one water molecule.

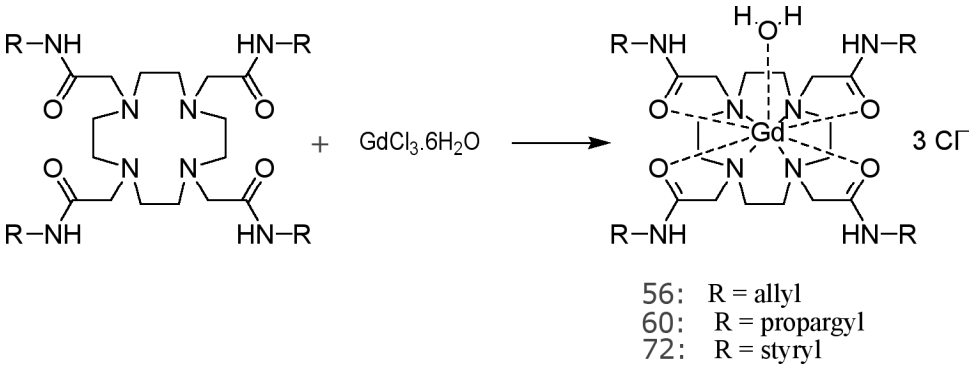

Figure 5.2.3.1 Sythesis of gadolinium monomers. DOTA-tetraamides (left) react with $GdCl_3$ salt to

form the Gd-DOTA complex (right). R denotes the allyl, propargyl or stryrl branching arm of the DOTA-tetraamide.

Name	Chemical name	MW (kD
56	Gd-1,4,7,10-tetrakis(2-styrylcarbamoylmethyl)-1,4,7,10-tetraazacyclododecar	906.55
60	Gd-1,4,7,10-tetrakis(allylcarbamoylmethyl)-1,4,7,10-tetraazacyclododecane	842.38
72	Gd-1,4,7,10-tetrakis(2-propynylcarbamoylmethyl)-1,4,7,10-tetraazacyclodode	834.29

Figure 5.2.3.2 Monomer variants and their chemical names. MW denotes molecular weight in kiloDaltons.

Polymers were synthesised with the propargyl-derivative of DOTA-tetraamide (monomer 72) as ligand, with diazide linkers (Figure 5.2.3.3), by thermal cycloaddition or click chemistry. A number of compounds with different ligand:linker ratios were synthesised, summarised below (Table 5.2.3.2). Polymers were either synthesised using gadolinium-loaded (g-polymers) or unloaded (e-polymers) ligands. Where unloaded ligands were used, partial gadolinium loading occurred subsequent to polymer synthesis by reacting with a known amount of gadolinium salt. The concentration of gadolinium in polymeric chelates was determined by Inducively coupled plasma mass spectrometry (ICP) analysis at the Natural History Museum using Varian Vista Axial Pro ICP-AES. Polymer molecular weight (MW) was determined by GPC chromatography. Based on the known molecular weight of the component ligand and linker and their expected ratio, it was estimated that most polymers were composed of 3-5 monomer units. The expected polymer size was significantly larger than this observed size, and it is not clear why the polymer reaction limits polymer size to only 3-5 monomers. Polymers e(1.65:1) and e(1.33:1) were mostly insoluble in water, and only the soluble fraction was used for MRI and cell viability assays.

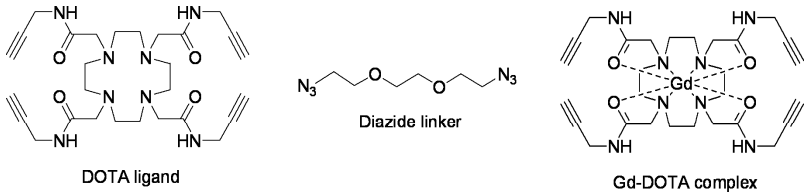

Figure 5.2.3.3 Components of the gadolinium complex. Gadolinium unloaded propargyl-derivatives of DOTA-tetraamide ligand (left), the diazide linker (middle) and gadolinium-loaded DOTA-tetraamide ligand(right).

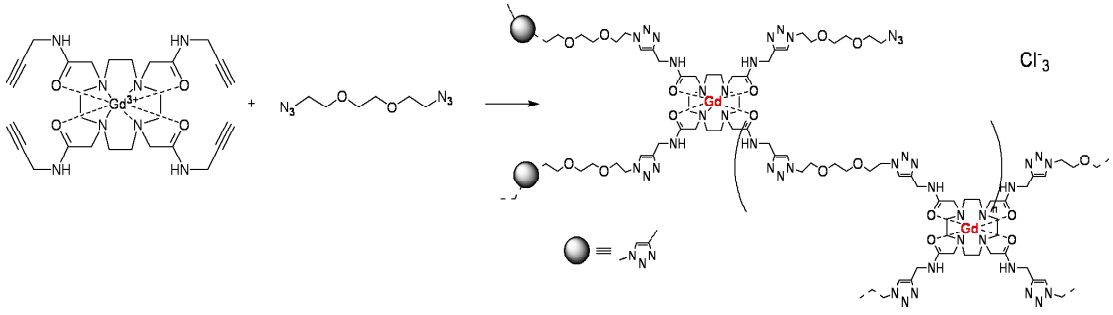

Figure 5.2.3.4 Polymerisation of Gd-loaded DOTA-tetraamide to form g-polymer.

Polymer	Ligand:Linker	Gadolinium-loading
$e_{(2:1)}50$	1:0.5	50%
$e_{(2:1)}80$	1:0.5	80%
$e_{(1.5:1)}50$	1:0.67	50%
$e_{(1.5:1)}80$	1:0.67	80%
$e_{(1.33:1)}50$	1:0.75	50%
$e_{(1.33:1)}80$	1:0.75	80%
$e_{(1.165:1)}50$	1:0.86	50%
$g_{(1.5:1)}$	1:0.67	100%
$g_{(1:2)}$	1:2	100%
$g_{(1:4)}$	1:4	100%
$g_{(1:6)}$	1:6	100%

Figure 5.2.3.5. Table of synthesised polymers, ligand:linker ratio and Gd-loading percentage. 'g' denotes polymerisation from Gd-loaded DOTA-tetraamide ligand units, 'e' denotes polymerisation from 'empty' DOTA-tetraamide ligands.

5.3. Results:

5.3.1. Longitudinal relaxivity of monomers at 2.35T.

Longitudinal relaxivity (r_1) values were calculated using the equation:

$$\frac{1}{T_1^{obs}} = \frac{1}{T_1^0} + r_1[Gd]$$

$$\frac{1}{T_1^{obs}} \approx \frac{1}{T_1^0} + r_1[Gd]$$

where T_1^{obs} is the observed T_1 of a given solution or tissue containing the contrast agent; T_1^0 is the T_1 of the solution or tissue without contrast agent (water), $[Gd]$ is the concentration of Gd^{3+}, and

r_1 is the longitudinal relaxivity. The slope of $1/T_1^{obs}$ vs [*Gd*] will give the relaxivity of the gadolinium complex. T_1 values at 2.35T were measured for a range of gadolinium complex concentrations (Table 5.3.1.1):

	56		**60**		**72**	
mM	**T_1**	**$1/T_1$**	**T_1**	**$1/T_1$**	**T_1**	**$1/T_1$**
0	2480.0	4.03E-04	2510.0	3.98E-04	2490.0	4.01E-04
0.1	1330.0	7.51E-04	1560.0	6.42E-04	1730.0	5.79E-04
0.2	932.6	1.07E-03	1110.0	8.97E-04	1290.0	7.77E-04
0.4	480.3	2.08E-03	619.6	1.61E-03	736.4	1.36E-03
0.7	321.4	3.11E-03	433.1	2.31E-03	511.2	1.96E-03
0.8	279.6	3.58E-03	396.1	2.52E-03	422.1	2.37E-03
1	241.2	4.15E-03	325.7	3.07E-03	371.8	2.69E-03
1.3	194.5	5.14E-03	273.0	3.66E-03	298.5	3.35E-03
1.7	142.2	7.03E-03	202.3	4.94E-03	202.3	4.94E-03
2.5	81.7	1.22E-02	129.5	7.72E-03	129.5	7.72E-03

Figure 5.3.1.1. T1 values for monomers 56, 60 and 72 across a range of concentrations, measured at 2.35T.

T_1 values for Gd-DOTA and Gd-DTPA were also measured (Table 3.1.2):

	Gd-DTPA	
mM	T1	1/T1
0	2.40E+03	4.16E-04
0.1	1.01E+03	9.86E-04
0.2	681.0476	1.47E-03
0.4	393.6303	2.54E-03
0.5	309.0985	3.24E-03
1	177.2756	5.64E-03

	Gd-DOTA	
mM	**T_1**	**$1/T_1$**
0	2925.499236	0.000341822
0.5	460.3998573	0.002172025
0.8	294.3751387	0.003397026
1	214.6680073	0.004658356
1.5	132.3600984	0.007555147
2	93.1515016	0.0107352

Figure 5.3.1.2. T1 values for Gd-DTPA and Gd-DOTA across a range of concentrations at 2.35T.

From these data, $1/T_1$ was plotted against [Gd] to obtain the r_1 relaxivity value for each gadolinium complex (Figure 5.3.1.1).

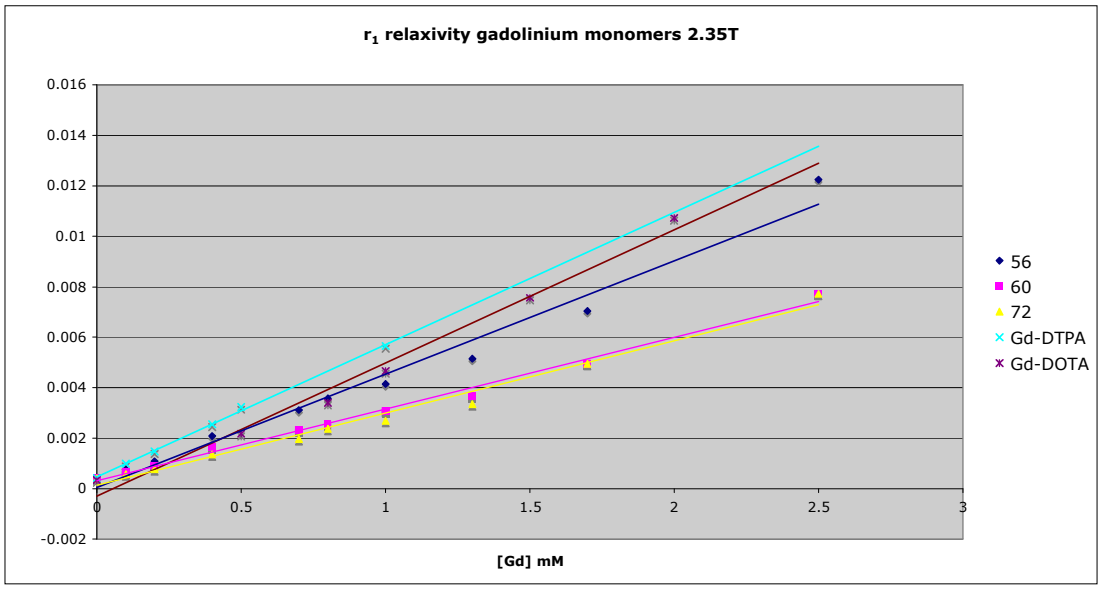

Figure 5.3.1.3. Graph of gadolinium concentration [Gd] against $1/T_1$ for monomers 56, 60 and 72, Gd-DOTA and Gd-DTPA.

From this graph (Figure 5.3.1.1), the following relaxivity values were calculated (Table 5.3.1.4):

compound	r_1 ($mM\ s^{-1}$)
Gd-DTPA	5.2471
Gd-DOTA	5.277
56	4.4891
60	2.8383
72	2.8622

Figure 5.3.1.4. Relaxivity values calculated from the slope of [Gd] vs $1/T_1$ for each monomer from Figure 5.3.1.1.

5.3.2. Transverse Relaxation of monomers at 2.35T

Transverse relaxivity values (r_2) were calculated using the equation:

$$\frac{1}{T_2^{obs}} = \frac{1}{T_2^{0}} + r_2[Gd]$$

where T_2^{obs} is the observed T_2 of a given solution or tissue containing the contrast agent; T_2^0 is the T_2 of the solution or tissue without contrast agent, [Gd] is the concentration of the Gd^{3+}, and r2 is the transverse relaxivity. The slope of $1/T_2^{obs}$ vs [Gd] will give the relaxivity of the gadolinium complex. T_2 values at 2.35T were measured for a range of gadolinium complex concentrations (Table 5.3.2.1):

	56		**60**		**72**	
mM	T_2	$1/T_2$	T_2	$1/T_2$	T_2	$1/T_2$
0	887.2741	0.001127047	828.8924	0.001206429	754.5281	0.001325332
0.4	363.4771	0.002751205	404.2957	0.002473437	286.0481	0.003495916
0.7	320.4794	0.003120325	380.323	0.002629344	393.9962	0.002538096
1	260.2279	0.003842785	270.9828	0.003690271	269.7793	0.003706734
1.3	225.023	0.00444399	190.847	0.005239799	264.4606	0.003781282
2.5	119.9127	0.0083394	95.8814	0.010429552	124.6159	0.008024658

Figure 5.3.2.1. T_2 values for Gd monomers at 2.35T.

For these data, $1/T_2$ was plotted against [Gd] to obtain the r_2 relaxivity value for each gadolinium complex (Figure 5.3.2.1).

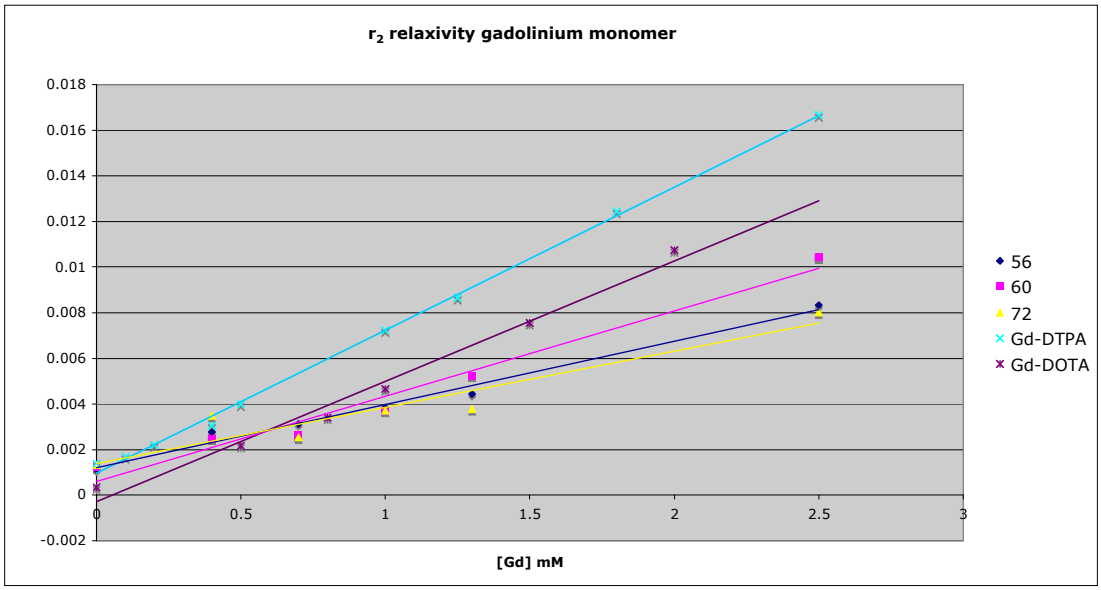

Figure 5.3.2.2. r_2 relaxivity curves for gadolinium monomers at 2.35T.

The r_1 and r_2 relaxivity for each gadolinium complex is summarised below (Table 5.3.2.2):

2.35T

	r_1 (mM s^{-1})	r_2 (mM s^{-1})
Gd-DTPA	5.2471	6.3287
Gd-DOTA	5.277	4.528
56	4.4891	2.7775
60	2.8383	3.7391
72	2.8622	2.4729

Figure 5.3.2.3. r_1 and r_2 relaxivity of gadolinium monomers at 2.35T.

The 0.2mM Gd-DTPA was used as a standard for each acquisition, and the T_1 and T_2 of 0.0mM monomer (water) was also measured for each acquisition. The variability between acquisitions was calculated:

	T_1		**r_1**	
	H_2O	0.2mM Gd-DTPA	H_2O	0.2mM Gd-DTPA
mean	2734.257016	714.2277176	0.000366053	0.001406717
stdev	155.6213862	44.80328052	2.07101E-05	8.49241E-05

Figure 5.3.2.4. Variance in T_1 and r_1 for H_2O and the Gd-DTPA reference.

5.3.3. Relaxivity of monomers at 9.4T.

Longitudinal (Table 5.3.2.1) and transverse (Table 5.3.2.2) relaxivity was calculated at 9.4T.

	56		**60**		**72**	
mM	T1	1/T1	T1	1/T1	T1	1/T1
0	28015.914	3.5694E-05	28213.125	3.54445E-05	28015.914	3.5694E-05
0.4	5655.2	0.000176828	6412.565	0.000155944	7636.22	0.000130955
0.7	3715.884	0.000269115	4614.833	0.000216693	4855.24	0.000205963
1.3	2319.414	0.000431143	2933.708	0.000340866	3644.34	0.000274398
1.7	1717.213	0.000582339	2333.13	0.000428609	2689.605	0.000371802
2.5	1190.949	0.000839667	1583.045	0.000631694	1883.167	0.00053102

Figure 5.3.3.1 T_1 values for gadolinium monomers at 0-3 mM concentration

	56		**60**		**72**	
mM	T2	1/T2	T2	1/T2	T2	1/T2
0	6936.823	0.000144158	5024.039	0.000199043		
0.4	2125.426	0.000470494	2988.472	0.000334619	2313.841	0.000432182
0.7	1691.982	0.000591023	2532.088	0.000394931	3123.81	0.000320122
1.3	1666.052	0.000600221	1712.774	0.000583848	2353.07	0.000424977
1.7	928.275	0.001077267	1284.038	0.000778793	1471.818	0.000679432
2.5	859.567	0.001163376	996.286	0.001003728	660.87	0.001513157

Figure 5.3.3.2 T_2 values for gadolinium monomers at 0-3 mM concentration

T_1 and T_2 was also calculated for Gd-DTPA at 9.4T (Table 5.3.3.3).

	Gd-DTPA			
mM	T1	1/T1	T2	1/T2
2.5	698.736	0.001431156	744.433	0.001343304
1.8	1088.065	0.000919063	988.127	0.001012016
1.25	1504	0.000664894	1270.25	0.000787247
0.2	7177.163	0.000139331	4220.98	0.000236912

Figure 5.3.3.3 T_1 and T_2 values for Gd-DTPA

For these data, $1/T_1$ and $1/T_2$ was plotted against [Gd] to obtain r_1 and r_2 relaxivity values for each gadolinium complex at 9.4T (Figure 5.3.3.1).

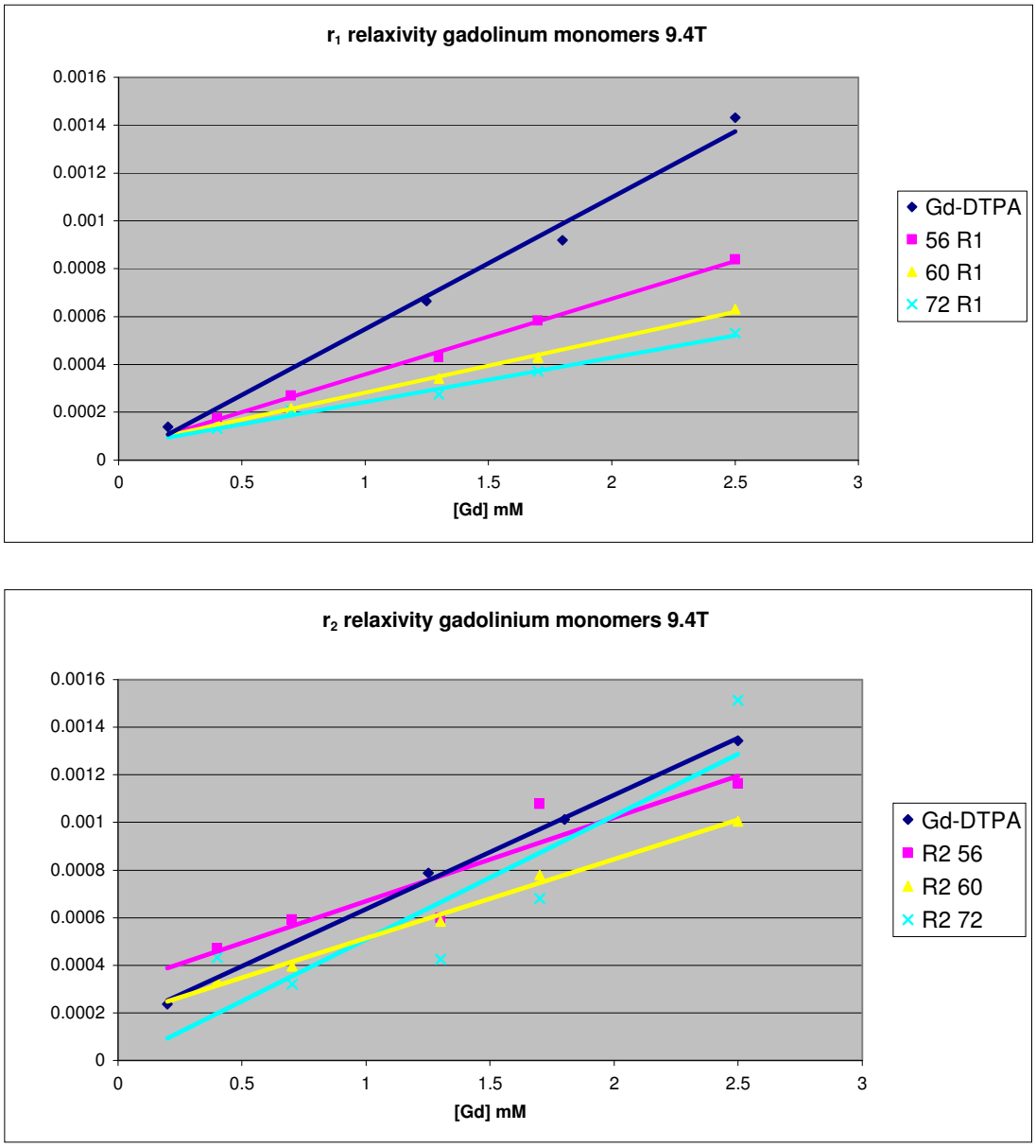

Figure 5.3.3.4 r_1 and r_2 relaxivity curves for monomers at 9.4T.

The r_1 and r_2 relaxivity at 9.4T for each gadolinium complex is summarised below (Table 5.3.2.4):

	2.35T		**9.4T**	
	r_1 (mM s^{-1})	***r_2 (mM s^{-1})***	***r_1 (mM s^{-1})***	***r_2 (mM s^{-1})***
Gd-DTPA	5.2471	6.3287	5.5067	4.8195
Gd-DOTA	5.277	4.528		
56	4.4891	2.7775	3.1573	3.9592
60	2.8383	3.7391	2.253	3.4087
72	2.8622	2.4729	2.8577	4.7913

Figure 5.3.3.5 r_1 and r_2 values for all monomers at 2.45T and 9.4T

5.3.4. Monomer cell viability.

Next, monomers were assessed for their effect on cell viability in the neural stem cell line ST14A. Cells were incubated in a range of concentrations of gadolinium monomers - 0-3mM for the Alamar Blue assay, and 0-1mM for the MTT assay – to assess cell metabolism. Across the range of concentrations, gadolinium monomers 56, 60 and 72 showed similar metabolic activity as control cells not exposed to gadolinium (Figure 5.3.4.1; ANOVA, $p>0.05$).

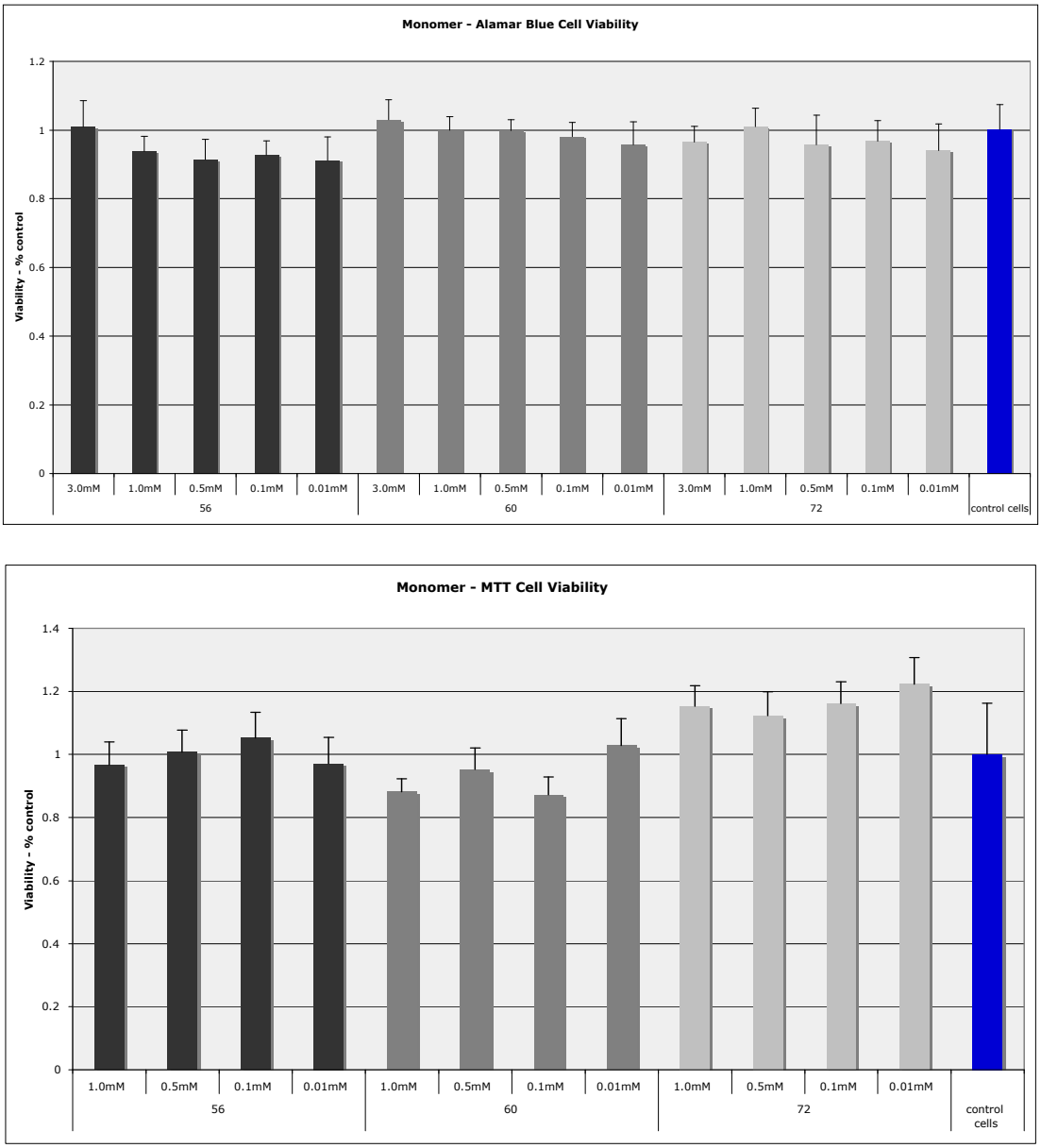

Figure 5.3.4.1 Cell viability assays for gadolinium monomers in ST14A cell line. Top, Alamar Blue assay. Bottom, MTT assay.

5.3.5. MRI imaging of monomer-labelled neural stem cells

Neural stem cells were incubated with 0.01mM, 0.1mM and 1.0mM of each of the monomers for 24 hours to assess cell labelling. Cells were then washed in EBSS and fixed in 4% PFA in PBS for cell imaging. Fixed cells were pelleted into 250ul eppendorfs and imaged at 2.35T to measure T_1 and T_2. Cell pellets of monomer-labelled cells were imaged at 2.35T. T_1 and T_2 relaxation decreased as the gadolinium incubation concentration increased, where T1 decreased by up to 60% compared to control unlabelled cells, in cells incubated at the highest concentration of

compound 56 and 72. This indicates that cells can be labelled and retain the gadolinium contrast agent following incubation, and that gadolinium labelling affects T_1 and T_2 of cells relative to control, unlabelled cells. For 60 1.0mM, it was not possible to measure T_1 and T_2 , and T_2 in 72 1.0mM, due to lack of signal.

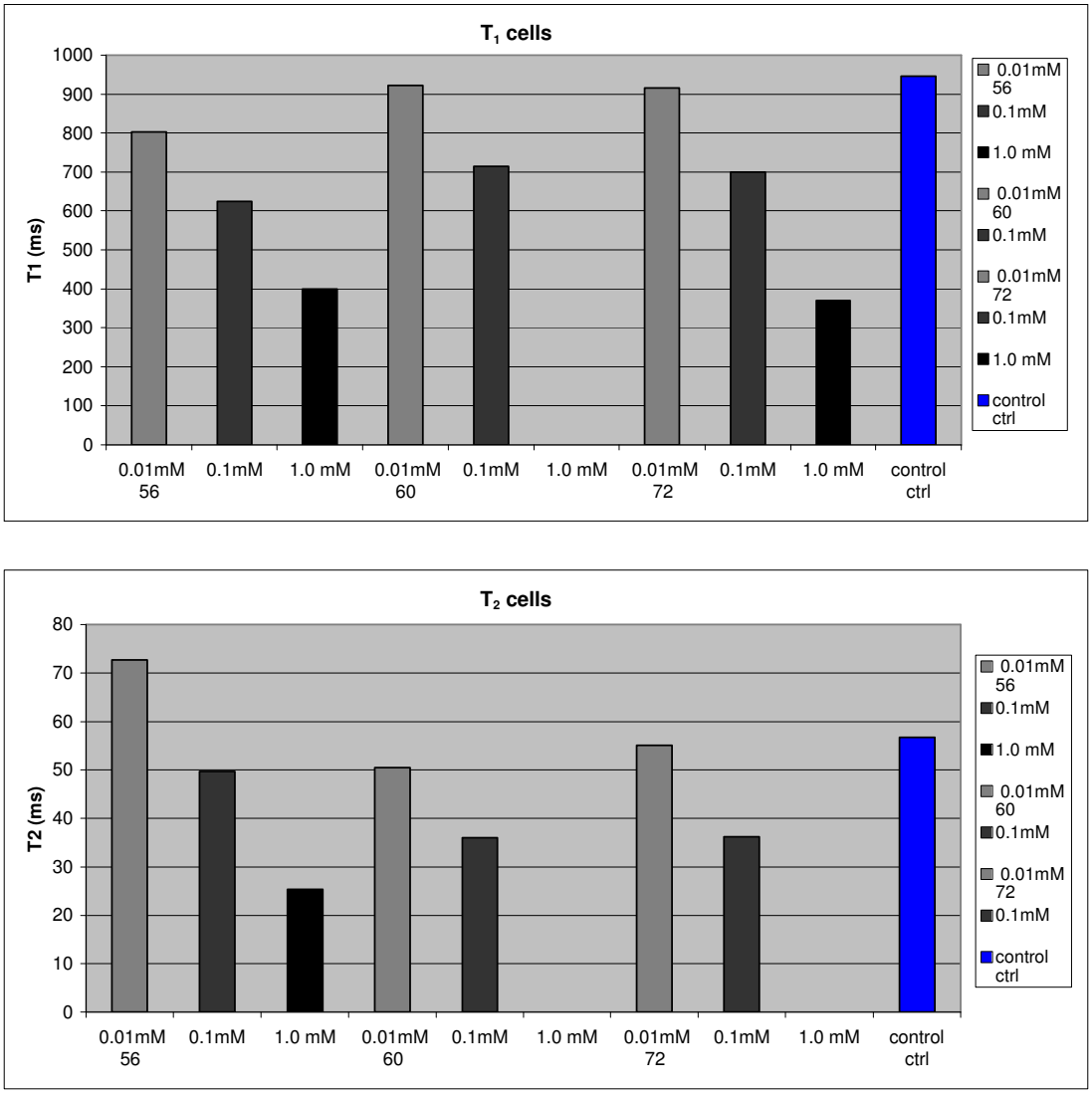

Figure 5.3.5.1T_1 and T_2 of gadolinium monomer-labelled cells at 2.35T.

	T_1	T_2
control	945.5262	56.6679
56 0.01mM	802.9539	72.7408
56 0.1mM	623.8157	49.6278
56 1.0 mM	399.4852	25.3204
60 0.01mM	921.8495	50.4671
60 0.1mM	714.5837	35.9959
60 1.0 mM		
72 0.01mM	915.3766	55.0261
72 0.1mM	699.4756	36.2085
72 1.0mM	370.0727	

Figure 5.3.5.2 T_1 and T_2 of gadolinium monomer-labelled cells at 2.35T.

5.3.6. T_1-weighted cell imaging at 2.35T and 9.4T

T_1-weighted (T1W) images were also acquired at 2.35T and 9.4T to assess the contrast generated relative to control, unlabelled cells at both field strengths. Positive contrast was observed in monomer 56 relative to control cells at 2.35T but not 9.4T. In monomers 60 and 72, a T_2 effect was observed in the T_1-weighted images, which resulted in negative contrast relative to the control cells. This effect was most apparent in monomer 60, which had the greatest r_2 relaxivity in solution (Figure 5.3.6.1).

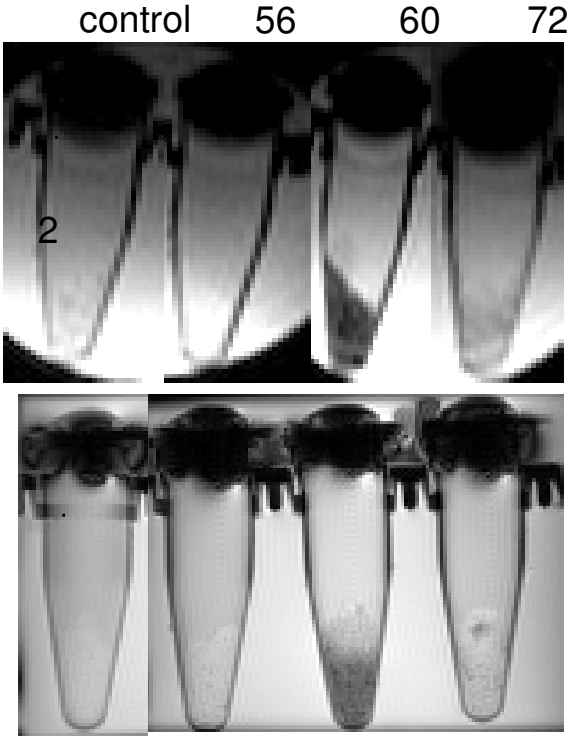

Figure 5.3.6.1.MRI of cells labelled with 1.0mM 56, 60, 72 gadolinium monomer at 2.35T and 9.4T. Top, T1W MRI of labelled cells at 2.35T. Bottom, T1W MRI of labelled cells at 9.4T.

5.3.7. Relaxivity of gadolinium polymers

Polymers were synthesised from the monomer 72. Although this monomer did not have the highest r_1 relaxivity of the monomers assessed, the carbon triple bonds of the propargyl groups on the four branching arms were required to react with the diazide linkers to synthesise the hyperbranched polymer. As discussed in the methods section, the following polymers were synthesised, with different ligand:linker ratios and gadolinium loading (Table 5.3.7.1), with an average polymerisation of 3-5 monomer units.

Polymer	**Ligand:Linker**	**Gadolinium-loading**
$e_{(2:1)}50$	1:0.5	50%
$e_{(2:1)}80$	1:0.5	80%
$e_{(1.5:1)}50$	1:0.67	50%
$e_{(1.5:1)}80$	1:0.67	80%
$e_{(1.33:1)}50$	1:0.75	50%
$e_{(1.33:1)}80$	1:0.75	80%
$e_{(1.165:1)}50$	1:0.86	50%
$g_{(1.5:1)}$	1:0.67	100%
$g_{(1:2)}$	1:2	100%
$g_{(1:4)}$	1:4	100%
$g_{(1:6)}$	1:6	100%

Figure 5.3.7.1 Gadolinium polymers synthesised from the monomer 72 and diazide linkers.

r_1 and r_2 relaxivity was calculated for each polymer at 2.35T (Table 5.3.7.2). Polymer $e_{(1.5:1)}50$ had the highest r1 relaxivity of all polymers. Polymers $e_{(1.5:1)}50$, $e_{(1.33:1)}50$, $e_{(2:1)}80$, and $e_{(2:1)}50$ had r_1 values greater than monomer 72. None of the 100% loaded polymers (g-polymers) had r_1 relaxivity greater than monomer 72. No clear pattern in gadolinium loading effect on r_1 relaxivity was observed among the e-polymers, and neither was a relationship between ligand:linker ratio and relaxivity observed.

2.35T

	r1 (mM s-1)	*r2 (mM s-1)*
Gd-DTPA	5.2471	6.3287
Dotarem	5.277	4.528
56	4.4891	2.7775
60	2.8383	3.7391
72	2.8622	2.4729
e$_{(1.165:1)}$50	1.9855	1.5302
e$_{(1.33:1)}$50	3.2401	1.4544
e$_{(1.33:1)}$80	0.8602	0.9612
e$_{(1.5:1)}$50	4.522	4.4952
e$_{(1.5:1)}$80	2.4464	3.8205
e$_{(2:1)}$50	2.9858	4.804
e$_{(2:1)}$80	3.3829	3.432
g$_{(1.5:1)}$	3.054	4.0973
g$_{(1:2)}$	2.4779	2.6983
g$_{(1:4)}$	2.2802	2.4435
g$_{(1:6)}$	2.5628	3.0891

Figure 5.3.7.2 r_1 and r_2 relaxivity of gadolinium polymers at 2.35T.

r_1 and r_2 relaxivity was calculated for $e_{(1.5:1)}50$, $g_{(1.5:1)}$, $g_{(1:4)}$ at 9.4T, and r_1 values were slightly lower at 9.4T than 2.35T (Table 5.3.7.3).

9.4T

	r1 (mM s-1)	*r2 (mM s-1)*
Gd-DTPA	5.5067	4.8195
56	3.1573	3.9592
60	2.253	3.4087
72	2.8577	4.7913
e$_{(1.5:1)}$50	4.5139	0.6772
g$_{(1.5:1)}$	2.5063	8.09
g$_{(1:4)}$	2.0411	4.0237

Figure 5.3.7.3 r_1 and r_2 relaxivity of gadolinium polymers at 9.4T

5.3.8. Polymer cell viability

Polymers were then assessed for their effect on cell viability in the neural stem cell line ST14A. Cells were incubated in a range of concentrations of polymers, 0-1.0mM, to assess cell metabolism using the Alamar Blue and MTT assays (Figure 3.8.1). Polymers $e_{(2:1)}50$, $e_{(1.33:1)}50$, $g_{(1.5:1)}$, $g_{(1:2)}$, and $g_{(1:6)}$ were not assessed because they formed a precipitate when mixed with the cell culture medium. In some polymers cell viability at 1.0mM was not assessed due to a lack of sufficient synthesised polymer for the experiment.

In the Alamar blue assay, a trend of increasing aberrance from control cell metabolic activity at higher concentrations was observed in all e-polymers, but not the g(1:4) g-polymer or Gd-DOTA (ANOVA, $p<0.05$ for $e_{(1.5:1)50}$, $e_{(1.5:1)80}$, $e_{(1.65:1)80}$, $e_{(1.65:1)50}$, $g_{(1:4)}$, $e_{(2.1)80}$). All cell conditions were also photographed after the absorbance reading (Figure 3.8.2). Although the absorbance readings suggest an increase in metabolic activity relative to control cells, the microscopy indicated that at higher absorbance readings, cell death and cell lysis had occurred. Although cells were washed between polymer incubation and Alamar blue assay, cell lysis products from the 4 h assay interval may have interfered with the absorbance reading, resulting in high rather than low absorbance readings to indicate cell death.

In the MTT assay, a similar trend in metabolic activity was not observed. In all e-polymers, a decreased metabolic activity relative to control cells was observed, at least at low concentrations. The MTT requires an additional experimental step of cell fixation and washing, which may have partially, but not fully, removed cell lysis products, leading to mixed results at higher concentrations.

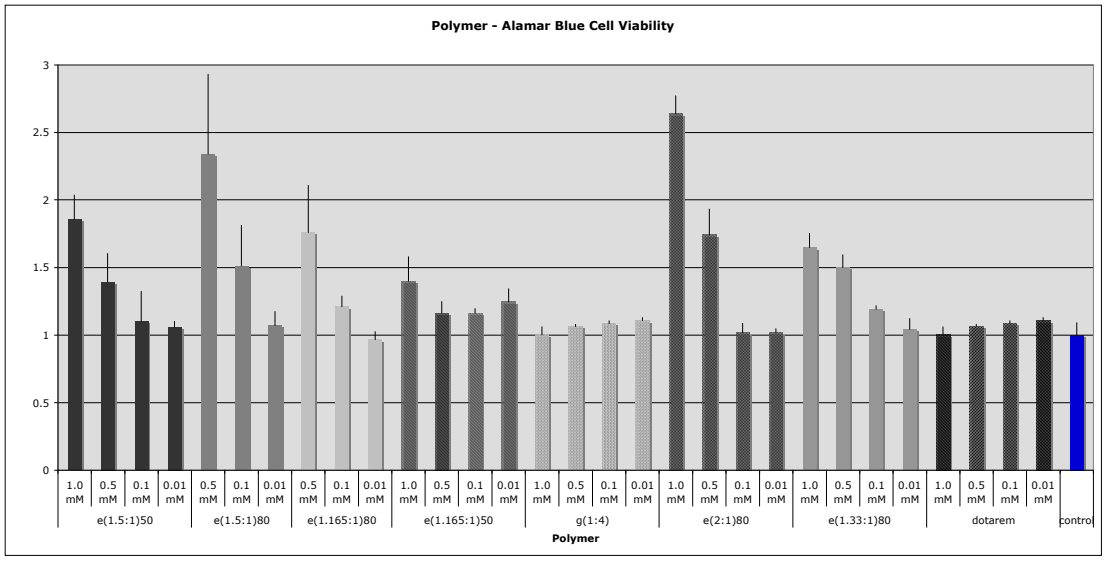

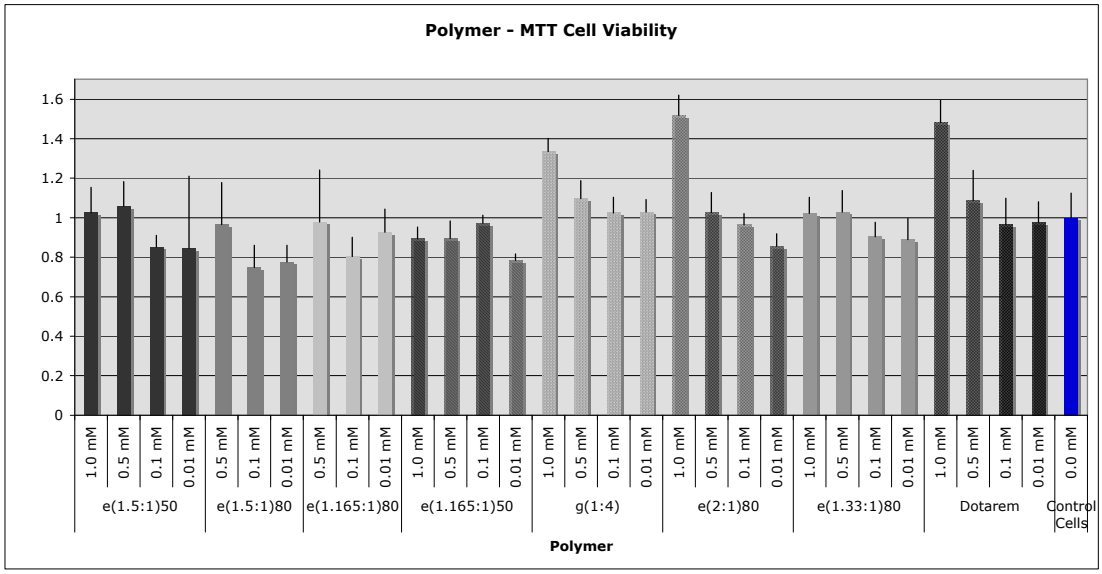

Figure 5.3.8.1 Cell viability assays for gadolinium polymers. Top, Alamar Blue assay. Bottom, MTT assay.

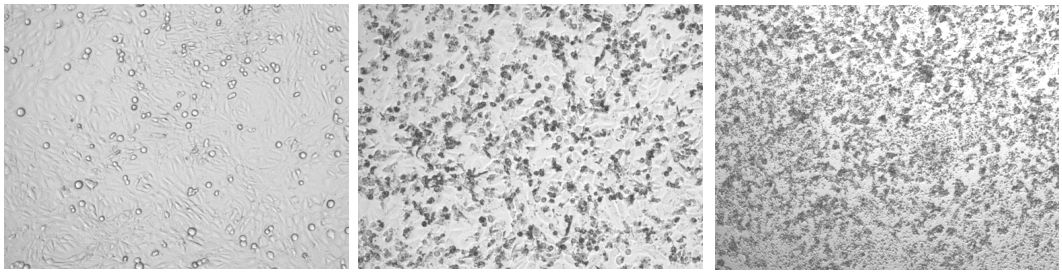

Figure 5.3.8.2 Light micrographs of cells after incubation with gadolinium polymers. A, example of healthy confluent cells. B, example of intermediate mixed population of dead and living cells. C, cell death and cell debris. Scale bar, 200um.

5.4. Discussion:

In summary, r_1 and r_2 relaxivity, cell viability and cell labelling was assessed for allyl-, styryl, and propargyl-derivatives of the Gd-DOTA-tetraamide monomer. Gadolinium polymers based on the propargyl-derivative were synthesised, with varying ligand:linker ratios and gadolinium loading, to determine optimum polymer design for high r_1 relaxivity. Cell viability was also assessed for polymers.

For monomers, r_1 and r_2 relaxivity were lower than Gd-DOTA or Gd-DTPA, at 2.35T and 9.4T. For all monomers, r_1 and r_2 relaxivity were lower at 9.4T than 2.35T. No trend was observed for r_2 relaxivity across field strengths.

	2.35T		**9.4T**	
	r_1 (mM s^{-1})	***r_2 (mM s^{-1})***	***r_1 (mM s^{-1})***	***r_2 (mM s^{-1})***
Gd-DTPA	5.2471	6.3287	5.5067	4.8195
Gd-DOTA	5.277	4.528		
56	4.4891	2.7775	3.1573	3.9592
60	2.8383	3.7391	2.253	3.4087
72	2.8622	2.4729	2.8577	4.7913

Figure 5.4.1 Summary of r_1 and r_2 relaxivity for gadolinium monomers at 2.35T and 9.4T

Cell viability was good for all monomers. Cells incubated with monomers could be labelled and imaged. No histological stain exists for gadolinium, but T_1 and T_2 effects were observed in pelleted labelled cells. T_1-weighted positive contrast was observed in monomer 56 but not monomers 60 or 72, where negative contrast was observed. One possible explanation for this could be a strong T2 effect in the cells. Dependent on the route of cell internalisation, gadolinium monomers may be sequestered in endosomes or lysosomes. If water exchange between cell components (eg between endosome and cytoplasm) is slow relative to the optimal water exchange rate of the monomer, the r_1 of the complex will be decreased due to less water gaining access to the Gd^{3+} ion. In this situation, the inner sphere effects of gadolinium may be limited. Additionally, at high concentrations, paramagnetic contrast agents can affect T_2 through outer sphere effects of gadolinium, decreasing signal intensity locally on T_2-weighted images (Modo et al., 2005). If this is the case, cell labelling can be modified to promote cytoplasmic localisation, for example by electroporation or liposome transfection. Electron microscopy analysis will be necessary to determine the internal localisation of the contrast agents. The chemistry of the monomer branching arms appears to have a significant effect on cell labelling, and T_1 and T_2.

Polymer $e_{(1.5:1)}50$ had the highest r1 relaxivity of all polymers, with $e_{(1.33:1)}50$, $e_{(2:1)}80$, and $e_{(2:1)}50$

also recording r_1 values greater than monomer 72. The mean polymer was composed of only 3-5 monomer units, which was much less than expected. The effect of a larger macromolecule in increasing r_1 relaxivity will also be less than expected, but an increased r_1 relaxivity was still observed. Optimising the synthesis reaction to obtain higher molecular weight polymers with greater monomer units per polymer may lead to a further increase in r1 relaxivity.

None of the 100% loaded polymers (g-polymers) had r_1 relaxivity greater than monomer 72. These initial results suggest that partial loading of polymers with gadolinium yields higher r_1 relaxivity values than 100% loading, however ligand:linker ratios were also different for g-polymers compared to e-polymers, so few direct comparisons can be made. No clear pattern in gadolinium loading effect on r_1 relaxivity was observed among the e-polymers, and neither was a relationship between ligand:linker ratio and relaxivity observed.

Sample	**ligand:linker**	**Gd^{3+} loading**	**r1**	**r2**
$e_{(1.165:1)}$50	1:0.86	50%	1.9855	1.5302
$e_{(1.33:1)}$50	1:0.75	50%	3.2401	1.4544
$e_{(1.33:1)}$80	1:0.75	80%	0.8602	0.9612
$e_{(1.5:1)}$50	1:0.67	50%	4.522	4.4952
$e_{(1.5:1)}$80	1:0.67	80%	2.4464	3.8205
$e_{(2:1)}$50	1:0.50	50%	2.9858	4.804
$e_{(2:1)}$80	1:0.50	80%	3.3829	3.432
$g_{(1.5:1)}$	1:0.67	100%	3.054	4.0973
$g_{(1:2)}$	1:2	100%	2.4779	2.6983
$g_{(1:4)}$	1:4	100%	2.2802	2.4435
$g_{(1:6)}$	1:6	100%	2.5628	3.0891

Figure 5.4.2 Summary of r_1 and r_2 relaxivity for gadolinium polymers at 2.35T

Cell viability was reduced for polymers, relative to control cells and gadolinium monomers, and viability assays were confirmed with microscopy. Monomer 72, the ligand from which the polymer was synthesised, did not affect cell viability in Alamar Blue or MTT assays, so the viability effects may be due to the polymer size or the presence of diazides. This must be further investigated for polymers to be considered candidate contrast agents for cellular imaging. In future studies, incubated cells will be imaged as a cell pellet to determine polymer internalisation and effect on T_1-weighted contrast.

Most g-polymers reacted with the cell culture medium to form a precipitate, possibly reacting with the phenol red indicator dye, as the precipitate formed was red. Further viability tests with g-

polymers could be carried out in culture medium without phenol red. The polymer may also be reacting with fetal calf serum, in which case cell culture in serum-free medium may be optimised for cell labelling.

Further optimization of the polymers would be required before they have the potential to be an improved MRI contrast agent to what is currently available. The monomeric chelates had lower r1 relaxivity compared to Gd-DTPA or Gd-DOTA, and relaxivity was not significantly increased in the polymers. Optimisation of polymer size and gadolinium loading might lead to improved r1 relaxivity. Labelling efficiency and cellular localisation could be optimized by the use of targeting vectors or transfection agents.

In conclusion, the characterisation of novel gadolinium monomer and polymer contrast agents is described. R1 and r2 relaxivity was measured for a number of gadolinium-based monomer and polymer compounds at 2.35T and 9.4T. Relaxivity was comparable or less than Gd-DOTA or Gd-DTPA. For monomers, cytotoxicity was low, but most polymers had a toxic effect on the ST14A neural stem cell line. For optimal contrast agent design, compound chemistry, relaxivity, and cytotoxicity must all be considered at early stages of design.

6. *In vivo magnetic resonance imaging of endogenous neuroblasts labelled with a ferumoxide-polycation complex*

6.1. Introduction

Neural stem and progenitor cells (NPC) persist in the adult brain (Reynolds et al., 1992; Morshead et al., 1994), and have been identified in the subventricular zone (SVZ) of the lateral ventricles (Merkle et al., 2006; varez-Buylla et al., 2004; varez-Buylla et al., 2002), a region which is capable of generating new neurons in the mature brain. NPC proliferate, generating neuroblasts that migrate along the rostral migratory stream (RMS) to the olfactory bulb (OB), where they differentiate into olfactory interneurons (Lois et al., 1993). In pathological environments, for example following cerebral ischaemia, neural stem and progenitor cells and neuroblasts respond by proliferation and migration towards sites of injury (Arvidsson et al., 2002; Parent et al., 2002; Zhang et al., 2001; Kokaia et al., 2006). This intrinsic sensitivity and responsiveness to disease states raises the prospect of developing therapeutic strategies to enhance the neurogenic response of the SVZ and contribution to brain repair (Tureyen et al., 2005; (Consiglio et al., 2004).

Development of methods capable of monitoring and tracking of endogenous NSC in an *in vivo* imaging system would be of great benefit to the understanding of neuroblast migration away from the SVZ under normal and pathological conditions. Currently, only a few cell tracing methods allow for *in vivo* labelling of endogenous NPC. The most commonly used labelling methods for adult neural stem cells are bromodeoxyuridine (BrdU) (Taupin et al., 2007),; retroviral GFP transduction (Tanaka et al., 2004; Levison et al., 1997); and Cre/loxP transgenic systems such as the targeted expression of CRE recombinase, where expression of GFP or other reporter genes are activated under the promoter of a stem cell gene of interest (Garcia et al., 2004; Young et al., 2007). All of these labelling methods require histological preparation and the use of fluorescence microscopy for imaging.

In vivo monitoring of endogenous NPC has been reported using magnetic resonance spectroscopy (^{1}H-MRS) and MRI contrast agents. Manganas *et al* observed a prominent peak in the spectroscopic profile of NPC, which was identified as a metabolic biomarker exclusive to NPC, and this could be spatially resolved using ^{1}H-MRS in the rodent and human brain (Manganas et al., 2007). Using this method, they were able to distinguish neural stem cells from non-neural stem cells and from mature neural cell types. The limitation of this method is that NPC, as they migrate away from the SVZ, adopt a mature phenotype at their end destination of the OB or infarct lesion, and would lose the unique biomarker expression.

MRI contrast agents have been used to label neural stem cells *in* vitro (Hoehn et al., 2002; Modo et al., 2002) and transplanted labelled cells have been monitored *in vivo* under normal and pathological conditions. Neural stem cells labelled with iron oxide-based MRI contrast agents have been transplanted into the rodent brain following cerebral ischaemia, and monitored over several weeks

using MRI (Hoehn et al., 2002; Arbab et al., 2006). Endogenous cell labelling using MRI contrast agents has been achieved peripherally, where iron oxide MRI contrast agents are preferentially phagocytosed by circulating macrophages (Weber et al., 2005; (Wiart et al., 2007).Within the nervous system, Shapiro *et al* demonstrated that NSC could be labelled *in vivo* with iron oxide beads, Bangs particles, and their migration through the RMS to the OB was successfully imaged (Shapiro et al., 2006). In a subsequent study, Sumner *et al* confirmed that NPC in the SEZ internalise the iron oxide beads and give rise to migrating neuroblasts (Sumner et al., 2009). When the NPC population was subjected to ablation by Ara-C after injection of the iron oxide beads, no new migrating neuroblasts were generated and no hypointense signal loss was observed in the RMS on MRI images. Both of these studies were carried out by injection of a large volume of contrast agent in the ventricles using micron-sized iron oxide particles, and imaged at high magnetic field strength.

In this work we have chosen to focus on Endorem, which is a ferumoxide MRI contrast agent composed of dextran-coated superparamagnetic iron oxide nanoparticles (SPIO) with a diameter of 150 nm, and has FDA approval for MRI contrast imaging in humans. Endorem has been used *in vitro* for cell labelling and tracking using multiple cell types: NPC, mesenchymal, hematopoeitic, and embryonic stem cells (Kustermann et al., 2008; Suzuki et al., 2007; Ben-Hur et al., 2007; Modo et al., 2002; Arbab et al., 2004). It is well tolerated by labelled cells and does not interfere with cell metabolism, cell division or differentiation (Arbab et al., 2005). Furthermore we have used Protamine sulphate, which is a transfection agent used to enhance cell labelling with Endorem in *in vitro* systems, to form the FePro complex (Arbab et al., 2005).

The aim of our study was to develop and optimize a methodology for endogenous cell labeling with future applications for tracking neuroblast migration in the normal and pathological brain. In Chapter 4, we demonstrated that the FePro complex could efficiently label cells *in vitro* at lower concentrations and with greater iron oxide uptake per cell than labeling with Endorem. Our hypothesis was that using a SPIO such as Endorem or the FePro particle would increase labeling efficiency at the SVZ with a smaller injection volume of SPIO than has been required in previous studies with the Bangs MION particles. In this study, the aim was to label the endogenous population of NPC by stereotactic injection of Endorem or FePro into the lateral ventricles adjacent to the SVZ, and to visualise neuroblast migration in the RMS in the normal brain. We observed that while intraventricular injection of Endorem resulted in its distribution throughout the ventricular system and into the periventricular space, the FePro complex was localised to the lateral ventricle. Brains imaged 28 days following injection identified the FePro complex in the RMS using both low (2.35T) and high (9.4T) magnetic field strength systems. Histology confirmed that the FePro complex was localised to the SVZ and RMS, and that neuroblasts within the RMS were labelled with the FePro complex.

6.2. Materials and Methods

6.2.1. Intraventricular injections

Twenty six adult male 220g Sprague-Dawley rats (Charles Rivers, UK) were used. Animals were stereotactically injected with either Endorem (Guerbet Laboratories Ltd, UK; n=5), FePro (n=18), or PBS control (n=3) into the left lateral ventricle. Animals were anaesthetised with 2% isofluorane and 100% O_2 and their head secured and aligned in a stereotactic frame. Body temperature was maintained at 37ºC by use of a rectal thermometer probe and heating mat. Animals were injected with 2.5 µl at 0.2 µl min^{-1} Endorem, FePro, or a control injection of PBS. In two animals, an injection volume of 20 µl FePro was used. The coordinates used were AP -0.08, ML +0.14; DV -0.38. To form the FePro complex, Endorem was mixed with 1mg/ml protamine sulphate (CellTech, UK) in a ratio of 9 µl : 5 µl and incubated for 10 minutes prior to injection. All procedures were in accordance with the UK Animals (Scientific) Procedures Act of 1986, and approved by the UCL Research Ethics Committee. All reagents supplied by Sigma-Aldrich UK unless stated otherwise.

6.2.2. In vivo and ex vivo MRI

MRI animal studies were performed using a 2.35T horizontal magnet with a 120 mm bore (Oxford Instruments Eynsham,UK), interfaced to a Surrey Medical Imaging Systems (SMIS, UK) console. A volume coil (60 mm length) was used to transmit radiofrequency excitation pulses. The magnetic resonance signals were detected using a passively decoupled, single loop, surface coil of 2 cm diameter positioned on the dorsal aspect of the head. Animals were anaesthetised with 2% isofluorane and 100% O_2, and secured on a stereotactic probe for imaging. Body temperature was maintained at 37ºC. Animals were imaged at 48 hours or four weeks post-injection. The 2D T2-weighted spin echo images were acquired with the following parameters: TR = 3000 ms, TE = 28 ms, FOV 30 mm, slice thickness 1 mm, matrix 128 x 128 voxels , 234^2 µm in-plane resolution, 4 averages; or TR = 1500 ms TE =120 ms, FOV 30 mm, slice thickness 1 mm, matrix 128 x 64 voxels, in plane resolution 234 µm x 469 µm, 16 averages.. The 3D gradient echo sequence was performed using the following parameters: TR = 80 ms, TE = 25 ms, FOV 25 mm, matrix 192 x 192 x 146 voxels, resolution 130 µm x 130 µm x 171 µm.. Following MRI, animals were transcardially perfused fixed with 0.9% saline at 4ºC followed by 4% paraformaldehyde (PFA; Sigma-Aldrich, UK) in phosphate buffered saline (PBS) containing 1 mM Gd-DTPA for *ex vivo* MRI. Perfuse-fixed whole brains including the olfactory bulb were removed from the skull after fixation and transferred to a 50 ml Falcon tube containing PFA. In some animals (n=4) the brains were used for ex vivo imaging before freezing for histology. Ex vivo imaging was also performed using a 9.4T horizontal 20 cm bore Varian VNMRS system using a 39 mm RF coil (RAPID Biomedical GmbH, Germany) and a 3D gradient-echo sequence with the following parameters: 2.56^3 cm FOV, 512 x 512 x 512 matrix (256 mm^3), TR=70 ms, TE=10 ms, flip angle 30º, 2 averages.

6.2.3. *Cellular MRI*

CD133+ cells were isolated from peripheral blood of donors stimulated with GCSF using CD133 microbeads (Miltenyi Biotech). CD133+ cells were labelled with Endorem at day 9 of culturing using 0.5 mg Fe/ml of growth medium and were washed twice in 15ml 1xPBS. These cells contained on average 3.9 pg iron oxide, as measured by superconducting quantum interference device (SQUID), and approximately 75% of cells contained. For differential cell labelling (DfL), suspension CD133+ cells were separated from adherent CD133+ cells, and labelled for 22 or 23 hours, followed by additional labelling for 2 hours with the adherent fraction. Labelled cells were washed twice in 15ml 1xPBS and used in experiments as described below. SPIO, as measured by isolation through a magnetic column (Miltenyi Biotech). Labelled-labelled (DfL) CD133+ cells were embedded in low melting point agarose (0.5%, 37^{o}C) at the following concentrations of: 745, 165, 49.5, 16.5 and 0 cells (0.5%, 37 x103/ml in 250 μl eppendorf tubes) and were rapidly cooled prior to horizontal alignment in a 4% agarose phantom in a 9.4T horizontal bore Varian system. Tubes were scanned in a single 0.5 mm slice at the RF isocentre of a 3935 mm coil (RAPID Biomedical GmbH, Germany). T2* weighted images were acquired using a gradient echo sequence (TE=25ms, TR=200ms, FA=30, 5122 matrix) and T2* maps were obtained from 20 echo times (TE 2.5-30ms, TR=200, FA=30, 2562 matrix) using the ImageJ MRI Analysis Calculator plugin (Schmidt, K., ImageJ, U. S. National Institutes of Health, Bethesda, MA USA.)

6.2.4. *Histology*

For immunohistochemistry and histology, fixed brains were left in 1% PFA overnight, transferred to 30% sucrose solution and left at 4^{o}C for 2 days, then frozen and stored at -80^{o}C. Coronal brain sections of 30 or 15 μm thickness were taken on a cryostat. Prussian blue stain for iron was performed with nuclear fast red counterstain or hematoxylin eosin staining. For Prussian blue staining, sections were incubated in 6% hydrochloric acid and 4% potassium ferrocyanide (Sigma-Aldrich, UK) for 20 minutes, then washed in PBS. Sections were then stained with nuclear fast red or hematoxylin eosin stain, and deyhydrated in 95 then 100% ethanol. Sections were transferred to Histoclear for 5 minutes, and mounted using DPX mountant. For immunohistochemistry, sections were incubated in 10% foetal calf serum with 0.1% Triton-X for 30 minutes, followed by goat anti-doublecortin (1:50, Santa Cruz Biotechnology) mouse anti-nestin (1:50; rat401, Developmental Biology Hybridoma Bank) or rabbit anti-GFAP (1:1000; Chemicon) overnight at 4^{o}C. For immunofluorescence staining, sections were washed in PBS and incubated in secondary antibody for one hour. Sections were washed in PBS and mounted with mountant medium (Citifluor Ltd). For immunoperoxidase staining, sections were incubated in 3% hydrogen peroxide for 10 minutes, followed by biotinylated anti-goat (1: 500, Dako) for one hour, and streptavidin-HRP (1:500, Dako) for one hour, with a 10 minute PBS wash between each incubation. Sections were then stained for

Prussian blue and nuclear fast red counterstain. Sections were dehydrated in ethanol and histoclear, and mounted in DPX mountant. For fluorescence microscopy, sections were incubated in cy3 anti-goat, cy3 anti-mouse, or FITC anti-rabbit with Hoescht nuclear stain, and mounted using Citifluor mounting medium. Sections were photographed using a Zeiss Axiophot microscope, OpenLab imaging software and Jenoptik digital camera, or a Leica TCS SP2 confocal microscope for fluorescence imaging. Confocal reflectance microscopy was used to detect iron oxide in the Endorem nanoparticles. The 488nm excitation laser was used and the light acquisition was adjusted to +/- 10 nm of the excitation wavelength to detect signal reflected by magnetite crystals in the nanoparticles. This method has been described to detect submicroscopic magnetite particles in large volumes of tissue (Green et al, 2001).All reagents supplied by Sigma-Aldrich UK unless stated otherwise.

6.3. Results

6.3.1. Distribution of Endorem following intraventricular injection.

Endorem was injected into the left lateral ventricle, which resulted in a hypointensity in ventricles ipsi- and contralateral to the injection site, as well as in the periventricular area medial to the ventricles, on 2.35T MRI spin echo images at 48 hours post-injection. Figure 6.3.1.1A is a coronal section at the level of the lateral ventricles, in which a dark appearance due to the paramagnetic effect of the iron oxide can be observed throughout the lateral ventricles and periventricular area. The inset shows a coronal section at the same level in a sham-injected animal. Multislice imaging demonstrated that the hypointensity extended from 1 mm anterior and 6 mm posterior to the slice shown, extending to the third ventricle.

Prussian blue histology was performed to detect the distribution of iron within and around the ventricles. Prussian blue iron detection on histological sections was compatible with *in vivo* MRI images, which demonstrated that Endorem was present in the anatomical areas displaying hypointensity on MRI images. Figures 6.3.1.1B-D show that Endorem is present in the ventricles as well as in the ventricular ependymal cell layer, the choroid plexus and the periventricular area. Within the lateral ventricle, Endorem was predominantly present in the medial wall, but was also detected in the lateral wall and the choroid plexus. Unexpectedly, the Prussian blue stain extended out from the medial, but not lateral, ependymal layer. Endorem was detected in the periventricular space medial to the lateral ventricles, but not in the striatum lateral to the ventricles. Endorem distribution in the septum appeared heterogeneous, where iron was observed in the dorsal nuclei – the triangular and lateral septal nuclei, septohippocampal and ventrohippocampal nuclei, and the fornix (Figure 6.3.1.1C, and data not shown). In addition, Endorem in the medial periventricular space was present both as dense clusters, as well as diffuse particles, which may indicate intracellular and extracellular iron, respectively (Figure 6.3.1.1D). Some Endorem was present along the injection tract. Endorem

was observed outside of the lateral in all animals with intraventricular administration of Endorem.

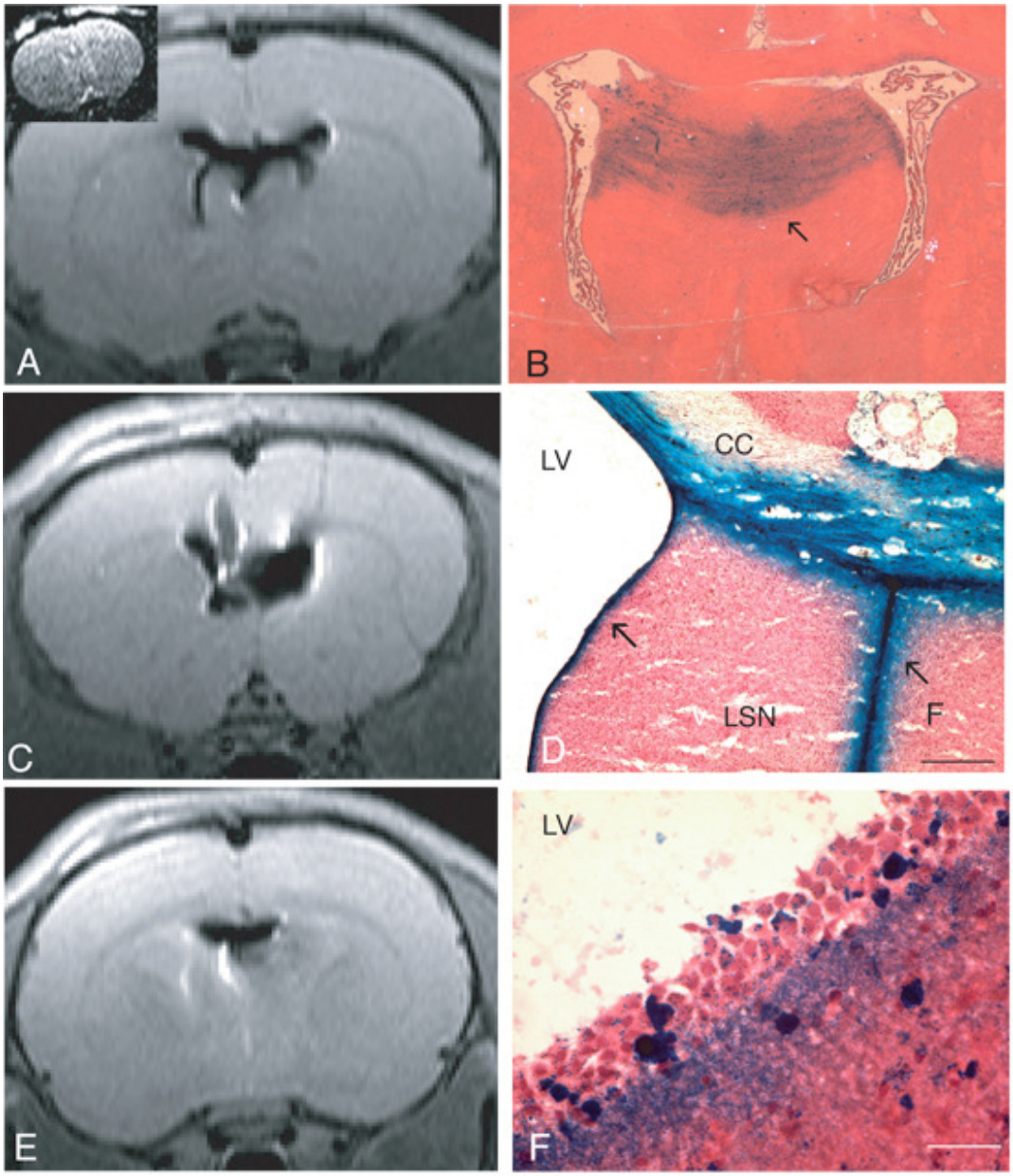

Figure 6.3.1.1 Endorem injection into the left lateral ventricle. A, 2D coronal MRI image at the level of the lateral ventricles.Hypointensity is seen in the ventricles and in the periventricular space medial to the ventricles, which indicates that Endorem is outside of the lateral ventricle. Inset: control, PBS-injection. No hypointensity is observed. **C**, 2D coronal MRI image 1mm anterior to the SVZ slice, showing Endorem distribution in both ventricles and in the medial periventricular space. **E**, 2D coronal MRI image 1mm rostral to the SVZ slice, showing Endorem distribtion in the medial periventricular space. **B, D, F** Prussian blue (PB) histology staining for iron, coronal sections. B, PB present in the periventricular space between left and right ventricles (arrow). D, PB in the corpus callosum (CC), lateral septal nucleus (LSN), fornix (F), and medial wall of the lateral ventricle (black arrow). Scale bar, 100um. F, high magnification view of medial wall of lateral ventricle (LV) and periventricularventricular space. Scale bar, 30um.

6.3.2. Localization of the FePro complex following intraventricular injection

In contrast to our observations following intraventricular microinjection of Endorem, injection of the FePro complex into the left lateral ventricle generated hypointensity in 2.35T MRI spin echo images in the left lateral ventricle only, in all animals. Hypointense contrast was absent from the periventricular area or the right lateral ventricle, at 48 hours post-injection. Figure 2A shows a coronal section at the level of the lateral ventricles 48 hours following intraventricular injection, demonstrating that the FePro is restricted to the left lateral ventricle only (Figure 6.3.2.1A, arrow). No hypointensity was observed in the right lateral ventricle, or in the periventricular space between the ventricles.

The Prussian blue histological stain for iron was compatible with *in vivo* MRI images, and confirmed that FePro was detected in the medial and lateral walls of the left lateral ventricle, and in the choroid plexus (not shown), but absent from the periventricular spaces medial and lateral to the ventricles (Figure 6.3.2.1B). In contrast to intraventricular injection of Endorem, FePro labelling was predominantly localised to the ependymal and subependymal layers of the medial and lateral walls of the ventricle.

Confocal reflectance microscopy analysis indicated that cell incorporation of the FePro contrast agent was predominantly in Nestin+ progenitor cells and ependymal cells of the SVZ (6.3.2.1C), as well as the GFAP+ astrocyte population in the SVZ (Figure 6.3.2.1D). At the 48 hour timepoint, no FePro-labelled Doublecortin+ neuroblasts were observed in the SVZ or RMS in sections analysed.

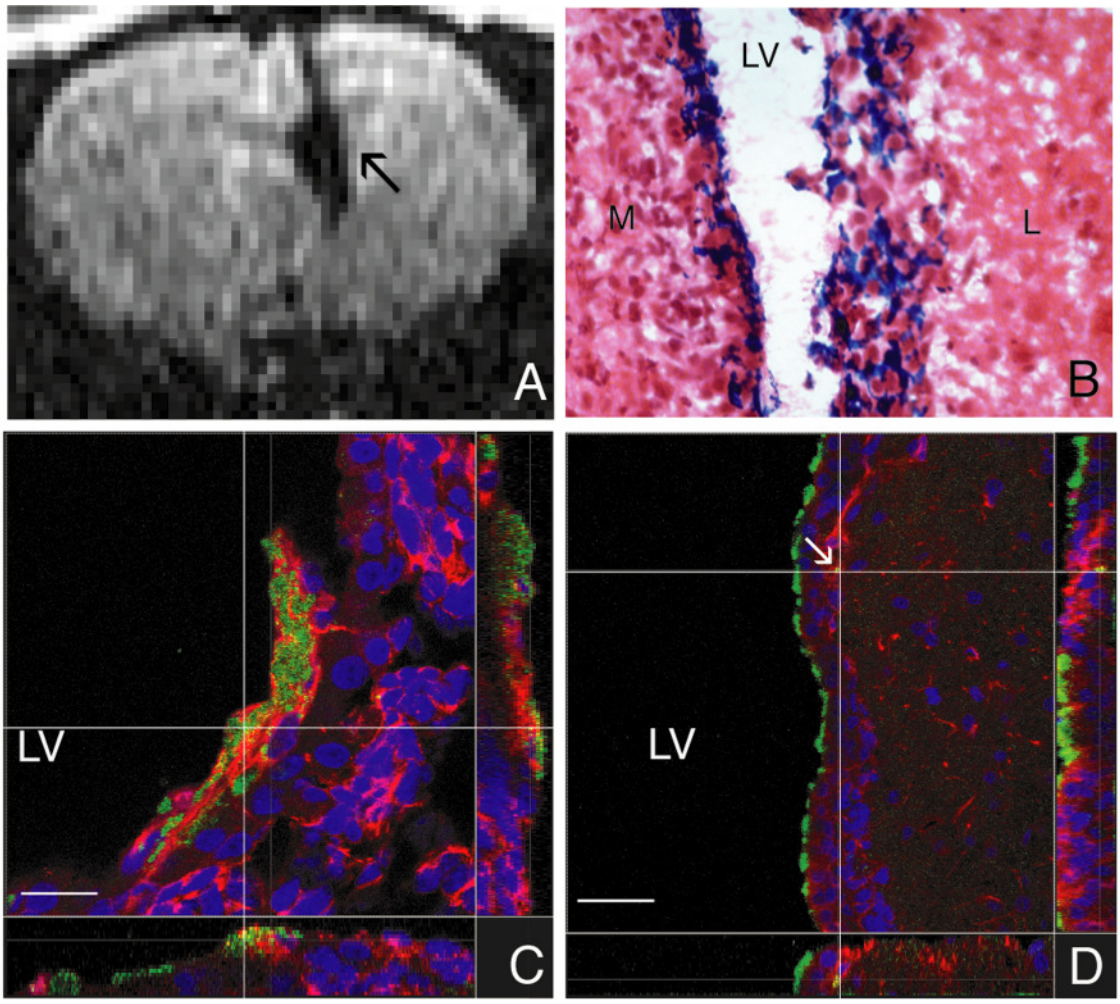

Figure 6.3.2.1 FePro injection into the left lateral ventricle. A, 2D coronal MRI image at the level of the lateral ventricles.Contrast is seen in the left ventricle only (white arrow) and not in the periventricular space medial to the ventricles, indicating that the contrast agent is retained within the ventricle. **B,** Prussian blue histology staining for iron shows iron restricted to the medial and lateral walls of the left lateral ventricle (LV). No PB is observed in the periventricular spaces medial (M) or lateral (L) to the ventricle. **C, D,** Immunohistochemistry and reflectance mode confocal microscopy for the detection of iron show Nestin-positive (C, red) and GFAP-positive (D, green) cells in the SVZ labelled with the FePro contrast agent (yellow), indicating that the FePro contrast agent is incorporated by NPC and astrocytes in the SVZ. Scale bars: B, 30 μm; C, 30 μm; D, 50 μm.

6.3.3. Analysis of the FePro complex in the RMS and OB

Twenty eight days following intraventricular injection, *in vivo* and *ex vivo* 3D gradient echo images were acquired on the 2.35T system. Figure 3 shows *in vivo* and *ex vivo* sagittal view of the left hemisphere in two separate animals. Hypointensity was still observed in the left lateral ventricle on *in vivo* MRI images (Figure 6.3.3.1A, B), and remained absent from the periventricular space medial to the ventricles and from the right lateral ventricle, suggesting that up to this timepoint the FePro

remains restricted to the left lateral ventricle. Hypointensity was detected in the rostral migratory stream on *in vivo* and *ex vivo* images at low magnetic field strength (2.35T; Figure 6.3.3.1C-F). Hypointensity was also observed along the injection tract and in the subarachnoid space. However, little or no hypointense contrast was observed in the olfactory bulb at 28 days post-injection at low field strength. At this timepoint, neuroblasts would be expected to have migrated from the subventricular zone through the rostral migratory stream and arrived at the olfactory bulb.

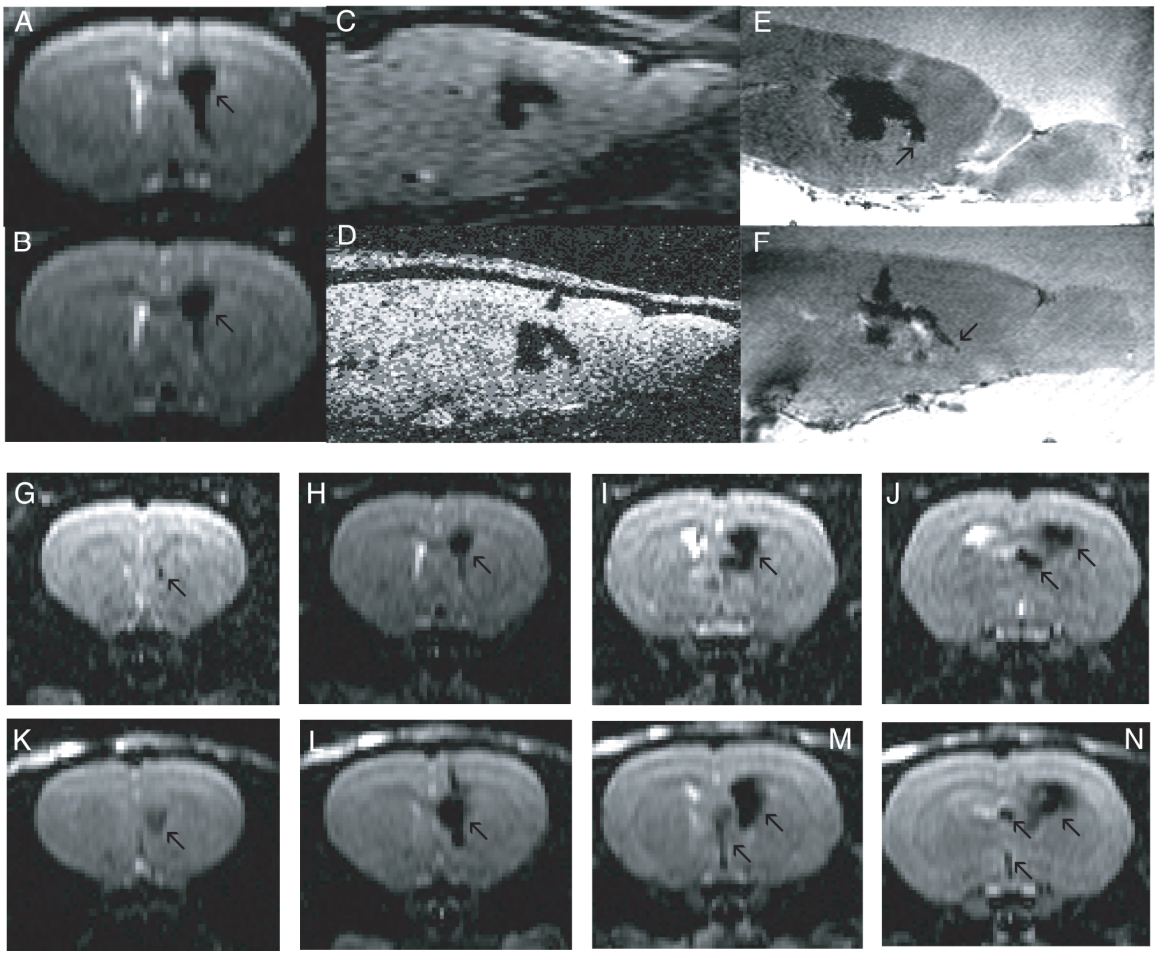

Figure 6.3.3.1 FePro labelling of the SVZ: MRI. A, B: coronal T2-weighted image at low magnetic field strength (2.35T) of FePro-injected left ventricle at 28 days post-injection in two separate animals. Contrast is seen in the left ventricle only, and no hypointensity is visible in the contralateral ventricle or septum. Arrows indicate hypointensity in the left ventricle.. **C, D:** *in vivo* T2*-weighted sagittal image of FePro-injected animals. **E, F:** *ex vivo* T2*-weighted sagittal image of separate animals after perfuse fixation. Arrows denote hypointensity in the RMS. G-N, 2D coronal T2-weighted images of 2 separate FePro-injected animals (G-J and K-N), showing FePro distribution 1mm anterior (G, K), 1mm posterior (I, M) and 2mm posterior (J, N) to the SVZ section (H, L). FePro is restricted to the left ventricle throughout the brain. Arrows denote FePro in the ventricles.

Perfused-fixed brains were also imaged on a 9.4T experimental system at the 28 day timepoint (Figure 6.3.3.2). On the high field system, increased spatial resolution and signal to noise was achieved compared to the low field 2.35T system, as well as increased sensitivity to the local field inhomogeneities associated with the iron oxide in the FePro complex. We observed greater susceptibility effects at the injection site of the lateral ventricles at 9.4T compared to 2.35T, as well as a 'blooming' effect that extended the hypointense contrast beyond the ventricles. In two animals injected with a larger volume of contrast agent, 20 μl FePro, the susceptibility effects extended into the ipsilateral striatum and cortex, the contralateral hemisphere, third and fourth ventricles, and the RMS (Figure 6.3.3.2A, inset). The high field data was in agreement with that observed at low field: hypointense contrast was detected in the left lateral ventricle and RMS. Additionally, some hypointense voxels were observed in the anterior RMS and at the OB (Figure 6.3.3.2B-E), in contrast to our data at low magnetic field strength.

Prussian blue stain for iron was performed to assess the distribution of the FePro complex in the brain. In all animals, Prussian Blue histology was compatible with *in vivo* and *ex vivo* MRI images. FePro-labelled cells were observed in the SVZ, RMS and OB granule cell layer, as well as in the choroid plexus and subarachnoid space (Figure 6.3.3.3). FePro-labelled cells were observed in the OB, despite no hypointensity being observed on *in vivo* or *ex vivo* MRI images at the OB at low field strength, but in agreement with our data at high field strength (Figure 6.3.3.3A, B). An average of 180 FePro-labelled cells were counted per RMS. The estimated total volume of the RMS from the anterior SVZ to the OB is 0.24 mm^3, based on histological quantification of mean RMS area and stereotactic calculation of total RMS length.2.4 X 10^4 μm^3. Our data therefore indicate that there are approximately 750 labelled cells per mm^3 in the RMS. To assess whether FePro-labelling provided adequate MR contrast for *in vivo* imaging at these concentrations, cells labelled with Endorem, containing 3.9 pg of iron oxide per cell, were suspended in agarose and imaged in an Eppendorf phantom using the 9.4T MRI system. Cells were clearly visible as signal voids due to the SPIO-induced decrease in T2*. At a concentration of 7508 cells/mm^3 suspended in agarose there was a 84% decrease in T2* compared to control unlabelled cells . Cells were detectable at dispersions of 8 cells/mm^2 due to the SPIO-induced decrease in T2* (T2* values: unlabelled cells = 107 100ms; labelled cells 2872 ms) and in corresponding signal intensity in T2*-weighted images indicating the detection of cells at these at high-field even at low numbers.

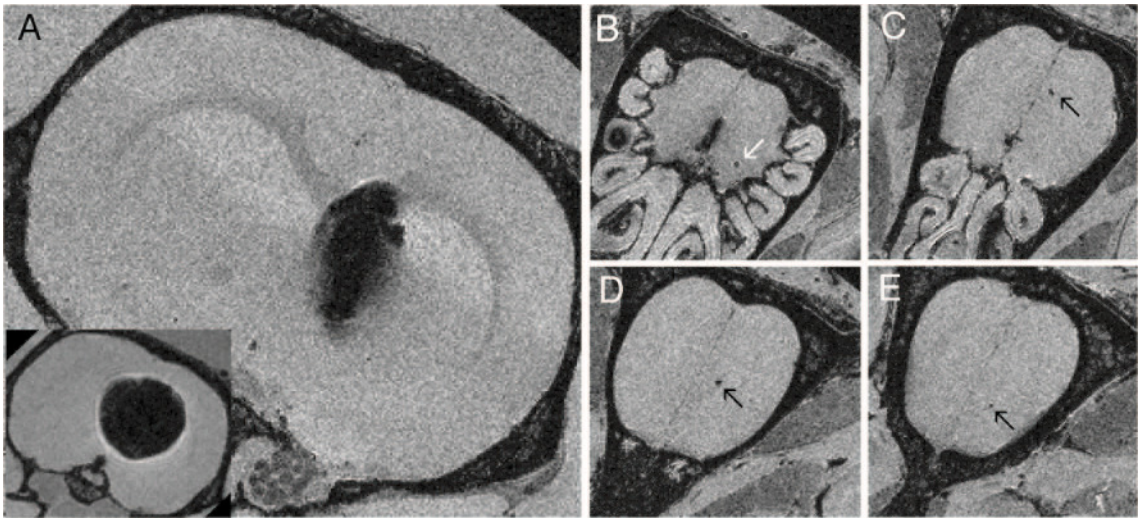

Figure 6.3.3.2 FePro labelling of the SVZ: high field 9.4T MRI. A, *Ex vivo* T2*-weighted coronal image of FePro-injected lateral ventricle at 28 days post-injection. **B-E,** coronal sections of the olfactory bulb. Arrows indicate punctate regions of hypointensity.

Prussian blue staining of coronal sections at 28 days post-injection did not detect FePro in the periventricular space or outside of the RMS. Doublecortin+ FePro-labelled cells were observed in the SVZ by confocal reflectance microscopy, and in the RMS by immunoperoxidase and horseradish peroxidase immunohistochemistry with Prussian blue staining, indicating that neuroblasts in the RMS are labelled with the FePro contrast agent (Figure 6.3.3.3E-H).

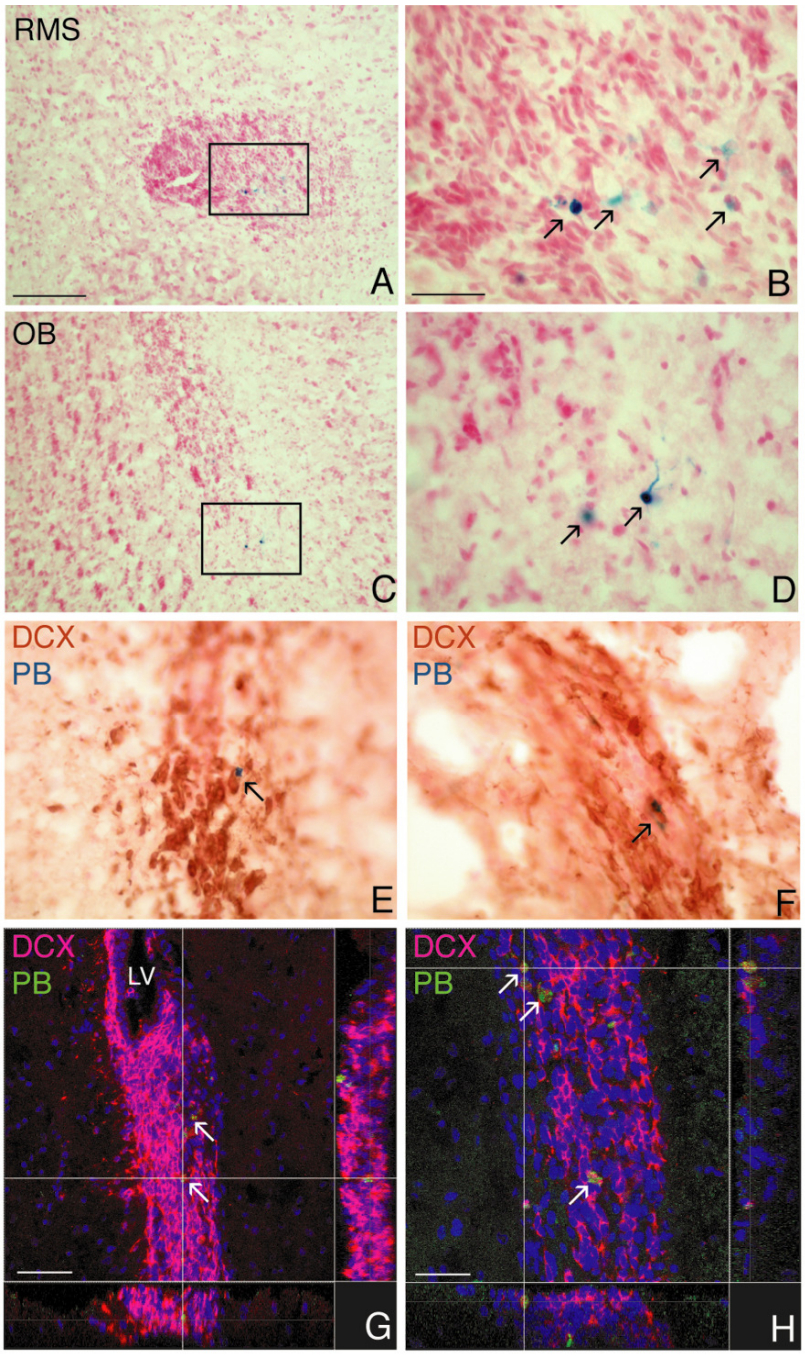

Figure 6.3.3.3 A-D. Prussian blue histology at 28 day timepoint. Prussian blue stain for iron oxide with nuclear fast red counterstain showing FePro-labelled cells in the rostral migratory stream (RMS), and olfactory bulb (OB) at 4 weeks post-injection. Scale bar, 200 μm. Blue box indicates area of adjacent high resolution insert. Arrows denote labelled cells. Scale bar, 40 μm. **E, F.** FePro-labelled cells in the RMS co-label with doublecortin. Brown, doublecortin positive neuroblasts (HRP) at 28 days post-FePro injection. Blue, FePro-labelled cells (prussian blue stain for iron). Arrows indicate FePro-labelled doublecortin-positive cells. Scale bar, 40 μm. **G, H** Immunofluorescent staining and reflectance mode confocal microscopy show Doublecortin-positive (red) FePro-labelled (yellow) cells in the SVZ (G) and RMS (H) at 28 days post-injection. Scale bars: A, C, 100 μm; B, D–F, 30 μm; G, 50 μm; H, 30 μm.

6.4. Discussion

In this study we demonstrate that NPC and neuroblasts can be labelled with MRI contrast agents at the SVZ, and migrating neuroblasts can be visualised using MRI in the RMS at low magnetic field strength. Two MRI contrast agent cell labelling approaches – using Endorem or and the FePro complex – were compared, and were shown to have very different distributions in the brain following intraventricular injection. Endorem injection resulted in its distribution throughout the ventricular system as well as in the periventricular space medial to the lateral ventricles. Therefore, Endorem may offer the potential to investigate the *in vivo* properties of the cerebrospinal fluid barrier in the brain and the transport of solutes throughout the brain using MRI, with potential applications for drug targeting. In contrast to Endorem, the FePro complex was restricted to its injection site, the left lateral ventricle. Furthermore, the FePro complex was detected in the SVZ and RMS at low and high magnetic field strength 28 days following intraventricular injection, and histology confirmed that neuroblasts within the RMS were labelled with the FePro complex. These results may facilitate the study of neuroblast migration by establishing a methodology for *in vivo* labelling and monitoring of the endogenous population.

6.4.1. Endorem distribution may reflect solute transport in the brain

Due to the observation of Endorem outside of the ventricle following intraventricular injection, Endorem was not a suitable MRI contrast agent for endogenous cell tracking. Endorem was observed within the lateral ventricles and in the periventricular space medial to the ventricles. It has previously been reported that CSF flow created by the ciliated ependymal cells within the ventricles is responsible for circulation of substances throughout the ventricular system (Sawamoto et al., 2006), and may account for the distribution of Endorem we observed throughout the ventricular system. We observed that Endorem moved more readily into the septum than into the striatum lateral to the ventricles, however the mechanism of this transport is not known. Endorem movement into the medial periventricular space may occur via transcytosis through ependymal cells –- as has been reported with horseradish peroxidase (Ueno et al., 2000)– via a paracellular route, or both. Endorem was detected in ependymal cells of the medial and lateral walls of the lateral ventricle, which would support active transcellular transport, but does not exclude the possibility of a paracellular route. Endorem particles in the periventricular space may be intracellular, extracellular, or both. Ferric iron, such as the iron oxide in Endorem, stored in the cellular compartment has been described as appearing as dense conglomerates of Prussian blue stain on histological sections, whereas free ferric iron appears pale faint blue (Schenck and Zimmerman, 2004). Within the periventricular space, in the septal nuclei between the ventricles, both types of Prussian blue staining was observed, suggesting

that Endorem may be present both extra- and intracellularly.

6.4.2. FePro complex does not diffuse into the periventricular space

Formation of the Endorem-protamine sulphate complex appears to inhibit the movement of Endorem into the periventricular space. In the absence of protamine sulphate, we have observed that Endorem is distributed throughout the periventricular space. This may be due to the larger molecular size of the aggregated Endorem particles within the FePro complex, inhibiting paracellular transport. Alternatively, protamine sulphate interaction with cell membranes may encourage or favour endocytosis and storage of the FePro complex within cells in contact with the complex. Protamine sulphate is a polycationic compound that is commonly used as a transfection agent for viral gene transfer. Its action is by aggregation of negatively-charged entities to create a complex, and increasing contact of the complex with cell membranes due to its positive charge. Endorem nanoparticles are coated with negatively-charged dextran, and protamine sulphate has been used in conjunction with Endorem *in vitro* for cell labelling (Arbab et al., 2005; Arbab et al., 2004). We have found that *in vitro*, protamine sulphate can increase cell uptake of the FePro complex four-fold compared to cell incubation with Endorem alone, as supported by quantification of cell iron content using the superconducting quantum interference device (SQUID, unpublished data). Other *in vitro* studies are in agreement with this data (Arbab et al., 2005).

6.4.3. FePro allows imaging of endogenous migrating neuroblasts

The FePro-labelled migrating neuroblasts produce hypointensity in MRI T2- and T2* -weighted images, observed in the RMS and OB. The FePro complex was detected in the SVZ, RMS on low field MRI images, and in the OB on images acquired at high field strength at 28 days post-injection.s. This is consistent with SVZ labelling observed at 2 days post-injection, and subsequent migration of labelled neuroblasts from the SVZ, detected later by MRI and Prussian blue staining for FePro. Immunohistochemistry indicates that at 48 hours post-injection, Nestin+ progenitor cells and GFAP+ astrocytes in the SVZ, of which a subpopulation are stem cells, have incorporated the FePro contrast agent. At later timepoints, we observed Doublecortin+ neuroblasts in the RMS labelled with the FePro complex. It is likely that this neuroblast labelling occurred at the lateral ventricles. Our hypothesis was that injection of MRI contrast agents into the lateral ventricle would be expected to non-selectively label cells in the region: neural stem cells, progenitor cells and neuroblasts, as well as ependymal cells and the choroid plexus. The data suggest that FePro-labelled stem or progenitor cells gave rise to neuroblasts that retained the FePro label, and migrated through the RMS and towards the OB.

The *in vivo* imaging of neuroblasts was achieved using a smaller injection concentration of iron oxide than previously reported by Shapiro *et al*, and without the addition of growth factors to promote cell

labelling at the SVZ. In this study, 2 μl of FePro complex was injected into the left lateral ventricle, in contrast to the 50 μl injection volume of Bangs particles and in some cases together with epidermal growth factor (10 μl, EGF)(Shapiro et al., 2006). The reduced susceptibility effects at the injection site, due to the smaller injection volume, will also permit imaging the short distance migration of neuroblasts in pathological environments, for example, their migration from the SVZ into the striatum following cerebral ischaemia. If there is endogenous neuroblast migration from the SVZ following an injury, it should be apparent using this method. In the two previous studies using the Bangs particles, the susceptibility effects from the 50ul injection of Bangs particles caused a 'blooming effect' into the striatum and cortex, therefore short distance neuroblast migration in response to brain injury is potentially obscured. Similarly in our study, increasing the injection volume to 20 μl FePro resulted in susceptibility effects extending into the striatum, cortex and contralateral hemisphere. The smaller 2 μl injection volume may also account for the lateralisation we observed in the ventricles, where the FePro complex did not diffuse throughout the CSF and into the contralateral ventricle, a result which will be of some experimental benefit in future studies.

This method of endogenous labelling of the SVZ with FePro complex has some limitations in that we observed a low number of labelled neuroblasts, particularly at longer distances from the injection site. While at 48 hours post-injection the SVZ appeared uniformly and non-selectively labelled with the FePro complex, at 28 days post-injection few FePro-labelled neuroblasts were observed in the OB on histological sections. FePro-labelled cells were observed throughout the RMS at 28 days post-injection, although the majority of FePro labelling remained at the SVZ. Given the low number of FePro-labelled neuroblasts within the RMS and at the OB, MRI detectability of FePro was good at both magnetic field strengths. Labelled neuroblasts at the beginning of the RMS, within the first millimeter distance from the anterior SVZ, could be detected at low field strength, and without interference from the susceptibility effects of the large concentration of iron oxide at the injection site. We were able to observe low cell numbers in the olfactory bulb using a 9.4T system, which was corroborated by *in vitro* phantom experiments.

Further possible limitations of the method are that the FePro complex persists at the injection site after the initial injection. FePro was detected in the SVZ after 28 days following injection. In future applications, this may limit the capturing of a time window of migration.,. It will provide, however, a cumulative indication of neuroblast migration from the time of injection onwards. Finally, it is possible that resident microglia may take up the FePro complex of neuroblasts if they die, and this would be indistinguishable on MRI images. However, the fact that most Prussian blue-positive cells in the RMS express Doublecortin suggests that this should not present a major obstacle. Furthermore, immunohistochemical detection of microglia in the RMS with the OX-42 antibody is low (data not shown). This is consistent with the finding by Shapiro et al (Shapiro et al., 2006), that only a small population of microglial cells contain Bangs particles in the RMS.

In conclusion, we have shown that intraventricular injection of Endorem results in its distribution throughout the ventricular system and into the periventricular space, whereas the FePro complex remains localised to the lateral ventricle. We have demonstrated that neuroblasts can be labelled with MRI contrast agents via the SVZ, and migrating neuroblasts can be visualised using MRI in the RMS at low and high magnetic field strengths. This novel methodology for *in vivo* labelling and monitoring of endogenous neuroblasts using MRI will be valuable for future applications in investigating neurogenesis under pathological conditions.

7. *Investigation of subventricular zone stem cell subpopulation contributions to neuroblast migration following cerebral ischaemia by lineage tracing*

7.1. Introduction

A population of neural stem cells (NSC) exists in the subventricular zone (SVZ) of the mature brain (Reynolds et al., 1992) and generates new neurons throughout adult life. In the normal brain, the neural stem cells divide to generate transit-amplifying daughter cells, which in turn generate neuroblasts that migrate through the rostral migratory stream (RMS) towards the olfactory bulb (OB), where they differentiate into olfactory bulb interneurons (Lledo et al., 2006g; Lledo et al., 2008). The neural stem cells have been characterised as a subpopulation of SVZ astrocytes, based on their expression of the astrocyte marker, glial fibrillary acidic protein (GFAP) (Doetsch et al., 1999a); . To date, no markers specific and exclusive to the NSC population have been identified, though they express a profile of markers shared by other cells types (GFAP, nestin, sox2, etc). This has made identifying stem cells difficult in immunohistochemical analysis, and has prevented the isolation of adult neural stem cells for cell culture and analysis. For this reason, few transgenic approaches to label NSC for *in vivo* characterisation have been successful.

Recent research suggests that the SVZ contains developmentally distinct stem cell populations, derived separately from the embryonic striatum and the embryonic cortex (Young et al., 2007a). In the study by Young *et al*, transgenic mice expressing Cre-recombinase under the transcription promoter of embryonic transcription factors – Gsh2 (expressed in the embryonic striatal germinal zone) and Emx1 (expressed in the embryonic cortex) (Fogarty et al., 2005; Kessaris et al., 2006)– were crossed with Rosa26-YFP reporter mice, in order to label the corresponding embryonic telencephalic regions with YFP. The transgenic mice were used to investigate whether these regionally distinct embryonic populations contribute differentially to the neural stem cell population in the adult SVZ, and to neurogenesis in the olfactory bulb. Gsh2- and Emx1-derived cells were both found to populate the SVZ, contribute to migratory neuroblast generation, and generate new olfactory neurons in the adult brain. The SVZ was composed predominantly of Gsh2-derived cells at the lateral wall and dorsolateral corner, with Emx1-derived cells also contributing to NSC in the dorsolateral corner (Figure 1.1).

Using a bromodeoxyuridine (BrdU) pulse to label newly dividing cells, Young *et al* demonstrated that the distinct stem cell populations made differential contributions to olfactory interneuron subtypes. Embryonic striatum-derived stem cells contribute disproportionately to the number of all newborn cells in the OB, in particular by generating all new Calbindin-positive and most Tyrosine hydroxylase-positive olfactory interneurons, whereas the cortex-derived stem cells generated the majority of Calretinin-positive interneurons. Additionally, it was found that embryonic cortex- and striatum-derived stem cells maintain expression of the Emx1 and Gsh2 throughout life, respectively (Young et

al., 2007a). Expression of these markers in adulthood can be further exploited through the development of tamoxifen-inducible Gsh2-Cre/R26-YFP ERt2 or Emx1-Cre/R26-YFP ERt2 transgenic mice, for further characterisation of these stem cell populations.

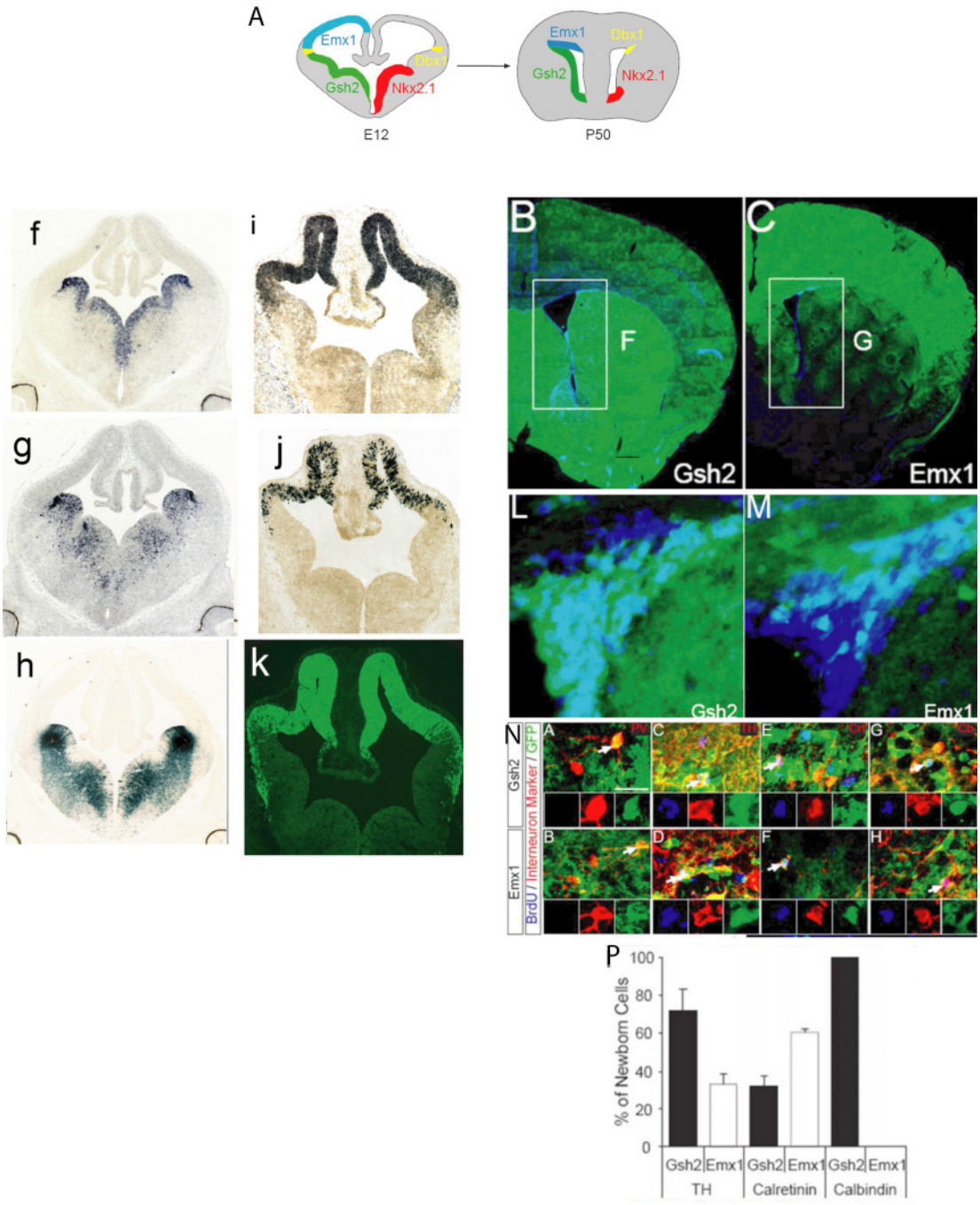

Figure 7.1.1. Emx1-Cre/R26-GFP and Gsh2-Cre/R26-GFP transgenic lines (from Young et al., 2007). **A**, Schematic depicting the different embryonic neuroepithelial domains and their relative contribution to generating the adult SVZ. **F-K** In situ hybridization for endogenous Gsh2 (f) or Cre (g) in E12.5 Gsh2-Cre/R26-GFP mice, and b-galactosidase enzymatic labeling (h) in Gsh2- Cre/ Rosa26R-lacZ embryos. In situ hybridization for endogenous Emx1 (i) or Cre (j) in E11.5 Emx1-Cre/R26-GFP mice and activation of the GFP reporter gene (k) in Emx1-Cre/R26-YFP / Rosa26R-GFP embryos. Scale bar, 400 µm. **B,C,** GFP-positive cells were detected by immuno-labeling in sections from Gsh2-Cre/R26-YFP

/Rosa26R-GFP mice (B) or Emx1-Cre/R26-YFP /Rosa26R-GFP mice (C). Each region of the embryonic neuroepithelium contributedpreferentially to distinct regions of the adult SVZ. **L,** Many GFP-positive cells were found in the SVZ in Gsh2-Cre/R26-YFP /R26-GFP mice. **M,** Significant numbers of GFP-labeled cells are present in the dorsal part of the SVZ in Emx1-Cre/R26-YFP /R26-GFP mice. **N,** Generation of new interneurons by distinct subpopulations of SVZ stem cells. Triple immunolabelling for BrdU (blue), GPF (green), and either Parvalbumin (A, B), Tyrosine Hydroxylase (TH) (C, D), Calretinin (Crt) (E, F) or Calbindin (Cb) (G, H) (red), four weeks after BrdU administration. **P,** Gsh2- and Emx1-derived stem cells generate different proportions of TH-, Crt- and Cb-positive neurons. Cb-positive neurons were exclusively Gsh2 (LGE)-derived.

This study and others (Willaime-Morawek et al, 2006) demonstrate that developmentally distinct subpopulations of neural stem cells populate the SVZ and contribute differentially to normal neurogenesis at the olfactory bulb. NSC at the SVZ are known to contribute to neurogenesis post-ischaemia, by the migration of neuroblasts into the ischaemic striatum and differentiation into striatal interneurons (Chopp et al., 2007; Dempsey and Kalluri, 2007; Hou et al., 2008; Kokaia and Lindvall, 2003; Kokaia et al., 2006; Ohab et al., 2006; Thored et al., 2006; Thored et al., 2007). Fewer studies have demonstrated neurogenesis in the ischaemic cortex, and the origin of the newborn cells is not confirmed (Magavi et al., 2000; Rakic, 2002). It is possible that differential contribution of NSC subpopulations at the SVZ determines the differential response to ischaemia in the stritatum and cortex. This study aims to determine the contribution of Gsh2-derived and Emx1-derived neural stem cell populations to the neurogenic response following ischaemia. Their contribution to the interneuron subpopulations in the normal striatum and cortex is also investigated as a baseline control measure.

The aim of this study was to investigate the contribution of these two neural stem cell populations – Gsh2- or Emx1-derived – to the ischaemic response, and to examine the *in vivo* behaviour of each neural stem cell population and their relative contributions to brain repair, using Gsh2-Cre/R26-GFP and Emx1-Cre/R26-GFP transgenic mice. To investigate this we used BrdU administration and the Cre-lox fate mapping approach in transgenic mice to determine which types of new cells are produced by the embryonic striatum-derived stem cells (in Gsh2-Cre/R26-YFP mice) or embryonic cortex-derived stem cells (Emx1-Cre/R26-YFP mice) at three timepoints following ischaemic injury – 1 week, 3 weeks and 5 weeks post-ischaemia. We found that both Gsh2- and Emx1-derived NSC proliferate and generate neuroblasts in the striatum but not in the cortex following ischaemia.

Oligodendrocyte precursor cells (OLPs) represent an additional population of proliferating cells in the adult brain, and are known to proliferate throughout adult life. The developmental origin of OLPs is in the ventricular zone of the developing brain, but they migrate and are distributed throughout all regions of the brain, including white matter, the cortex and striatum, by postnatal stages. OLPs express PDGFRα and NG2 proteoglycan, which become downregulated when

OLPs differentiate into mature oligodendrocytes. It has recently been reported that OLPs can also generate forebrain neurons in the normal adult brain in the piriform cortex (Rivers et al, 2008), and postnatal OLPs can generate astrocytes *in vitro* (Figure 7.1.2). In the normal brain, OLP contribution to projection neurons in the piriform cortex was found to be approximately 1.4%, however the function of these cells is unknown.

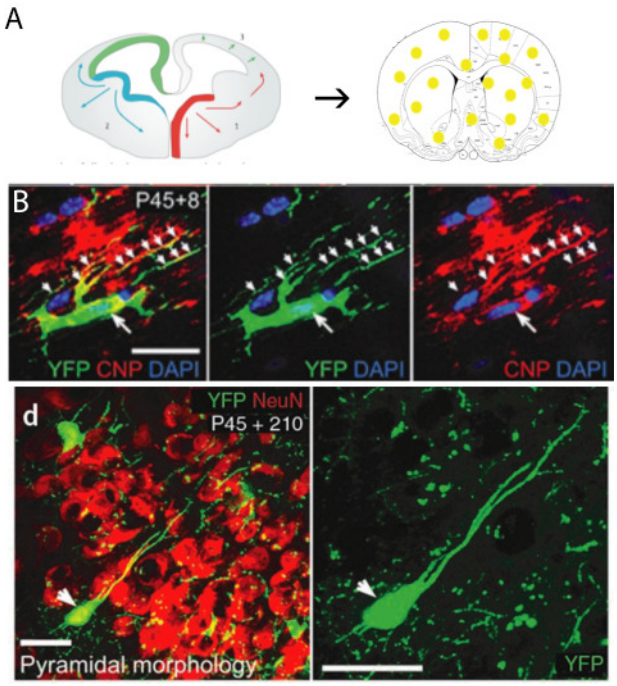

Figure 7.1.2. OLPs in the adult brain. (From Rivers et al, 2008). A, Schematic depicting the different embryonic neuroepithelial domains and their contribution to generating adult OLPs. B, In the corpus callosum 8 days after tamoxifen induction of GPF expression, some YFP+ cells expressed CNP in their cell bodies and proximal processes (arrows). D, YFP+ NeuN+ cells in the piriform cortex after 210 days after tamoxifen induction of GPF expression. Scale bars represent 30 μm.

It is possible that ischaemic damage will not only activate SVZ neural progenitor cells, but will additionally activate OLPs to replace oligoendrocytes that are lost or damaged. Some evidence suggests that oligodendrocytes are resistant to the initial ischaemic insult, but undergo apoptosis 24 to 48 hours after a transient ischaemic event (Mabuchi et al., 2000). Oligodendrocytes and OLPs have been shown to subsequently accumulate in the corpus callosum and border of the ischaemic lesion within 7 days, co-localising with reactive astrocytes and microglia at the infarct border (Aguirre and Gallo, 2004; Gottlieb et al., 2000; Mabuchi et al., 2000; Mandai et al., 1997; Ohta et al., 2003). It is unclear from these studies whether OLP accumulation after ischaemia is a function of OLP proliferation, or migration from other brain areas. It is also unclear whether OLP differentiation at later time points contributes to glial scar formation, remyelination or neurogenesis.

A further aim of this study was to investigate the effect of cerebral ischaemia on the proliferation and differentiation of resident oligodendrocyte precursor cells (OLPs) in the cortex, striatum and corpus callosum. Examining the effect of ischaemia on the SVZ stem cell population in conjunction with the oligodendrocyte population will help form a more complete understanding of the activity of endogenous progenitor cells following ischaemia, and their contribution to repair. Furthermore, the finding that OLPs can contribute to neurogenesis in the normal brain establishes oligodendrocyte precursor cells as a candidate cell type for contribution to neurogenesis after ischaemia. The previously generated PDGFRα-CreERt2/R26-YFP transgenic line was used to selectively label OLPs and trace their progeny and contribution to oligodendrogenesis after cerebral ischaemia. PDGFRα-CreERt2 mice carrying the Rosa26R-YFP allele received Tamoxifen prior to MCAO surgery in order to induce expression of YFP in OLPs at the time of ischaemia. We observed an increase in OLP proliferation in the striatum following cerebral ischaemia. OLPs contributed to mature oligodendrocyte generation and maintenance of the OLP population, but a proportion of OLP-derived cells were of unknown cell type. No OLP-derived neurons or neuroblasts were observed in the cortex, striatum or corpus callosum.

7.2. Methods

7.2.1. Transgenic mice

Adult male mice aged 90-120 days and > 25 g were used in this study. The generation of *Gsh2-Cre*, *Emx1-Cre,* and *PDGFRα-CreERt2* mice was described previously (Fogarty et al., 2005;Kessaris et al., 2006; Rivers et al. 2008). Each transgenic line was crossed with either of two Cre reporter lines: *Rosa26-enhanced Green Fluorescent Protein* (*R26-GFP*) (Mao et al., 2001; Jackson Laboratories) for Gsh2-Cre and Emx1-Cre, or *Rosa26-Yellow Fluorescent Protein* (*R26-YFP*) (Srinivas et al., 2001; generously supplied by S. Srinivas) for PDGFRα-CreERt2/R26-YFP. To activate Cre recombinase activity in *PDGFRα-CreERt2/R26-YFP* transgenics, tamoxifen (Sigma) was administered, at a concentration of 50 mg/ml in corn oil. Induction in adult mice was performed 7 days before MCAO surgery, and was achieved by administering 300 mg/kg Tamoxifen per day by gavage on five consecutive days.

7.2.2. BrdU labeling

To identify cells dividing in vivo, BrdU (Sigma) in PBS was administered as four 2 mg intra-peritoneal doses at a concentration of 20 mg/ml over 48 hours. The first dose of BrdU was administered at 48 hours post-MCAO surgery.

7.2.3. MCAO surgery

All procedures were in accordance with the UK Animals (Scientific) Procedures Act of 1986, and

approved by the UCL Research Ethics Committee. Forty four animals were used in the study: Gsh2-Cre/R26-GFP 1 week (n=5); Gsh2-Cre/R26-GFP 3 weeks (n=5); Gsh2-Cre/R26-GFP 5 weeks (n=5); Emx1-Cre/R26-GFP 1 week (n=4); Emx1-Cre/R26-GFP 3 week (n=5); Emx1-Cre/R26-GFP 5 week (n=6); PDGFRα-CreERt2/R26-YFP 1 week (n=5); PDGFRα-CreERt2/R26-YFP 3 weeks (n=3); PDGFRα-CreERt2/R26-YFP 5 weeks (n=3). Three animals received sham surgery. Mouse MCAO surgery was performed using the Koizumi model (Koizumi 1986). Animals were anaesthetised with 2% isofluorane and 100% O_2. Temperature was maintained with a feedback-controlled homeothermic blanket and rectal probe (Hamilton/ADI). The right common carotid artery was exposed. For mice, a 7-0 silicon-coated suture (Doccol) was inserted into the carotid artery and advance 7mm into the brain to reach the MCA bifurcation from the circle of Willis. The MCA was occluded for 30 minutes. Following occlusion, the MCA was reperfused by retracting the suture from the brain slowly over 2 minutes and animals recovered. Recovered animals were housed individually in clean cages and put on a wet food diet for the first 48 hours. For sham surgery, the surgical procedure and post-operative animal care was similar to described above, however during surgery the silicon-coated suture did not obstruct the MCA bifurcation. In PDGFRα-CreERt2/R26-YFP mice, animals received 5 mg/kg carprofen analgesic for 48 hours post-surgery, as prescribed by the UCL vet.

After surgery animals were recovered in individual cages lined with soft tissue bedding, and housed separately. In the first 48 hours, animals were fed a mixture of soft pellets and jelly, after which they were returned to hard pellets.

7.2.4. MRI

MRI animal studies were performed using a 2.35T horizontal magnet with a 120 mm bore (Oxford Instruments Eynsham, UK), interfaced to a Surrey Medical Imaging Systems (SMIS, UK) console. A volume coil (60 mm length) was used to transmit radiofrequency excitation pulses. The magnetic resonance signals were detected using passively decoupled, single loop, surface coil of 1cm diameter positioned on the dorsal aspect of the head. Animals were anaesthetised with 2% isofluorane and 100% O_2, and secured on a stereotactic probe for imaging. Body temperature was maintained at 37°C. A 2D spin echo (T2-weighted) sequence was used with the following parameters: TR = 1500ms; TE = 120ms; FOV 25 mm; 128 X 128 voxels; slice thickness 1 mm; 10 averages. Animals were imaged at 7, 21, or 35 days post-MCA occlusion surgery.

7.2.5. Tissue preparation

Following MRI, mice were anaesthetized with pentobarbitone and perfused through the ascending aorta, first with PBS and then with 4% (w/v) paraformaldehyde (PFA, Sigma) in PBS. Brains were removed, immersed in fresh 4% PFA and stored at 4°C overnight. Tissue was cryo-

protected in 20% sucrose in PBS for 24 hours. All brains were embedded in optimal cutting temperature (OCT) compound and coronal cryo-sections (20 μm nominal thickness) were collected onto SuperfrostPlus slides (BDH) or floated in PBS.

7.2.6. Immunohistochemistry

Initially, three mice were examined for each transgenic genotype and ischaemic timepoint. From each mouse, three coronal brain sections at the anterior SVZ/ MCA region were immunolabeled for each antibody staining condition. Sections were washed with PBS and permeabilized with blocking solution containing Triton-X100 before incubating overnight with rabbit anti- YFP (1:6000) or rat anti-YFP IgG2a (1:1000, Nacalai Tesque Inc.). Sections were washed three times with PBS, then incubated with AlexaFluor 488-conjugated anti-rabbit IgG or AlexaFluor 488-conjugated anti-rat IgG (1:1000; Invitrogen) in blocking solution. Some sections were treated with Hoescht 33258 nuclear label (1:1000; Sigma). Floating sections were transferred onto glass slides and mounted using Fluoromount (DAKO). Sections were co-stained with either CY3-conjugated mouse anti-GFAP (1:3000; Sigma); rabbit anti-GFAP (1:500; Dako); mouse anti-NeuN (1:500, Chemicon); rabbit anti-Calbindin (1:1000, Swant); rabbit anti-Calretinin (1:1000, Swant), rabbit anti-Parvalbumin (1:1000, Chemicon), guinea-pig anti-doublecortin (1:3000, Chemicon); mouse anti-PSA-NCAM IgM (1:1000, Chemicon); and detected with AlexaFluor 568-conjugated anti-mouse IgG1; AlexaFluor 568-conjugated anti-rabbit IgG; AlexaFluor 568-conjugated anti-mouse IgM (Invitrogen, all used at 1:1000;) or CY3-conjugated anti-guinea-pig (1:500, Pierce).

For BrdU immunohistochemistry, stained floating sections were subsequently collected onto glass slides and fixed with 70% ethanol/ 20% glacial acetic acid, then 20 minutes in 70% ethanol at -20°C. Slides were then washed with PBS / 1% Triton-X100 and treated with 6M HCl / 1% Triton X-100 in PBS for 15 minutes. Slides were then washed in PBS and incubated with anti-BrdU (1:15, ATCC mouse hybridoma) overnight at 4oC. Slides were washed in PBS and incubated with AlexaFluor 568-conjugated anti-mouse IgG1 or AlexaFluor 647-conjugated anti-mouse IgG1 (1:1000, Invitrogen) for one hour at room temperature.

7.2.7. Confocal Microscopy

Images were collected with a confocal microscope (Perkin Elmer). For quantification of cells in the PDGFRα-CreERt2/R26-YFP -CreERt2 transgenic line, a minimum of 6 non-overlapping fields in the ipsi- and contra-lateral cortex (from cingluate through to motor, somatosensory and insular cortex, but excluding the piriform cortex), striatum, and corpus callosum were examined per animal. Total YFP+ cells per frame, as well as percentage of NG2+/ CNP+/ NeuN+/ GFAP+ or Olig2+ YFP+ double-positive cells were counted. Statistical analysis was performed using analysis of variance (ANOVA), with Tukey post-hoc analysis.

7.3. Results:

7.3.1. Animal model mortality rates in Gsh2-Cre/R26-YFP, Emx1-Cre/R26-GFP and PDGFRα-CreERt2/R26-YFP

Recovery from the MCAO procedure was good; only 2% of animals died during surgery or during the recovery period before returning to normal housing. However, a high mortality rate in the 12-60 hour period after surgery was observed, and some animals died up to 8 days post-surgery. Mortality rates were 41.9% for Gsh2-Cre/R26-GFP and 42.9% for Emx1-Cre/R26-GFP transgenics. For PDGFRα-CreERt2/R26-YFP -CreERT2 transgenics, the initial mortality rate was very high at 83.3%. Post-operative care was adjusted, as recommended by the UCL vet, to include carprofen analgesic at 5 mg/kg/day for 48 hours post-surgery to improve outcome. Following this modification, mortality in the PDGFRα-CreERt2/R26-YFP -CreERT2 transgenic group was reduced to 50.0%. All animals analysed are from the carprofen-treated group. The mean weight at surgery was 27.1 ±2.1 for PDGFRα-CreERt2/R26-YFP -CreERT2, 29.0 ±2.9 for Emx1-Cre/R26-YFP , and 32.1 ±3.2 for Gsh2-Cre/R26-GFP mice.

7.3.2. MRI in Gsh2-Cre/R26-GFP and Emx1-Cre/R26-GFP transgenic mice.

Following cerebral ischaemia surgery, animals were imaged at 1 week, 3 weeks or 5 weeks post-ischaemia, prior to perfusion fixation, for confirmation and assessment of final lesion volume. We observed the evolution of hypointensity in the lesion at later timepoints on T2-weighted images, consistent with previous reported data (Figure 7.3.2.1A).

Whole brain total lesion volume and MCA territory lesion volume were assessed. We observed a time point effect but no transgenic effect. There was no difference in the total lesion volume, or lesion volume at the MCA territory, between Gsh2-Cre/R26-GFP and Emx1-Cre/R26-GFP transgenics at any timepoint, but lesion volumes between time points were significantly different (whole brain ANOVA, $p<0.005$; MCAO territory ANOVA, $p<0.001$; Figure 3.2.1B,C). For both whole brain and MCA territory lesion volumes, 3-week and 5-week lesion volumes significantly smaller than 1-week lesion volumes (Total, $p<0.01$; MCAO, $p<0.001$). Lesion volume as a proportion of the ipsilateral hemisphere (lesion fraction) was also assessed. We found that there was no difference between Gsh2-Cre/R26-GFP and Emx1-Cre/R26-GFP lesion fractions at each time point, but that lesion fractions were significantly different across timepoints (ANOVA, $p<0.001$; Figure 3.2.1C). In summary, no difference was observed between Gsh2-Cre/R26-GFP and Emx1-Cre/R26-GFP transgenics at 1-week, 3-week or 5-weeks post-ischaemia. Ischaemic lesions were significantly

reduced in volume and as a fraction of the ipsilateral hemisphere at 3- and 5-weeks, relative to 1-week post-ischaemia.

We also assessed the ratio of contralateral to ipsilateral hemisphere volume at the SVZ level. We observed that the ipsilateral total hemisphere volume decreased at 3-weeks and 5-weeks post-ischaemia, relative to the contralateral hemisphere, and compared to sham-operated animals (univariate ANOVA, $p<0.001$; Figure 7.3.2.1E).

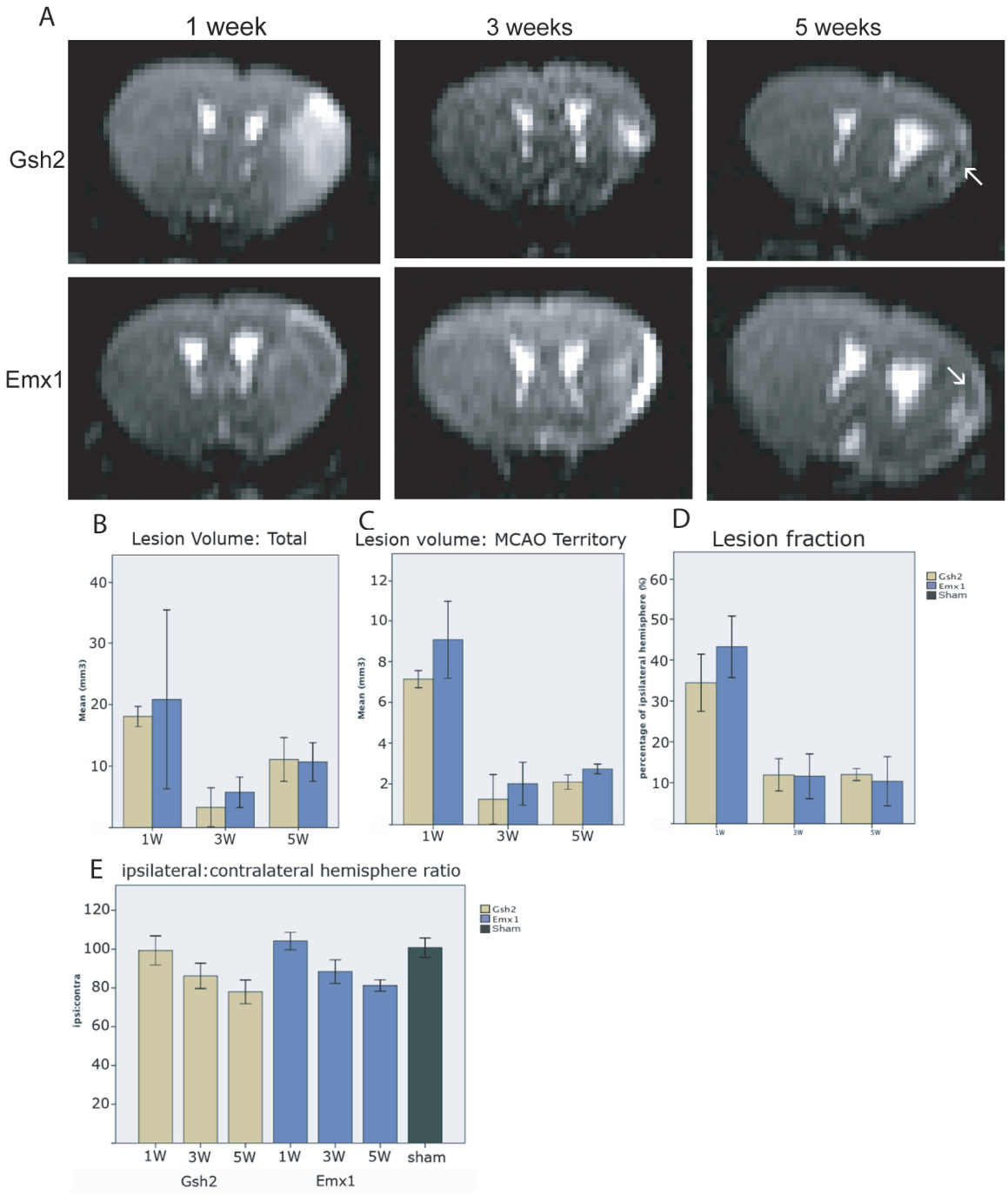

Figure 7.3.2.1. A, MRI of Gsh2-Cre/R26-GFP and Emx1-Cre/R26-GFP transgenic mice at 1, 3, and 5

weeks post-ischaemia. **B-D** Whole brain total lesion volume (B), lesion volume at the MCA territory (C) and lesion volume as a fraction of ischaemic hemisphere volume at the MCA territory (D) for Gsh2-Cre/R26-GFP (yellow) and Emx1-Cre/R26-GFP (violet) at 1, 3, and 5 weeks post-ischaemia. **E**, Ratio of ipsilateral to contralateral hemisphere volume in Gsh2-Cre/R26-GFP (yellow), Emx1-Cre/R26-GFP (violet), and sham-operated mice (grey). The ischaemic (ipsilateral) hemisphere decreases in volume over time relative to the non-ischaemic (contralateral) hemisphere over time.

7.3.3. Contribution of Emx1- and Gsh2-derived stem cells to proliferating and migrating neuroblasts.

Next, we assessed the capacity of Gsh2- and Emx1-derived NSC to proliferate, migrate, and generate new neurons following cerebral ischaemia by immunohistochemical analysis. NPC proliferation was observed in the SVZ at 1-week post-ischaemia in Gsh-2 animals (Figure 7.3.3.1). Preliminary observations indicate an increase in BrdU+ cells in the ipsilateral hemisphere relative to the contralateral hemisphere, with almost all BrdU+ cells PSA-NCAM+ and all were YFP+, whereas fewer BrdU+ cells in the contralateral SVZ were PSA-NCAM+, and some BrdU+YFP- cells were observed in this hemisphere (Figure 7.3.3.1). This suggests that following ischaemia, Gsh2-derived stem and progenitor cells are activated and respond by the proliferation and generation of neuroblasts.

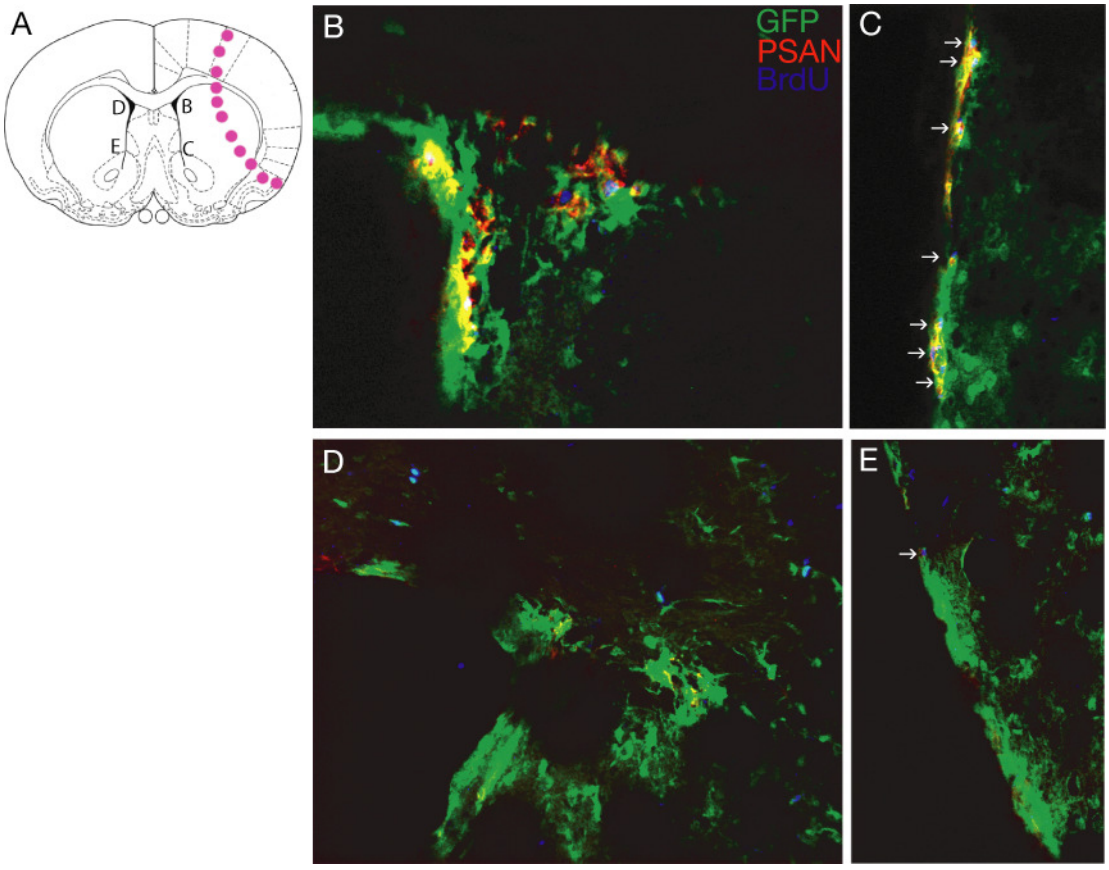

Figure 7.3.3.1. Proliferation at the SVZ at 1 week post-ischaemia in Gsh2-Cre/R26-GFP mouse. A, Schematic of a coronal section of adult brain at the SVZ, with ischaemic lesion demarcated (pink dots). **B-E**, Cell proliferation at the SVZ dorsolateral corner (B,D) and lateral wall (C,E) in the ischaemic (B,C) and contralateral (D,E) hemisphere. Green, GFP; red, PSA-NCAM; blue, BrdU. Arrows denote PSA-NCAM+ BrdU+ cells. Scale bars, 50um.

Consistent with other studies, in our preliminary observations we detected Doublecortin+ and PSA-NCAM+ neuroblasts migrating out from the subventricular zone ipsilateral to the lesion. At 5 weeks post-ischaemia, neuroblast streams were observed migrating from both the lateral wall and the dorsolateral corner of the ipsilateral ventricle into the striatum (Figure 7.3.3.2 C,G-I). No PSA-NCAM+ or Doublecortin+ cells were observed in the ipsilateral cortex. No neuroblast migration away from the SVZ into the striatum was observed in the contralateral hemisphere (Figure 7.3.3.2 D-E).

YFP+ Doublecortin+ BrdU+ cells were observed in Gsh2-Cre/R26-GFP transgenics, indicating that some neuroblasts migrating at 5 weeks originated between 2-4 days post-ischaemia from Gsh2-derived neural stem cells in the SVZ (Figure 7.3.3.2 J-K).

Figure 7.3.3.2 A-C shows a whole hemisphere profile of PSANCAM distribution in Gsh2 at 1-week (B), 5-week (C), and in the contralateral control hemisphere (A). PSANCAM expression is restricted to the SVZ in the contralateral hemisphere and at 1-week post-ischaemia. At 5 weeks post-ischaemia, we observed PSANCAM+ neuroblast streams migrating toward the lesion, and at the peri-infarct border.

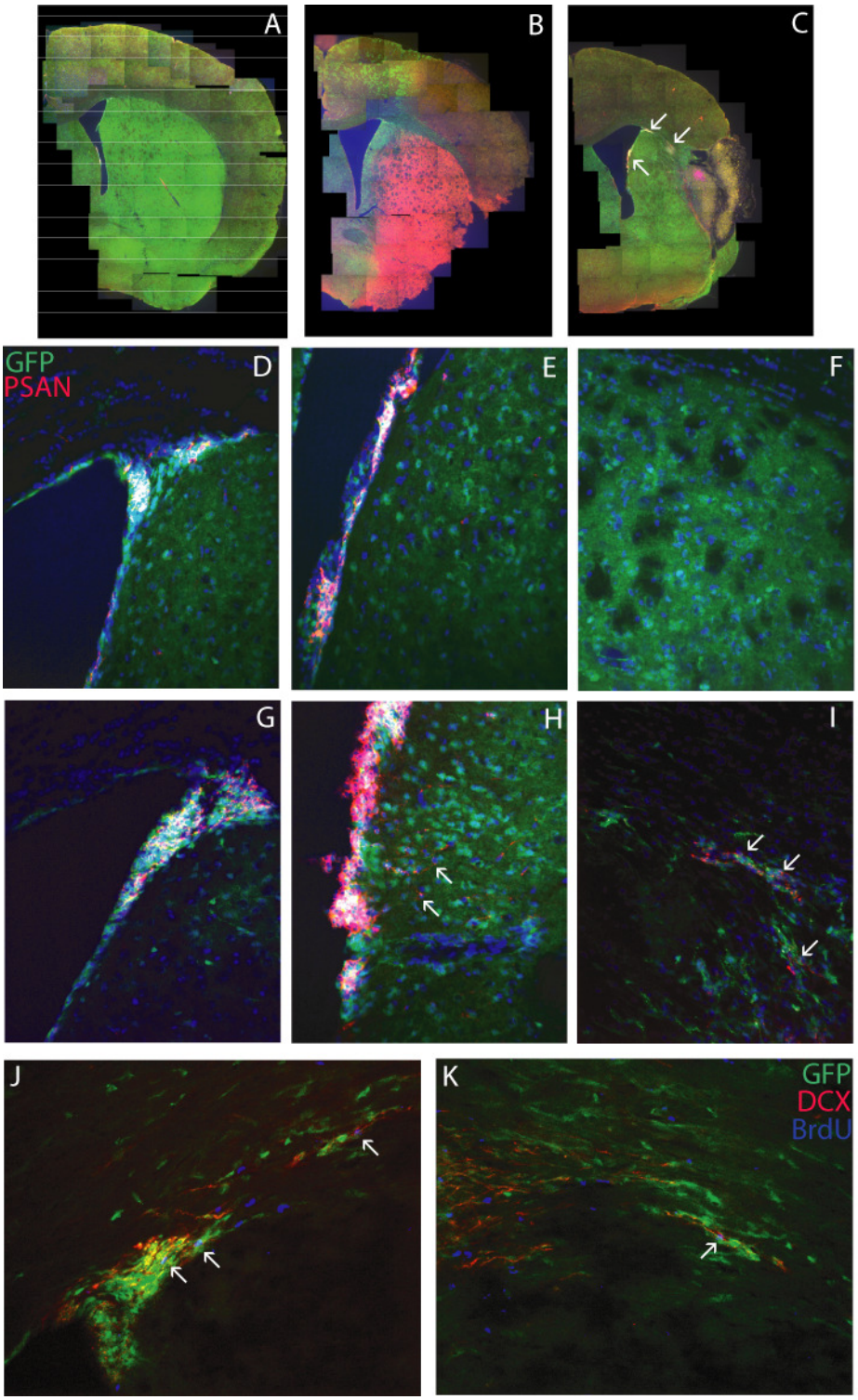

Figure 7.3.3.2. Neuroblast migration from the SVZ at 5W post-ischaemia in Gsh2-Cre/R26-GFP transgenic mice. A-C, Fluorescent microscopy of GFP and PSA-NCAM immunohistochemistry in contralateral (control) 5W (A), ipsilateral (ischaemic) 1W (B), and ipsilateral 5W (C) whole hemisphere, showing neuroblast migration from the SVZ toward the ischaemic lesion. **D-I**, higher magnification of SVZ and striatum at 5W post-ischaemia in control contralateral (D-F) and ischaemic ipsilateral (G-I) hemispheres. D,G, SVZ dorsolateral corner. E,H, SVZ dorsolateral wall. F,I, striatum. Arrows denote PSA-NCAM+ migrating

neuroblasts. Red, PSA-NCAM. Green, GFP. Blue, Hoescht nuclear dye. **J,K,** BrdU, GFP, and Doublecortin (DCX) at the SVZ dorsolateral corner (J) and dorsolateral migratory streatm (K) in the ipsilateral hemisphere at 5W post-ischaemia, showing newly-generated Gsh2-derived and non-Gsh2-derived neuroblasts migrating into the ischaemic striatum. Arrows denote BrdU+ GFP+ PSA-NCAM+ triple-immunolabelled cells. Scale bars, 50um.

YFP+ PSA-NCAM+ neuroblasts were observed in both Emx1-Cre/R26-GFP and Gsh2-Cre/R26-GFP transgenics, indicating that both stem cell populations contribute to new neuroblast generation in response to ischaemia (Figure 7.3.3.3). In the Emx1-Cre/R26-GFP mice, YFP+PSA-NCAM+ cells were predominantly observed in the dorsolateral stream of neuroblasts migrating from the dorsolateral corner of the SVZ, bordering the corpus callosum. No YFP+ neuroblasts were observed migrating in the striatum.

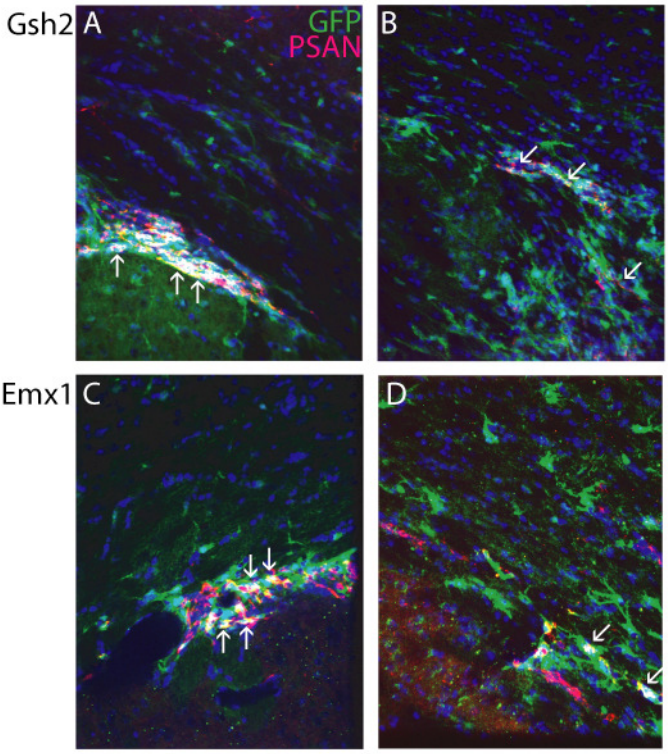

Figure 7.3.3.3. GFP and PSA-NCAM immunohistochemistry in Gsh2-Cre/R26-GFP. (A,B) and Emx1-Cre/R26-GFP (C,D) transgenic mice. **A,C**, SVZ dorsolateral corner. **B,D,** dorsolateral migratory stream. Arrows denote GFP+ PSA-NCAM+ double immunolabelled cells. Scale bars, 50um.

7.3.4. Contribution of Emx1- and Gsh2-derived populations cortical and striatal interneurons.

In order to assess the contribution of Emx1- and Gsh2-derived cells to neurogenesis following

ischaemia in the striatum or cortex, we must first assess the extent to which Emx1- and Gsh2-derived neurons are present in the normal brain. In the current literature this has been assessed at the olfactory bulb but not in the cortex or striatum (Young et al, 2007). We used the contralateral, non-ischaemic hemisphere as a control, to determine the normal contribution of Emx1- and Gsh2-derived cells to the interneuron populations in the adult cortex and striatum. In Gsh2-Cre/R26-GFP transgenics, both YFP+ and YFP- interneurons were observed to coexpress with NeuN (neuronal), Calretinin, Calbindin, Parvalbumin, and NPY in both the striatum and cortex (interneurons; Figure 7.3.4.1). This is expected as developmentally Gsh2-derived cells are known to contribute to the neuronal population in the striatum as well as to give rise to interneuron populations in the cortex. In Emx1-Cre/R26-GFP transgenics, we observed that Emx1-derived cells contributed to cortical neuron population, which is consistent with findings demonstrating that this developmental population gives rise to neurons in the cortex. We also observed YFP co-expression with NeuN and Crt in the striatum, which may indicate that some Emx1-derived cells can give rise to striatal neurons. This is an unexpected result and further quantification of these observations is necessary to confirm this finding. One other study (Willaime-Morawek et al, 2008) found that Emx1-derived neural stem cells give rise to a small proportion of striatal neurons expressing NeuN, Calretinin, Calbindin or DARPP32. At 5 weeks post-ischaemia, few or no BrdU+ YFP+ interneurons were observed in Gsh2-Cre/R26-GFP transgenics in the ipsilateral cortex or striatum (not shown), suggesting that NSC dividing between 2-4 days post-ischaemia do not give rise to mature interneurons.

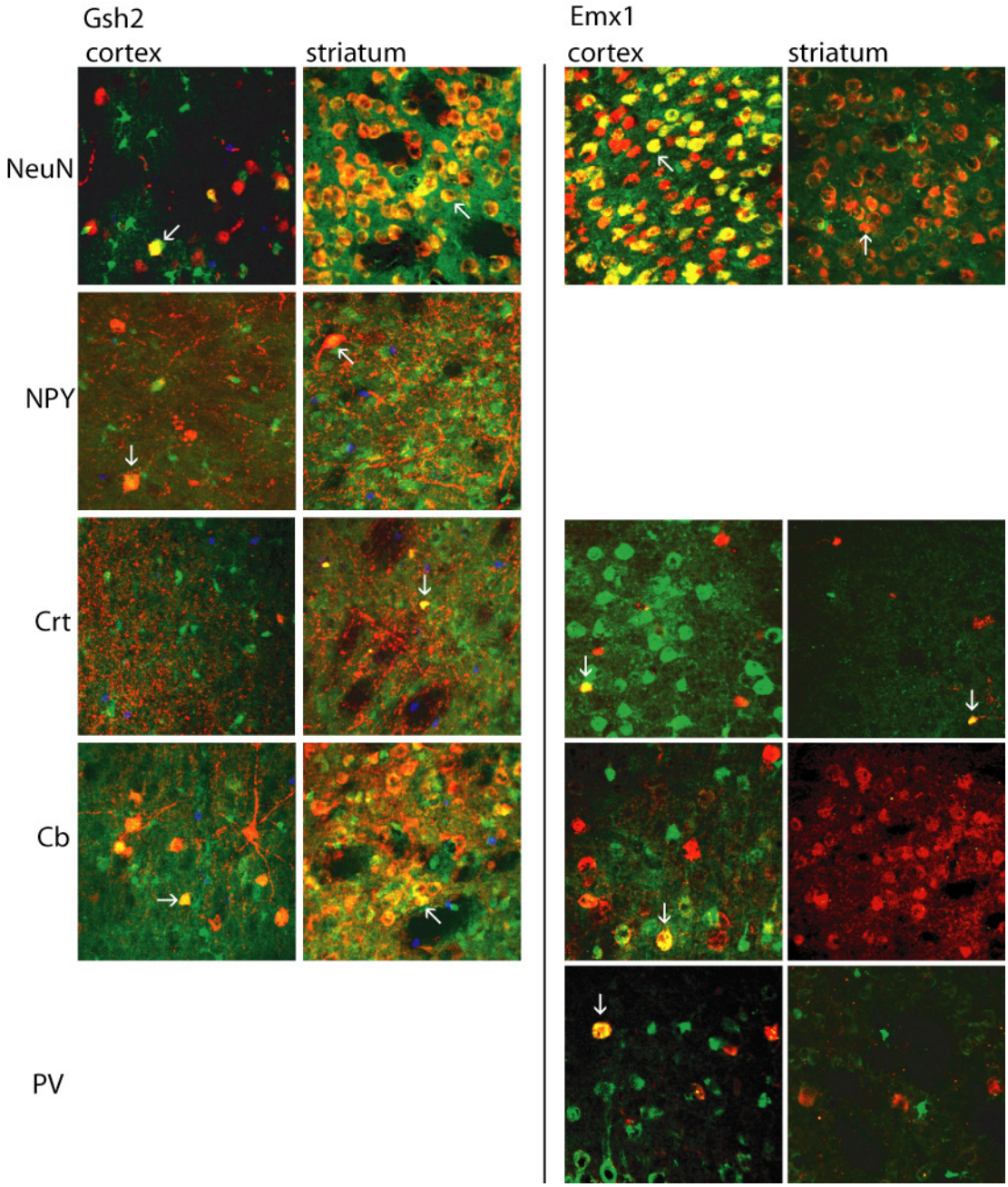

Figure 7.3.4.1. Contribution of Emx1- and Gsh2-derived populations cortical and striatal interneurons. Contralateral (control) striatum and cortex at 5W post-ischaemia. Red, interneuron markers (NeuN, neuron; NPY, neuropeptide Y; Crt, calretinin; Cb, calbindin; PV, parvabumin. Green, GFP. Arrows denote GFP+ interneuron+ cells. Left, Gsh2-Cre/R26-GFP transgenic. Right, Emx1-Cre/R26-GFP transgenic. Scale bars, 30um.

Very few BrdU+ NeuN+ or interneuron marker-positive (calretinin, calbindin, NPY, parvabumin) cells were observed in the peri-infarct region, ipsilateral or contralateral cortex or striatum. Figure

3.4.2 A shows a BrdU+ NPY+ GFP- cell in the ipsilateral striatum of Gsh2-Cre/R26-GFP transgenic at 5-weeks post-ischaemia. BrdU+ YFP+ cells were also observed in the cortex and striatum (Figure 7.3.4.2 B). These cells may be proliferating astrocytes or oligodendrocyte precursors whose developmental origin was Gsh2 or Emx1 embryonic telencephalic regions. The observed BrdU+ YFP- cells may represent proliferating microglia. These results may indicate that cells proliferating at 2 to 4 days post-ischaemia in the SVZ have a low contribution to post-ischaemia neurogenesis, and may have died by the 5 week timepoint. In conclusion, both Gsh2- and Emx1-derived NPC at the SVZ respond to cerebral ischaemia by proliferation and migration to the lesion site by 5 weeks post-ischaemia.

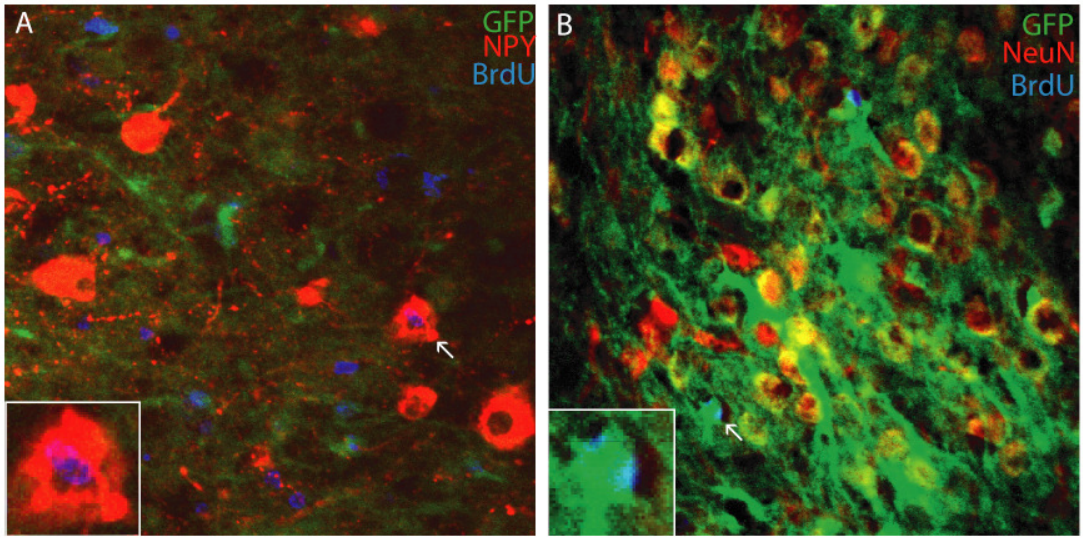

Figure 7.3.4.2. Cell proliferation in the ischaemic hemisphere at 5W post-ischaemia in the Gsh2-Cre/R26-GFP transgenic mouse. A, BrdU+ NPY+ double-immunolabelled interneuron (arrow) in the ischaemic striatum. **B,** GFP+ BrdU+ NeuN- cell in the ischaemic striatum (arrow). Scale bars, 30 um. Insets, high magnification of cells.

7.3.5. MRI and ischaemic lesion in PDGFRα-CreERt2/R26-YFP mice

At 1 week post-ischaemia, lesions in PDGFRα-CreERt2/R26-YFP animals were predominantly located in the striatum (Figure 7.3.5.1). At 3 and 5 weeks, lesions were not apparent on MRI images, but could be detected with hematoxylin-eosin staining on histological sections (Figure 7.3.5.1). Enlarged ventricles in the ipsilateral hemisphere were also observed on MRI images. These differences in lesion size and character may be due to modifications of the experimental protocol to include tamoxifen administration prior to MCAO surgery, and are considered in the Discussion section.

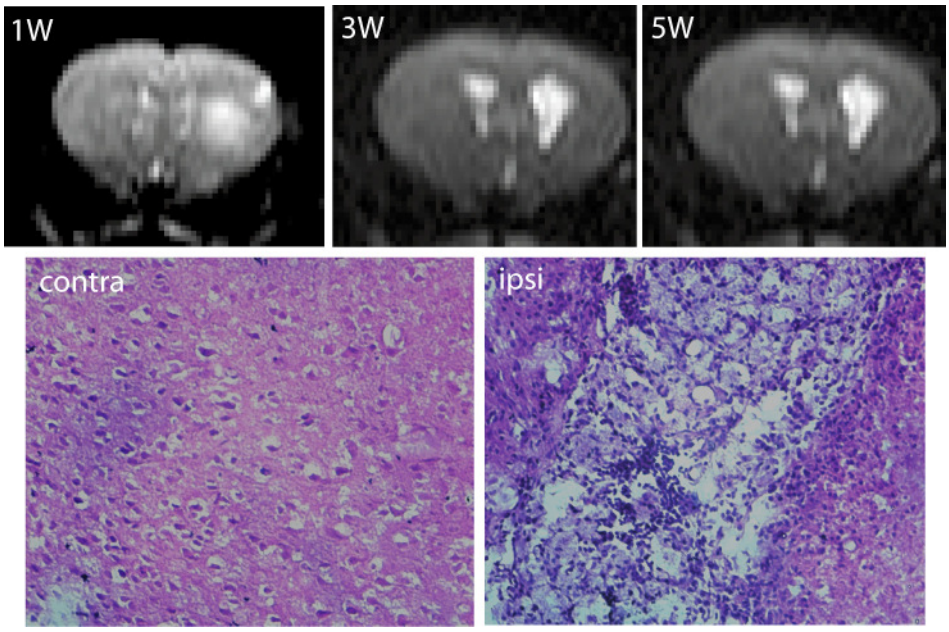

Figure 7.3.5.1. Ischaemic lesion in the PDGFRα-CreERt2/R26-YFP-iCreERT2 transgenic mouse. Top row, Coronal spin-echo MRI images of the MCA territory at 1, 3, and 5 weeeks post-ischaemia. Bottom row, hematoxylin-eosin histological stain in the contralateral (non-ischaemic) and ipsilateral (ischaemic) cortex. Scale bars, 50 um.

7.3.6. Distribution of YFP+ cells post-ischaemia

We assessed the distribution of YFP+ cells in the ipsilateral and contralateral cortex, striatum and corpus callosum at 1 week post-ischaemia. We observed an increase in YFP+ cells in the ipsilateral striatum, relative to all other groups: contralateral striatum, contra- and ipsilateral cortex and corpus callosum (ANOVA, $p<0.001$; Figure 7.3.7.1G). We did not observe any difference in YFP+ cell distribution between ipsilateral and contralateral hemispheres in the cortex or corpus callosum at 1 week post-ischaemia. This pattern of YFP+ cell distribution remained similar at 5 weeks post-ischaemia. YFP+ cells remained elevated in the ipsilateral striatum relative to the contralateral side, cortex and corpus callosum (Fig 7.3.7.1G; ANOVA, $p<0.001$).

7.3.7. Fate of PDGFRα-CreERt2/R26-YFP- expressing cells

Next, we assessed the fate of YFP+ cells in the ischaemic brain. OLP-derived cells may take a number of differentiation pathways following ischaemia: they may remain undifferentiated (1); differentiate into mature oligodendrocytes or neurons (2); or differentiate into astrocytes or another unknown cell type (3). We initially assessed the first two scenarios, as previous studies confirm that OLPs have the capacity to differentiate into neurons *in vivo*.

We observed that a proportion of YFP+ cells remained undifferentiated OLPs in all brain regions, as characterised by NG2 expression. At 1 week post-ischaemia, the proportion of YFP+ NG2+ cells was comparatively consistent across brain regions and hemispheres except in the ipsilateral striatum, where we observed a decrease in the percentage of YFP+NG2+ cells (ANOVA, $p<0.005$; Fig 7.3.7.1). We observed some YFP+NG2+ cells that were also BrdU+, indicating that that these cells were generated after the ischaemic event (Fig 7.3.7.2). These results suggest that OLP proliferate in response to cerebral ischaemia, but the newly generated cells do not remain as undifferentiated OLP.

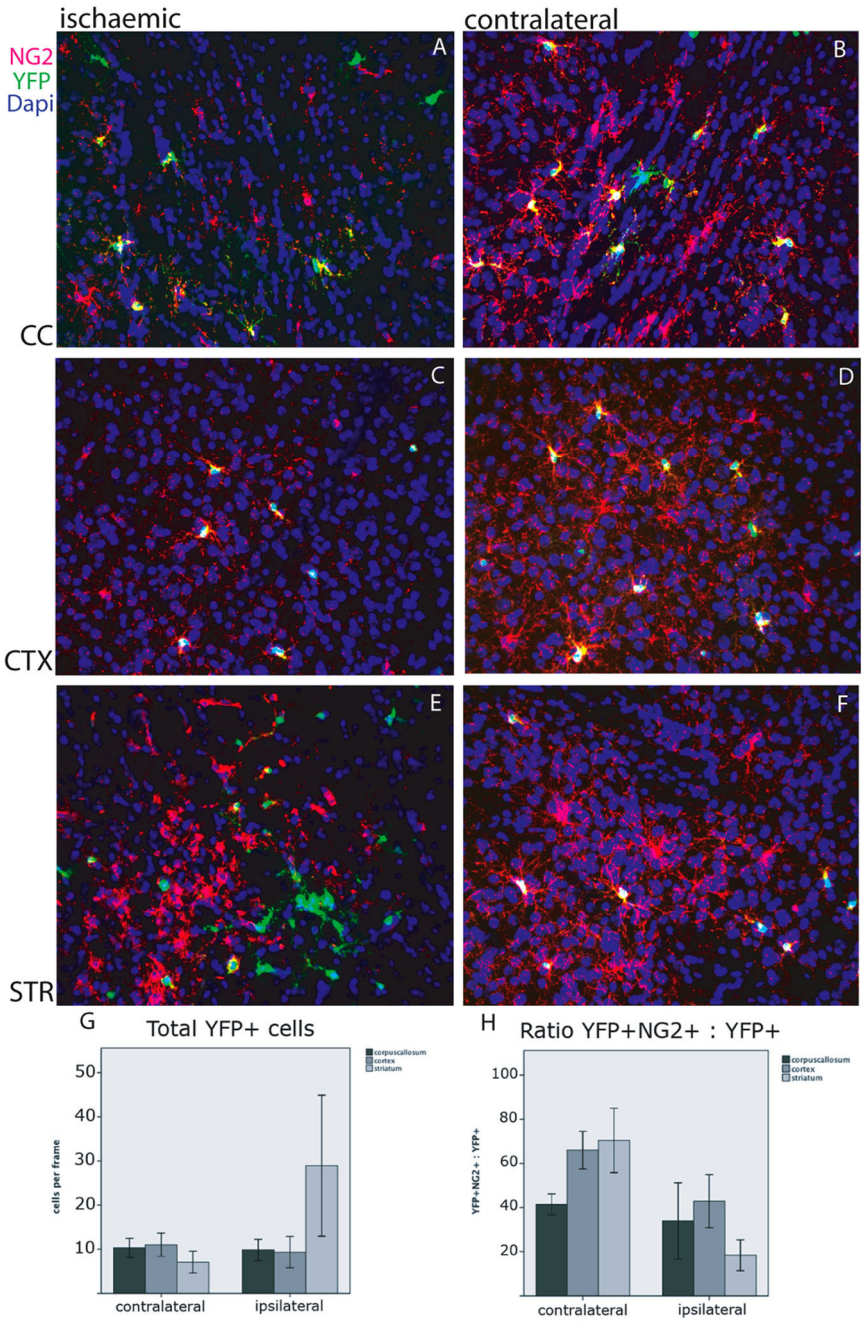

Figure 7.3.7.1. Distribution of YFP+ cells at 5W post-ischaemia in PDGFRa-CreERT2/R26-YFP transgenic mouse. A-F, YFP (green) and NG2 (red) expression in the corpus callosum (CC; A,B), cortex (CTX; C,D), and striatum (STR; E,F) in the ischaemic (A,C,E) and contralateral control (B,D,F) hemispheres. **G,** YFP+ cell counts in the ipsilateral ischaemic and contralateral control corpus callosum, cortex, and striatum. **H,** YFP+ NG2+ double immunolabelled cells as a percentage of total YFP+ cells in the ipsi- and contralateral corpus callosum, cortex and striatum. Scale bars, 50um.

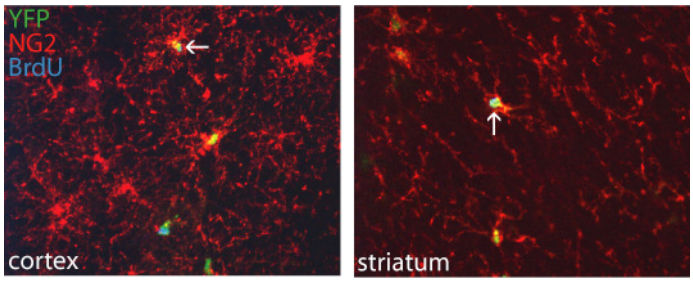

Figure 7.3.7.2. Proliferation of OLPs following cerebral ischaemia. BrdU+ GFP+ NG2+ cells in the ischaemic cortex and striatum at 5W post-ischaemia in the PDGFRa-iCreERT2 transgenic mouse. Arrows denote triple-immunolabelled cells. Scale bar, 50 um.

We then examined whether the YFP+ cells were differentiated mature oligodendrocytes. CNP is an early marker for mature myelinating oligodendrocytes. At 1-, 3- (not shown) and 5-weeks post-ischaemia, we observed both YFP+ CNP+ and YFP+CNP- cells in all brain regions: ipsi- and contralateral striatum, cortex and corpus callosum (Figures 7.3.7.3G-L). These results indicate that OLPs can contribute to oligodendrogenesis from early stages following cerebral ischaemia.

We also examined whether YFP+ cells differentiated into neurons (Figure 7.3.7.3 A-E). In the sections studied, we did not observe any YFP+NeuN+ cells at 1 week or 5-weeks post-ischaemia in the contralateral or ipsilateral striatum, cortex or corpus callosum, excluding the piriform cortex which was not counted. These preliminary results suggest that OLP do not contribute in any significant amount to neurogenesis outside of the piriform cortex.

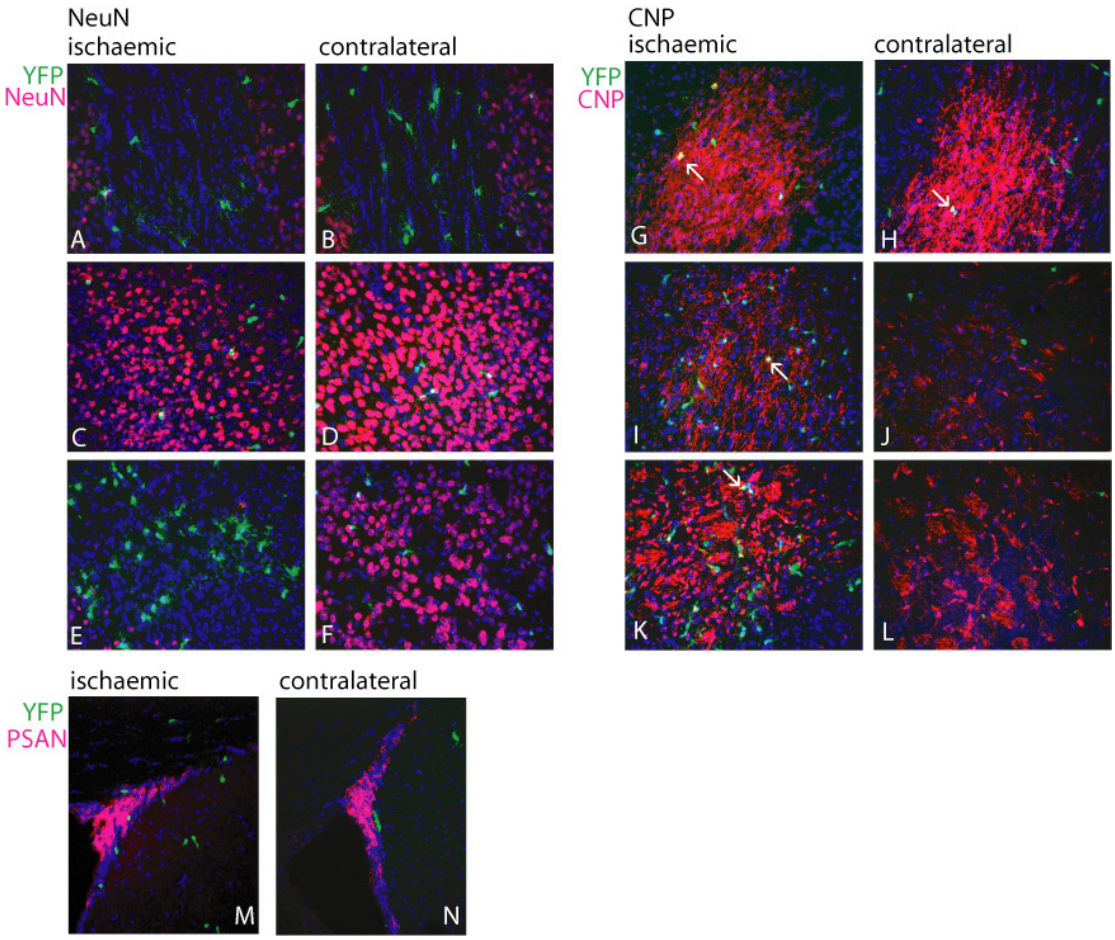

Figure 7.3.7.3. Identity of YFP+ cells at 5W post-ischaemia. A-F, NeuN and YFP expression in the corpus callosum (A,B); cortex (C,D); and striatum (E,F) in the ipsilateral ischaemic (A,C,E) and contralateral control (B,D,F) hemispheres. No NeuN+ YFP+ cells were observed. **G-L,** CNP expression in the corpus callosum (G,H); cortex (I,J); and striatum (K,L) in the ipsilateral (G,I,K) and contralateral (H,J,L) hemispheres. Arrows denote CNP+ YFP+ double-immunolabelled cells. M, N, PSA-NCAM and GFP expression at the SVZ. No PSA-NCAM+ YFP+ cells were observed. Scale bars, 50 um.

7.4. Discussion:

In this study, we explore the fate of different populations of endogenous progenitors in the brain following cerebral ischaemia: neural stem and progenitors in the SVZ, and oligodendrocyte precursor cells (OLPs).

7.4.1. Gsh2/Emx1 neural stem and progenitor cells

In this study, the reduction in ipsilateral hemisphere volume over time may represent secondary, delayed neuronal death in the ischaemic hemisphere, lesion compaction, brain reorganisation or a combination of these factors

Although we only observed neuroblast migration from the SVZ into the striatum and not into the cortex after ischaemia, these neuroblasts were a mixed population originating from Gsh2- and Emx1-derived neural stem cells. The restriction of migration to the striatum following focal middle cerebral artery occlusion has been previously reported (Arvidsson, 2002). Our results suggest that the embryonic lineage of the distinct neural stem cell populations in the SVZ does not restrict their capacity to migrate, as we observed both embryonic cortex (Emx1) and embryonic striatum (Gsh2) derived neuroblast migration in the striatum.

Lack of neuroblast migration to the cortex may be a result of several factors. Neuroblasts must cross the corpus callosum to reach the cortex from the SVZ. We observed neuroblast migration from the dorsolateral corner of the SVZ and along the ventral edge of the corpus callosum where it meets the striatum. The corpus callosum may therefore be a barrier to neuroblast migration, or create a barrier for chemoattractive cues originating in the ischaemic cortex. In models of cerebral ischaemia where the lesion is exclusively in the cortex, neuroblast migration to the lesion boundary has been observed (Moorshead), which suggests that SVZ neuroblasts are able to overcome the corpus callosum boundary. Alternatively, the inflammatory response in the cortex may be different from that of the striatum, and may lack migratory cues for neuroblast recruitment. Finally, there may be a latent migration to the cortex that occurs later than neuroblast migration to the striatum, which peaks at 4-5 weeks post-ischaemia.

In this study, BrdU was administered between 48 and 96 hours post-ischaemia. We observed BrdU+ neuroblasts at the SVZ at 1 week post-ischaemia, but few BrdU+ neurons in the ischaemic striatum at 5 weeks post-ischaemia. This suggests that the proliferation at the SVZ during this time contributes little to neurogenesis in the lesion. It is possible that SVZ proliferation at later timepoints contributes more to neurogenesis post-ischaemia, and there are several options for evaluating this.

In future studies, a cumulative approach to labelling could be used. BrdU could be administered over longer periods, for example by adding BrdU to the drinking water over several days or weeks. Alternatively, additional groups could be included in the study to examine proliferative activity at 7 days and 10 days post-ischaemia in Gsh2-Cre/R26-GFP and Emx1-Cre/R26-GFP mice. Immunohisochemistry with mitotic markers would also give an indication of cell proliferation at each timepoint.

Caution must be used when interpreting BrdU activity in cell stress environments such as cerebral ischaemia. Damaged or degenerating neurons can also express mitotic markers and initiate DNA synthesis while undergoing DNA repair or apoptosis (Rakic, 2002). Under normal conditions the level of DNA repair in the brain is low (Schmitz et al., 1999), and BrdU immunohistochemistry is not sensitive enough to detect this activity. And even after inducing DNA damage by ionising radiation, BrdU has not been detected by immunohistochemistry in vivo or in vitro (Taupin, 2007). The

sensitivity may be due to the levels of BrdU incorporation into the cell, where proliferation involves the replication of the entire genome, and DNA repair replaces approximately 100 nucleotides per repair site (Taupin, 2007). However, Pawelczyk et al recently demonstrated that BrdU could be transferred from BrdU-labelled cells to macrophages in an in vitro Boyden chamber model of inflammation, albeit in small quantities (Pawelczyk et al., 2008).

Immunohistochemistry with mitotic markers are a secondary option for assessing cell proliferation and would give an indication of cell proliferation at the time of sacrifice – eg at 1, 3 and 5 weeks post-ischaemia. However, some markers of mitosis may also be upregulated during DNA repair. PCNA is expressed in the DNA synthesis phase of replication, G1 and S-phase, but under cell stress is involved in the RAD6-dependednt DNA repair pathway. Phospho-histone 3 is involved in chromosome condensation during mitosis, is not recruited into DNA repair pathways, and is commonly used as a marker for cell proliferation in in vitro DNA damage studies. Ki-67 is expressed in the G1, S and G2 phases of the cell cycle, and is also used as a marker in DNA damage studies(Hall et al., 1993; Iatropoulos and Williams, 1996).

7.4.2. PDGFRα-CreERt2/R26-YFP

We observed an increase in proliferation of OLPs in the ischaemic lesion. Few studies have examined the role of oligodendrocyte precursors after ischaemia. Our results suggest that they proliferate locally in response to ischaemia, however their long-term fate remains unknown. We found that the majority of OLPs did not express NG2 at 1 week post-ischaemia, suggesting that by this timepoint they were undergoing differentiation. We identified CNP+ cells at 1 week and 5 weeks post-ischaemia, however the majority of GFP+ cells were CNP-negative, suggesting the OLP differentiation was not predominantly into mature oligodendrocytes. Our results do not suggest that OLPs are a contributor to post-ischaemic neurogenesis, although it is possible that a very small percentage can differentiate into neurons.

What is the fate of the OLP progeny? Do the OLP progeny contribute to injury or repair mechanisms after ischaemia? There is scope for the role of the OLPs following ischaemia to be further explored. It is possible that while OLPs do not mature fully into myelinating oligodendrocytes after ischaemia, they begin differentiation into an intermediate cell type and retain an oligodendroglial identity. Immunohistochemistry for oligodendroglial markers such as Sox10 could determine if OLPs in the ischaemic lesion exit the oligodendroglial lineage. Similarly, while we observed very few NeuN- or interneuron-positive cells at 5 weeks post-ischaemia in the ipsilateral striatum and cortex, it is possible that OLPs were differentiating into immature neuronal cells. Immunohistochemistry for early neuronal markers such as β3-tubulin would determine whether a larger proportion of OLPs were contributing to neurogenesis. Finally, it is possible that OLPs are

differentiating into other glial cell types, for example astrocytes.

In contrast to the Gsh2-Cre/R26-GFP and Emx1-Cre/R26-GFP transgenic lines, the use of the inducible PDGFRα-CreERt2/R26-YFP -CreERT2 transgenic allowed us to define the initiation of GFP expression, and to selectively label the OLP population immediately prior to cerebral ischaemia. Our data therefore represent the fate of resident OLP at the time of ischaemia. However, we encountered several limitations in using this model. Induction of GFP expression requires Tamoxifen treatment, which we administered by gavage between 7 and 2 days prior to MCAO surgery, allowing 2 days for wash out. Initially, we observed a high mortality in these animals relative to the Gsh2-Cre/R26-GFP and Emx1-Cre/R26-GFP transgenic lines. Tamoxifen is a selective estrogen receptor modulator, and is commonly used in treatment for breast cancer. Its activity on estrogen receptors has been exploited in this transgenic line to selectively activate Cre recombinase in cells expressing the estrogen receptor 2 under the PDGFRα-CreERt2/R26-YFP promotor. However, there are several known side effects of Tamoxifen, including the increased risk of blood clotting and stroke, as well as fatigue, nausea and pain. Tamoxifen has also been shown to be neuroprotective following cerebral ischaemia (Wakade et al., 2008; Zhang et al., 2007b; Zhang et al., 2005b).

7.4.3. Animal mortality and lesion variability

We observed increased mortality in the PDGFRα-CreERt2/R26-YFP -CreERT2 transgenic line. Mortality resulting from the MCAO surgery itself was kept to a minimum (less than 2%) by minimising tissue damage at the neck area, minimising the surgery time, working in a sterile environment, and the post-operative care procedure. Tamoxifen treatment has known side effects, and additionally mice may have increased stress from extensive handling and gavage. Though the age of all mice in the study was 3 to 4 months of age, the mean weight of the PDGFRα-CreERt2/R26-YFP -CreERT2 mice was the lowest of all groups, suggesting that the mice may have been stressed. In future studies, it will be important to weigh mice prior to Tamoxifen treatment as well as at regular intervals following ischaemia.

We also observed a different lesion pathology in the PDGFRα-CreERt2/R26-YFP -CreERT2 mice, where the lesion was restricted to the striatum at 1 week post-ischaemia, and lesions were not detectable on MRI at 3- and 5-weeks post-ischaemia. A similar observation was reported by Wegener et al, who describe exclusively subcortical infarctions after MCAO surgery, which 'were characterised by a complete resolution of initially increased T1 and T2 relaxation times by 10 weeks (Wegener et al., 2006). Consistent with our findings, the authors detected selective neuronal death and gliosis in histological lesions.

It is possible that the vasculature of this transgenic line differs slightly from the Gsh2-Cre/R26-GFP

and Emx1-Cre/R26-GFP mice and could lead to a different lesion type. It is also possible that the combined use of carprofen and Tamoxifen conferred neuroprotection to the mice which resulted in a reduced lesion volume. There is scope for optimisation of the timing of Tamoxifen administration, post-operative care and monitoring will be undertaken to improve mortality rates and lesion volume, if possible in future studies.

7.4.4. Future work

There is opportunity for further work resulting from our findings. The contribution of Gsh2 and Emx1-derived cells to neuroblast generation after stroke can be quantified. Neuroblasts in the rostral migratory stream may proliferate or exit the stream in response to ischaemia, and this can be characterised. As discussed above, BrdU administration protocols can be modified or extended to label more proliferating neural stem cells, and the contribution of Gsh2- and Emx1-derived cells to the generation of mature neurons can be further characterised.

Futher work will include further characterisation of the fate of the OLP progeny, as well as investigation of the contribution of OLPs to neurogenesis in the piriform cortex. Finally, MRI was performed at the final timepoint on a 2.35T system, for quantification of lesion volume. In future studies, longitudinal data may be acquired in mice up to the final timepoint, to assess the evolution of lesion volume. In this study we observed a decrease in mean lesion volume at later timepoints. However, due to the high mortality rate, it is unclear whether mice surviving have smaller lesion volumes, or whether, consistent with other studies and our findings in the rat, lesion size decreases in individual animals at later timepoints. In vivo imaging using high-field system will increase spatial resolution, and imaging of physiological parameters such as cerebral blood flow and oedema could further characterise the infarct core and penumbra (Weber et al., 2005).

These experiments will provide essential knowledge into possible targets for the directed exploitation of SVZ stem cell populations in order to enhance endogenous brain repair. This study will also determine the contribution of each stem cell population to neurogenesis following injury. Better understanding of these issues will contribute to our knowledge of CNS injury, and may identify therapeutic targets.

8. *Discussion*

This thesis investigated methods of labeling and tracking of endogenous or grafted neural progenitor cells using MRI contrast agents, and their potential application to *in vivo* imaging of NPC migration after cerebral ischaemia. Cell labelling with iron oxide MRI contrast agents was optimised, and novel gadolinium-based MRI contrast agents were characterized. Labelled cells could be imaged *in vivo* in a model of cerebral ischaemia, but endogenous, pathological sources of iron oxide were also observed, and confounded cellular imaging. A method of in situ labelling of endogenous NPC with MRI contrast agents was developed and optimised, and endogenous NPC migration following cerebral ischaemia was investigated by transgenic lineage tracing. In the future, these approaches could be combined to longitudinally track subpopulations of SVZ NPC after cerebral ischamia.

First, an iron oxide-based MRI contrast agent and labelling method was investigated and optimized *in vitro* in a fetal NPC cell culture model. The FePro contrast agent labelling method maximised iron oxide uptake by cells, relative to incubation with Endorem alone, and generated hypointense contrast on MRI images. In addition, the FePro contrast agent was non-toxic to NPC, did not alter labelled cell metabolism relative to control cells, and did not interfere with NPC neurosphere formation or differentiation. *In vivo* cell tracking of FePro-labelled cells was then investigated in a model of cerebral ischaemia, where grafted cells were imaged over four weeks after cerebral ischaemia. Grafted cells were identified at the lesion site on MRI images, but an endogenous hypointense contrast was also observed to evolve over time within the lesioned tissue, in all animals. Endogenous ferric iron was observed in the lesion on histological sections. In addition to investigating the source of endogenous iron following ischaemia, there is scope to optimise other study parameters to increase graft survival and migration after ischaemia. These can include the timepoint and location of the graft, and the use of immunosuppressant drugs.

This study raises important issues surrounding the use of MRI and MRI contrast agents for longitudinal cell tracking studies in models of injury, where the evolution of endogenous contrast over time within lesioned tissue can be a source of uncertainty in image interpretation. Blood brain barrier breakdown, microhemorrhage and iron dysregulation after ischaemia, leading to iron accumulation in the lesion, are possible causes of the evolution of T_2 hypointensity, and delayed neuronal death. Brain iron accumulation after the ischaemic event may contribute to the development of a neurotoxic environment that leads to delayed neuronal death. The sources of iron are likely from both the degradation of blood products as a consequence of BBB breakdown or microhemorrhages following the ischaemic insult, as well as endogenous brain iron stores which may contribute to, and exacerbate, free radical damage after ischaemia. Together, the studies described above confirm our observation that the evolution of the ischaemic lesion is a dynamic process occurring over several weeks following cerebral ischaemia, and delayed neuronal death may reshape the lesion at later time points.

Next, we considered the development of gadolinium-based MRI contrast agents for cellular labeling and

tracking, as an alternative to the iron oxide-based agents, in collaboration with Imperial College chemistry department. Monomeric and polymeric Gd-DOTA chelates were synthesized and designed for maximal r_1 relaxivity, and their relaxivity and effects on cell viability were assessed. Through this approach, we identified a number of candidate polymeric Gd-DOTA chelates with high relaxivity and low cytotoxicity for use in cellular imaging and tracking studies.

For monomers, r_1 and r_2 relaxivity were lower than Gd-DOTA or Gd-DTPA, at 2.35T and 9.4T. For all monomers, r_1 and r_2 relaxivity were lower at 9.4T than 2.35T. Cell viability for monomer-labelled cells was not different than control cells, and cells could be labelled and imaged using MRI. While T_1-weighted positive contrast was observed in monomer 56, hypointense contrast was observed in monomers 60 or 72, possibly due to T2 effects of these monomer becoming dominant within labelled cells. Electron microscopy analysis will be necessary to determine the internal localisation of the contrast agents. The chemistry of the monomer branching arms appears to have a significant effect on cell labelling, and T_1 and T_2.

Although the mean number of monomer units in the polymers was lower than expected, several partially-loaded polymers has greater r1 relaxivity than the monomer from which it was synthesized, whereas this was not observed with any of the 100%-loaded polymers. Optimising the synthesis reaction to obtain higher molecular weight polymers with greater monomer units per polymer may lead to a further increase in r1 relaxivity. Cell viability was reduced for polymers, relative to control cells and gadolinium monomers, and viability assays were confirmed with microscopy. Monomer 72, the ligand from which the polymer was synthesised, did not affect cell viability in Alamar Blue or MTT assays, so the viability effects may be due to the polymer size or the presence of diazides. This must be further investigated for polymers to be considered candidate contrast agents for cellular imaging. For optimal contrast agent design, compound chemistry, relaxivity, and cytotoxicity must all be considered at early stages of design.

To investigate the endogenous NPC population, a method of *in situ* labeling of endogenous NPC with the MRI contrast agent FePro was developed. In this study we demonstrate that NPC and neuroblasts can be labelled with MRI contrast agents at the SVZ, and migrating neuroblasts can be visualised using MRI in the RMS at low magnetic field strength. Histology confirmed that neuroblasts within the RMS were labelled with the FePro complex. These results may facilitate the study of neuroblast migration by establishing a methodology for *in vivo* labelling and monitoring of the endogenous population.

The *in vivo* imaging of neuroblasts was achieved using a smaller injection concentration of iron oxide than previously reported, and without the addition of growth factors to promote cell labelling at the SVZ. The reduced susceptibility effects at the injection site, due to the smaller injection volume, will also permit imaging the short distance migration of neuroblasts in pathological environments, for example, their migration from the SVZ into the striatum following cerebral ischaemia. If there is endogenous neuroblast migration from the SVZ following an injury, it should be apparent using this method.

This method of endogenous labelling of the SVZ with FePro complex has some limitations in that we observed a low number of labelled neuroblasts, particularly at longer distances from the injection site. These

studies demonstrate that MRI contrast agents offer the potential for *in vivo*, longitudinal tracking of NPC migration, in both grafted and endogenous NPC populations. Coupled with transgenic lineage tracing, and used in animal models of CNS injury such as cerebral ischaemia, labeling and tracking the migration of NSC with MRI contrast agents can contribute to our understanding of NPC biology in pathological environments.

We use transgenic lineage tracing to explore the fate of different populations of endogenous progenitors in the brain following cerebral ischaemia: neural stem and progenitors in the SVZ, and oligodendrocyte precursor cells (OLPs). We observed neuroblast migration from the SVZ into the striatum after ischaemia, and these neuroblasts were a mixed population originating from Gsh2- and Emx1-derived neural stem cells. Further assessment of the contribution of neuroblasts to neurogenesis and newborn neurons after ischaemia is the subject of future studies.

We also observed an increase in proliferation of OLPs at the ischaemic lesion. We found that the majority of OLPs did not express the OLP marker NG2 at 1 week post-ischaemia, suggesting that by this timepoint they were undergoing differentiation. We identified CNP+ myelin-producing oligodendrocyte cells at 1 week and 5 weeks post-ischaemia, however the majority of GFP+ cells were CNP-negative, suggesting the OLP differentiation was not predominantly into mature oligodendrocytes. The fate of proliferating OLPs after ischaemia remains uncertain, and is the subject of future studies. Our results do not suggest that OLPs are a contributor to post-ischaemic neurogenesis, although it is possible that a very small percentage can differentiate into neurons.

9. Reference List

Aarum J, Sandberg K, Haeberlein SL, Persson MA, 2003. Migration and differentiation of neural precursor cells can be directed by microglia. Proc. Natl. Acad. Sci. U. S. A 100: 15983-15988.

Aboody KS, Brown A, Rainov NG, Bower KA, Liu S, Yang W, Small JE, Herrlinger U, Ourednik V, Black PM, Breakefield XO, Snyder EY, 2000. Neural stem cells display extensive tropism for pathology in adult brain: evidence from intracranial gliomas. Proc. Natl. Acad. Sci. U. S. A 97: 12846-12851.

Abrous DN, Koehl M, Le MM, 2005. Adult neurogenesis: from precursors to network and physiology. Physiol Rev. 85: 523-569.

Aguirre A, Gallo V, 2004. Postnatal neurogenesis and gliogenesis in the olfactory bulb from NG2-expressing progenitors of the subventricular zone. J. Neurosci. 24: 10530-10541.

Ahn S, Joyner AL, 2005. In vivo analysis of quiescent adult neural stem cells responding to Sonic hedgehog. Nature 437: 894-897.

Aime S, Cabella C, Colombatto S, Geninatti CS, Gianolio E, Maggioni F, 2002. Insights into the use of paramagnetic Gd(III) complexes in MR-molecular imaging investigations. J. Magn Reson. Imaging 16: 394-406.

Ajami B, Bennett JL, Krieger C, Tetzlaff W, Rossi FM, 2007. Local self-renewal can sustain CNS microglia maintenance and function throughout adult life. Nat. Neurosci. 10: 1538-1543.

Alkayed NJ, Harukuni I, Kimes AS, London ED, Traystman RJ, Hurn PD, 1998. Gender-linked brain injury in experimental stroke. Stroke 29: 159-165.

Aloisi F, 2001. Immune function of microglia. Glia 36: 165-179.

Alonso G, 2005. NG2 proteoglycan-expressing cells of the adult rat brain: possible involvement in the formation of glial scar astrocytes following stab wound. Glia 49: 318-338.

Alonso M, Ortega-Perez I, Grubb MS, Bourgeois JP, Charneau P, Lledo PM, 2008. Turning astrocytes from the rostral migratory stream into neurons: a role for the olfactory sensory organ. J. Neurosci. 28: 11089-11102.

Anderson SA, Lee KK, Frank JA, 2006. Gadolinium-fullerenol as a paramagnetic contrast agent for cellular imaging. Invest Radiol. 41: 332-338.

Arbab AS, Bashaw LA, Miller BR, Jordan EK, Bulte JW, Frank JA, 2003. Intracytoplasmic tagging of cells with ferumoxides and transfection agent for cellular magnetic resonance imaging after cell transplantation: methods and techniques. Transplantation 76: 1123-1130.

Arbab AS, Frank JA, 2008. Cellular MRI and its role in stem cell therapy. Regen. Med. 3: 199-215.

Arbab AS, Liu W, Frank JA, 2006. Cellular magnetic resonance imaging: current status and future prospects. Expert. Rev. Med. Devices 3: 427-439.

Arbab AS, Wilson LB, Ashari P, Jordan EK, Lewis BK, Frank JA, 2005a. A model of lysosomal metabolism of dextran coated superparamagnetic iron oxide (SPIO) nanoparticles: implications for cellular magnetic resonance imaging. NMR Biomed. 18: 383-389.

Arbab AS, Yocum GT, Kalish H, Jordan EK, Anderson SA, Khakoo AY, Read EJ, Frank JA, 2004. Efficient magnetic cell labeling with protamine sulfate complexed to ferumoxides for cellular MRI. Blood 104: 1217-1223.

Arbab AS, Yocum GT, Rad AM, Khakoo AY, Fellowes V, Read EJ, Frank JA, 2005b. Labeling of cells with ferumoxides-protamine sulfate complexes does not inhibit function or differentiation capacity of hematopoietic or mesenchymal stem

cells. NMR Biomed. 18: 553-559.

Armengou A, Davalos A, 2002. A review of the state of research into the role of iron in stroke. J. Nutr. Health Aging 6: 207-208.

Artemov D, Bhujwalla ZM, Bulte JW, 2004. Magnetic resonance imaging of cell surface receptors using targeted contrast agents. Curr. Pharm. Biotechnol. 5: 485-494.

Arvidsson A, Collin T, Kirik D, Kokaia Z, Lindvall O, 2002. Neuronal replacement from endogenous precursors in the adult brain after stroke. Nat. Med. 8: 963-970.

Arvidsson A, Kokaia Z, Lindvall O, 2001. N-methyl-D-aspartate receptor-mediated increase of neurogenesis in adult rat dentate gyrus following stroke. Eur. J. Neurosci. 14: 10-18.

Asahi M, Sumii T, Fini ME, Itohara S, Lo EH, 2001. Matrix metalloproteinase 2 gene knockout has no effect on acute brain injury after focal ischemia. Neuroreport 12: 3003-3007.

Astrup J, Symon L, Branston NM, Lassen NA, 1977. Cortical evoked potential and extracellular K+ and H+ at critical levels of brain ischemia. Stroke 8: 51-57.

Athiraman H, Jiang Q, Ding GL, Zhang L, Zhang ZG, Wang L, Arbab AS, Li Q, Panda S, Ledbetter K, Rad AM, Chopp M, 2009. Investigation of relationships between transverse relaxation rate, diffusion coefficient, and labeled cell concentration in ischemic rat brain using MRI. Magn Reson. Med. 61: 587-594.

Ay I, Sugimori H, Finklestein SP, 2001. Intravenous basic fibroblast growth factor (bFGF) decreases DNA fragmentation and prevents downregulation of Bcl-2 expression in the ischemic brain following middle cerebral artery occlusion in rats. Brain Res. Mol. Brain Res. 87: 71-80.

Bachoud-Levi AC, Deglon N, Nguyen JP, Bloch J, Bourdet C, Winkel L, Remy P, Goddard M, Lefaucheur JP, Brugieres P, Baudic S, Cesaro P, Peschanski M, Aebischer P, 2000. Neuroprotective gene therapy for Huntington's disease using a polymer encapsulated BHK cell line engineered to secrete human CNTF. Hum. Gene Ther. 11: 1723-1729.

Bang OY, Lee JS, Lee PH, Lee G, 2005. Autologous mesenchymal stem cell transplantation in stroke patients. Ann. Neurol. 57: 874-882.

Barberi T, Klivenyi P, Calingasan NY, Lee H, Kawamata H, Loonam K, Perrier AL, Bruses J, Rubio ME, Topf N, Tabar V, Harrison NL, Beal MF, Moore MA, Studer L, 2003. Neural subtype specification of fertilization and nuclear transfer embryonic stem cells and application in parkinsonian mice. Nat. Biotechnol. 21: 1200-1207.

Barres BA, Hart IK, Coles HS, Burne JF, Voyvodic JT, Richardson WD, Raff MC, 1992. Cell death in the oligodendrocyte lineage. J. Neurobiol. 23: 1221-1230.

Beauquis J, Roig P, Homo-Delarche F, De NA, Saravia F, 2006. Reduced hippocampal neurogenesis and number of hilar neurones in streptozotocin-induced diabetic mice: reversion by antidepressant treatment. Eur. J. Neurosci. 23: 1539-1546.

Bedard A, Parent A, 2004. Evidence of newly generated neurons in the human olfactory bulb. Brain Res. Dev. Brain Res. 151: 159-168.

Belachew S, Chittajallu R, Aguirre AA, Yuan X, Kirby M, Anderson S, Gallo V, 2003. Postnatal NG2 proteoglycan-expressing progenitor cells are intrinsically multipotent and generate functional neurons. J. Cell Biol. 161: 169-186.

Ben-Hur T, Einstein O, Mizrachi-Kol R, Ben-Menachem O, Reinhartz E, Karussis D, Abramsky O, 2003. Transplanted multipotential neural precursor cells migrate into the inflamed white matter in response to experimental autoimmune encephalomyelitis. Glia 41: 73-80.

Benraiss A, Chmielnicki E, Lerner K, Roh D, Goldman SA, 2001. Adenoviral brain-derived neurotrophic factor induces both neostriatal and olfactory neuronal recruitment from endogenous progenitor cells in the adult forebrain. J. Neurosci. 21: 6718-6731.

Berg D, Youdim MB, 2006. Role of iron in neurodegenerative disorders. Top. Magn Reson. Imaging 17: 5-17.

Berger C, Hiestand P, Kindler-Baumann D, Rudin M, Rausch M, 2006. Analysis of lesion development during acute inflammation and remission in a rat model of experimental autoimmune encephalomyelitis by visualization of macrophage infiltration, demyelination and blood-brain barrier damage. NMR Biomed. 19: 101-107.

Bergles DE, Roberts JD, Somogyi P, Jahr CE, 2000. Glutamatergic synapses on oligodendrocyte precursor cells in the hippocampus. Nature 405: 187-191.

Bernardino L, Agasse F, Silva B, Ferreira R, Grade S, Malva JO, 2008. Tumor necrosis factor-alpha modulates survival, proliferation, and neuronal differentiation in neonatal subventricular zone cell cultures. Stem Cells 26: 2361-2371.

Bernier PJ, Vinet J, Cossette M, Parent A, 2000. Characterization of the subventricular zone of the adult human brain: evidence for the involvement of Bcl-2. Neurosci. Res. 37: 67-78.

Bhardwaj RD, Curtis MA, Spalding KL, Buchholz BA, Fink D, Bjork-Eriksson T, Nordborg C, Gage FH, Druid H, Eriksson PS, Frisen J, 2006. Neocortical neurogenesis in humans is restricted to development. Proc. Natl. Acad. Sci. U. S. A 103: 12564-12568.

Bible E, Chau DY, Alexander MR, Price J, Shakesheff KM, Modo M, 2009. The support of neural stem cells transplanted into stroke-induced brain cavities by PLGA particles. Biomaterials 30: 2985-2994.

Bicknese AR, Goodwin HS, Quinn CO, Henderson VC, Chien SN, Wall DA, 2002. Human umbilical cord blood cells can be induced to express markers for neurons and glia. Cell Transplant. 11: 261-264.

Bidmon HJ, Emde B, Oermann E, Kubitz R, Witte OW, Zilles K, 2001. Heme oxygenase-1 (HSP-32) and heme oxygenase-2 induction in neurons and glial cells of cerebral regions and its relation to iron accumulation after focal cortical photothrombosis. Exp. Neurol. 168: 1-22.

Bishop GM, Robinson SR, 2001. Quantitative analysis of cell death and ferritin expression in response to cortical iron: implications for hypoxia-ischemia and stroke. Brain Res. 907: 175-187.

Bjorklund LM, Sanchez-Pernaute R, Chung S, Andersson T, Chen IY, McNaught KS, Brownell AL, Jenkins BG, Wahlestedt C, Kim KS, Isacson O, 2002. Embryonic stem cells develop into functional dopaminergic neurons after transplantation in a Parkinson rat model. Proc. Natl. Acad. Sci. U. S. A 99: 2344-2349.

Bliss T, Guzman R, Daadi M, Steinberg GK, 2007. Cell transplantation therapy for stroke. Stroke 38: 817-826.

Block ML, Hong JS, 2007. Chronic microglial activation and progressive dopaminergic neurotoxicity. Biochem. Soc. Trans. 35: 1127-1132.

Block ML, Zecca L, Hong JS, 2007. Microglia-mediated neurotoxicity: uncovering the molecular mechanisms. Nat. Rev. Neurosci. 8: 57-69.

Bogler O, Wren D, Barnett SC, Land H, Noble M, 1990. Cooperation between two growth factors promotes extended self-renewal and inhibits differentiation of oligodendrocyte-type-2 astrocyte (O-2A) progenitor cells. Proc. Natl. Acad. Sci. U. S. A 87: 6368-6372.

Bonaguidi MA, McGuire T, Hu M, Kan L, Samanta J, Kessler JA, 2005. LIF and BMP signaling generate separate and discrete types of GFAP-expressing cells. Development 132: 5503-5514.

Bonfanti L, Peretto P, 2007a. Radial glial origin of the adult neural stem cells in the subventricular zone. Prog. Neurobiol. 83: 24-36.

Borlongan CV, Hadman M, Sanberg CD, Sanberg PR, 2004. Central nervous system entry of peripherally injected umbilical cord blood cells is not required for neuroprotection in stroke. Stroke 35: 2385-2389.

Bradbury MS, Panagiotakos G, Chan BK, Tomishima M, Zanzonico P, Vider J, Ponomarev V, Studer L, Tabar V, 2007. Optical bioluminescence imaging of human ES cell progeny in the rodent CNS. J. Neurochem. 102: 2029-2039.

Brekke C, Morgan SC, Lowe AS, Meade TJ, Price J, Williams SC, Modo M, 2007. The in vitro effects of a bimodal contrast agent on cellular functions and relaxometry. NMR Biomed. 20: 77-89.

Broom KA, Anthony DC, Blamire AM, Waters S, Styles P, Perry VH, Sibson NR, 2005. MRI reveals that early changes in cerebral blood volume preced blood-brain barrier breakdown and overt pathology in MS-like lesions in rat brain. JCBFM. 25: 204-216.

Brunner EJ, Marmot MG, White IR, O'Brien JR, Etherington MD, Slavin BM, Kearney EM, Smith GD, 1993. Gender and employment grade differences in blood cholesterol, apolipoproteins and haemostatic factors in the Whitehall II study. Atherosclerosis 102: 195-207.

Brustle O, 1999. Building brains: neural chimeras in the study of nervous system development and repair. Brain Pathol. 9: 527-545.

Brustle O, Choudhary K, Karram K, Huttner A, Murray K, Dubois-Dalcq M, McKay RD, 1998. Chimeric brains generated by intraventricular transplantation of fetal human brain cells into embryonic rats. Nat. Biotechnol. 16: 1040-1044.

Brustle O, Spiro AC, Karram K, Choudhary K, Okabe S, McKay RD, 1997. In vitro-generated neural precursors participate in mammalian brain development. Proc. Natl. Acad. Sci. U. S. A 94: 14809-14814.

Bu J, Akhtar N, Nishiyama A, 2001. Transient expression of the NG2 proteoglycan by a subpopulation of activated macrophages in an excitotoxic hippocampal lesion. Glia 34: 296-310.

Bu J, Banki A, Wu Q, Nishiyama A, 2004. Increased NG2(+) glial cell proliferation and oligodendrocyte generation in the hypomyelinating mutant shiverer. Glia 48: 51-63.

Buffo A, Vosko MR, Erturk D, Hamann GF, Jucker M, Rowitch D, Gotz M, 2005. Expression pattern of the transcription factor Olig2 in response to brain injuries: implications for neuronal repair. Proc. Natl. Acad. Sci. U. S. A 102: 18183-18188.

Buhnemann C, Scholz A, Bernreuther C, Malik CY, Braun H, Schachner M, Reymann KG, Dihne M, 2006. Neuronal differentiation of transplanted embryonic stem cell-derived precursors in stroke lesions of adult rats. Brain 129: 3238-3248.

Bulte JW, Douglas T, Mann S, Frankel RB, Moskowitz BM, Brooks RA, Baumgarner CD, Vymazal J, Strub MP, Frank JA, 1994. Magnetoferritin: characterization of a novel superparamagnetic MR contrast agent. J. Magn Reson. Imaging 4: 497-505.

Bulte JW, Douglas T, Witwer B, Zhang SC, Strable E, Lewis BK, Zywicke H, Miller B, van GP, Moskowitz BM, Duncan ID, Frank JA, 2001. Magnetodendrimers allow endosomal magnetic labeling and in vivo tracking of stem cells. Nat. Biotechnol. 19: 1141-1147.

Bulte JW, Kraitchman DL, 2004b. Monitoring cell therapy using iron oxide MR contrast agents. Curr. Pharm. Biotechnol. 5: 567-584.

Bulte JW, Kraitchman DL, 2004a. Monitoring cell therapy using iron oxide MR contrast agents. Curr. Pharm. Biotechnol. 5: 567-584.

Burns KA, Ayoub AE, Breunig JJ, Adhami F, Weng WL, Colbert MC, Rakic P, Kuan CY, 2007. Nestin-CreER mice reveal DNA synthesis by nonapoptotic neurons following cerebral ischemia hypoxia. Cereb. Cortex 17: 2585-2592.

Burt RK, Loh Y, Cohen B, Stefoski D, Balabanov R, Katsamakis G, Oyama Y, Russell EJ, Stern J, Muraro P, Rose J, Testori A, Bucha J, Jovanovic B, Milanetti F, Storek J, Voltarelli JC, Burns WH, 2009. Autologous non-myeloablative haemopoietic stem cell transplantation in relapsing-remitting multiple sclerosis: a phase I/II study. Lancet Neurol. 8: 244-253.

Busza AL, Allen KL, King MD, van BN, Williams SR, Gadian DG, 1992. Diffusion-weighted imaging studies of cerebral ischemia in gerbils. Potential relevance to energy failure. Stroke 23: 1602-1612.

Butovsky O, Ziv Y, Schwartz A, Landa G, Talpalar AE, Pluchino S, Martino G, Schwartz M, 2006. Microglia activated by IL-4 or IFN-gamma differentially induce neurogenesis and oligodendrogenesis from adult stem/progenitor cells. Mol. Cell Neurosci. 31: 149-160.

Cacci E, jmone-Cat MA, Anelli T, Biagioni S, Minghetti L, 2008. In vitro neuronal and glial differentiation from embryonic or adult neural precursor cells are differently affected by chronic or acute activation of microglia. Glia 56: 412-425.

Calamante F, Lythgoe MF, Pell GS, Thomas DL, King MD, Busza AL, Sotak CH, Williams SR, Ordidge RJ, Gadian DG, 1999a. Early changes in water diffusion, perfusion, T1, and T2 during focal cerebral ischemia in the rat studied at 8.5 T. Magn Reson. Med. 41: 479-485.

Calamante F, Thomas DL, Pell GS, Wiersma J, Turner R, 1999b. Measuring cerebral blood flow using magnetic resonance imaging techniques. J. Cereb. Blood Flow Metab 19: 701-735.

Camarero G, Leon Y, Gorospe I, De PF, Alsina B, Giraldez F, Varela-Nieto I, 2003. Insulin-like growth factor 1 is required for survival of transit-amplifying neuroblasts and differentiation of otic neurons. Dev. Biol. 262: 242-253.

Capone C, Frigerio S, Fumagalli S, Gelati M, Principato MC, Storini C, Montinaro M, Kraftsik R, De CM, Parati E, De Simoni MG, 2007. Neurosphere-derived cells exert a neuroprotective action by changing the ischemic microenvironment. PLoS. ONE. 2: e373.

Caravan P, Ellison JJ, McMurry TJ, Lauffer RB, 1999. Gadolinium(III) Chelates as MRI Contrast Agents: Structure, Dynamics, and Applications. Chem. Rev. 99: 2293-2352.

Carbonell T, Rama R, 2007. Iron, oxidative stress and early neurological deterioration in ischemic stroke. Curr. Med. Chem. 14: 857-874.

Carlen M, Meletis K, Goritz C, Darsalia V, Evergren E, Tanigaki K, Amendola M, Barnabe-Heider F, Yeung MS, Naldini L, Honjo T, Kokaia Z, Shupliakov O, Cassidy RM, Lindvall O, Frisen J, 2009. Forebrain ependymal cells are Notch-dependent and generate neuroblasts and astrocytes after stroke. Nat. Neurosci. 12: 259-267.

Carmichael ST, 2005. Rodent models of focal stroke: size, mechanism, and purpose. NeuroRx. 2: 396-409.

Cattaneo E, Conti L, 1998. Generation and characterization of embryonic striatal conditionally immortalized ST14A cells. J. Neurosci. Res. 53: 223-234.

Chang YC, Shyu WC, Lin SZ, Li H, 2007. Regenerative therapy for stroke. Cell Transplant. 16: 171-181.

Chen J, Li Y, Wang L, Zhang Z, Lu D, Lu M, Chopp M, 2001. Therapeutic benefit of intravenous administration of bone marrow stromal cells after cerebral ischemia in rats. Stroke 32: 1005-1011.

Chen J, Zacharek A, Zhang C, Jiang H, Li Y, Roberts C, Lu M, Kapke A, Chopp M, 2005. Endothelial nitric oxide synthase regulates brain-derived neurotrophic factor expression and neurogenesis after stroke in mice. J. Neurosci. 25: 2366-2375.

Chen J, Zhang ZG, Li Y, Wang L, Xu YX, Gautam SC, Lu M, Zhu Z, Chopp M, 2003. Intravenous administration of human bone marrow stromal cells induces angiogenesis in the ischemic boundary zone after stroke in rats. Circ. Res. 92: 692-699.

Chen Y, Sun FY, 2007. Age-related decrease of striatal neurogenesis is associated with apoptosis of neural precursors and newborn neurons in rat brain after ischemia. Brain Res. 1166: 9-19.

Chiasson BJ, Tropepe V, Morshead CM, van der KD, 1999. Adult mammalian forebrain ependymal and subependymal cells demonstrate proliferative potential, but only subependymal cells have neural stem cell characteristics. J. Neurosci. 19: 4462-4471.

Chopp M, Li Y, 2002. Treatment of neural injury with marrow stromal cells. Lancet Neurol. 1: 92-100.

Chopp M, Zhang ZG, Jiang Q, 2007. Neurogenesis, angiogenesis, and MRI indices of functional recovery from stroke. Stroke 38: 827-831.

Chu K, Jung KH, Kim SJ, Lee ST, Kim J, Park HK, Song EC, Kim SU, Kim M, Lee SK, Roh JK, 2008. Transplantation of human neural stem cells protect against ischemia in a preventive mode via hypoxia-inducible factor-1alpha stabilization in the host brain. Brain Res. 1207: 182-192.

Chu K, Kim M, Park KI, Jeong SW, Park HK, Jung KH, Lee ST, Kang L, Lee K, Park DK, Kim SU, Roh JK, 2004. Human neural stem cells improve sensorimotor deficits in the adult rat brain with experimental focal ischemia. Brain Res. 1016: 145-153.

Clark RK, Lee EV, Fish CJ, White RF, Price WJ, Jonak ZL, Feuerstein GZ, Barone FC, 1993. Development of tissue damage, inflammation and resolution following stroke: an immunohistochemical and quantitative planimetric study. Brain

Res. Bull. 31: 565-572.

Clelland CD, Barker RA, Watts C, 2008. Cell therapy in Huntington disease. Neurosurg. Focus. 24: E9.

Cohen B, Dafni H, Meir G, Harmelin A, Neeman M, 2005. Ferritin as an endogenous MRI reporter for noninvasive imaging of gene expression in C6 glioma tumors. Neoplasia. 7: 109-117.

Consiglio A, Gritti A, Dolcetta D, Follenzi A, Bordignon C, Gage FH, Vescovi AL, Naldini L, 2004. Robust in vivo gene transfer into adult mammalian neural stem cells by lentiviral vectors. Proc. Natl. Acad. Sci. U. S. A 101: 14835-14840.

Cornetta K, Anderson WF, 1989. Protamine sulfate as an effective alternative to polybrene in retroviral-mediated gene-transfer: implications for human gene therapy. J. Virol. Methods 23: 187-194.

Coskun V, Wu H, Blanchi B, Tsao S, Kim K, Zhao J, Biancotti JC, Hutnick L, Krueger RC, Jr., Fan G, de VJ, Sun YE, 2008. CD133+ neural stem cells in the ependyma of mammalian postnatal forebrain. Proc. Natl. Acad. Sci. U. S. A 105: 1026-1031.

Cunningham LA, Wetzel M, Rosenberg GA, 2005. Multiple roles for MMPs and TIMPs in cerebral ischemia. Glia 50: 329-339.

Daadi MM, Maag AL, Steinberg GK, 2008. Adherent self-renewable human embryonic stem cell-derived neural stem cell line: functional engraftment in experimental stroke model. PLoS. ONE. 3: e1644.

Danielisova V, Gottlieb M, Burda J, 2002. Iron deposition after transient forebrain ischemia in rat brain. Neurochem. Res. 27: 237-242.

Dar A, Kollet O, Lapidot T, 2006. Mutual, reciprocal SDF-1/CXCR4 interactions between hematopoietic and bone marrow stromal cells regulate human stem cell migration and development in NOD/SCID chimeric mice. Exp. Hematol. 34: 967-975.

Darsalia V, Heldmann U, Lindvall O, Kokaia Z, 2005. Stroke-induced neurogenesis in aged brain. Stroke 36: 1790-1795.

Darsalia V, Kallur T, Kokaia Z, 2007. Survival, migration and neuronal differentiation of human fetal striatal and cortical neural stem cells grafted in stroke-damaged rat striatum. Eur. J. Neurosci. 26: 605-614.

Dawson MR, Levine JM, Reynolds R, 2000. NG2-expressing cells in the central nervous system: are they oligodendroglial progenitors? J. Neurosci. Res. 61: 471-479.

Dayer AG, Jenny B, Sauvain MO, Potter G, Salmon P, Zgraggen E, Kanemitsu M, Gascon E, Sizonenko S, Trono D, Kiss JZ, 2007. Expression of FGF-2 in neural progenitor cells enhances their potential for cellular brain repair in the rodent cortex. Brain 130: 2962-2976.

De CM, Joniau M, 1988. Magnetoliposomes. Formation and structural characterization. Eur. Biophys. J. 15: 311-319.

Deans AE, Wadghiri YZ, Bernas LM, Yu X, Rutt BK, Turnbull DH, 2006. Cellular MRI contrast via coexpression of transferrin receptor and ferritin. Magn Reson. Med. 56: 51-59.

del Zoppo GJ, Milner R, Mabuchi T, Hung S, Wang X, Berg GI, Koziol JA, 2007. Microglial activation and matrix protease generation during focal cerebral ischemia. Stroke 38: 646-651.

Dempsey RJ, Kalluri HS, 2007. Ischemia-induced neurogenesis: role of growth factors. Neurosurg. Clin. N. Am. 18: 183-90, xi.

Dempsey RJ, Sailor KA, Bowen KK, Tureyen K, Vemuganti R, 2003. Stroke-induced progenitor cell proliferation in adult spontaneously hypertensive rat brain: effect of exogenous IGF-1 and GDNF. J. Neurochem. 87: 586-597.

Dezawa M, Hoshino M, Ide C, 2005. Treatment of neurodegenerative diseases using adult bone marrow stromal cell-derived neurons. Expert. Opin. Biol. Ther. 5: 427-435.

Dijkhuizen RM, Nicolay K, 2003. Magnetic resonance imaging in experimental models of brain disorders. J. Cereb. Blood Flow Metab 23: 1383-1402.

Dittmar MS, Vatankhah B, Fehm NP, Schuierer G, Bogdahn U, Horn M, Schlachetzki F, 2006. Fischer-344 rats are unsuitable for the MCAO filament model due to their cerebrovascular anatomy. J. Neurosci. Methods 156: 50-54.

Djukic M, Mildner A, Schmidt H, Czesnik D, Bruck W, Priller J, Nau R, Prinz M, 2006. Circulating monocytes engraft in the brain, differentiate into microglia and contribute to the pathology following meningitis in mice. Brain 129: 2394-2403.

Doetsch F, 2003h. The glial identity of neural stem cells. Nat. Neurosci. 6: 1127-1134

Doetsch F, 2003i. A niche for adult neural stem cells. Curr. Opin. Genet. Dev. 13: 543-550.

Doetsch F, Caille I, Lim DA, Garcia-Verdugo JM, varez-Buylla A, 1999a. Subventricular zone astrocytes are neural stem cells in the adult mammalian brain. Cell 97: 703-716.

Doetsch F, Garcia-Verdugo JM, varez-Buylla A, 1999b. Regeneration of a germinal layer in the adult mammalian brain. Proc. Natl. Acad. Sci. U. S. A 96: 11619-11624.

Doetsch F, Petreanu L, Caille I, Garcia-Verdugo JM, varez-Buylla A, 2002. EGF converts transit-amplifying neurogenic precursors in the adult brain into multipotent stem cells. Neuron 36: 1021-1034.

Dousset V, Delalande C, Ballarino L, Quesson B, Seilhan D, Coussemacq M, Thiaudiere E, Brochet B, Canioni P, Caille JM, 1999. In vivo macrophage activity imaging in the central nervous system detected by magnetic resonance. Magn Reson. Med. 41: 329-333.

Dranovsky A, Hen R, 2006. Hippocampal neurogenesis: regulation by stress and antidepressants. Biol. Psychiatry 59: 1136-1143.

Duggal N, Schmidt-Kastner R, Hakim AM, 1997. Nestin expression in reactive astrocytes following focal cerebral ischemia in rats. Brain Res. 768: 1-9.

Durukan A, Tatlisumak T, 2007. Acute ischemic stroke: overview of major experimental rodent models, pathophysiology, and therapy of focal cerebral ischemia. Pharmacol. Biochem. Behav. 87: 179-197.

Dutton AH, Tokuyasu KT, Singer SJ, 1979. Iron-dextran antibody conjugates: General method for simultaneous staining of two components in high-resolution immunoelectron microscopy. Proc. Natl. Acad. Sci. U. S. A 76: 3392-3396.

Ehrenreich H, Hasselblatt M, Dembowski C, Cepek L, Lewczuk P, Stiefel M, Rustenbeck HH, Breiter N, Jacob S, Knerlich F, Bohn M, Poser W, Ruther E, Kochen M, Gefeller O, Gleiter C, Wessel TC, De RM, Itri L, Prange H, Cerami A, Brines M, Siren AL, 2002. Erythropoietin therapy for acute stroke is both safe and beneficial. Mol. Med. 8: 495-505.

Einstein O, Fainstein N, Vaknin I, Mizrachi-Kol R, Reihartz E, Grigoriadis N, Lavon I, Baniyash M, Lassmann H, Ben-Hur T, 2007. Neural precursors attenuate autoimmune encephalomyelitis by peripheral immunosuppression. Ann. Neurol. 61: 209-218.

Einstein O, Grigoriadis N, Mizrachi-Kol R, Reinhartz E, Polyzoidou E, Lavon I, Milonas I, Karussis D, Abramsky O, Ben-Hur T, 2006. Transplanted neural precursor cells reduce brain inflammation to attenuate chronic experimental autoimmune encephalomyelitis. Exp. Neurol. 198: 275-284.

Ekdahl CT, Claasen JH, Bonde S, Kokaia Z, Lindvall O, 2003. Inflammation is detrimental for neurogenesis in adult brain. Proc. Natl. Acad. Sci. U. S. A 100: 13632-13637.

Ekdahl CT, Kokaia Z, Lindvall O, 2009. Brain inflammation and adult neurogenesis: the dual role of microglia. Neuroscience 158: 1021-1029.

Endoh M, Pulsinelli WA, Wagner JA, 1994. Transient global ischemia induces dynamic changes in the expression of bFGF and the FGF receptor. Brain Res. Mol. Brain Res. 22: 76-88.

Engel U, Wolswijk G, 1996. Oligodendrocyte-type-2 astrocyte (O-2A) progenitor cells derived from adult rat spinal cord: in vitro characteristics and response to PDGF, bFGF and NT-3. Glia 16: 16-26.

Ernst C, Christie BR, 2005. Nestin-expressing cells and their relationship to mitotically active cells in the subventricular zones of the adult rat. Eur. J. Neurosci. 22: 3059-3066.

Faulkner JR, Herrmann JE, Woo MJ, Tansey KE, Doan NB, Sofroniew MV, 2004. Reactive astrocytes protect tissue and preserve function after spinal cord injury. J. Neurosci. 24: 2143-2155.

Fisher M, 2004. The ischemic penumbra: identification, evolution and treatment concepts. Cerebrovasc. Dis. 17 Suppl 1: 1-6.

Floris S, Blezer EL, Schreibelt G, Dopp E, van der Pol SM, Schadee-Eestermans IL, Nicolay K, Dijkstra CD, de Vries HE, 2004. Blood-brain barrier permeability and monocyte infiltration in experimental allergic encephalomyelitis: a quantitative MRI study. Brain 127: 616-627.

Flugel A, Bradl M, Kreutzberg GW, Graeber MB, 2001. Transformation of donor-derived bone marrow precursors into host microglia during autoimmune CNS inflammation and during the retrograde response to axotomy. J. Neurosci. Res. 66: 74-82.

Fogarty M, Richardson WD, Kessaris N, 2005. A subset of oligodendrocytes generated from radial glia in the dorsal spinal cord. Development 132: 1951-1959.

Fowlkes JL, Serra DM, Bunn RC, Thrailkill KM, Enghild JJ, Nagase H, 2004. Regulation of insulin-like growth factor (IGF)-I action by matrix metalloproteinase-3 involves selective disruption of IGF-I/IGF-binding protein-3 complexes. Endocrinology 145: 620-626.

Franklin RJ, Gilson JM, Blakemore WF, 1997. Local recruitment of remyelinating cells in the repair of demyelination in the central nervous system. J. Neurosci. Res. 50: 337-344.

Friel R, van der SS, Mee PJ, 2005a. Embryonic stem cells: understanding their history, cell biology and signalling. Adv. Drug Deliv. Rev. 57: 1894-1903.

Friel R, van der SS, Mee PJ, 2005b. Embryonic stem cells: understanding their history, cell biology and signalling. Adv. Drug Deliv. Rev. 57: 1894-1903.

Fruttiger M, Karlsson L, Hall AC, Abramsson A, Calver AR, Bostrom H, Willetts K, Bertold CH, Heath JK, Betsholtz C, Richardson WD, 1999. Defective oligodendrocyte development and severe hypomyelination in PDGF-A knockout mice. Development 126: 457-467.

Fu Y, Raatschen HJ, Nitecki DE, Wendland MF, Novikov V, Fournier LS, Cyran C, Rogut V, Shames DM, Brasch RC, 2007. Cascade polymeric MRI contrast media derived from poly(ethylene glycol) cores: initial syntheses and characterizations. Biomacromolecules. 8: 1519-1529.

Fujie W, Kirino T, Tomukai N, Iwasawa T, Tamura A, 1990. Progressive shrinkage of the thalamus following middle cerebral artery occlusion in rats. Stroke 21: 1485-1488.

Fujimura M, Morita-Fujimura Y, Kawase M, Copin JC, Calagui B, Epstein CJ, Chan PH, 1999. Manganese superoxide dismutase mediates the early release of mitochondrial cytochrome C and subsequent DNA fragmentation after permanent focal cerebral ischemia in mice. J. Neurosci. 19: 3414-3422.

Fujioka M, Taoka T, Matsuo Y, Mishima K, Ogoshi K, Kondo Y, Tsuda M, Fujiwara M, Asano T, Sakaki T, Miyasaki A, Park D, Siesjo BK, 2003. Magnetic resonance imaging shows delayed ischemic striatal neurodegeneration. Ann. Neurol. 54: 732-747.

Gaasch JA, Lockman PR, Geldenhuys WJ, Allen DD, Van der Schyf CJ, 2007. Brain iron toxicity: differential responses of astrocytes, neurons, and endothelial cells. Neurochem. Res. 32: 1196-1208.

Gage FH, 2000. Mammalian neural stem cells. Science 287: 1433-1438.

Gage FH, Coates PW, Palmer TD, Kuhn HG, Fisher LJ, Suhonen JO, Peterson DA, Suhr ST, Ray J, 1995. Survival and differentiation of adult neuronal progenitor cells transplanted to the adult brain. Proc. Natl. Acad. Sci. U. S. A 92: 11879-11883.

Gage FH, Kempermann G, Palmer TD, Peterson DA, Ray J, 1998. Multipotent progenitor cells in the adult dentate gyrus. J. Neurobiol. 36: 249-266.

Garcia JH, Liu KF, Ye ZR, Gutierrez JA, 1997. Incomplete infarct and delayed neuronal death after transient middle cerebral artery occlusion in rats. Stroke 28: 2303-2309.

Gasche Y, Soccal PM, Kanemitsu M, Copin JC, 2006. Matrix metalloproteinases and diseases of the central nervous system with a special emphasis on ischemic brain. Front Biosci. 11: 1289-1301.

Geninatti CS, Bussolati B, Tei L, Grange C, Esposito G, Lanzardo S, Camussi G, Aime S, 2006. Magnetic resonance visualization of tumor angiogenesis by targeting neural cell adhesion molecules with the highly sensitive gadolinium-loaded apoferritin probe. Cancer Res. 66: 9196-9201.

Genove G, DeMarco U, Xu H, Goins WF, Ahrens ET, 2005. A new transgene reporter for in vivo magnetic resonance imaging. Nat. Med. 11: 450-454.

Gerriets T, Stolz E, Walberer M, Muller C, Kluge A, Bachmann A, Fisher M, Kaps M, Bachmann G, 2004. Noninvasive quantification of brain edema and the space-occupying effect in rat stroke models using magnetic resonance imaging. Stroke 35: 566-571.

Gharbawie OA, Auer RN, Whishaw IQ, 2006. Subcortical middle cerebral artery ischemia abolishes the digit flexion and closing used for grasping in rat skilled reaching. Neuroscience 137: 1107-1118.

Gharbawie OA, Whishaw IQ, 2006. Parallel stages of learning and recovery of skilled reaching after motor cortex stroke: "oppositions" organize normal and compensatory movements. Behav. Brain Res. 175: 249-262.

Ghashghaei HT, Lai C, Anton ES, 2007a. Neuronal migration in the adult brain: are we there yet? Nat. Rev. Neurosci. 8: 141-151.

Gheusi G, Cremer H, McLean H, Chazal G, Vincent JD, Lledo PM, 2000. Importance of newly generated neurons in the adult olfactory bulb for odor discrimination. Proc. Natl. Acad. Sci. U. S. A 97: 1823-1828.

Ginsberg MD, 1990. Local metabolic responses to cerebral ischemia. Cerebrovasc. Brain Metab Rev. 2: 58-93.

Girouard H, Iadecola C, 2006. Neurovascular coupling in the normal brain and in hypertension, stroke, and Alzheimer disease. J. Appl. Physiol 100: 328-335.

Gong C, Wang TW, Huang HS, Parent JM, 2007. Reelin regulates neuronal progenitor migration in intact and epileptic hippocampus. J. Neurosci. 27: 1803-1811.

Gottlieb M, Domercq M, Matute C, 2000. Altered expression of the glutamate transporter EAAC1 in neurons and immature oligodendrocytes after transient forebrain ischemia. J. Cereb. Blood Flow Metab 20: 678-687.

Gould E, Beylin A, Tanapat P, Reeves A, Shors TJ, 1999. Learning enhances adult neurogenesis in the hippocampal formation. Nat. Neurosci. 2: 260-265.

Gould E, McEwen BS, Tanapat P, Galea LA, Fuchs E, 1997. Neurogenesis in the dentate gyrus of the adult tree shrew is regulated by psychosocial stress and NMDA receptor activation. J. Neurosci. 17: 2492-2498.

Gregersen R, Lambertsen K, Finsen B, 2000. Microglia and macrophages are the major source of tumor necrosis factor in permanent middle cerebral artery occlusion in mice. J. Cereb. Blood Flow Metab 20: 53-65.

Gritti A, Bonfanti L, Doetsch F, Caille I, varez-Buylla A, Lim DA, Galli R, Verdugo JM, Herrera DG, Vescovi AL, 2002. Multipotent neural stem cells reside into the rostral extension and olfactory bulb of adult rodents. J. Neurosci. 22: 437-445.

Groves AK, Barnett SC, Franklin RJ, Crang AJ, Mayer M, Blakemore WF, Noble M, 1993. Repair of demyelinated lesions by transplantation of purified O-2A progenitor cells. Nature 362: 453-455.

Gu W, Brannstrom T, Wester P, 2000. Cortical neurogenesis in adult rats after reversible photothrombotic stroke. J. Cereb. Blood Flow Metab 20: 1166-1173.

Guzman R, Bliss T, De Los AA, Moseley M, Palmer T, Steinberg G, 2008. Neural progenitor cells transplanted into the uninjured brain undergo targeted migration after stroke onset. J. Neurosci. Res. 86: 873-882.

Guzman R, Uchida N, Bliss TM, He D, Christopherson KK, Stellwagen D, Capela A, Greve J, Malenka RC, Moseley ME, Palmer TD, Steinberg GK, 2007. Long-term monitoring of transplanted human neural stem cells in developmental and pathological contexts with MRI. Proc. Natl. Acad. Sci. U. S. A 104: 10211-10216.

Hagg T, 2005. Molecular regulation of adult CNS neurogenesis: an integrated view. Trends Neurosci. 28: 589-595.

Hakumaki JM, Grohn OH, Tyynela K, Valonen P, Yla-Herttuala S, Kauppinen RA, 2002. Early gene therapy-induced apoptotic response in BT4C gliomas by magnetic resonance relaxation contrast T1 in the rotating frame. Cancer Gene Ther. 9: 338-345.

Hall PA, McKee PH, Menage HD, Dover R, Lane DP, 1993. High levels of p53 protein in UV-irradiated normal human skin. Oncogene 8: 203-207.

Hanisch UK, Kettenmann H, 2007. Microglia: active sensor and versatile effector cells in the normal and pathologic brain. Nat. Neurosci. 10: 1387-1394.

Hardy SA, Maltman DJ, Przyborski SA, 2008. Mesenchymal stem cells as mediators of neural differentiation. Curr. Stem Cell Res. Ther. 3: 43-52.

Hartfuss E, Galli R, Heins N, Gotz M, 2001. Characterization of CNS precursor subtypes and radial glia. Dev. Biol. 229: 15-30.

Hata R, Mies G, Wiessner C, Fritze K, Hesselbarth D, Brinker G, Hossmann KA, 1998. A reproducible model of middle cerebral artery occlusion in mice: hemodynamic, biochemical, and magnetic resonance imaging. J. Cereb. Blood Flow Metab 18: 367-375.

Hauser KF, Houdi AA, Turbek CS, Elde RP, Maxson W, III, 2000. Opioids intrinsically inhibit the genesis of mouse cerebellar granule neuron precursors in vitro: differential impact of mu and delta receptor activation on proliferation and neurite elongation. Eur. J. Neurosci. 12: 1281-1293.

Hauser RA, Sandberg PR, Freeman TB, Stoessl AJ, 2002. Bilateral human fetal striatal transplantation in Huntington's disease. Neurology 58: 1704.

Hawrylak N, Ghosh P, Broadus J, Schlueter C, Greenough WT, Lauterbur PC, 1993. Nuclear magnetic resonance (NMR) imaging of iron oxide-labeled neural transplants. Exp. Neurol. 121: 181-192.

Hayashi J, Takagi Y, Fukuda H, Imazato T, Nishimura M, Fujimoto M, Takahashi J, Hashimoto N, Nozaki K, 2006. Primate embryonic stem cell-derived neuronal progenitors transplanted into ischemic brain. J. Cereb. Blood Flow Metab 26: 906-914.

Hayashi T, Abe K, Suzuki H, Itoyama Y, 1997. Rapid induction of vascular endothelial growth factor gene expression after transient middle cerebral artery occlusion in rats. Stroke 28: 2039-2044.

Hayashi T, Noshita N, Sugawara T, Chan PH, 2003. Temporal profile of angiogenesis and expression of related genes in the brain after ischemia. J. Cereb. Blood Flow Metab 23: 166-180.

Hazell AS, 2007. Excitotoxic mechanisms in stroke: an update of concepts and treatment strategies. Neurochem. Int. 50: 941-953.

Heldmann U, Thored P, Claasen JH, Arvidsson A, Kokaia Z, Lindvall O, 2005. TNF-alpha antibody infusion impairs

survival of stroke-generated neuroblasts in adult rat brain. Exp. Neurol. 196: 204-208.

Hemingway H, Shipley M, Macfarlane P, Marmot M, 2000. Impact of socioeconomic status on coronary mortality in people with symptoms, electrocardiographic abnormalities, both or neither: the original Whitehall study 25 year follow up. J. Epidemiol. Community Health 54: 510-516.

Hening TD, Saborowski O, Golovko D, Boddington S, Bauer JS, Fu Y, Meier R, Pietsch H, Sennino B, McDonald DM, drup-Link HE, 2007. Cell labeling with the positive MR contrast agent Gadofluorine M. Eur. Radiol. 17: 1226-1234.

Hermann P, Kotek J, Kubicek V, Lukes I, 2008. Gadolinium(III) complexes as MRI contrast agents: ligand design and properties of the complexes. Dalton Trans.: 3027-3047.

Herrera DG, Garcia-Verdugo JM, varez-Buylla A, 1999. Adult-derived neural precursors transplanted into multiple regions in the adult brain. Ann. Neurol. 46: 867-877.

Herrera DG, Yague AG, Johnsen-Soriano S, Bosch-Morell F, Collado-Morente L, Muriach M, Romero FJ, Garcia-Verdugo JM, 2003. Selective impairment of hippocampal neurogenesis by chronic alcoholism: protective effects of an antioxidant. Proc. Natl. Acad. Sci. U. S. A 100: 7919-7924.

Hicks AU, MacLellan CL, Chernenko GA, Corbett D, 2008. Long-term assessment of enriched housing and subventricular zone derived cell transplantation after focal ischemia in rats. Brain Res. 1231: 103-112.

Hoehn M, Kustermann E, Blunk J, Wiedermann D, Trapp T, Wecker S, Focking M, Arnold H, Hescheler J, Fleischmann BK, Schwindt W, Buhrle C, 2002. Monitoring of implanted stem cell migration in vivo: a highly resolved in vivo magnetic resonance imaging investigation of experimental stroke in rat. Proc. Natl. Acad. Sci. U. S. A 99: 16267-16272.

Hoehn M, Wiedermann D, Justicia C, Ramos-Cabrer P, Kruttwig K, Farr T, Himmelreich U, 2007. Cell tracking using magnetic resonance imaging. J. Physiol 584: 25-30.

Hou SW, Wang YQ, Xu M, Shen DH, Wang JJ, Huang F, Yu Z, Sun FY, 2008. Functional integration of newly generated neurons into striatum after cerebral ischemia in the adult rat brain. Stroke 39: 2837-2844.

Hsieh J, Aimone JB, Kaspar BK, Kuwabara T, Nakashima K, Gage FH, 2004. IGF-I instructs multipotent adult neural progenitor cells to become oligodendrocytes. J. Cell Biol. 164: 111-122.

Hua R, Doucette R, Walz W, 2008. Doublecortin-expressing cells in the ischemic penumbra of a small-vessel stroke. J. Neurosci. Res. 86: 883-893.

Huang J, Upadhyay UM, Tamargo RJ, 2006. Inflammation in stroke and focal cerebral ischemia. Surg. Neurol. 66: 232-245.

Hunter AJ, Hatcher J, Virley D, Nelson P, Irving E, Hadingham SJ, Parsons AA, 2000. Functional assessments in mice and rats after focal stroke. Neuropharmacology 39: 806-816.

Iatropoulos MJ, Williams GM, 1996. Proliferation markers. Exp. Toxicol. Pathol. 48: 175-181.

Iizuka H, Sakatani K, Young W, 1990. Neural damage in the rat thalamus after cortical infarcts. Stroke 21: 790-794.

Imitola J, Raddassi K, Park KI, Mueller FJ, Nieto M, Teng YD, Frenkel D, Li J, Sidman RL, Walsh CA, Snyder EY, Khoury SJ, 2004. Directed migration of neural stem cells to sites of CNS injury by the stromal cell-derived factor 1alpha/CXC chemokine receptor 4 pathway. Proc. Natl. Acad. Sci. U. S. A 101: 18117-18122.

Iosif RE, Ahlenius H, Ekdahl CT, Darsalia V, Thored P, Jovinge S, Kokaia Z, Lindvall O, 2008. Suppression of stroke-induced progenitor proliferation in adult subventricular zone by tumor necrosis factor receptor 1. J. Cereb. Blood Flow Metab 28: 1574-1587.

Ishibashi S, Sakaguchi M, Kuroiwa T, Yamasaki M, Kanemura Y, Shizuko I, Shimazaki T, Onodera M, Okano H, Mizusawa H, 2004. Human neural stem/progenitor cells, expanded in long-term neurosphere culture, promote functional recovery after focal ischemia in Mongolian gerbils. J. Neurosci. Res. 78: 215-223.

Jander S, Schroeter M, Saleh A, 2007. Imaging inflammation in acute brain ischemia. Stroke 38: 642-645.

Jiang Q, Zhang ZG, Ding GL, Zhang L, Ewing JR, Wang L, Zhang R, Li L, Lu M, Meng H, Arbab AS, Hu J, Li QJ, Pourabdollah Nejad DS, Athiraman H, Chopp M, 2005. Investigation of neural progenitor cell induced angiogenesis after embolic stroke in rat using MRI. Neuroimage. 28: 698-707.

Jiang W, Gu W, Brannstrom T, Rosqvist R, Wester P, 2001. Cortical neurogenesis in adult rats after transient middle cerebral artery occlusion. Stroke 32: 1201-1207.

Jiao J, Chen DF, 2008. Induction of neurogenesis in nonconventional neurogenic regions of the adult central nervous system by niche astrocyte-produced signals. Stem Cells 26: 1221-1230.

Jiao JW, Feldheim DA, Chen DF, 2008. Ephrins as negative regulators of adult neurogenesis in diverse regions of the central nervous system. Proc. Natl. Acad. Sci. U. S. A 105: 8778-8783.

Jin K, Mao XO, Del Rio GG, Jin L, Greenberg DA, 2005. Heparin-binding epidermal growth factor-like growth factor stimulates cell proliferation in cerebral cortical cultures through phosphatidylinositol 3'-kinase and mitogen-activated protein kinase. J. Neurosci. Res. 81: 497-505.

Jin K, Minami M, Lan JQ, Mao XO, Batteur S, Simon RP, Greenberg DA, 2001. Neurogenesis in dentate subgranular zone and rostral subventricular zone after focal cerebral ischemia in the rat. Proc. Natl. Acad. Sci. U. S. A 98: 4710-4715.

Jin K, Sun Y, Xie L, Peel A, Mao XO, Batteur S, Greenberg DA, 2003. Directed migration of neuronal precursors into the ischemic cerebral cortex and striatum. Mol. Cell Neurosci. 24: 171-189.

Jin K, Zhu Y, Sun Y, Mao XO, Xie L, Greenberg DA, 2002. Vascular endothelial growth factor (VEGF) stimulates neurogenesis in vitro and in vivo. Proc. Natl. Acad. Sci. U. S. A 99: 11946-11950.

Johnston SC, Mendis S, Mathers CD, 2009. Global variation in stroke burden and mortality: estimates from monitoring, surveillance, and modelling. Lancet Neurol. 8: 345-354.

Josephson L, Tung CH, Moore A, Weissleder R, 1999. High-efficiency intracellular magnetic labeling with novel superparamagnetic-Tat peptide conjugates. Bioconjug. Chem. 10: 186-191.

Justicia C, Ramos-Cabrer P, Hoehn M, 2008. MRI detection of secondary damage after stroke: chronic iron accumulation in the thalamus of the rat brain. Stroke 39: 1541-1547.

Kabalka G, Buonocore E, Hubner K, Moss T, Norley N, Huang L, 1987. Gadolinium-labeled liposomes: targeted MR contrast agents for the liver and spleen. Radiology 163: 255-258.

Kaji K, Norrby K, Paca A, Mileikovsky M, Mohseni P, Woltjen K, 2009. Virus-free induction of pluripotency and subsequent excision of reprogramming factors. Nature 458: 771-775.

Kalluri HS, Vemuganti R, Dempsey RJ, 2007. Mechanism of insulin-like growth factor I-mediated proliferation of adult neural progenitor cells: role of Akt. Eur. J. Neurosci. 25: 1041-1048.

Kamada H, Yu F, Nito C, Chan PH, 2007. Influence of hyperglycemia on oxidative stress and matrix metalloproteinase-9 activation after focal cerebral ischemia/reperfusion in rats: relation to blood-brain barrier dysfunction. Stroke 38: 1044-1049.

Kaplan MS, Hinds JW, 1977. Neurogenesis in the adult rat: electron microscopic analysis of light radioautographs. Science 197: 1092-1094.

Kappeler C, Saillour Y, Baudoin JP, Tuy FP, Alvarez C, Houbron C, Gaspar P, Hamard G, Chelly J, Metin C, Francis F, 2006. Branching and nucleokinesis defects in migrating interneurons derived from doublecortin knockout mice. Hum. Mol. Genet. 15: 1387-1400.

Karadottir R, Hamilton NB, Bakiri Y, Attwell D, 2008. Spiking and nonspiking classes of oligodendrocyte precursor glia in CNS white matter. Nat. Neurosci. 11: 450-456.

Karagiannis ED, Popel AS, 2006. Distinct modes of collagen type I proteolysis by matrix metalloproteinase (MMP) 2 and membrane type I MMP during the migration of a tip endothelial cell: insights from a computational model. J. Theor. Biol. 238: 124-145.

Keene CD, Sonnen JA, Swanson PD, Kopyov O, Leverenz JB, Bird TD, Montine TJ, 2007. Neural transplantation in Huntington disease: long-term grafts in two patients. Neurology 68: 2093-2098.

Keller G, 2005. Embryonic stem cell differentiation: emergence of a new era in biology and medicine. Genes Dev. 19: 1129-1155.

Kelly S, Bliss TM, Shah AK, Sun GH, Ma M, Foo WC, Masel J, Yenari MA, Weissman IL, Uchida N, Palmer T, Steinberg GK, 2004. Transplanted human fetal neural stem cells survive, migrate, and differentiate in ischemic rat cerebral cortex. Proc. Natl. Acad. Sci. U. S. A 101: 11839-11844.

Kessaris N, Fogarty M, Iannarelli P, Grist M, Wegner M, Richardson WD, 2006. Competing waves of oligodendrocytes in the forebrain and postnatal elimination of an embryonic lineage. Nat. Neurosci. 9: 173-179.

Kim DE, Schellingerhout D, Ishii K, Shah K, Weissleder R, 2004. Imaging of stem cell recruitment to ischemic infarcts in a murine model. Stroke 35: 952-957.

Kirschenbaum B, Doetsch F, Lois C, varez-Buylla A, 1999. Adult subventricular zone neuronal precursors continue to proliferate and migrate in the absence of the olfactory bulb. J. Neurosci. 19: 2171-2180.

Kitagawa H, Sasaki C, Sakai K, Mori A, Mitsumoto Y, Mori T, Fukuchi Y, Setoguchi Y, Abe K, 1999. Adenovirus-mediated gene transfer of glial cell line-derived neurotrophic factor prevents ischemic brain injury after transient middle cerebral artery occlusion in rats. J. Cereb. Blood Flow Metab 19: 1336-1344.

Kitano H, Kirsch JR, Hurn PD, Murphy SJ, 2007. Inhalational anesthetics as neuroprotectants or chemical preconditioning agents in ischemic brain. J Cereb. Blood Flow Metab 27: 1108-1128.

Kleinschnitz C, Bendszus M, Frank M, Solymosi L, Toyka KV, Stoll G, 2003. In vivo monitoring of macrophage infiltration in experimental ischemic brain lesions by magnetic resonance imaging. J. Cereb. Blood Flow Metab 23: 1356-1361.

Kobayashi T, Ahlenius H, Thored P, Kobayashi R, Kokaia Z, Lindvall O, 2006. Intracerebral infusion of glial cell line-derived neurotrophic factor promotes striatal neurogenesis after stroke in adult rats. Stroke 37: 2361-2367.

Koistinaho J, Miettinen S, Keinanen R, Vartiainen N, Roivainen R, Laitinen JT, 1996. Long-term induction of haem oxygenase-1 (HSP-32) in astrocytes and microglia following transient focal brain ischaemia in the rat. Eur. J. Neurosci. 8: 2265-2272.

Koizumi J YYNTOG. Experimental studies of ischemic brain edema, I: a new experimental model of cerebral embolism in rats in which recirculation can be introduced in the ischemic area. Jpn J Stroke 8, 1-8. 1986.
Ref Type: Generic

Koizumi H, Higginbotham H, Poon T, Tanaka T, Brinkman BC, Gleeson JG, 2006. Doublecortin maintains bipolar shape and nuclear translocation during migration in the adult forebrain. Nat. Neurosci. 9: 779-786.

Kokaia Z, Lindvall O, 2003. Neurogenesis after ischaemic brain insults. Curr. Opin. Neurobiol. 13: 127-132.

Kokaia Z, Thored P, Arvidsson A, Lindvall O, 2006. Regulation of stroke-induced neurogenesis in adult brain--recent scientific progress. Cereb. Cortex 16 Suppl 1: i162-i167.

Kokaia Z, Zhao Q, Kokaia M, Elmer E, Metsis M, Smith ML, Siesjo BK, Lindvall O, 1995. Regulation of brain-derived neurotrophic factor gene expression after transient middle cerebral artery occlusion with and without brain damage. Exp. Neurol. 136: 73-88.

Komitova M, Mattsson B, Johansson BB, Eriksson PS, 2005. Enriched environment increases neural stem/progenitor cell proliferation and neurogenesis in the subventricular zone of stroke-lesioned adult rats. Stroke 36: 1278-1282.

Kondo T, Raff M, 2000. Oligodendrocyte precursor cells reprogrammed to become multipotential CNS stem cells. Science 289: 1754-1757.

Kondo Y, Asanuma M, Nishibayashi S, Iwata E, Ogawa N, 1997. Late-onset lipid peroxidation and neuronal cell death following transient forebrain ischemia in rat brain. Brain Res. 772: 37-44.

Kondziolka D, Steinberg GK, Wechsler L, Meltzer CC, Elder E, Gebel J, Decesare S, Jovin T, Zafonte R, Lebowitz J, Flickinger JC, Tong D, Marks MP, Jamieson C, Luu D, Bell-Stephens T, Teraoka J, 2005. Neurotransplantation for patients with subcortical motor stroke: a phase 2 randomized trial. J. Neurosurg. 103: 38-45.

Kondziolka D, Wechsler L, Gebel J, Decesare S, Elder E, Meltzer CC, 2003. Neuronal transplantation for motor stroke: from the laboratory to the clinic. Phys. Med. Rehabil. Clin. N. Am. 14: S153-60, xi.

Kondziolka D, Wechsler L, Goldstein S, Meltzer C, Thulborn KR, Gebel J, Jannetta P, Decesare S, Elder EM, McGrogan M, Reitman MA, Bynum L, 2000. Transplantation of cultured human neuronal cells for patients with stroke. Neurology 55: 565-569.

Kondziolka D, Wechsler L, Tyler-Kabara E, Achim C, 2002. The role of cell therapy for stroke. Neurosurg. Focus. 13: e1.

Korde AS, Pettigrew LC, Craddock SD, Pocernich CB, Waldmeier PC, Maragos WF, 2007. Protective effects of NIM811 in transient focal cerebral ischemia suggest involvement of the mitochondrial permeability transition. J. Neurotrauma 24: 895-908.

Kraitchman DL, Bulte JW, 2008. Imaging of stem cells using MRI. Basic Res. Cardiol. 103: 105-113.

Kresse M, Wagner S, Pfefferer D, Lawaczeck R, Elste V, Semmler W, 1998. Targeting of ultrasmall superparamagnetic iron oxide (USPIO) particles to tumor cells in vivo by using transferrin receptor pathways. Magn Reson. Med. 40: 236-242.

Kuhn HG, Winkler J, Kempermann G, Thal LJ, Gage FH, 1997. Epidermal growth factor and fibroblast growth factor-2 have different effects on neural progenitors in the adult rat brain. J. Neurosci. 17: 5820-5829.

Kukley M, Capetillo-Zarate E, Dietrich D, 2007. Vesicular glutamate release from axons in white matter. Nat. Neurosci. 10: 311-320.

Kurozumi K, Nakamura K, Tamiya T, Kawano Y, Ishii K, Kobune M, Hirai S, Uchida H, Sasaki K, Ito Y, Kato K, Honmou O, Houkin K, Date I, Hamada H, 2005. Mesenchymal stem cells that produce neurotrophic factors reduce ischemic damage in the rat middle cerebral artery occlusion model. Mol. Ther. 11: 96-104.

Kurozumi K, Nakamura K, Tamiya T, Kawano Y, Kobune M, Hirai S, Uchida H, Sasaki K, Ito Y, Kato K, Honmou O, Houkin K, Date I, Hamada H, 2004. BDNF gene-modified mesenchymal stem cells promote functional recovery and reduce infarct size in the rat middle cerebral artery occlusion model. Mol. Ther. 9: 189-197.

Kurz T, Terman A, Brunk UT, 2007. Autophagy, ageing and apoptosis: the role of oxidative stress and lysosomal iron. Arch. Biochem. Biophys. 462: 220-230.

Ladeby R, Wirenfeldt M, Dalmau I, Gregersen R, Garcia-Ovejero D, Babcock A, Owens T, Finsen B, 2005a. Proliferating resident microglia express the stem cell antigen CD34 in response to acute neural injury. Glia 50: 121-131.

Ladeby R, Wirenfeldt M, Garcia-Ovejero D, Fenger C, ssing-Olesen L, Dalmau I, Finsen B, 2005b. Microglial cell population dynamics in the injured adult central nervous system. Brain Res. Brain Res. Rev. 48: 196-206.

Lagace DC, Whitman MC, Noonan MA, Ables JL, DeCarolis NA, Arguello AA, Donovan MH, Fischer SJ, Farnbauch LA, Beech RD, DiLeone RJ, Greer CA, Mandyam CD, Eisch AJ, 2007. Dynamic contribution of nestin-expressing stem cells to adult neurogenesis. J. Neurosci. 27: 12623-12629.

Lai AY, Todd KG, 2006. Microglia in cerebral ischemia: molecular actions and interactions. Can. J. Physiol Pharmacol. 84: 49-59.

Lai B, Mao XO, Xie L, Jin K, Greenberg DA, 2008. Electrophysiological neurodifferentiation of subventricular zone-

derived precursor cells following stroke. Neurosci. Lett. 442: 305-308.

Lalancette-Hebert M, Gowing G, Simard A, Weng YC, Kriz J, 2007. Selective ablation of proliferating microglial cells exacerbates ischemic injury in the brain. J. Neurosci. 27: 2596-2605.

Lappalainen RS, Narkilahti S, Huhtala T, Liimatainen T, Suuronen T, Narvanen A, Suuronen R, Hovatta O, Jolkkonen J, 2008. The SPECT imaging shows the accumulation of neural progenitor cells into internal organs after systemic administration in middle cerebral artery occlusion rats. Neurosci. Lett. 440: 246-250.

Lattuada L, Demattio S, Vincenzi V, Cabella C, Visigalli M, Aime S, Crich SG, Gianolio E, 2006. Magnetic resonance imaging of tumor cells by targeting the amino acid transport system. Bioorg. Med. Chem. Lett. 16: 4111-4114.

Lazarini F, Tham TN, Casanova P, renzana-Seisdedos F, Dubois-Dalcq M, 2003. Role of the alpha-chemokine stromal cell-derived factor (SDF-1) in the developing and mature central nervous system. Glia 42: 139-148.

Lee HJ, Kim KS, Park IH, Kim SU, 2007. Human neural stem cells over-expressing VEGF provide neuroprotection, angiogenesis and functional recovery in mouse stroke model. PLoS. ONE. 2: e156.

Lee J, Seroogy KB, Mattson MP, 2002. Dietary restriction enhances neurotrophin expression and neurogenesis in the hippocampus of adult mice. J. Neurochem. 80: 539-547.

Lee SR, Kim HY, Rogowska J, Zhao BQ, Bhide P, Parent JM, Lo EH, 2006. Involvement of matrix metalloproteinase in neuroblast cell migration from the subventricular zone after stroke. J. Neurosci. 26: 3491-3495.

Lee ST, Chu K, Jung KH, Kim SJ, Kim DH, Kang KM, Hong NH, Kim JH, Ban JJ, Park HK, Kim SU, Park CG, Lee SK, Kim M, Roh JK, 2008. Anti-inflammatory mechanism of intravascular neural stem cell transplantation in haemorrhagic stroke. Brain 131: 616-629.

Leker RR, Soldner F, Velasco I, Gavin DK, ndroutsellis-Theotokis A, McKay RD, 2007. Long-lasting regeneration after ischemia in the cerebral cortex. Stroke 38: 153-161.

Lepore AC, Walczak P, Rao MS, Fischer I, Bulte JW, 2006. MR imaging of lineage-restricted neural precursors following transplantation into the adult spinal cord. Exp. Neurol. 201: 49-59.

Levine JM, Reynolds R, 1999. Activation and proliferation of endogenous oligodendrocyte precursor cells during ethidium bromide-induced demyelination. Exp. Neurol. 160: 333-347.

Lewin M, Carlesso N, Tung CH, Tang XW, Cory D, Scadden DT, Weissleder R, 2000. Tat peptide-derivatized magnetic nanoparticles allow in vivo tracking and recovery of progenitor cells. Nat. Biotechnol. 18: 410-414.

Li L, Schatteman GC, Oppenheim RW, Lei M, Bowen-Pope DF, Houenou LJ, 1996. Altered development of spinal cord in the mouse mutant (Patch) lacking the PDGF receptor alpha-subunit gene. Brain Res. Dev. Brain Res. 96: 204-209.

Li Y, Chen J, Chen XG, Wang L, Gautam SC, Xu YX, Katakowski M, Zhang LJ, Lu M, Janakiraman N, Chopp M, 2002. Human marrow stromal cell therapy for stroke in rat: neurotrophins and functional recovery. Neurology 59: 514-523.

Li Y, Chen J, Chopp M, 2001a. Adult bone marrow transplantation after stroke in adult rats. Cell Transplant. 10: 31-40.

Li Y, Chen J, Wang L, Lu M, Chopp M, 2001b. Treatment of stroke in rat with intracarotid administration of marrow stromal cells. Neurology 56: 1666-1672.

Li Y, Chen J, Zhang CL, Wang L, Lu D, Katakowski M, Gao Q, Shen LH, Zhang J, Lu M, Chopp M, 2005. Gliosis and brain remodeling after treatment of stroke in rats with marrow stromal cells. Glia 49: 407-417.

Li Y, Chopp M, 2009. Marrow stromal cell transplantation in stroke and traumatic brain injury. Neurosci. Lett. 456: 120-123.

Li Y, Chopp M, 1999. Temporal profile of nestin expression after focal cerebral ischemia in adult rat. Brain Res. 838: 1-10.

Li Y, Chopp M, Chen J, Wang L, Gautam SC, Xu YX, Zhang Z, 2000. Intrastriatal transplantation of bone marrow nonhematopoietic cells improves functional recovery after stroke in adult mice. J. Cereb. Blood Flow Metab 20: 1311-1319.

Lichtenwalner RJ, Parent JM, 2006. Adult neurogenesis and the ischemic forebrain. J. Cereb. Blood Flow Metab 26: 1-20.

Lim DA, Fishell GJ, varez-Buylla A, 1997. Postnatal mouse subventricular zone neuronal precursors can migrate and differentiate within multiple levels of the developing neuraxis. Proc. Natl. Acad. Sci. U. S. A 94: 14832-14836.

Lim DA, Huang YC, varez-Buylla A, 2007. The adult neural stem cell niche: lessons for future neural cell replacement strategies. Neurosurg. Clin. N. Am. 18: 81-92, ix.

Lim DA, Tramontin AD, Trevejo JM, Herrera DG, Garcia-Verdugo JM, varez-Buylla A, 2000. Noggin antagonizes BMP signaling to create a niche for adult neurogenesis. Neuron 28: 713-726.

Lin RC, Matesic DF, Marvin M, McKay RD, Brustle O, 1995. Re-expression of the intermediate filament nestin in reactive astrocytes. Neurobiol. Dis. 2: 79-85.

Lindqvist A, Mohapel P, Bouter B, Frielingsdorf H, Pizzo D, Brundin P, Erlanson-Albertsson C, 2006. High-fat diet impairs hippocampal neurogenesis in male rats. Eur. J. Neurol. 13: 1385-1388.

Lindsey BW, Tropepe V, 2006. A comparative framework for understanding the biological principles of adult neurogenesis. Prog. Neurobiol. 80: 281-307.

Lindvall O, Kokaia Z, 2004. Recovery and rehabilitation in stroke: stem cells. Stroke 35: 2691-2694.

Lindvall O, Kokaia Z, 2006. Stem cells for the treatment of neurological disorders. Nature 441: 1094-1096.

Liour SS, Yu RK, 2003. Differentiation of radial glia-like cells from embryonic stem cells. Glia 42: 109-117.

Liu XS, Chopp M, Santra M, Hozeska-Solgot A, Zhang RL, Wang L, Teng H, Lu M, Zhang ZG, 2008. Functional response to SDF1 alpha through over-expression of CXCR4 on adult subventricular zone progenitor cells. Brain Res. 1226: 18-26.

Liu XS, Zhang ZG, Zhang RL, Gregg S, Morris DC, Wang Y, Chopp M, 2007a. Stroke induces gene profile changes associated with neurogenesis and angiogenesis in adult subventricular zone progenitor cells. J. Cereb. Blood Flow Metab 27: 564-574.

Liu Z, Fan Y, Won SJ, Neumann M, Hu D, Zhou L, Weinstein PR, Liu J, 2007b. Chronic treatment with minocycline preserves adult new neurons and reduces functional impairment after focal cerebral ischemia. Stroke 38: 146-152.

Lledo PM, Alonso M, Grubb MS, 2006a. Adult neurogenesis and functional plasticity in neuronal circuits. Nat. Rev. Neurosci. 7: 179-193.

Lledo PM, Merkle FT, varez-Buylla A, 2008. Origin and function of olfactory bulb interneuron diversity. Trends Neurosci. 31: 392-400.

Lo EH, 2008. A new penumbra: transitioning from injury into repair after stroke. Nat. Med. 14: 497-500.

Lo EH, Moskowitz MA, Jacobs TP, 2005. Exciting, radical, suicidal: how brain cells die after stroke. Stroke 36: 189-192.

Lois C, Garcia-Verdugo JM, varez-Buylla A, 1996. Chain migration of neuronal precursors. Science 271: 978-981.

Lois C, varez-Buylla A, 1993. Proliferating subventricular zone cells in the adult mammalian forebrain can differentiate into neurons and glia. Proc. Natl. Acad. Sci. U. S. A 90: 2074-2077.

Lois C, varez-Buylla A, 1994. Long-distance neuronal migration in the adult mammalian brain. Science 264: 1145-1148.

Lu D, Sanberg PR, Mahmood A, Li Y, Wang L, Sanchez-Ramos J, Chopp M, 2002. Intravenous administration of human umbilical cord blood reduces neurological deficit in the rat after traumatic brain injury. Cell Transplant. 11: 275-281.

Luengo-Fernandez R, Gray AM, Rothwell PM, 2009. Effect of urgent treatment for transient ischaemic attack and minor stroke on disability and hospital costs (EXPRESS study): a prospective population-based sequential comparison. Lancet Neurol. 8: 235-243.

Lythgoe MF, Sibson NR, Harris NG, 2003. Neuroimaging of animal models of brain disease. Br. Med. Bull. 65: 235-257.

Ma M, Ma Y, Yi X, Guo R, Zhu W, Fan X, Xu G, Frey WH, Liu X, 2008. Intranasal delivery of transforming growth factor-beta1 in mice after stroke reduces infarct volume and increases neurogenesis in the subventricular zone. BMC. Neurosci. 9: 117.

Mabuchi T, Kitagawa K, Ohtsuki T, Kuwabara K, Yagita Y, Yanagihara T, Hori M, Matsumoto M, 2000. Contribution of microglia/macrophages to expansion of infarction and response of oligodendrocytes after focal cerebral ischemia in rats. Stroke 31: 1735-1743.

Magavi SS, Leavitt BR, Macklis JD, 2000. Induction of neurogenesis in the neocortex of adult mice. Nature 405: 951-955.

Magnitsky S, Watson DJ, Walton RM, Pickup S, Bulte JW, Wolfe JH, Poptani H, 2005. In vivo and ex vivo MRI detection of localized and disseminated neural stem cell grafts in the mouse brain. Neuroimage. 26: 744-754.

Malatesta P, Hack MA, Hartfuss E, Kettenmann H, Klinkert W, Kirchhoff F, Gotz M, 2003. Neuronal or glial progeny: regional differences in radial glia fate. Neuron 37: 751-764.

Malberg JE, Eisch AJ, Nestler EJ, Duman RS, 2000. Chronic antidepressant treatment increases neurogenesis in adult rat hippocampus. J. Neurosci. 20: 9104-9110.

Mandai K, Matsumoto M, Kitagawa K, Matsushita K, Ohtsuki T, Mabuchi T, Colman DR, Kamada T, Yanagihara T, 1997. Ischemic damage and subsequent proliferation of oligodendrocytes in focal cerebral ischemia. Neuroscience 77: 849-861.

Manganas LN, Zhang X, Li Y, Hazel RD, Smith SD, Wagshul ME, Henn F, Benveniste H, Djuric PM, Enikolopov G, Maletic-Savatic M, 2007. Magnetic resonance spectroscopy identifies neural progenitor cells in the live human brain. Science 318: 980-985.

Marchal G, Beaudouin V, Rioux P, de lS, V, Le DF, Viader F, Derlon JM, Baron JC, 1996. Prolonged persistence of substantial volumes of potentially viable brain tissue after stroke: a correlative PET-CT study with voxel-based data analysis. Stroke 27: 599-606.

Marmot MG, Smith GD, Stansfeld S, Patel C, North F, Head J, White I, Brunner E, Feeney A, 1991. Health inequalities among British civil servants: the Whitehall II study. Lancet 337: 1387-1393.

Martens DJ, Seaberg RM, van der KD, 2002. In vivo infusions of exogenous growth factors into the fourth ventricle of the adult mouse brain increase the proliferation of neural progenitors around the fourth ventricle and the central canal of the spinal cord. Eur. J. Neurosci. 16: 1045-1057.

Martino G, Pluchino S, 2006. The therapeutic potential of neural stem cells. Nat. Rev. Neurosci. 7: 395-406.

Maurer MH, Thomas C, Burgers HF, Kuschinsky W, 2008. Transplantation of adult neural progenitor cells transfected with vascular endothelial growth factor rescues grafted cells in the rat brain. Int. J. Biol. Sci. 4: 1-7.

Mayzel-Oreg O, Omae T, Kazemi M, Li F, Fisher M, Cohen Y, Sotak CH, 2004. Microsphere-induced embolic stroke: an MRI study. Magn Reson. Med. 51: 1232-1238.

McBride JL, Behrstock SP, Chen EY, Jakel RJ, Siegel I, Svendsen CN, Kordower JH, 2004. Human neural stem cell transplants improve motor function in a rat model of Huntington's disease. J. Comp Neurol. 475: 211-219.

McCurdy RD, Feron F, McGrath JJ, kay-Sim A, 2005. Regulation of adult olfactory neurogenesis by insulin-like growth factor-I. Eur. J. Neurosci. 22: 1581-1588.

McGrath KE, Koniski AD, Maltby KM, McGann JK, Palis J, 1999. Embryonic expression and function of the chemokine SDF-1 and its receptor, CXCR4. Dev. Biol. 213: 442-456.

McTigue DM, Tripathi RB, 2008. The life, death, and replacement of oligodendrocytes in the adult CNS. J. Neurochem. 107: 1-19.

Mergenthaler P, Dirnagl U, Meisel A, 2004. Pathophysiology of stroke: lessons from animal models. Metab Brain Dis. 19: 151-167.

Merkle FT, Tramontin AD, Garcia-Verdugo JM, varez-Buylla A, 2004. Radial glia give rise to adult neural stem cells in the subventricular zone. Proc. Natl. Acad. Sci. U. S. A 101: 17528-17532.

Merkle FT, varez-Buylla A, 2006. Neural stem cells in mammalian development. Curr. Opin. Cell Biol. 18: 704-709.

Milosevic A, Noctor SC, Martinez-Cerdeno V, Kriegstein AR, Goldman JE, 2008. Progenitors from the postnatal forebrain subventricular zone differentiate into cerebellar-like interneurons and cerebellar-specific astrocytes upon transplantation. Mol. Cell Neurosci. 39: 324-334.

Ming GL, Song H, 2005. Adult neurogenesis in the mammalian central nervous system. Annu. Rev. Neurosci. 28: 223-250.

Minger SL, Ekonomou A, Carta EM, Chinoy A, Perry RH, Ballard CG, 2007. Endogenous neurogenesis in the human brain following cerebral infarction. Regen. Med. 2: 69-74.

Mirescu C, Peters JD, Gould E, 2004. Early life experience alters response of adult neurogenesis to stress. Nat. Neurosci. 7: 841-846.

Modo M, Beech JS, Meade TJ, Williams SC, Price J, 2008. A chronic 1 year assessment of MRI contrast agent-labelled neural stem cell transplants in stroke. Neuroimage.

Modo M, Cash D, Mellodew K, Williams SC, Fraser SE, Meade TJ, Price J, Hodges H, 2002a. Tracking transplanted stem cell migration using bifunctional, contrast agent-enhanced, magnetic resonance imaging. Neuroimage. 17: 803-811.

Modo M, Hoehn M, Bulte JW, 2005. Cellular MR imaging. Mol. Imaging 4: 143-164.

Modo M, Mellodew K, Cash D, Fraser SE, Meade TJ, Price J, Williams SC, 2004. Mapping transplanted stem cell migration after a stroke: a serial, in vivo magnetic resonance imaging study. Neuroimage. 21: 311-317.

Modo M, Rezaie P, Heuschling P, Patel S, Male DK, Hodges H, 2002b. Transplantation of neural stem cells in a rat model of stroke: assessment of short-term graft survival and acute host immunological response. Brain Res. 958: 70-82.

Modo M, Stroemer RP, Tang E, Patel S, Hodges H, 2002c. Effects of implantation site of stem cell grafts on behavioral recovery from stroke damage. Stroke 33: 2270-2278.

Mokdad AH, Bales VS, Greenlund KJ, Mensah GA, 2003. Public health surveillance for disease prevention: lessons from the behavioral risk factor surveillance system. Ethn. Dis. 13: S19-S23.

Monje ML, Toda H, Palmer TD, 2003. Inflammatory blockade restores adult hippocampal neurogenesis. Science 302: 1760-1765.

Moore A, Basilion JP, Chiocca EA, Weissleder R, 1998. Measuring transferrin receptor gene expression by NMR imaging. Biochim. Biophys. Acta 1402: 239-249.

Moos T, 2002. Brain iron homeostasis. Dan. Med. Bull. 49: 279-301.

Morgan SC, Taylor DL, Pocock JM, 2004. Microglia release activators of neuronal proliferation mediated by activation of mitogen-activated protein kinase, phosphatidylinositol-3-kinase/Akt and delta-Notch signalling cascades. J. Neurochem. 90: 89-101.

Morshead CM, Reynolds BA, Craig CG, McBurney MW, Staines WA, Morassutti D, Weiss S, van der KD, 1994b. Neural stem cells in the adult mammalian forebrain: a relatively quiescent subpopulation of subependymal cells. Neuron 13: 1071-1082.

Morshead CM, Reynolds BA, Craig CG, McBurney MW, Staines WA, Morassutti D, Weiss S, van der KD, 1994a. Neural stem cells in the adult mammalian forebrain: a relatively quiescent subpopulation of subependymal cells. Neuron 13: 1071-1082.

Nabika T, Cui Z, Masuda J, 2004. The stroke-prone spontaneously hypertensive rat: how good is it as a model for cerebrovascular diseases? Cell Mol. Neurobiol. 24: 639-646.

Nakamura T, Xi G, Hua Y, Hoff JT, Keep RF, 2003. Nestin expression after experimental intracerebral hemorrhage. Brain Res. 981: 108-117.

Nakanishi M, Niidome T, Matsuda S, Akaike A, Kihara T, Sugimoto H, 2007. Microglia-derived interleukin-6 and leukaemia inhibitory factor promote astrocytic differentiation of neural stem/progenitor cells. Eur. J. Neurosci. 25: 649-658.

Napoli I, Neumann H, 2009. Microglial clearance function in health and disease. Neuroscience 158: 1030-1038.

National Audit Office. Department of Health - Reducing brain damage: faster access to better stroke care. 2005. London, National Audit Office.
Ref Type: Generic

Nawashiro H, Brenner M, Fukui S, Shima K, Hallenbeck JM, 2000. High susceptibility to cerebral ischemia in GFAP-null mice. J. Cereb. Blood Flow Metab 20: 1040-1044.

Nawashiro H, Martin D, Hallenbeck JM, 1997. Neuroprotective effects of TNF binding protein in focal cerebral ischemia. Brain Res. 778: 265-271.

Naylor AS, Persson AI, Eriksson PS, Jonsdottir IH, Thorlin T, 2005a. Extended voluntary running inhibits exercise-induced adult hippocampal progenitor proliferation in the spontaneously hypertensive rat. J. Neurophysiol. 93: 2406-2414.

Naylor M, Bowen KK, Sailor KA, Dempsey RJ, Vemuganti R, 2005b. Preconditioning-induced ischemic tolerance stimulates growth factor expression and neurogenesis in adult rat hippocampus. Neurochem. Int. 47: 565-572.

Neumann-Haefelin T, Kastrup A, de CA, Yenari MA, Ringer T, Sun GH, Moseley ME, 2000. Serial MRI after transient focal cerebral ischemia in rats: dynamics of tissue injury, blood-brain barrier damage, and edema formation. Stroke 31: 1965-1972.

Ni HT, Hu S, Sheng WS, Olson JM, Cheeran MC, Chan AS, Lokensgard JR, Peterson PK, 2004. High-level expression of functional chemokine receptor CXCR4 on human neural precursor cells. Brain Res. Dev. Brain Res. 152: 159-169.

Ninomiya M, Yamashita T, Araki N, Okano H, Sawamoto K, 2006. Enhanced neurogenesis in the ischemic striatum following EGF-induced expansion of transit-amplifying cells in the subventricular zone. Neurosci. Lett. 403: 63-67.

Nishiyama A, 1998. Glial progenitor cells in normal and pathological states. Keio J. Med. 47: 205-208.

Nishiyama A, 2007. Polydendrocytes: NG2 cells with many roles in development and repair of the CNS. Neuroscientist. 13: 62-76.

Nishiyama A, Komitova M, Suzuki R, Zhu X, 2009. Polydendrocytes (NG2 cells): multifunctional cells with lineage plasticity. Nat. Rev. Neurosci. 10: 9-22.

Nishiyama A, Yu M, Drazba JA, Tuohy VK, 1997. Normal and reactive NG2+ glial cells are distinct from resting and activated microglia. J. Neurosci. Res. 48: 299-312.

Noble M, Murray K, Stroobant P, Waterfield MD, Riddle P, 1988. Platelet-derived growth factor promotes division and motility and inhibits premature differentiation of the oligodendrocyte/type-2 astrocyte progenitor cell. Nature 333: 560-562.

Noctor SC, Flint AC, Weissman TA, Wong WS, Clinton BK, Kriegstein AR, 2002b. Dividing precursor cells of the embryonic cortical ventricular zone have morphological and molecular characteristics of radial glia. J. Neurosci. 22: 3161-

3173.

Noctor SC, Flint AC, Weissman TA, Wong WS, Clinton BK, Kriegstein AR, 2002a. Dividing precursor cells of the embryonic cortical ventricular zone have morphological and molecular characteristics of radial glia. J. Neurosci. 22: 3161-3173.

Noctor SC, Martinez-Cerdeno V, Ivic L, Kriegstein AR, 2004. Cortical neurons arise in symmetric and asymmetric division zones and migrate through specific phases. Nat. Neurosci. 7: 136-144.

Ocbina PJ, Dizon ML, Shin L, Szele FG, 2006. Doublecortin is necessary for the migration of adult subventricular zone cells from neurospheres. Mol. Cell Neurosci. 33: 126-135.

Ogawa D, Okada Y, Nakamura M, Kanemura Y, Okano HJ, Matsuzaki Y, Shimazaki T, Ito M, Ikeda E, Tamiya T, Nagao S, Okano H, 2009. Evaluation of human fetal neural stem/progenitor cells as a source for cell replacement therapy for neurological disorders: properties and tumorigenicity after long-term in vitro maintenance. J. Neurosci. Res. 87: 307-317.

Ohab JJ, Fleming S, Blesch A, Carmichael ST, 2006. A neurovascular niche for neurogenesis after stroke. J. Neurosci. 26: 13007-13016.

Ohta K, Iwai M, Sato K, Omori N, Nagano I, Shoji M, Abe K, 2003. Dissociative increase of oligodendrocyte progenitor cells between young and aged rats after transient cerebral ischemia. Acta Neurochir. Suppl 86: 187-189.

Otaegi G, Yusta-Boyo MJ, Vergano-Vera E, Mendez-Gomez HR, Carrera AC, Abad JL, Gonzalez M, de la Rosa EJ, Vicario-Abejon C, De PF, 2006. Modulation of the PI 3-kinase-Akt signalling pathway by IGF-I and PTEN regulates the differentiation of neural stem/precursor cells. J. Cell Sci. 119: 2739-2748.

Ourednik J, Ourednik V, Lynch WP, Schachner M, Snyder EY, 2002. Neural stem cells display an inherent mechanism for rescuing dysfunctional neurons. Nat. Biotechnol. 20: 1103-1110.

Ourednik V, Ourednik J, Park KI, Teng YD, Aboody KA, Auguste KI, Taylor RM, Tate BA, Snyder EY, 2000. Neural stem cells are uniquely suited for cell replacement and gene therapy in the CNS. Novartis. Found. Symp. 231: 242-262.

Ozerdem U, Grako KA, hlin-Huppe K, Monosov E, Stallcup WB, 2001. NG2 proteoglycan is expressed exclusively by mural cells during vascular morphogenesis. Dev. Dyn. 222: 218-227.

Palmer C, Menzies SL, Roberts RL, Pavlick G, Connor JR, 1999a. Changes in iron histochemistry after hypoxic-ischemic brain injury in the neonatal rat. J. Neurosci. Res. 56: 60-71.

Palmer TD, Markakis EA, Willhoite AR, Safar F, Gage FH, 1999b. Fibroblast growth factor-2 activates a latent neurogenic program in neural stem cells from diverse regions of the adult CNS. J. Neurosci. 19: 8487-8497.

Palmer TD, Ray J, Gage FH, 1995. FGF-2-responsive neuronal progenitors reside in proliferative and quiescent regions of the adult rodent brain. Mol. Cell Neurosci. 6: 474-486.

Palmer TD, Willhoite AR, Gage FH, 2000. Vascular niche for adult hippocampal neurogenesis. J. Comp Neurol. 425: 479-494.

Panickar KS, Norenberg MD, 2005. Astrocytes in cerebral ischemic injury: morphological and general considerations. Glia 50: 287-298.

Panizzo RA, Kyrtatos PG, Price AN, Gadian DG, Ferretti P, Lythgoe MF, 2009. In vivo magnetic resonance imaging of endogenous neuroblasts labelled with a ferumoxide-polycation complex. Neuroimage. 44: 1239-1246.

Papadopoulos SM, Chandler WF, Salamat MS, Topol EJ, Sackellares JC, 1987. Recombinant human tissue-type plasminogen activator therapy in acute thromboembolic stroke. J. Neurosurg. 67: 394-398.

Parent JM, Vexler ZS, Gong C, Derugin N, Ferriero DM, 2002. Rat forebrain neurogenesis and striatal neuron replacement after focal stroke. Ann. Neurol. 52: 802-813.

Pawelczyk E, Arbab AS, Chaudhry A, Balakumaran A, Robey PG, Frank JA, 2008. In vitro model of bromodeoxyuridine or iron oxide nanoparticle uptake by activated macrophages from labeled stem cells: implications for cellular therapy. Stem Cells 26: 1366-1375.

Payne J, Shibasaki F, Mercola M, 1997. Spina bifida occulta in homozygous Patch mouse embryos. Dev. Dyn. 209: 105-116.

Pekny M, Nilsson M, 2005. Astrocyte activation and reactive gliosis. Glia 50: 427-434.

Pencea V, Bingaman KD, Freedman LJ, Luskin MB, 2001a. Neurogenesis in the subventricular zone and rostral migratory stream of the neonatal and adult primate forebrain. Exp. Neurol. 172: 1-16.

Pencea V, Bingaman KD, Wiegand SJ, Luskin MB, 2001b. Infusion of brain-derived neurotrophic factor into the lateral ventricle of the adult rat leads to new neurons in the parenchyma of the striatum, septum, thalamus, and hypothalamus. J. Neurosci. 21: 6706-6717.

Petreanu L, varez-Buylla A, 2002. Maturation and death of adult-born olfactory bulb granule neurons: role of olfaction. J. Neurosci. 22: 6106-6113.

Pittet MJ, Swirski FK, Reynolds F, Josephson L, Weissleder R, 2006. Labeling of immune cells for in vivo imaging using magnetofluorescent nanoparticles. Nat. Protoc. 1: 73-79.

Pluchino S, Martino G, 2005. The therapeutic use of stem cells for myelin repair in autoimmune demyelinating disorders. J. Neurol. Sci. 233: 117-119.

Pluchino S, Quattrini A, Brambilla E, Gritti A, Salani G, Dina G, Galli R, Del CU, Amadio S, Bergami A, Furlan R, Comi G, Vescovi AL, Martino G, 2003. Injection of adult neurospheres induces recovery in a chronic model of multiple sclerosis. Nature 422: 688-694.

Politi LS, Bacigaluppi M, Brambilla E, Cadioli M, Falini A, Comi G, Scotti G, Martino G, Pluchino S, 2007. Magnetic-resonance-based tracking and quantification of intravenously injected neural stem cell accumulation in the brains of mice with experimental multiple sclerosis. Stem Cells 25: 2583-2592.

Pollock K, Stroemer P, Patel S, Stevanato L, Hope A, Miljan E, Dong Z, Hodges H, Price J, Sinden JD, 2006. A conditionally immortal clonal stem cell line from human cortical neuroepithelium for the treatment of ischemic stroke. Exp. Neurol. 199: 143-155.

Porter CD, Lukacs KV, Box G, Takeuchi Y, Collins MK, 1998. Cationic liposomes enhance the rate of transduction by a recombinant retroviral vector in vitro and in vivo. J. Virol. 72: 4832-4840.

Powers JM, 1984. Medical therapy of stroke. Ariz. Med. 41: 390-392.

Powrozek TA, Sari Y, Singh RP, Zhou FC, 2004. Neurotransmitters and substances of abuse: effects on adult neurogenesis. Curr. Neurovasc. Res. 1: 251-260.

Priller J, Flugel A, Wehner T, Boentert M, Haas CA, Prinz M, Fernandez-Klett F, Prass K, Bechmann I, de Boer BA, Frotscher M, Kreutzberg GW, Persons DA, Dirnagl U, 2001. Targeting gene-modified hematopoietic cells to the central nervous system: use of green fluorescent protein uncovers microglial engraftment. Nat. Med. 7: 1356-1361.

Pringle NP, Mudhar HS, Collarini EJ, Richardson WD, 1992. PDGF receptors in the rat CNS: during late neurogenesis, PDGF alpha-receptor expression appears to be restricted to glial cells of the oligodendrocyte lineage. Development 115: 535-551.

Raber J, Fan Y, Matsumori Y, Liu Z, Weinstein PR, Fike JR, Liu J, 2004. Irradiation attenuates neurogenesis and exacerbates ischemia-induced deficits. Ann. Neurol. 55: 381-389.

Raff MC, Barres BA, Burne JF, Coles HS, Ishizaki Y, Jacobson MD, 1993. Programmed cell death and the control of cell survival: lessons from the nervous system. Science 262: 695-700.

Rakic P, 2002. Adult neurogenesis in mammals: an identity crisis. J. Neurosci. 22: 614-618.

Rausch M, Baumann D, Neubacher U, Rudin M, 2002. In-vivo visualization of phagocytotic cells in rat brains after transient ischemia by USPIO. NMR Biomed. 15: 278-283.

Rausch M, Sauter A, Frohlich J, Neubacher U, Radu EW, Rudin M, 2001. Dynamic patterns of USPIO enhancement can be observed in macrophages after ischemic brain damage. Magn Reson. Med. 46: 1018-1022.

Ravikumar R, McEwen ML, Springer JE, 2007. Post-treatment with the cyclosporin derivative, NIM811, reduced indices of cell death and increased the volume of spared tissue in the acute period following spinal cord contusion. J. Neurotrauma 24: 1618-1630.

Raynal I, Prigent P, Peyramaure S, Najid A, Rebuzzi C, Corot C, 2004. Macrophage endocytosis of superparamagnetic iron oxide nanoparticles: mechanisms and comparison of ferumoxides and ferumoxtran-10. Invest Radiol. 39: 56-63.

Rempe DA, Kent TA, 2002. Using bone marrow stromal cells for treatment of stroke. Neurology 59: 486-487.

Reumers V, Deroose CM, Krylyshkina O, Nuyts J, Geraerts M, Mortelmans L, Gijsbers R, Van den HC, Debyser Z, Baekelandt V, 2008. Noninvasive and quantitative monitoring of adult neuronal stem cell migration in mouse brain using bioluminescence imaging. Stem Cells 26: 2382-2390.

Reuter I, Tai YF, Pavese N, Chaudhuri KR, Mason S, Polkey CE, Clough C, Brooks DJ, Barker RA, Piccini P, 2008. Long-term clinical and positron emission tomography outcome of fetal striatal transplantation in Huntington's disease. J. Neurol. Neurosurg. Psychiatry 79: 948-951.

Reynolds BA, Tetzlaff W, Weiss S, 1992. A multipotent EGF-responsive striatal embryonic progenitor cell produces neurons and astrocytes. J. Neurosci. 12: 4565-4574.

Reynolds BA, Weiss S, 1992. Generation of neurons and astrocytes from isolated cells of the adult mammalian central nervous system. Science 255: 1707-1710.

Richardson WD, Pringle N, Mosley MJ, Westermark B, Dubois-Dalcq M, 1988. A role for platelet-derived growth factor in normal gliogenesis in the central nervous system. Cell 53: 309-319.

Rivers LE, Young KM, Rizzi M, Jamen F, Psachoulia K, Wade A, Kessaris N, Richardson WD, 2008. PDGFRA/NG2 glia generate myelinating oligodendrocytes and piriform projection neurons in adult mice. Nat. Neurosci. 11: 1392-1401.

Robertson TL, Kato H, Gordon T, Kagan A, Rhoads GG, Land CE, Worth RM, Belsky JL, Dock DS, Miyanishi M, Kawamoto S, 1977. Epidemiologic studies of coronary heart disease and stroke in Japanese men living in Japan, Hawaii and California. Coronary heart disease risk factors in Japan and Hawaii. Am. J. Cardiol. 39: 244-249.

Robin AM, Zhang ZG, Wang L, Zhang RL, Katakowski M, Zhang L, Wang Y, Zhang C, Chopp M, 2006. Stromal cell-derived factor 1alpha mediates neural progenitor cell motility after focal cerebral ischemia. J. Cereb. Blood Flow Metab 26: 125-134.

Rochefort C, Gheusi G, Vincent JD, Lledo PM, 2002. Enriched odor exposure increases the number of newborn neurons in the adult olfactory bulb and improves odor memory. J. Neurosci. 22: 2679-2689.

Roitbak T, Li L, Cunningham LA, 2008. Neural stem/progenitor cells promote endothelial cell morphogenesis and protect endothelial cells against ischemia via HIF-1alpha-regulated VEGF signaling. J. Cereb. Blood Flow Metab 28: 1530-1542.

Rouault TA, Cooperman S, 2006. Brain iron metabolism. Semin. Pediatr. Neurol. 13: 142-148.

Royal College of Physicians. National clinical guidelines for stroke. 2007. London, Royal College of Physicians.
Ref Type: Generic

Rudelius M, drup-Link HE, Heinzmann U, Piontek G, Settles M, Link TM, Schlegel J, 2003. Highly efficient paramagnetic labelling of embryonic and neuronal stem cells. Eur. J. Nucl. Med. Mol. Imaging 30: 1038-1044.

Rusa R, Alkayed NJ, Crain BJ, Traystman RJ, Kimes AS, London ED, Klaus JA, Hurn PD, 1999. 17beta-estradiol reduces stroke injury in estrogen-deficient female animals. Stroke 30: 1665-1670.

Saccardi R, Kozak T, Bocelli-Tyndall C, Fassas A, Kazis A, Havrdova E, Carreras E, Saiz A, Lowenberg B, te Boekhorst PA, Gualandio F, Openshaw H, Longo G, Pagliai F, Massacesi L, Deconink E, Ouyang J, Nagore FJ, Besalduch J, Lisukov IA, Bonini A, Merelli E, Slavino S, Gratwohl A, Passweg J, Tyndall A, Steck AJ, Andolina M, Capobianco M, Martin JL, Lugaresi A, Meucci G, Saez RA, Clark RE, Fernandez MN, Fouillard L, Herstenstein B, Koza V, Cocco E, Baurmann H, Mancardi GL, 2006. Autologous stem cell transplantation for progressive multiple sclerosis: update of the European Group for Blood and Marrow Transplantation autoimmune diseases working party database. Mult. Scler. 12: 814-823.

Saleh A, Wiedermann D, Schroeter M, Jonkmanns C, Jander S, Hoehn M, 2004. Central nervous system inflammatory response after cerebral infarction as detected by magnetic resonance imaging. NMR Biomed. 17: 163-169.

Sanberg PR, Willing AE, Garbuzova-Davis S, Saporta S, Liu G, Sanberg CD, Bickford PC, Klasko SK, El-Badri NS, 2005. Umbilical cord blood-derived stem cells and brain repair. Ann. N. Y. Acad. Sci. 1049: 67-83.

Sanchez-Ramos JR, Song S, Kamath SG, Zigova T, Willing A, Cardozo-Pelaez F, Stedeford T, Chopp M, Sanberg PR, 2001. Expression of neural markers in human umbilical cord blood. Exp. Neurol. 171: 109-115.

Savitt JM, Dawson VL, Dawson TM, 2006. Diagnosis and treatment of Parkinson disease: molecules to medicine. J. Clin. Invest 116: 1744-1754.

Savitz SI, Dinsmore J, Wu J, Henderson GV, Stieg P, Caplan LR, 2005. Neurotransplantation of fetal porcine cells in patients with basal ganglia infarcts: a preliminary safety and feasibility study. Cerebrovasc. Dis. 20: 101-107.

Sawamoto K, Wichterle H, Gonzalez-Perez O, Cholfin JA, Yamada M, Spassky N, Murcia NS, Garcia-Verdugo JM, Marin O, Rubenstein JL, Tessier-Lavigne M, Okano H, varez-Buylla A, 2006. New neurons follow the flow of cerebrospinal fluid in the adult brain. Science 311: 629-632.

Sbarbati A, Reggiani A, Nicolato E, Arban R, Bernardi P, Lunati E, Asperio RM, Marzola P, Osculati F, 2002. Correlation MRI/ultrastructure in cerebral ischemic lesions: application to the interpretation of cortical layered areas. Magn Reson. Imaging 20: 479-486.

Schanzer A, Wachs FP, Wilhelm D, Acker T, Cooper-Kuhn C, Beck H, Winkler J, Aigner L, Plate KH, Kuhn HG, 2004. Direct stimulation of adult neural stem cells in vitro and neurogenesis in vivo by vascular endothelial growth factor. Brain Pathol. 14: 237-248.

Schenck JF, Zimmerman EA, 2004. High-field magnetic resonance imaging of brain iron: birth of a biomarker? NMR Biomed. 17: 433-445.

Schilling M, Besselmann M, Leonhard C, Mueller M, Ringelstein EB, Kiefer R, 2003. Microglial activation precedes and predominates over macrophage infiltration in transient focal cerebral ischemia: a study in green fluorescent protein transgenic bone marrow chimeric mice. Exp. Neurol. 183: 25-33.

Schmandt T, Meents E, Gossrau G, Gornik V, Okabe S, Brustle O, 2005. High-purity lineage selection of embryonic stem cell-derived neurons. Stem Cells Dev. 14: 55-64.

Schmitz C, Axmacher B, Zunker U, Korr H, 1999. Age-related changes of DNA repair and mitochondrial DNA synthesis in the mouse brain. Acta Neuropathol. 97: 71-81.

Schroeter M, Saleh A, Wiedermann D, Hoehn M, Jander S, 2004. Histochemical detection of ultrasmall superparamagnetic iron oxide (USPIO) contrast medium uptake in experimental brain ischemia. Magn Reson. Med. 52: 403-406.

Seidenfaden R, Desoeuvre A, Bosio A, Virard I, Cremer H, 2006. Glial conversion of SVZ-derived committed neuronal precursors after ectopic grafting into the adult brain. Mol. Cell Neurosci. 32: 187-198.

Selim MH, Ratan RR, 2004. The role of iron neurotoxicity in ischemic stroke. Ageing Res. Rev. 3: 345-353.

Sgubin D, Aztiria E, Perin A, Longatti P, Leanza G, 2007. Activation of endogenous neural stem cells in the adult human brain following subarachnoid hemorrhage. J. Neurosci. Res. 85: 1647-1655.

Shah K, 2009. Imaging neural stem cell fate in mouse model of glioma. Curr. Protoc. Stem Cell Biol. Chapter 5: Unit.

Shaked I, Tchoresh D, Gersner R, Meiri G, Mordechai S, Xiao X, Hart RP, Schwartz M, 2005. Protective autoimmunity: interferon-gamma enables microglia to remove glutamate without evoking inflammatory mediators. J. Neurochem. 92: 997-1009.

Shapiro EM, Gonzalez-Perez O, Manuel Garcia-Verdugo J, varez-Buylla A, Koretsky AP, 2006a. Magnetic resonance imaging of the migration of neuronal precursors generated in the adult rodent brain. Neuroimage. 32: 1150-1157.

Shapiro EM, Sharer K, Skrtic S, Koretsky AP, 2006b. In vivo detection of single cells by MRI. Magn Reson. Med. 55: 242-249.

Sharp FR, Lu A, Tang Y, Millhorn DE, 2000. Multiple molecular penumbras after focal cerebral ischemia. J. Cereb. Blood Flow Metab 20: 1011-1032.

Shen LH, Li Y, Chen J, Zacharek A, Gao Q, Kapke A, Lu M, Raginski K, Vanguri P, Smith A, Chopp M, 2007. Therapeutic benefit of bone marrow stromal cells administered 1 month after stroke. J. Cereb. Blood Flow Metab 27: 6-13.

Shen LH, Li Y, Chen J, Zhang J, Vanguri P, Borneman J, Chopp M, 2006. Intracarotid transplantation of bone marrow stromal cells increases axon-myelin remodeling after stroke. Neuroscience 137: 393-399.

Shen Q, Wang Y, Kokovay E, Lin G, Chuang SM, Goderie SK, Roysam B, Temple S, 2008. Adult SVZ stem cells lie in a vascular niche: a quantitative analysis of niche cell-cell interactions. Cell Stem Cell 3: 289-300.

Shin YC, Choi KY, Kim WG, 2007. Cyclosporin A has a protective effect with induced upregulation of Hsp70 and nNOS on severe spinal cord ischemic injury in rabbits. J. Invest Surg. 20: 113-120.

Shingo T, Sorokan ST, Shimazaki T, Weiss S, 2001. Erythropoietin regulates the in vitro and in vivo production of neuronal progenitors by mammalian forebrain neural stem cells. J. Neurosci. 21: 9733-9743.

Shyu WC, Lin SZ, Yen PS, Su CY, Chen DC, Wang HJ, Li H, 2008. Stromal cell-derived factor-1 alpha promotes neuroprotection, angiogenesis, and mobilization/homing of bone marrow-derived cells in stroke rats. J. Pharmacol. Exp. Ther. 324: 834-849.

Simmons DA, Casale M, Alcon B, Pham N, Narayan N, Lynch G, 2007. Ferritin accumulation in dystrophic microglia is an early event in the development of Huntington's disease. Glia 55: 1074-1084.

Sipe JC, Lee P, Beutler E, 2002. Brain iron metabolism and neurodegenerative disorders. Dev. Neurosci. 24: 188-196.

Smukler SR, Runciman SB, Xu S, van der KD, 2006. Embryonic stem cells assume a primitive neural stem cell fate in the absence of extrinsic influences. J. Cell Biol. 172: 79-90.

Snyder EY, Yoon C, Flax JD, Macklis JD, 1997. Multipotent neural precursors can differentiate toward replacement of neurons undergoing targeted apoptotic degeneration in adult mouse neocortex. Proc. Natl. Acad. Sci. U. S. A 94: 11663-11668.

Sofroniew MV, 2005. Reactive astrocytes in neural repair and protection. Neuroscientist. 11: 400-407.

Son BR, Marquez-Curtis LA, Kucia M, Wysoczynski M, Turner AR, Ratajczak J, Ratajczak MZ, Janowska-Wieczorek A, 2006. Migration of bone marrow and cord blood mesenchymal stem cells in vitro is regulated by stromal-derived factor-1-CXCR4 and hepatocyte growth factor-c-met axes and involves matrix metalloproteinases. Stem Cells 24: 1254-1264.

Song HJ, Stevens CF, Gage FH, 2002. Neural stem cells from adult hippocampus develop essential properties of functional CNS neurons. Nat. Neurosci. 5: 438-445.

Sorgi FL, Bhattacharya S, Huang L, 1997. Protamine sulfate enhances lipid-mediated gene transfer. Gene Ther. 4: 961-968.

Soriano SG, Lipton SA, Wang YF, Xiao M, Springer TA, Gutierrez-Ramos JC, Hickey PR, 1996. Intercellular adhesion molecule-1-deficient mice are less susceptible to cerebral ischemia-reperfusion injury. Ann. Neurol. 39: 618-624.

Spassky N, Merkle FT, Flames N, Tramontin AD, Garcia-Verdugo JM, varez-Buylla A, 2005. Adult ependymal cells are

postmitotic and are derived from radial glial cells during embryogenesis. J. Neurosci. 25: 10-18.

Stuckey DJ, Carr CA, Martin-Rendon E, Tyler DJ, Willmott C, Cassidy PJ, Hale SJ, Schneider JE, Tatton L, Harding SE, Radda GK, Watt S, Clarke K, 2006. Iron particles for noninvasive monitoring of bone marrow stromal cell engraftment into, and isolation of viable engrafted donor cells from, the heart. Stem Cells 24: 1968-1975.

Stumm RK, Rummel J, Junker V, Culmsee C, Pfeiffer M, Krieglstein J, Hollt V, Schulz S, 2002. A dual role for the SDF-1/CXCR4 chemokine receptor system in adult brain: isoform-selective regulation of SDF-1 expression modulates CXCR4-dependent neuronal plasticity and cerebral leukocyte recruitment after focal ischemia. J. Neurosci. 22: 5865-5878.

Sugawara T, Fujimura M, Noshita N, Kim GW, Saito A, Hayashi T, Narasimhan P, Maier CM, Chan PH, 2004. Neuronal death/survival signaling pathways in cerebral ischemia. NeuroRx. 1: 17-25.

Sugiura S, Kitagawa K, Tanaka S, Todo K, Omura-Matsuoka E, Sasaki T, Mabuchi T, Matsushita K, Yagita Y, Hori M, 2005. Adenovirus-mediated gene transfer of heparin-binding epidermal growth factor-like growth factor enhances neurogenesis and angiogenesis after focal cerebral ischemia in rats. Stroke 36: 859-864.

Suhonen JO, Peterson DA, Ray J, Gage FH, 1996. Differentiation of adult hippocampus-derived progenitors into olfactory neurons in vivo. Nature 383: 624-627.

Sumner JP, Shapiro EM, Maric D, Conroy R, Koretsky AP, 2009. In vivo labeling of adult neural progenitors for MRI with micron sized particles of iron oxide: quantification of labeled cell phenotype. Neuroimage. 44: 671-678.

Suzuki Y, Zhang S, Kundu P, Yeung AC, Robbins RC, Yang PC, 2007. In vitro comparison of the biological effects of three transfection methods for magnetically labeling mouse embryonic stem cells with ferumoxides. Magn Reson. Med. 57: 1173-1179.

Taguchi A, Soma T, Tanaka H, Kanda T, Nishimura H, Yoshikawa H, Tsukamoto Y, Iso H, Fujimori Y, Stern DM, Naritomi H, Matsuyama T, 2004. Administration of CD34+ cells after stroke enhances neurogenesis via angiogenesis in a mouse model. J. Clin. Invest 114: 330-338.

Takahashi K, Okita K, Nakagawa M, Yamanaka S, 2007. Induction of pluripotent stem cells from fibroblast cultures. Nat. Protoc. 2: 3081-3089.

Takahashi K, Yamanaka S, 2006. Induction of pluripotent stem cells from mouse embryonic and adult fibroblast cultures by defined factors. Cell 126: 663-676.

Takahashi K, Yasuhara T, Shingo T, Muraoka K, Kameda M, Takeuchi A, Yano A, Kurozumi K, Agari T, Miyoshi Y, Kinugasa K, Date I, 2008. Embryonic neural stem cells transplanted in middle cerebral artery occlusion model of rats demonstrated potent therapeutic effects, compared to adult neural stem cells. Brain Res. 1234: 172-182.

Takami K, Iwane M, Kiyota Y, Miyamoto M, Tsukuda R, Shiosaka S, 1992. Increase of basic fibroblast growth factor immunoreactivity and its mRNA level in rat brain following transient forebrain ischemia. Exp. Brain Res. 90: 1-10.

Takasawa K, Kitagawa K, Yagita Y, Sasaki T, Tanaka S, Matsushita K, Ohstuki T, Miyata T, Okano H, Hori M, Matsumoto M, 2002. Increased proliferation of neural progenitor cells but reduced survival of newborn cells in the contralateral hippocampus after focal cerebral ischemia in rats. J. Cereb. Blood Flow Metab 22: 299-307.

Tamura A, Graham DI, McCulloch J, Teasdale GM, 1981. Focal cerebral ischaemia in the rat: 1. Description of technique and early neuropathological consequences following middle cerebral artery occlusion. J. Cereb. Blood Flow Metab 1: 53-60.

Tanaka N, Sasahara M, Ohno M, Higashiyama S, Hayase Y, Shimada M, 1999. Heparin-binding epidermal growth factor-like growth factor mRNA expression in neonatal rat brain with hypoxic/ischemic injury. Brain Res. 827: 130-138.

Tanaka R, Komine-Kobayashi M, Mochizuki H, Yamada M, Furuya T, Migita M, Shimada T, Mizuno Y, Urabe T, 2003. Migration of enhanced green fluorescent protein expressing bone marrow-derived microglia/macrophage into the mouse brain following permanent focal ischemia. Neuroscience 117: 531-539.

Tatlisumak T, Takano K, Carano RA, Miller LP, Foster AC, Fisher M, 1998a. Delayed treatment with an adenosine kinase

inhibitor, GP683, attenuates infarct size in rats with temporary middle cerebral artery occlusion. Stroke 29: 1952-1958.

Tatlisumak T, Takano K, Meiler MR, Fisher M, 1998b. A glycine site antagonist, ZD9379, reduces number of spreading depressions and infarct size in rats with permanent middle cerebral artery occlusion. Stroke 29: 190-195.

Taupin P, 2007. BrdU immunohistochemistry for studying adult neurogenesis: paradigms, pitfalls, limitations, and validation. Brain Res. Rev. 53: 198-214.

Tavazoie M, Van d, V, Silva-Vargas V, Louissaint M, Colonna L, Zaidi B, Garcia-Verdugo JM, Doetsch F, 2008. A specialized vascular niche for adult neural stem cells. Cell Stem Cell 3: 279-288.

Tejima E, Zhao BQ, Tsuji K, Rosell A, van LK, Gonzalez RG, Montaner J, Wang X, Lo EH, 2007. Astrocytic induction of matrix metalloproteinase-9 and edema in brain hemorrhage. J. Cereb. Blood Flow Metab 27: 460-468.

The Stroke Association. Stroke Statistics. 2006a. London, The Stroke Association.
Ref Type: Generic

The Stroke Association. Stroke Statistics. 2006b. London, The Stroke Association.
Ref Type: Generic

Thomas DL, Lythgoe MF, Pell GS, Calamante F, Ordidge RJ, 2000. The measurement of diffusion and perfusion in biological systems using magnetic resonance imaging. Phys. Med. Biol. 45: R97-138.

Thompson KJ, Shoham S, Connor JR, 2001. Iron and neurodegenerative disorders. Brain Res. Bull. 55: 155-164.

Thomson JA, Itskovitz-Eldor J, Shapiro SS, Waknitz MA, Swiergiel JJ, Marshall VS, Jones JM, 1998. Embryonic stem cell lines derived from human blastocysts. Science 282: 1145-1147.

Thored P, Arvidsson A, Cacci E, Ahlenius H, Kallur T, Darsalia V, Ekdahl CT, Kokaia Z, Lindvall O, 2006. Persistent production of neurons from adult brain stem cells during recovery after stroke. Stem Cells 24: 739-747.

Thored P, Wood J, Arvidsson A, Cammenga J, Kokaia Z, Lindvall O, 2007. Long-term neuroblast migration along blood vessels in an area with transient angiogenesis and increased vascularization after stroke. Stroke 38: 3032-3039.

Tran PB, Ren D, Veldhouse TJ, Miller RJ, 2004. Chemokine receptors are expressed widely by embryonic and adult neural progenitor cells. J. Neurosci. Res. 76: 20-34.

Tropepe V, Hitoshi S, Sirard C, Mak TW, Rossant J, van der KD, 2001. Direct neural fate specification from embryonic stem cells: a primitive mammalian neural stem cell stage acquired through a default mechanism. Neuron 30: 65-78.

Trounson A, 2005. Human embryonic stem cell derivation and directed differentiation. Ernst. Schering. Res. Found. Workshop: 27-44.

Tsai PT, Ohab JJ, Kertesz N, Groszer M, Matter C, Gao J, Liu X, Wu H, Carmichael ST, 2006. A critical role of erythropoietin receptor in neurogenesis and post-stroke recovery. J. Neurosci. 26: 1269-1274.

Tureyen K, Vemuganti R, Sailor KA, Dempsey RJ, 2005. Ideal suture diameter is critical for consistent middle cerebral artery occlusion in mice. Neurosurgery 56: 196-200.

Tweedle MF, 1992. Physicochemical properties of gadoteridol and other magnetic resonance contrast agents. Invest Radiol. 27 Suppl 1: S2-S6.

Ueno M, Akiguchi I, Hosokawa M, Kotani H, Kanenishi K, Sakamoto H, 2000. Blood-brain barrier permeability in the periventricular areas of the normal mouse brain. Acta Neuropathol. 99: 385-392.

Vallieres L, Campbell IL, Gage FH, Sawchenko PE, 2002. Reduced hippocampal neurogenesis in adult transgenic mice with chronic astrocytic production of interleukin-6. J. Neurosci. 22: 486-492.

van Lookeren CM, Thomas GR, Thibodeaux H, Palmer JT, Williams SP, Lowe DG, van BN, 1999. Secondary reduction in

the apparent diffusion coefficient of water, increase in cerebral blood volume, and delayed neuronal death after middle cerebral artery occlusion and early reperfusion in the rat. J. Cereb. Blood Flow Metab 19: 1354-1364.

van PH, Christie BR, Sejnowski TJ, Gage FH, 1999. Running enhances neurogenesis, learning, and long-term potentiation in mice. Proc. Natl. Acad. Sci. U. S. A 96: 13427-13431.

van PH, Schinder AF, Christie BR, Toni N, Palmer TD, Gage FH, 2002. Functional neurogenesis in the adult hippocampus. Nature 415: 1030-1034.

Alvarez-Buylla A, Garcia-Verdugo JM, 2002. Neurogenesis in adult subventricular zone. J. Neurosci. 22: 629-634.

Alvarez-Buylla A, Lim DA, 2004. For the long run: maintaining germinal niches in the adult brain. Neuron 41: 683-686.

Veizovic T, Beech JS, Stroemer RP, Watson WP, Hodges H, 2001. Resolution of stroke deficits following contralateral grafts of conditionally immortal neuroepithelial stem cells. Stroke 32: 1012-1019.

Vendrame M, Cassady J, Newcomb J, Butler T, Pennypacker KR, Zigova T, Sanberg CD, Sanberg PR, Willing AE, 2004. Infusion of human umbilical cord blood cells in a rat model of stroke dose-dependently rescues behavioral deficits and reduces infarct volume. Stroke 35: 2390-2395.

Vescovi AL, Reynolds BA, Fraser DD, Weiss S, 1993. bFGF regulates the proliferative fate of unipotent (neuronal) and bipotent (neuronal/astroglial) EGF-generated CNS progenitor cells. Neuron 11: 951-966.

Vise WM, Schuier F, Hossmann KA, Takagi S, Zulch KJ, 1977. Cerebral microembolization. I. Pathophysiological studies. Arch. Neurol. 34: 660-665.

Wagner JP, Black IB, Cicco-Bloom E, 1999. Stimulation of neonatal and adult brain neurogenesis by subcutaneous injection of basic fibroblast growth factor. J. Neurosci. 19: 6006-6016.

Wakade C, Khan MM, De Sevilla LM, Zhang QG, Mahesh VB, Brann DW, 2008. Tamoxifen neuroprotection in cerebral ischemia involves attenuation of kinase activation and superoxide production and potentiation of mitochondrial superoxide dismutase. Endocrinology 149: 367-379.

Walczak P, Ruiz-Cabello J, Kedziorek DA, Gilad AA, Lin S, Barnett B, Qin L, Levitsky H, Bulte JW, 2006. Magnetoelectroporation: improved labeling of neural stem cells and leukocytes for cellular magnetic resonance imaging using a single FDA-approved agent. Nanomedicine. 2: 89-94.

Walton NM, Sutter BM, Laywell ED, Levkoff LH, Kearns SM, Marshall GP, Scheffler B, Steindler DA, 2006. Microglia instruct subventricular zone neurogenesis. Glia 54: 815-825.

Wang L, Zhang Z, Wang Y, Zhang R, Chopp M, 2004. Treatment of stroke with erythropoietin enhances neurogenesis and angiogenesis and improves neurological function in rats. Stroke 35: 1732-1737.

Wang L, Zhang ZG, Zhang RL, Gregg SR, Hozeska-Solgot A, Letourneau Y, Wang Y, Chopp M, 2006. Matrix metalloproteinase 2 (MMP2) and MMP9 secreted by erythropoietin-activated endothelial cells promote neural progenitor cell migration. J. Neurosci. 26: 5996-6003.

Wang Q, Tang XN, Yenari MA, 2007a. The inflammatory response in stroke. J. Neuroimmunol. 184: 53-68.

Wang Y, Jin K, Mao XO, Xie L, Banwait S, Marti HH, Greenberg DA, 2007b. VEGF-overexpressing transgenic mice show enhanced post-ischemic neurogenesis and neuromigration. J. Neurosci. Res. 85: 740-747.

Weber R, Ramos-Cabrer P, Hoehn M, 2006. Present status of magnetic resonance imaging and spectroscopy in animal stroke models. J. Cereb. Blood Flow Metab 26: 591-604.

Weber R, Wegener S, Ramos-Cabrer P, Wiedermann D, Hoehn M, 2005. MRI detection of macrophage activity after experimental stroke in rats: new indicators for late appearance of vascular degradation? Magn Reson. Med. 54: 59-66.

Wegener S, Weber R, Ramos-Cabrer P, Uhlenkueken U, Sprenger C, Wiedermann D, Villringer A, Hoehn M, 2006.

Temporal profile of T2-weighted MRI distinguishes between pannecrosis and selective neuronal death after transient focal cerebral ischemia in the rat. J. Cereb. Blood Flow Metab 26: 38-47.

Weinstein PR, Hong S, Sharp FR, 2004. Molecular identification of the ischemic penumbra. Stroke 35: 2666-2670.

Wenning GK, Odin P, Morrish P, Rehncrona S, Widner H, Brundin P, Rothwell JC, Brown R, Gustavii B, Hagell P, Jahanshahi M, Sawle G, Bjorklund A, Brooks DJ, Marsden CD, Quinn NP, Lindvall O, 1997. Short- and long-term survival and function of unilateral intrastriatal dopaminergic grafts in Parkinson's disease. Ann. Neurol. 42: 95-107.

Wiart M, Davoust N, Pialat JB, Desestret V, Moucharrafie S, Cho TH, Mutin M, Langlois JB, Beuf O, Honnorat J, Nighoghossian N, Berthezene Y, 2007. MRI monitoring of neuroinflammation in mouse focal ischemia. Stroke 38: 131-137.

Wichterle H, Garcia-Verdugo JM, Herrera DG, varez-Buylla A, 1999. Young neurons from medial ganglionic eminence disperse in adult and embryonic brain. Nat. Neurosci. 2: 461-466.

Wichterle H, Lieberam I, Porter JA, Jessell TM, 2002. Directed differentiation of embryonic stem cells into motor neurons. Cell 110: 385-397.

Widera D, Holtkamp W, Entschladen F, Niggemann B, Zanker K, Kaltschmidt B, Kaltschmidt C, 2004. MCP-1 induces migration of adult neural stem cells. Eur. J. Cell Biol. 83: 381-387.

Wiener EC, Konda S, Shadron A, Brechbiel M, Gansow O, 1997. Targeting dendrimer-chelates to tumors and tumor cells expressing the high-affinity folate receptor. Invest Radiol. 32: 748-754.

Wiese C, Rolletschek A, Kania G, Blyszczuk P, Tarasov KV, Tarasova Y, Wersto RP, Boheler KR, Wobus AM, 2004. Nestin expression--a property of multi-lineage progenitor cells? Cell Mol. Life Sci. 61: 2510-2522.

Willaime-Morawek S, Seaberg R, Batista C, Labbé E, Attisano L, Gorski JA, Jones KR, Kam A, Morshead CM, van der Kooy D. Embryonic cortical neural stem cells migrate ventrally and persist as postnatal striatal stem cells. J Cell Biol, Vol. 175, No. 1, October 9, 2006 159–168.

Willaime-Morawek S, van der KD, 2008. Cortex- and striatum- derived neural stem cells produce distinct progeny in the olfactory bulb and striatum. Eur. J. Neurosci. 27: 2354-2362.

Windrem MS, Nunes MC, Rashbaum WK, Schwartz TH, Goodman RA, McKhann G, Roy NS, Goldman SA, 2004. Fetal and adult human oligodendrocyte progenitor cell isolates myelinate the congenitally dysmyelinated brain. Nat. Med. 10: 93-97.

Wolswijk G, 2002. Oligodendrocyte precursor cells in the demyelinated multiple sclerosis spinal cord. Brain 125: 338-349.

Wolswijk G, Noble M, 1989. Identification of an adult-specific glial progenitor cell. Development 105: 387-400.

Wong LF, Ralph GS, Walmsley LE, Bienemann AS, Parham S, Kingsman SM, Uney JB, Mazarakis ND, 2005. Lentiviral-mediated delivery of Bcl-2 or GDNF protects against excitotoxicity in the rat hippocampus. Mol. Ther. 11: 89-95.

Woodruff RH, Fruttiger M, Richardson WD, Franklin RJ, 2004. Platelet-derived growth factor regulates oligodendrocyte progenitor numbers in adult CNS and their response following CNS demyelination. Mol. Cell Neurosci. 25: 252-262.

Wren D, Wolswijk G, Noble M, 1992. In vitro analysis of the origin and maintenance of O-2Aadult progenitor cells. J. Cell Biol. 116: 167-176.

Yamaguchi T, Miyata K, Shibasaki F, Isshiki A, Uchino H, 2006. Effect of cyclosporin a on immediate early gene in rat global ischemia and its neuroprotection. J. Pharmacol. Sci. 100: 73-81.

Yamashita T, Ninomiya M, Hernandez AP, Garcia-Verdugo JM, Sunabori T, Sakaguchi M, Adachi K, Kojima T, Hirota Y, Kawase T, Araki N, Abe K, Okano H, Sawamoto K, 2006. Subventricular zone-derived neuroblasts migrate and differentiate into mature neurons in the post-stroke adult striatum. J. Neurosci. 26: 6627-6636.

Yan YP, Sailor KA, Vemuganti R, Dempsey RJ, 2006. Insulin-like growth factor-1 is an endogenous mediator of focal ischemia-induced neural progenitor proliferation. Eur. J. Neurosci. 24: 45-54.

Ying QL, Stavridis M, Griffiths D, Li M, Smith A, 2003. Conversion of embryonic stem cells into neuroectodermal precursors in adherent monoculture. Nat. Biotechnol. 21: 183-186.

Yoo S, Wrathall JR, 2007. Mixed primary culture and clonal analysis provide evidence that NG2 proteoglycan-expressing cells after spinal cord injury are glial progenitors. Dev. Neurobiol. 67: 860-874.

Yoshimura S, Takagi Y, Harada J, Teramoto T, Thomas SS, Waeber C, Bakowska JC, Breakefield XO, Moskowitz MA, 2001. FGF-2 regulation of neurogenesis in adult hippocampus after brain injury. Proc. Natl. Acad. Sci. U. S. A 98: 5874-5879.

Young KM, Fogarty M, Kessaris N, Richardson WD, 2007b. Subventricular zone stem cells are heterogeneous with respect to their embryonic origins and neurogenic fates in the adult olfactory bulb. J. Neurosci. 27: 8286-8296.

Young KM, Fogarty M, Kessaris N, Richardson WD, 2007c. Subventricular zone stem cells are heterogeneous with respect to their embryonic origins and neurogenic fates in the adult olfactory bulb. J. Neurosci. 27: 8286-8296.

Young KM, Fogarty M, Kessaris N, Richardson WD, 2007a. Subventricular zone stem cells are heterogeneous with respect to their embryonic origins and neurogenic fates in the adult olfactory bulb. J. Neurosci. 27: 8286-8296.

Yrjanheikki J, Tikka T, Keinanen R, Goldsteins G, Chan PH, Koistinaho J, 1999. A tetracycline derivative, minocycline, reduces inflammation and protects against focal cerebral ischemia with a wide therapeutic window. Proc. Natl. Acad. Sci. U. S. A 96: 13496-13500.

Yu J, Vodyanik MA, Smuga-Otto K, ntosiewicz-Bourget J, Frane JL, Tian S, Nie J, Jonsdottir GA, Ruotti V, Stewart R, Slukvin II, Thomson JA, 2007. Induced pluripotent stem cell lines derived from human somatic cells. Science 318: 1917-1920.

Zhang H, Vutskits L, Calaora V, Durbec P, Kiss JZ, 2004a. A role for the polysialic acid-neural cell adhesion molecule in PDGF-induced chemotaxis of oligodendrocyte precursor cells. J. Cell Sci. 117: 93-103.

Zhang P, Li J, Liu Y, Chen X, Kang Q, 2009. Transplanted human embryonic neural stem cells survive, migrate, differentiate and increase endogenous nestin expression in adult rat cortical peri-infarction zone. Neuropathology.

Zhang R, Zhang Z, Wang L, Wang Y, Gousev A, Zhang L, Ho KL, Morshead C, Chopp M, 2004b. Activated neural stem cells contribute to stroke-induced neurogenesis and neuroblast migration toward the infarct boundary in adult rats. J. Cereb. Blood Flow Metab 24: 441-448.

Zhang R, Zhang Z, Zhang C, Zhang L, Robin A, Wang Y, Lu M, Chopp M, 2004c. Stroke transiently increases subventricular zone cell division from asymmetric to symmetric and increases neuronal differentiation in the adult rat. J. Neurosci. 24: 5810-5815.

Zhang RL, Zhang ZG, Chopp M, 2005a. Neurogenesis in the adult ischemic brain: generation, migration, survival, and restorative therapy. Neuroscientist. 11: 408-416.

Zhang RL, Zhang ZG, Wang Y, Letourneau Y, Liu XS, Zhang X, Gregg SR, Wang L, Chopp M, 2007a. Stroke induces ependymal cell transformation into radial glia in the subventricular zone of the adult rodent brain. J. Cereb. Blood Flow Metab 27: 1201-1212.

Zhang Y, Jin Y, Behr MJ, Feustel PJ, Morrison JP, Kimelberg HK, 2005b. Behavioral and histological neuroprotection by tamoxifen after reversible focal cerebral ischemia. Exp. Neurol. 196: 41-46.

Zhang Y, Milatovic D, Aschner M, Feustel PJ, Kimelberg HK, 2007b. Neuroprotection by tamoxifen in focal cerebral ischemia is not mediated by an agonist action at estrogen receptors but is associated with antioxidant activity. Exp. Neurol. 204: 819-827.

Zhang Z, Jiang Q, Jiang F, Ding G, Zhang R, Wang L, Zhang L, Robin AM, Katakowski M, Chopp M, 2004d. In vivo magnetic resonance imaging tracks adult neural progenitor cell targeting of brain tumor. Neuroimage. 23: 281-287.

Zhang ZG, Jiang Q, Zhang R, Zhang L, Wang L, Zhang L, Arniego P, Ho KL, Chopp M, 2003. Magnetic resonance imaging and neurosphere therapy of stroke in rat. Ann. Neurol. 53: 259-263.

Zhao BQ, Tejima E, Lo EH, 2007. Neurovascular proteases in brain injury, hemorrhage and remodeling after stroke. Stroke 38: 748-752.

Zhao BQ, Wang S, Kim HY, Storrie H, Rosen BR, Mooney DJ, Wang X, Lo EH, 2006. Role of matrix metalloproteinases in delayed cortical responses after stroke. Nat. Med. 12: 441-445.

Zhao C, Deng W, Gage FH, 2008. Mechanisms and functional implications of adult neurogenesis. Cell 132: 645-660.

Zhu DY, Liu SH, Sun HS, Lu YM, 2003. Expression of inducible nitric oxide synthase after focal cerebral ischemia stimulates neurogenesis in the adult rodent dentate gyrus. J. Neurosci. 23: 223-229.

Zhu W, Mao Y, Zhao Y, Zhou LF, Wang Y, Zhu JH, Zhu Y, Yang GY, 2005. Transplantation of vascular endothelial growth factor-transfected neural stem cells into the rat brain provides neuroprotection after transient focal cerebral ischemia. Neurosurgery 57: 325-333.

Zhu X, Hill RA, Nishiyama A, 2008. NG2 cells generate oligodendrocytes and gray matter astrocytes in the spinal cord. Neuron Glia Biol. 4: 19-26.

Zigova T, Song S, Willing AE, Hudson JE, Newman MB, Saporta S, Sanchez-Ramos J, Sanberg PR, 2002. Human umbilical cord blood cells express neural antigens after transplantation into the developing rat brain. Cell Transplant. 11: 265-274.

Ziskin JL, Nishiyama A, Rubio M, Fukaya M, Bergles DE, 2007. Vesicular release of glutamate from unmyelinated axons in white matter. Nat. Neurosci. 10: 321-330.

Ziv Y, Ron N, Butovsky O, Landa G, Sudai E, Greenberg N, Cohen H, Kipnis J, Schwartz M, 2006. Immune cells contribute to the maintenance of neurogenesis and spatial learning abilities in adulthood. Nat. Neurosci. 9: 268-275.